Plantwide Optimizing Control for the Continuous Bio-Ethanol Production Process

vorgelegt von
M.Eng. Silvia Mercedes Ochoa Cáceres
aus Bucaramanga (Kolumbien)

Von der Fakultät III - Prozesswissenschaften
der Technischen Universität Berlin
zur Erlangung des akademischen Grades
Doktor der Ingenieurwissenschaften
Dr. - Ing.

genehmigte Dissertation

Promotionsausschuss:

Vorsitzender: Prof. Dr.-Ing. habil. Rudibert King
Berichter: Prof. Dr.-Ing. habil. Prof. h.c. Dr. h.c. Günter Wozny
Berichter: Prof. Dr.-Ing. habil. Jens-Uwe Repke

Tag der wissenschaftliche Aussprache: 26.04.2010

Berlin 2010

D 83

Dedicado

A mis padres por su amor y apoyo incondicional.

A Huguis por ser mi inspiración y el sol de mi vida.

Man muss Optimist sein

Max Planck

Vorwort

Die vorliegende Arbeit entstand während meiner Tätigkeit als wissenschaftliche Mitarbeiterin am Fachgebiet Dynamik und Betrieb technischer Anlagen an der Technischen Universität Berlin. Mein ganz besonderer Dank gilt meinem Doktorvater, Herrn Prof. Dr.-Ing. Günter Wozny, für die sowohl durch hohe Anforderungen als auch durch große gewährte Freiräume geprägte Betreuung dieser Arbeit. Er stand immer als Ansprechpartner zur Verfügung und gewährte mir stets einen großen wissenschaftlichen Gestaltungsspielraum.

Herrn Prof. Dr. Jens-Uwe Repke danke ich für die Übernahme des Koreferats. Darüber hinaus möchte ich mich für sein persönliches Engagement, besonders seine ständige Gesprächsbereitschaft und die Unterstützung bedanken. Bei Herr Prof. Dr. Rudibert King bedanke ich mich für die Übernahme des Prüfungsvorsitzes.

Für die finanzielle Förderung dieser Arbeit danke ich dem DAAD und der Antioquia Universität von Kolumbien. Weiterhin bedanke Ich mich beim Dr.-Ing. Frank Beuster des ehemaligen PIPES-Programm Manager und sehr guten Freund.

Weiterhin bedanke ich mich bei Prof. Dae Ryok Yang von der Korea University für die externe Betreuung während meiner Zeit in der Korea Universität. Herrn Professor Dr. Frank-Jürgen Methner möchte ich für die Einführung in der fermentative Technologie im seine Fachgebiet danken. Für die Zusammenarbeit mit Professor Velislava Luybenova und Professor Maya Ignatova von der Bulgarian Academy of Sciences und mit Dr. Ing. Georgi Kostov von der Plovdiv Universität während meiner Zeit in Bulgarien danke ich sehr.

Ich bedanke mich bei allen Freunden und Kollegen für die freundliche und ausgezeichnete Zusammenarbeit die Unterstützung und das gute Arbeitsklima. Besonders hohen Anteil daran hatten Dipl.-Ing. Teresa del Pozo, Dr. Ing. Ahrim Yoo, Dr.

Ing. Liang Cheng, Dr. Ing. Dong Kyu Kim, Dr. Ing. Harvey Arellano-Garcia, Dr. Ing. Tilman Barz, Dipl. Ing. Oliver Schach, und M. Sc. Matan Beery. Am Ende, meiner größer danken zum Dipl.-Inf. Carolina Becker, das Lateinamerikanische Stückchen in Fachgebiet und super Freundin die immer für mich da war.

I would also like to thank M. Eng. Miguel Ricardo Hernandez-Garcia from University of South California for the opportunity to use high performance computation in some of the simulations.

Mi agradecimiento de todo corazón a mis padres por su amor y apoyo incondicional durante toda mi vida. A Huguis por ser mi compañero en esta gran aventura que es la vida, y por ser mi sol especialmente durante los 4 inolvidables inviernos que viví en Berlín. A mis hermanos Liliana y David, por su apoyo y complicidad. A Elsita y José Miguel por su amor y por acogerme cálidamente como parte de su hogar. A todos, gracias por su apoyo, confianza y amor que me han permitido culminar exitosamente una de mis más grandes metas.

Señor Dios te agradezco infinitamente y de todo corazón por regalarme cada día, por permitirme disfrutar de mi trabajo, por cada una de las bendiciones que me has regalado durante mi vida, por todas las experiencias vividas en estos cuatro años y especialmente por la culminación con éxito de este proyecto.

Berlin, April 2010

Abstract

In this work, the Plantwide Control (PWC) problem of a continuous bio-ethanol process is investigated from a Plantwide Optimizing Control (PWOC) perspective. A PWOC methodology is proposed which addresses this problem by integrating real-time optimization and control for optimal operation. The PWOC methodology consists of two main tasks. The first is a local control-oriented task related to the identification and design of necessary local control loops required for satisfying the primary objectives of the process (e.g. safe operation, environmental and equipment protection, etc.). The second is a Plantwide control-oriented task in which the available control degrees of freedom are used for maximizing the process profitability. This means that, excluding the local loops, no pre-defined set points will be either regulated or tracked. The core of the PWOC methodology proposed is the formulation of a Dynamic Real time optimization (D-RTO) problem for the complete process. In this work, two new approaches are proposed for reducing the computational effort of solving this problem in real time. First, it is proposed to shrink the search region in the optimization problem based on the effect of disturbances (both, known and unknown) on the profitability of the process. Second, a new stochastic global optimization algorithm denoted as Molecular-Inspired parallel Tempering (MIPT) is proposed for solving the D-RTO problem. The performance of the MIPT algorithm is evaluated in different challenging case studies, demonstrating to be a very competitive and efficient algorithm, reaching the global optimum with 100% success ratio in most cases without requiring much computational effort. It is shown that incorporating the shrinking approach and the MIPT algorithm results in a very efficient approach for solving the complex problem of controlling a complete, highly interconnected plant, such as the bio-ethanol production process. In addition, two different PWOC approaches have been considered: A Single-Layer Direct Optimizing Control (PWOC-one-layer) and a Multi-Layer without Coordination approach (PWOC-two-layer). The performance of the PWOC-one-layer and PWOC-two-layer schemes is analyzed under three different disturbance scenarios: a known disturbance in the feed concentration, an unknown disturbance in the kinetics parameters of fermentation, and a sudden increase in the raw material price. The performance of the PWOC approaches facing these challenges is compared to the performance when a decentralized Plantwide architecture (i.e. multiple single PID loops) is used, a typical configuration in industry, demonstrating the benefits of using Plantwide Optimization-based Control strategies towards reaching maximum profitability.

Zusammenfassung

In der vorliegenden Arbeit wurde die *Plantwide Optimizing Control* (PWOC) für die kontinuierliche Bio-Ethanolproduktion untersucht. Diese Methode integriert *Real-Time Optimization* (RTO) und Regelung für den optimalen Betrieb in zwei verschiedene Aufgaben. Die erste ist eine lokale dezentralisierte Regelungsaufgabe, die aus der Identifizierung und dem Entwurf benötigter lokaler Regelkreise für die Erfüllung der Primärregelungsziele des Prozess (z.B. sicherer Betrieb, Umweltschutz, Anlageschutz, usw.) besteht. Die zweite ist eine anlagenweite (plantwide) Regelungsaufgabe, die die verfügbaren Freiheitsgrade nutzt um die Prozessrentabilität zu maximieren. Das heißt, dass außer den lokalen Regelkreisen, keine festgelegten Sollwerte vorgegeben werden. Das Prinzip des PWOC Methode ist die Formulierung eines *Dynamic Real-Time Optimization* (D-RTO) Problems für den ganzen Prozess. Die Berechnungsdauer der Lösung der D-RTO wird durch die Ausführung einer neuen Methode zur Verkleinerung des Durchsuchungsbereich und durch eine neue stochastiche globale Optimierungsmethode (*Molecular-Inspired Parallel Tempering* - MIPT) stark reduziert. Die Leistung des MIPT Optimierungsalgorithmus wird für verschiedene Probleme bewertet. Es wird nachgewiesen, dass MIPT eine sehr effiziente und hilfreiche Methode ist. Die Verwendung der neuen Methode zur Verkleinerung des Durchsuchungsbereichs und der MIPT Optimierungsmethode führen zu einer leistungsfähigen Lösung des komplizierten *Plantwide Control* (PWC) Problems (z.B. für den kontinuierlichen Bio-Ethanol Produktionsprozess). Zwei verschiedene PWOC Architekturen werden verwendet: Die *Single-Layer Direct Optimizing Control* Architektur und die *Multi-Layer without Coordination* Architektur. Die Ergebnisse für jede Architektur sind für drei Störungsszenarien untersucht worden: eine bekannte Störung in der Zulaufkonzentration, eine unbekannte Störung in den kinetischen Parametern der Fermentation, und eine unerwartete Steigerung der Rohstoffpreise. Die Leistung der PWOC Architekturen werden mit der Leistung einer dezentralisierten Architektur (mehrere PID Regelkreise) verglichen. Es ist klar geworden, dass die PWOC Methode eine äußerst effiziente Strategie für die Maximierung der Prozessrentabilität darstellt.

Table of Contents

Page

List of Symbols

Latin letters

Symbol	Description	Unit
a	Molecular size	Å
a_{act}	Specific α-amylase activity	U/kg
ads	Molecular sieves adsorption potential	kg/kg
A_T	Cross section of tank	m^2
A_{tray}	Tray wet area	m^2
B_1	Flow of bottoms in distillation column (stillage)	kmol/h
B_2	Flow of bottoms in rectification column	kmol/h
C_p	Molar heat capacity	J/kmolK
d	Disturbance	
d_{ij}	Distance between molecules i and j (in the space of decision variables)	
e	Error	
e_1	α-amylase concentration	kg/m^3
$e_{1,1}$	α-amylase concentration in α-amylase feed stream	kg/m^3
e_2	Glucoamylase concentration	kg/m^3
$e_{2,3}$	Glucoamylase concentration in glucoamylase feed stream	kg/m^3
E_a	Activation energy	J/mol
E	Ethanol concentration	kg/m^3
E_F	Ethanol concentration in fermentor	kg/m^3
E_L	Ethanol concentration in liquefaction tank	kg/m^3
E_S	Ethanol concentration in saccharification tank	kg/m^3
M	Mayer term in objective function	
E_m	Constant of biomass growth inhibition by ethanol	kg/m^3
D_1	Flow of distillate in distillation column	kmol/h
D_2	Flow of distillate in distillation column	kmol/h

Symbol	Description	Unit
F_0	Starch slurry feed stream	kg/h
F_1	α-amylase feed stream	kg/h
F_2	Output stream from liquefaction tank	kg/h
F_3	Glucoamylase feed stream	kg/h
F_4	Output stream from saccharification tank	kg/h
F_5	Fresh yeast feed stream	kg/h
F_6	Liquid output stream from fermentor	kg/h
F_7	Cells retained by filter	kg/h
F_8	Biomass purge stream	kg/h
F_9	Biomass to treatment tank	kg/h
F_{10}	Fresh water feed stream to treatment tank	kg/h
F_{11}	Ethanol recycle stream from flash to fermentor	kg/h
F_{12}	Vent gas output from fermentor	kg/h
F_{13}	Yeast-free stream from filter	kg/h
F_{14}	Liquid output from flash	kmol/h
F_{15}	Water recycle stream from flash to fermentor	kmol/h
F_{16}	Feed stream to distillation column	kmol/h
F_{17}	Vapor output from flash	kmol/h
F_{18}	CO_2 stream to scrubber	kmol/h
F_{19}	Feed sidestream to rectification column	kmol/h
F_{20}	Fuel-grade ethanol product stream	kg/h
F_{21}	Lutter water recycle stream	kg/h
F_{22}	Fresh water feed stream to liquefaction tank	kg/h
F_{23}	Total water feed stream to liquefaction tank	kg/h
F_{B1}	Molar flowrate of bottoms from distillation column	kmol/h
F_{B2}	Molar flowrate of bottoms from rectification column	kmol/h
F_{Bm}	Random force	
F_{D1}	Molar flowrate of distillate from distillation column	kmol/h
F_{D2}	Molar flowrate of distillate from rectification column	kmol/h
F_f	Friction force	
F_{global}	Global optimum	
F_{obj}	Objective function	

Symbol	Description	Unit
F_{opt}	Current best value of objective function	
F_{rep}	Repulsion force	
g	Equality constraint	
g_{act}	Specific glucoamylase activity	U/kg
G	Gibbs Free Energy in PT, MIPT	
G	Glucose concentration	kg/m^3
G_F	Glucose concentration in fermentor	kg/m^3
G_m	Constant of biomass growth inhibition by glucose	kg/m^3
G_S	Glucose concentration in saccharification tank	kg/m^3
h	Inequality constraint	
$h_{0,ref}$	Molar enthalpy at reference temperature	J/kmol
h_l	Molar enthalpy of liquid	J/kmol
h_v	Molar enthalpy of vapor	J/kmol
H_{B1}	Level in reboiler of distillation column	m
H_{B2}	Level in reboiler of rectification column	m
H_{D1}	Level in reflux drum of distillation column	m
H_{D2}	Level in reflux drum of rectification column	m
H_F	Level in fermentor	m
H_L	Level in liquefaction tank	m
H_S	Level in saccharification tank	m
i	Iteration counter, replica counter	
j	Replica counter	
J	Objective function	
k	Particle counter	
k_3	Kinetic rate constant of dextrin consumption	m^3/Uh
k_B	Boltzmann's constant	J/K
k_{de}	Kinetic rate constant of α-amylase deactivation	1/h
k_{dP}	Constant of cellular death by ethanol	m^3/kg
k_{dT}	Kinetic rate constant of cellular death	1/h
k_g	Kinetic rate constant of starch gelatinization	1/h
k_i	Product inhibition constant	kg/m^3
k_m	Michaelis-Menten constant	kg/m^3
k_{mlt}	Kinetic rate constant of dextrin production	1/h
K_1	Repulsion force constant in MIPT	
K_2	Random force constant in MIPT	

Symbol	Description	Unit
K_3	Metropolis constant in MIPT	
K_C	Controller gain	
K_i	Constant of biomass growth decay by glucose	m^3/kg
ℓ	Lagrange term in objective function	
L	Liquid flow rate in distillation column	kmol/h
$L_{1,rect}$	Liquid output flow rate from the first stage (reboiler) in rectification column	kmol/h
$minf_E$	Minimum fraction of explorer molecules in MIPT	
m_{lt}	Maltotriose concentration	kg/m^3
$m_{lt,L}$	Maltotriose concentration in liquefaction tank	kg/m^3
$m_{lt,S}$	Maltotriose concentration in saccharification tank	kg/m^3
m_{MS}	Mass of molecular sieves in an adsorption unit	kg
m_p	Kinetic constant of ethanol production during cell maintenance	1/h
m_X	Kinetic constant of substrate consumption during cell maintenance	1/h
M	Molar liquid holdup in trays	kmol
M	Mayer term in objective function	
M_{ads}	Rate of mass adsorption by molecular sieves	kg/h
n_c	Number of components	
n_{dv}	Number of decision variables	
n_f	Non-fermentable concentration	kg/m^3
n_m	Number of molecules	
N	Total number of elements	
N_{T1}	Number of trays in distillation column	
N_{T2}	Number of trays in rectification column	
NRC	Success ratio	
p	Probability density function	
P	Pressure	Pa
P	Weighting matrix for smooth operation in MPC formulation	

Symbol	Description	Unit
P_{acc}	Probability of acceptance using Metropolis condition	
P_{t1}	Pressure at the top of distillation column	Pa
P_{t2}	Pressure at the top of rectification column	Pa
P_v	Vapor pressure	Pa
q	Vapor fraction in column feed stream	
Q	Heat duty in process model	J/h
Q	Weighting matrix for output regulation in MPC formulation	
Q_{C1}	Heat duty in total condenser of distillation column	J/h
Q_{C2}	Heat duty in partial condenser of rectification column	J/h
Q_{R1}	Heat duty in reboiler of distillation column	J/h
Q_{R2}	Heat duty in reboiler of rectification column	J/h
r	Uniform random number	
r_d	Rate of cells death	kg/m^3h
r_{de}	Rate of α-amylase deactivation	U/m^3h
r_{evap}	Rate of evaporation	kmol/h
r_g	Rate of gelatinization	kg/m^3h
r_{mtl}	Rate of dextrins production	kg/m^3h
$r_{mtl,S}$	Rate of dextrins consumption in saccharification	kg/m^3h
r_p	Rate of ethanol production	kg/m^3h
r_s	Rate of glucose consumption	kg/m^3h
r_X	Rate of biomass growth	kg/m^3h
R	Weighting matrix for manipulated variable regulation in MPC formulation	
R	Universal gas constant	J/molK
R_1	Reflux flow rate in distillation column	kmol/h
R_2	Reflux flow rate in rectification column	kmol/h
S_g	Gelatinized starch concentration	kg/m^3
$S_{g,L}$	Gelatinized starch concentration in liquefaction tank	kg/m^3
S_{ung}	Ungelatinized starch concentration	kg/m^3
$S_{ung,0}$	Ungelatinized starch concentration in starch feed stream	kg/m^3

Symbol	Description	Unit
$S_{ung,L}$	Ungelatinized starch concentration in liquefaction tank	kg/m^3
t	Time	h
t_0	Initial time	h
t_{opt}	Optimization horizon	h
t_{reg}	Regeneration period of molecular sieves unit	h
T	Temperature	K
u	Manipulated variable	
u_{max}	Upper bound of manipulated variable	
u_{min}	Lower bound of manipulated variable	
U	Vector of manipulated variables	
u_{Loc}	Local manipulated variable	
u_{PW}	Plantwide manipulated variable	
v	Particle/molecule velocity	
v	Volume of liquid in tray	m^3
V	Vapor flow rate in distillation column	kmol/h
V_F	Volume of liquid in fermentor	m^3
V_L	Volume of liquid in liquefaction tank	m^3
V_S	Volume of liquid in saccharification tank	m^3
VB_1	Boilup vapour flowrate in distillation column	kmol/h
VB_2	Boilup vapour flowrate in rectification column	kmol/h
w	Water concentration	kg/m^3
w	Molecular weight	kg/kmol
w	Economic weight factors in profitability objective function	
w_d	Economic weight factor related to disturbances	
w_{ij}	Gain factor manipulated variable – disturbance	
$w_{i\Phi}$	Gain factor manipulated variable – profitability	
w_u	Economic weight factor related to manipulated variables	
w_y	Economic weight factor related to outputs	
x	State in process model	
x_0	Initial state in process model	

Symbol	Description	Unit
x	Decision variable in optimization problem	
x	Liquid mole fraction in distillation trays	
x_{E20}	Ethanol mass fraction in product	
x_{EB1}	Mass fraction of ethanol in bottoms of distillation column	
x_{EB2}	Mass fraction of ethanol in bottoms of rectification column	
x_{ED1}	Mass fraction of ethanol in distillate of distillation column	
x_{ED2}	Mass fraction of ethanol in distillate of rectification column	
x_{w20}	Water mass fraction in product	
x_{wD2}	Water mass fraction in distillate of rectification column	
X	Vector of decision variables in optimization problem	
X	Vector of states in process model	
$\hat{X}$	Vector of estimated states in process model	
X_d	Dead biomass concentration	kg/m^3
X_m	Constant of biomass growth inhibition by biomass	kg/m^3
X_t	Total biomass concentration	kg/m^3
$X_{t,F}$	Total biomass concentration in fermentor	kg/m^3
X_v	Viable biomass concentration	kg/m^3
y	Output variable	
y	Vapor mole fraction	
Y	Vector of outputs	
Y_{PX}	Yield of ethanol per mass of cells	kg/kg
Y_{XS}	Yield of biomass per mass of substrate consumed	kg/kg
z	Overall mole fraction	
z_Φ	Dummy variable	

Greek letters

Symbol	Description	Unit
β	Annealing parameter	1/J
Δ	Difference operator	
ε	Tolerance	
ϕ	Factors in PSO	
Φ	Profitability function	
γ	Friction coefficient	
γ	Activity coefficient in VLE model	
γ_X	Ratio of dry cell weight per wet cell volume	kg/m^3
Γ	Performance objective function in MPC	
λ	Molar heat of vaporization	J/kmol
μ	Mean value of a Gaussian distribution	
μ_{max}	Specific rate of cells growth	1/h
ρ	Density	kg/m^3
σ	Standard deviation	
σ^2	Variance	
τ_I	Integral time of PID controller	h
ξ	Random number	

Subscripts

Symbol	Description
C	Condenser
F	Fermentation
i	i-th iteration
l	liquid
L	Liquefaction
max	Maximum
min	Minimum
opt	Optimal
pw	Plantwide
R	Reboiler
ref	Reference
sp	Set point
ss	Steady state
S	Saccharification
v	Vapor

Abbreviations

AC	Composition control
AD	Azeotropic distillation
ADP	Adenosine Diphosphate
ATP	Adenosine Triphosphate
BRS	Blind Random Search
CSTR	Continuous stirred tank reactor
D	Drum in process flowsheet
DDGs	Dried Distillers Grains
D-RTO	Dynamic Real-Time Optimization
E	Explorer molecule in MIPT
ED	Extractive distillation
F	Filter in process flowsheet
FC	Flow control
GA	Genetic Algorithms
GO	Global Optimization
GRAD	Gradient-based optimization method
HE	Heat exchanger in process flowsheet
LC	Level control
LRS	Localized Random Search
MC	Monte Carlo
MINLP	Mixed-Integer Nonlinear Programming
MIPT	Molecular-Inspired Parallel Tempering Algorithm
MPC	Model Predictive Control
NLP	Nonlinear Programming
NMPC	Nonlinear Model Predictive Control
OU	Operating Unit
P	Pump in process flowsheet
PC	Pressure control
PI	Proportional-Integral controller
PID	Proportional-Integral-Derivative controller
PSD	Pressure Swing Distillation
PSO	Particle Swarm Optimization
PT	Parallel Tempering
PWC	Plantwide Control
PWOC	Plantwide Optimizing Control
R	Refiner molecule in MIPT
R	Reactor in process flowsheet

RTO	Real-Time Optimization
SA	Simulated Annealing
SISO	Single Input – Single Output
SQP	Sequential Quadratic Programming
SSF	Simultaneous Saccharification-Fermentation
T	Tower in process flowsheet
V	Vessel in process flowsheet

1. Introduction

In the year 2000, the Intergovernmental Panel on Climate Change presented a scientific study concluding that if the emission of greenhouse gases, mainly CO_2, does not decrease, the global warming effect would dramatically increase the Earth temperature (up to 6°C on average), with devastating consequences for the environment and ecosystems, and consequently for mankind. The report presented in year 2000, clearly stated that the global warming is a real problem faced by the planet, and that the reduction of CO_2 emissions generated by transportation is a challenge for the political, economic and industrial sectors. The German federal government, in the framework of its climate protection program, has adopted policies for motivating the production and consumption of fuels from regenerative sources of energy (**Schmitz, 2003**). A recent report by the Saxon State Ministry of the Environment and Agriculture (**Grunert, 2005**) summarizes the situation of the Bio-ethanol industry in Germany, where it is reported that up to 2005, there were four bio-ethanol production plants already installed and operating with a total production capacity of ca. 600.000 m^3/year, using rye, triticale, corn and wheat as main raw materials. Furthermore, up to the same year, 7 additional plants were under construction with a planned capacity of 100.000 m^3/year each, in order to completely satisfy the internal bio-ethanol demand. As it can be noticed, the Bio-ethanol industry in Germany, and also worldwide, has become a very important sustainable alternative for replacing fuel-oils, in an effort to decrease the effects of fuels on the climate change.

The intention of this work is to offer an alternative for assuring the economical feasibility of the bio-ethanol process industry from a plantwide control and optimization perspectives. In the next Section, the motivating reasons for this work are explained. Then, a general description of the bio-ethanol production process is provided. Finally, at the end of the section, the outline of this work is presented.

1.1. Motivation to Plantwide Control for the Bio-ethanol process

Nowadays, bioprocess industry is an important part of the worldwide economy. Specifically, the bio-ethanol industry has experienced a significant growth in the last years because ethanol, as an environmentally friendly fuel, is considered an attractive alternative energy source. Fuel ethanol is considered today as a bulk product, whose consumption is expected to keep growing fast for the next 20 years, as reported by **Licht (2006)** and **Walter et al. (2008)** (Figure 1.1). Despite the growing market and favorable predictions, ethanol industry is at risk because the process is claimed to be economically infeasible, non-sustainable without governmental subsidies, and non-competitive with fuel oil prices today.

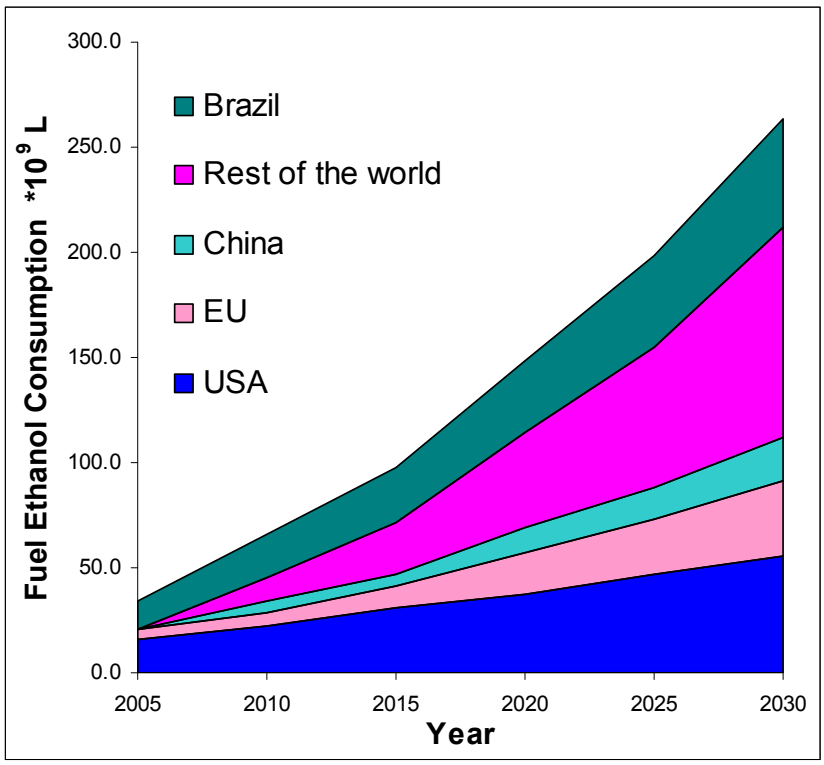

Figure 1.1 Fuel Ethanol consumption 2005-2030 (Source: **Walter et al. 2008**)

In order to assure the economical and environmental feasibility of the bio-ethanol industry, ethanol production has been continuously improved in very different ways. Examples of this progress include the genetic modifications of the microbial strains for building more ethanol-tolerant yeast, strains capable of carrying out simultaneously saccharification and fermentation tasks, and for the development of strains with capability for simultaneously fermenting hexoses and pentoses. Furthermore, the development of different purification

technologies for reducing energy consumption during the separation of the ethanol-water mixture has also been an active area of research, where new technologies such as pervaporation, extractive distillation, pressure swing adsorption using molecular sieves and pressure swing distillation with heat integration appear to be promising alternatives for improving the purification section in the bio-ethanol process. Recently, some efforts have been done from the Process system Engineering point of view, in which the focus has been to obtain an optimal design for the process, by minimizing energy consumption. For example, the work by **Karuppiah et al. (2008)** addressed the optimal design problem of a complete corn-based bio-ethanol plant, by formulating and solving a mixed integer nonlinear programming problem. The work by **Ahmetovic et al. (2010)** uses the results reported by **Karuppiah et al. (2008)**, for both, optimizing energy consumption and synthesizing an optimal process water network in corn-based ethanol plants. In the work by **Alvarado-Morales et al. (2009)**, a methodology is proposed and applied for analyzing and designing a bio-ethanol production process from lignocelullose, considering new alternatives for reducing the waste water generation, and different alternatives for downstream separation. Finally, the works by **Haelssig et al. (2008)** and by **Hoch and Espinosa (2008)** addresses the conceptual design of the purification section for the bio-ethanol process, looking for a significant reduction in energy demand. The mentioned works have shown the potential of the application of computer-aided tools to the bio-ethanol process, resulting in very interesting alternatives for reducing operating costs whereas saving energy and minimizing waste production. However, in addition to an optimal design of the process, it is important also to account for an efficient and appropriate control system for the process which should consider the interactions between the different operating units in the process. Traditionally, the control problem for the bio-ethanol process (and for bioprocesses in general) has been focused in controlling the fermentation section separately from the other process units. This is why, in the literature, it is possible to find many works regarding the modeling, estimation, and control of the isolated fermentation stage, but only few works addressing the control problem considering the process as an integrated dynamic production system consisting of more than one single process unit (i.e. accounting for interactions between the fermentation, cells recycle, and purification units). Some representative works in this direction include those by **Meleiro et al. (2009)** and **Costa et al. (2002)**, in which the model presented for controlling purposes includes more than one process equipment (i.e. fermentation, cells recycle and a flash vessel). However, in spite of accounting for the interaction between different process units, these works are still focused on the control of some state variables only in the fermentor, and lack of a suitable plantwide control formulation.

In the present work, the Plantwide Control (PWC) problem for the complete bio-ethanol process is addressed as an optimizing control problem based on Dynamic Real-Time Optimization (D-RTO), due to the following facts: the process is highly nonlinear and characterized by the coupling of slow and fast dynamics; there exist interactions between different operating units which cannot be neglected, also the quality and availability of the raw material change often, introducing disturbances into the process; and finally, the economical feasibility of the process can be effectively assured only if this is the main control objective of the plantwide strategy. Of course, an optimal process design should be the base for an efficient and economically feasible process, but this is not enough, because, despite optimal operation may be expected at the optimal operating point for the designed process, a real process is always affected by disturbances and uncertainties, which in many cases upset the process, driving the optimum to a very different operating point and thus resulting in significant economic losses.

It is important to notice that for solving the dynamic real time optimization problem that arises in the Plantwide optimizing control framework, it is desirable to use global optimization algorithms for solving the problem in order to avoid reaching a lower profit performance at a local optimum. As noted by **Lacks (2003)**, in large chemical processes the profit can be a nonlinear function of the operating conditions variables, and there may be local maxima, local minima and saddle points on the profit function space. Therefore, since the optimal operation of the process occurs at the conditions corresponding to the global maximum profit, it is important to search for the global optimum of the profit function by using global rather than local optimization algorithms. Although this last statement may seem obvious, usually real-time applications are solved using local optimization algorithms because of the larger computational requirements of global optimization procedures and the need to solve fast the real-time optimization problem. Trying to overcome these drawbacks, a new global optimization algorithm is proposed in Chapter 3, which has an excellent performance both in terms of finding the global optimum and requiring a reasonable computational demand.

Before concluding this section, it is important to clarify that the scope of Global Optimization (GO) is to find the absolutely best set of admissible conditions to achieve an objective under given constraints (**Neumaier, 2004**). In this work, such "admissible conditions" is the set of plantwide manipulated variables that lead the process to maximum profitability. Figure 1.2 shows an example of an optimization (maximization) problem consisting on a multimodal

objective function in two dimensions where the use of global optimization techniques is required in order to find the global maximum.

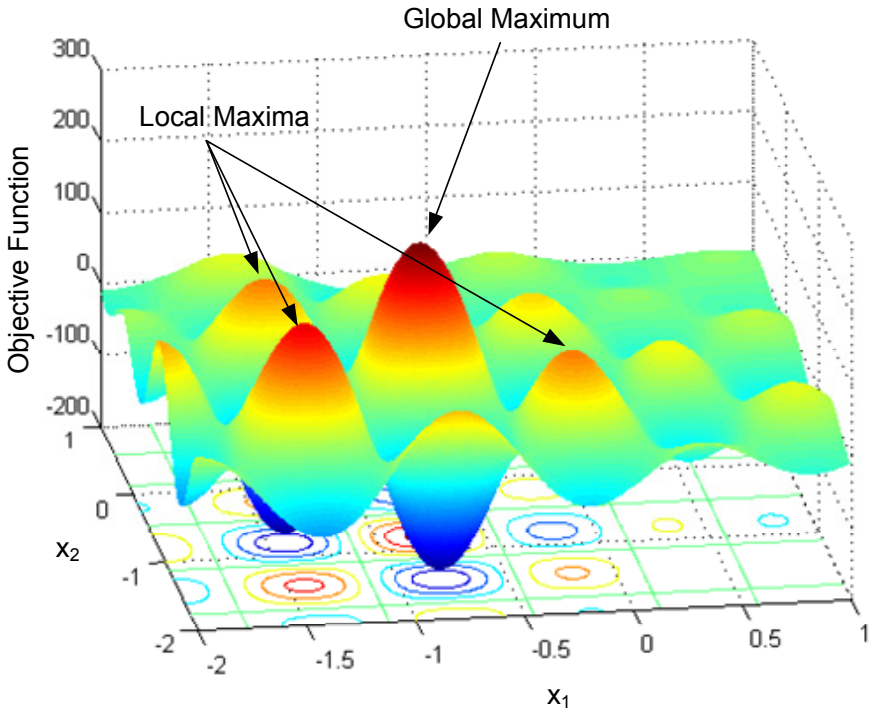

Figure 1.2 Global maximum and local maxima for the two-dimensional Shubert function. Only some of the local maxima are indicated by arrows. The Shubert function is described in Appendix B.1.

In general, deterministic or stochastic approaches can be used for solving GO problems. In this thesis, stochastic methods are investigated and compared with a new method proposed and developed in this work, which is denoted as the Molecular-Inspired Parallel Tempering Algorithm (MIPT) and is presented in Chapter 3.

1.2. Generalities of the Bio-ethanol process

Fuel-ethanol can be obtained from different raw materials (substrates), mainly from starchy materials, sugar crops and lignocellulosic materials. In general, the production process involves the stages shown in Figure 1.3. First, the polymeric substrates are broken down into monosaccharides through physical, chemical or enzymatic techniques, as appropriate. Then, the conversion of the sugars to alcohol by microbial fermentation (generally by yeasts) is carried out. Finally, the alcohol is recovered by distillation and it is purified in subsequent steps, to obtain fuel-grade ethanol (>99.8% wt).

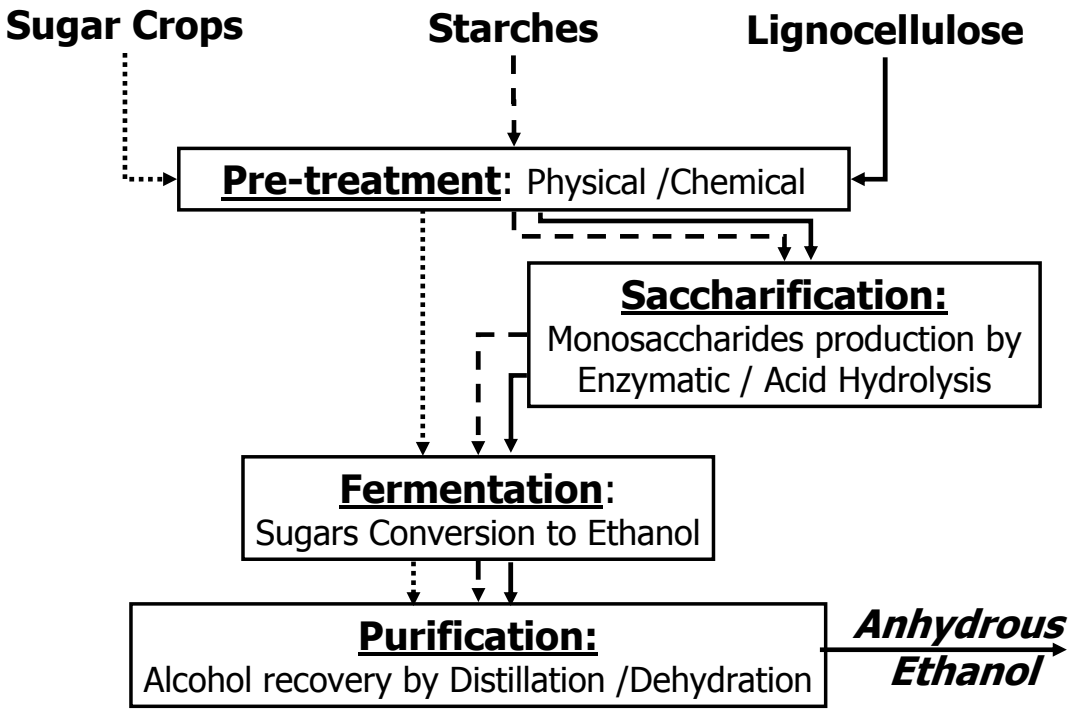

Figure 1.3 Main stages in fuel-ethanol production from different raw materials: Sugar crops (dotted line), Starches (dashed line) and Lignocellulose (solid line)

As it is mentioned by **Roehr (2001)** the selection of an appropriate substrate depends on a number of factors and one of the most important is the geographical climate of the intended production site. Thus, while starchy materials like corn, wheat, rice and potatoes are the most common substrates in Europe and North America; sugar cane, molasses, and cassava appear to provide the most promising supply of ethanol for tropical countries like Brazil. If well, lignocellulosic biomass is claimed to be a more convenient raw material for ethanol production (no competition between food and fuel production, low price, etc.), currently only few pilot plants worldwide produce ethanol from this raw material, mainly because saccharification is more difficult to carry out than in the case of starches, due to the presence of lignin which protects cellulose and hemicellulose against enzymatic action (thus increasing the pre-treatment costs); and because fermentation is also more complicated, as the substrate available for ethanol production consists on a mixture of pentoses and hexoses usually requiring the use of a genetically modified yeast strain.

In Germany, the most promising raw materials for ethanol production are cereals like wheat, rye, barley and triticale (**Jacobi and Hartman, 2005**). Figure 1.4 shows a general block diagram of the ethanol production process from starchy materials. The raw material is first milled (in the milling section) to the desired grain size in order to allow enzymatic attack for

breaking down the polysaccharide (starch) into monosaccharides (mainly glucose). Such enzymatic process is done in the hydrolysis stage (involving gelatinization, liquefaction and saccharification). After hydrolysis, the glucose fermentation to ethanol is carried out where a fermentation broth containing ethanol, water, some glucose and non-fermentable material is obtained, but also some CO_2 is produced. For obtaining fuel-ethanol, the fermentation broth is then sent to the purification section (distillation, rectification and dehydration). The CO_2 is sent to a scrubber whereas the stillage (a high valuable protein content by-product obtained at the distillation bottoms) is sent to the Dried Distillers Grains section where it is dried and treated for being sold as animal feed. A more detailed description, including the modelling of each stage in the process is given in Chapter 4 where the particular case study addressed in this work, namely the Bio-ethanol continuous process from starchy raw materials, is presented.

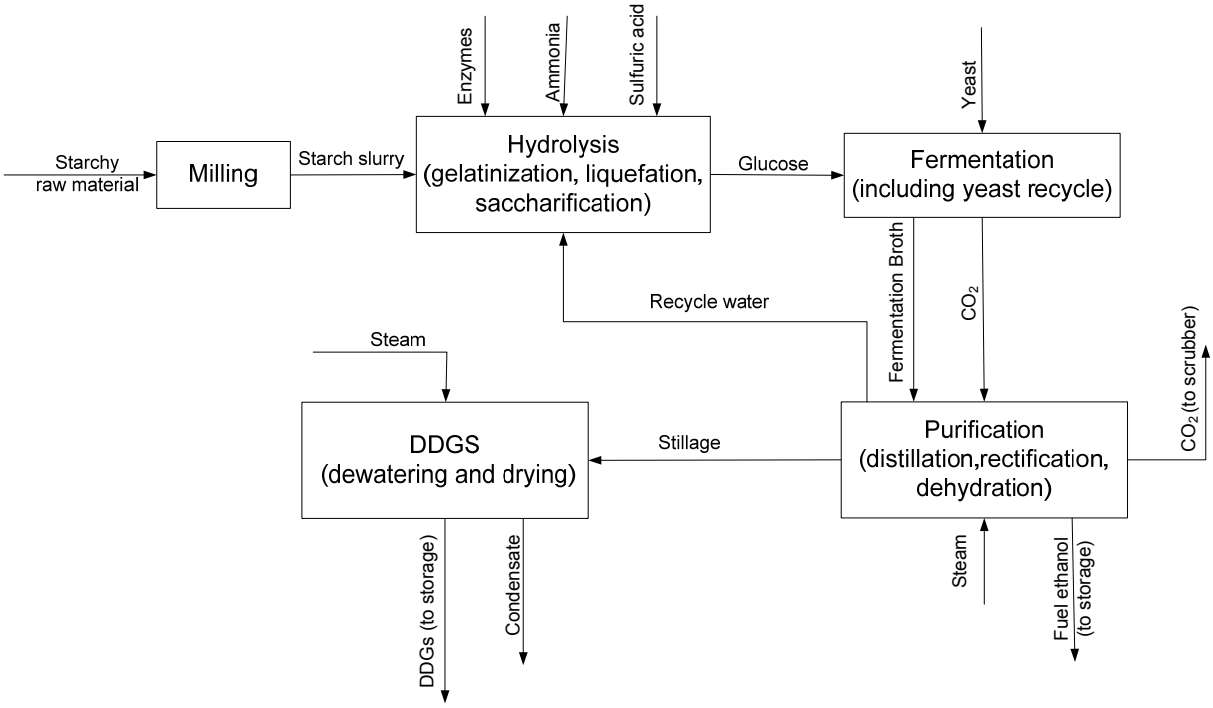

Figure 1.4 General block diagram for the ethanol production process from starch

1.3. Thesis Outline

The main purpose of this work is to present a novel approach for the Plantwide Control of bio-ethanol production, in which the main control objective is to maximize the profitability of the whole process. The core of the Plantwide Control approach proposed in this thesis is the formulation of a Dynamic Real time optimization (D-RTO) problem for the complete process.

As solving such a problem requires much computational effort and time, this work proposes two new approaches for dealing with the problem in real time. First, an approach for shrinking the search region of the optimization problem is proposed, which is based on the effect of the disturbances (both, known and unknown) in the profitability of the process. Second, a stochastic global optimization method is proposed for solving the D-RTO problem, which is used in a sequential formulation for finding the global optima values for the manipulated variables that lead to maximum profitability in a reasonable computation time. With this novel approach it is possible to solve the complex problem of controlling a complete (highly interconnected) plant, such as the bio-ethanol production process (which considers three recycle loops) and similar applications in the chemical and biochemical industry.

The thesis is organized as follows. Chapter 2 presents a review of the theoretical background in the plantwide control architectures that have been investigated in chemical processes applications during the last 20 years, including the decentralized, distributed, multilayer, and single-layer architectures. Furthermore, the background of the stochastic methods used in this work is also presented, namely, the localized random search algorithm, simulated annealing, particle swarm and genetic algorithms. The new global optimization method denoted as Molecular-Inspired Parallel tempering Algorithm is formulated in Chapter 3, where the performance of the method is tested in 6 challenging optimization problems and compared to the performance of other well-established optimization methods. As it is shown, the MIPT has an excellent performance in solving global optimization problems of different nature, showing to be a very promising algorithm for bioprocesses applications. The specific case study for plantwide optimizing control addressed in this work, that is, the bio-ethanol production from starchy raw materials is described in detail in Chapter 4, where the model developed for the entire process is presented. In Chapter 5, the Plantwide Optimizing Control (PWOC) methodology is presented. The proposed approach for PWOC is developed and explained in detail. In Section 5.2 the shrinking approach for reducing the search space of the D-RTO problem is introduced. Chapter 6 shows the application of the Plantwide Optimizing Control (PWOC) framework (using the Multi-layer and Single-layer architectures, denoted here as PWOC-two-layer and PWOC-one-layer, respectively) proposed in Chapter 5, where the shrinking approach as well as the MIPT algorithm is used in the solution strategy of the D-RTO problem that arises. The performance of the proposed PWOC approach (including the shrinking) is evaluated in three different scenarios. First, a known disturbance in the feed concentration (starch composition) is applied to the process. Second, a model mismatch is introduced on the kinetics parameters in the fermentation section of the

process. And third, a scenario that considers raw material price change is evaluated. The performance of PWOC facing these challenges is compared to the performance when a decentralized Plantwide architecture (i.e. multiple single PID loops) is used, which is a typical configuration in industry. Finally, conclusions and recommendations for future work are outlined in Chapter 7.

It is important to notice that the problem of controlling a complete process involves many different interconnected tasks, as it is represented in Figure 1.5, all of which are very important in real applications. In this work, the focus has been on the process control and optimization tasks, which require the development of a reliable process model. In addition, complete observability of the process based on reliable measures taken by accurate physical sensors has been assumed, and therefore, the data reconciliation and soft-sensing issues were not addressed. Furthermore, parameter identification was done off-line in order to reduce computational effort.

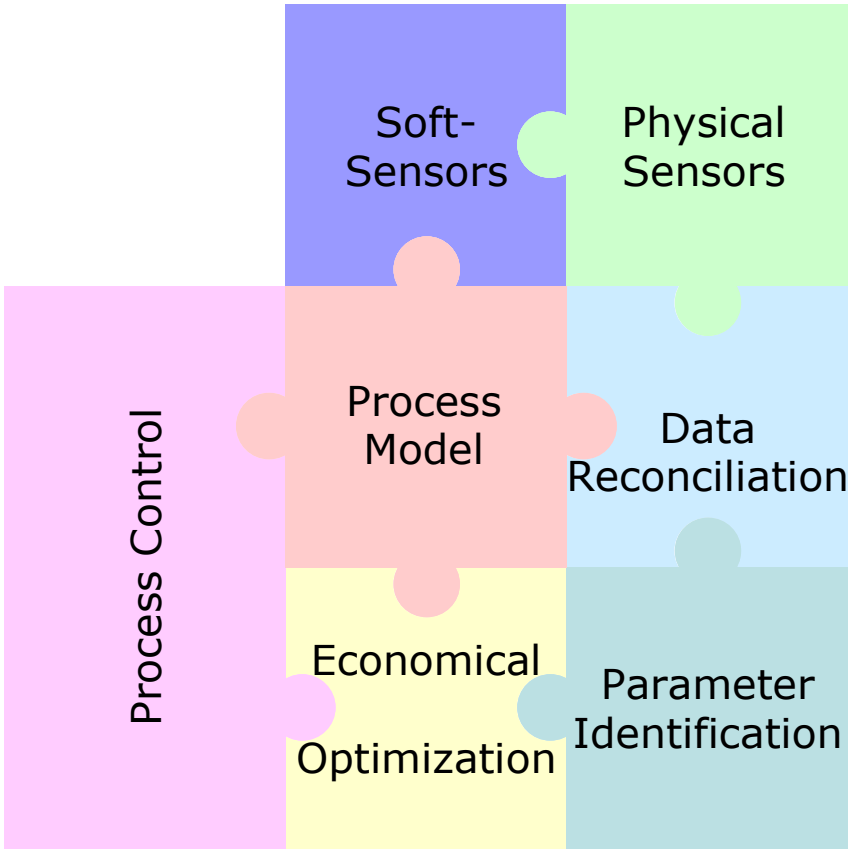

Figure 1.5 Interconnected tasks and tools for Plantwide Control

2. Theoretical Background

This research focuses on two main topics. The first is related to the control of a complete process plant (plantwide control), while the second is concerned on the use of stochastic global optimization as a tool for plantwide control. The purpose of this chapter is to summarize the theoretical background in these two topics.

2.1. Plantwide Control Architectures (PWC)

Since the pioneer work by **Buckley (1964)**, Plantwide Control (PWC) has attracted the attention of the process control community for more than 40 years. Through these years, different architectures have been used for tackling the problem of controlling a complete process. The intention of this section is to present a brief review of the several options reported for addressing PWC. One possible classification of the different PWC architectures is shown in Figure 2.1. In this classification, which agrees in some points with that presented by **Scattolini (2009)**, PWC approaches are presented in four main groups, characterized by the complexity of the model considered into the control system for describing the dynamics of the process and by the degree of communication between controllers of different operating units or between different layers of the control system hierarchy. These four main architectures considered are: Decentralized, Distributed, Multi-layer and Single-layer. Considering the complexity of the model, in the decentralized approach the need for a model of the process is avoided (with exception of decentralized MPC, which of course do need a process model). In the Distributed architecture, the usual case is to use linear dynamic models. The Multi-layer case usually makes use of a nonlinear steady state model in the optimization layer and a linear dynamic model in the controller layer as it will be explained in Section 2.1.3. Finally, since the operation of the control system in the Single-layer case relies on a centralized controller, it is desirable to consider a first-principles nonlinear dynamic model of the process in order to predict the process behavior as close as possible to reality.

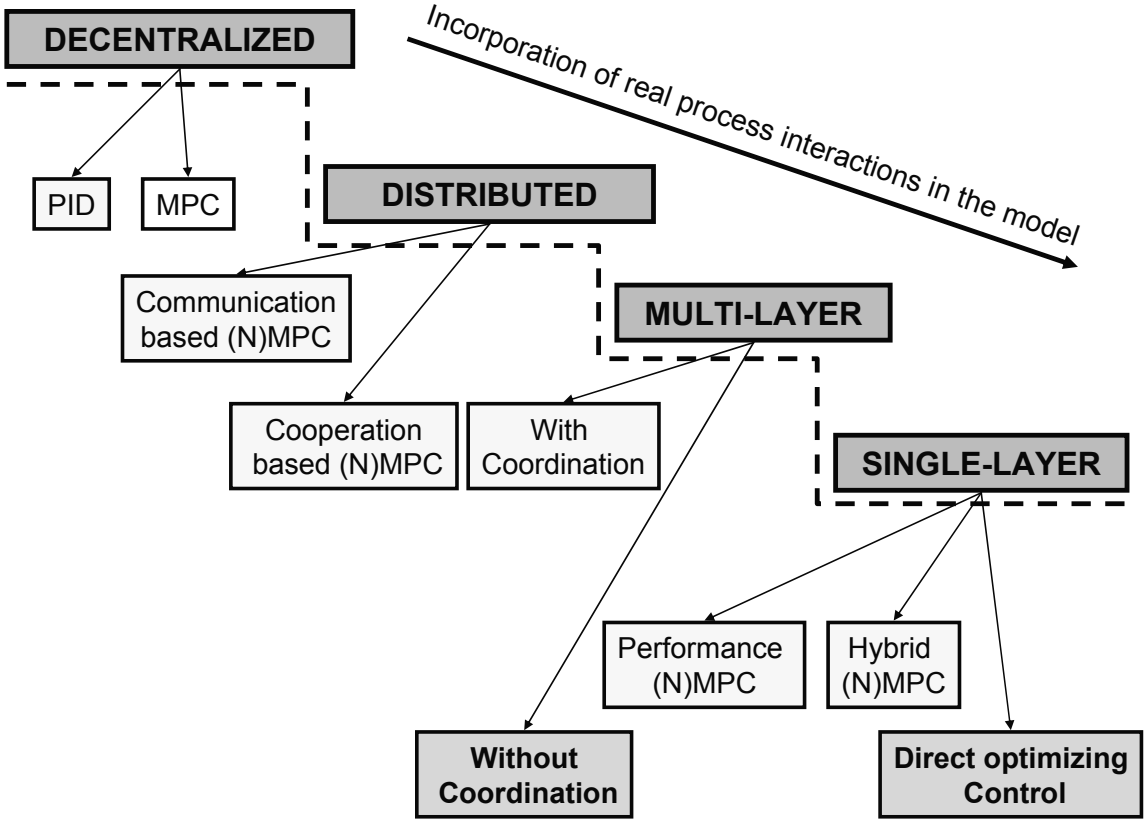

Figure 2.1 Classification of Plantwide Control architectures **(Ochoa et al. 2010a)**

In the following, the description of the architectures considered in Figure 2.1 is given, in which the main features as well as remarkable contributions specially dedicated to chemical process applications are emphasized.

For all architectures, let us assume a process (chemical or biochemical plant) composed of N different operating units (OU_1, OU_2, …,OU_n, …, OU_N), in which the vector of output variables to be regulated in OU_n is denoted as $Y_n=[y_{1n}, y_{2n}, ..., y_{in}, ..., y_{In}]$, where I is the number of controlled variables in each operating unit. Furthermore, the vector of manipulated variables in OU_n is written as $U_n=[u_{1n}, u_{2n}, ..., u_{jn}, ..., u_{Jn}]$, where J is the number of manipulated variables in each operating unit. Finally, the state vector $X_n=[x_{1n}, x_{2n}, ..., x_{kn}, ..., x_{Kn}]$ of operating unit OU_n is conformed by the K state variables in that operating unit.

2.1.1. Decentralized Architecture

The Decentralized architecture (Figure 2.2) consists usually of SISO PID loops in which different individual controllers ($C_{11,n}$, …, $C_{ij,n}$, …, $C_{IJ,n}$) are used in each operating unit OU_n for regulating each output variable y_{in} by manipulating u_{jn}. The main feature of this architecture is that the control system is actually composed of several individual controllers which do not

share any kind of information between them independently of whether or not the selection of the manipulated and controlled variables takes into account the interactions in the process, i.e. each controller operates independently of the others without receiving/sending information from/to any controller, acting as an "isolated entity". As noted by **Stephanopoulous and Ng (2000)**, most of the research activities in the topic of PWC up to the year 2000 addressed the PWC problem as the selection of the best input-output pairing for the implementation of SISO PID loops. However, the work by **Garcia and Morari (1984)** is a notable exception, in which a multivariable control scheme based on a multi-layer PWC architecture was proposed for controlling a benzene plant. As the decentralized approach is the simplest of the PWC structures (relying on PID controllers or linear dynamic models for the MPCs), it is still predominant in industry. The work by **Larsson and Skogestad (2000)** presents an excellent review in this topic and a mathematically-oriented design procedure based on the self-optimizing control concept (**Skogestad, 2000**). Recent works following these guidelines can be seen in **Araujo (2007)**, **Araujo et al. (2007a, 2007b, 2008)**, **Baldea et al. (2008)** and **Larsson et al. (2003)**. Other works in decentralized PWC architecture make use of an oriented process approach, in which mainly heuristics and simulation analysis are used. The books by **Luyben et al. (1998)** and **Luyben (2002)** present a popular heuristic procedure for developing decentralized PWC schemes. Other relevant works applying heuristics coupled with simulation for decentralized PWC include **Konda et al. (2005, 2006)**, **Lausch et al. (1998)**, **McAvoy and Ye (1993)**, **Price et al. (1994)** and **Vasudevan et al. (2009)**.

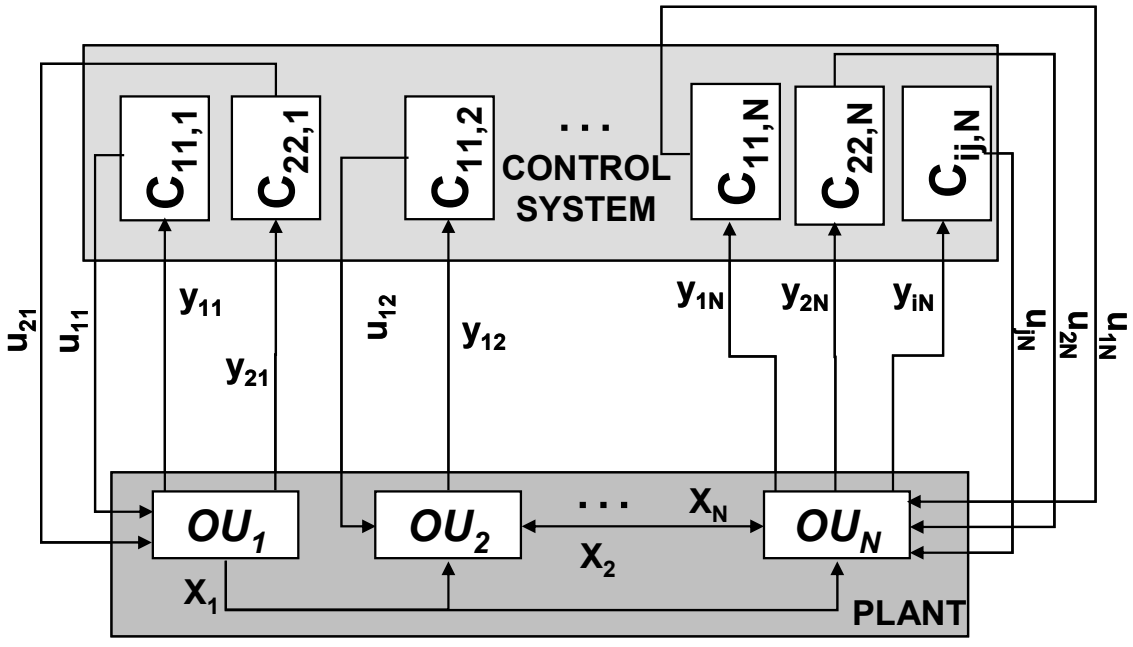

Figure 2.2 Decentralized architecture for Plantwide Control **(Ochoa et al., 2009a)**

2.1.2. Distributed Architecture

Most of the works in the remaining three architectures shown in Figure 2.1 make use of a multivariable controller. Two main reasons motivated the shift of the PWC problem from the paradigm of decentralized PID towards different alternatives **(Venkat et al., 2007)**:

1. The performance limitations of the decentralized architecture
2. The broad industrial impact of the Model Predictive Control (MPC) framework

In the Distributed architecture (Figure 2.3) each operating unit uses at least one MPC controller (MPC_n), which is in charge of controlling the outputs vector Y_n by manipulating the inputs U_n of the specific operating unit. The main feature in this architecture is that the multiple MPC controllers do exchange some information between them. Two basic Distributed-MPC approaches are the communication-based and the cooperation-based, which mainly differ that in the former, each controller has a local objective function whereas in the latter the objective function in each controller is a copy of the total objective function for the complete plant **(Rawlings and Stewart, 2008)**. Recent representative works addressing the PWC from the Distributed perspective are those by **Mercangöz and Doyle (2007)**, **Sun and El-Farra (2008)** and **Venkat et al. (2006, 2007)**.

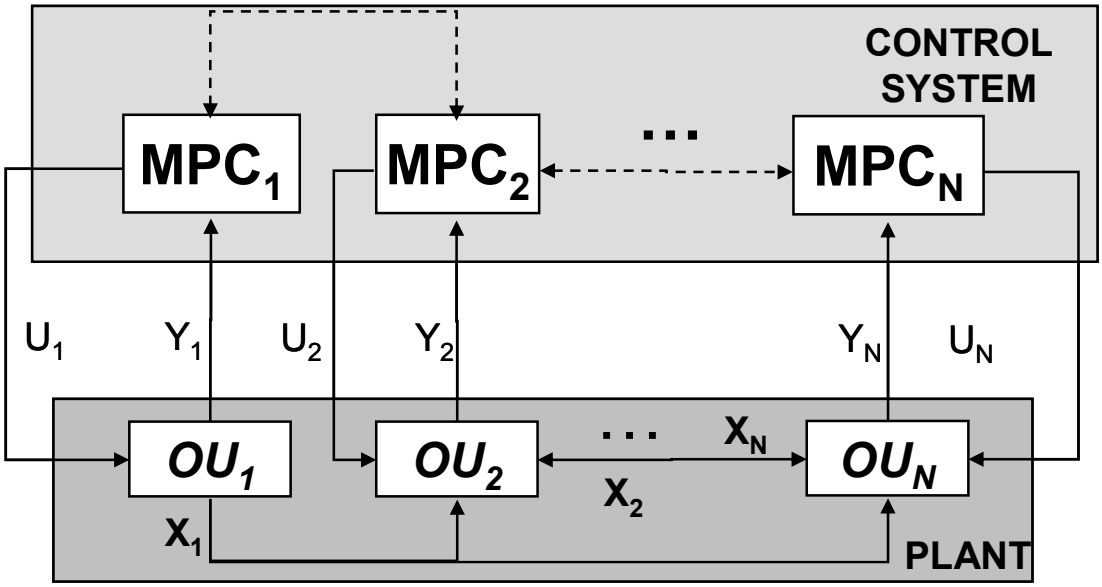

Figure 2.3 Distributed architecture for Plantwide Control **(Ochoa et al., 2009a)**

2.1.3. Multilayer Architecture

The Multi-layer architecture is a hierarchical structure that follows the guidelines given by **Findeisen et al. (1980)**, who classified the hierarchical control into multi-layer and multi-level. According to Findeisen's work, in the multi-layer case the control of a system is split into algorithms (layers), whereas in the multi-level case control it is divided into local goals and the action of each local control unit is coordinated by an additional superior unit. In Figure 2.1 it is proposed to sub-divide the Multi-layer (or hierarchical) architecture into: Multi-layer with Coordination (Figure 2.4) -denoted as Multi-level approach by Findeisen- and Multi-layer without Coordination (Figure 2.5). Both Multi-layer architectures are composed by at least two different layers, i.e. an optimization and a control layer. The optimization layer consists on a Real-Time Optimization (RTO) problem in which the main task is to compute optimal set point values ($Y_{sp,opt}$) for the set of controlled variables (Y_n) that minimizes an economic-type objective function. On the other hand, the control layer (MPC) is in charge of tracking those optimal set point values that come from the RTO-layer, minimizing a performance-type objective function. It is important to notice that the "connection" between RTO and MPC layers may suffer inconsistencies due to model mismatch (non-linear steady state vs. linear dynamic) and conflicting objectives **(Biegler and Zavala, 2009)**. Therefore, in the last years a proposal for replacing the steady state RTO by a Dynamic Real Time Optimization (D-RTO) layer has emerged (**Kadam et al., 2002, 2003**; **Kadam and Marquardt, 2004**).

2.1.3.1 Multilayer with Coordination Architecture

In this type of Multilayer architecture, a coordination layer is usually included between the RTO and the MPC layers. This coordinator usually manages information coming from both layers, and it is in charge of finding for each MPC_n a locally feasible set point ($Y_{n,sp}$) close to the global solution found by the RTO layer ($Y_{sp,opt}$). Then, each MPC_n is responsible of tracking the local set points ($Y_{n,sp}$) by calculating the vector of manipulated variables U_n for each operating unit. Further details can be found in the work by **Ying and Joseph (1999)** where the coordinator is stated as a linear or quadratic programming problem; in the works by **Lu (2003)** and **Tosukhowong et al. (2004)** in which a least-squares coordination collar is used; and in the work by **Cheng et al. (2007)**, where a price-driven method for coordination between the RTO and the MPC layers is applied. A final mention should be done regarding the difference between the Multi-layer with coordination and Distributed architectures. As both schemes include a kind of coordination, in the Distributed case the

coordination consists on exchanging some information between the local MPCs, whereas in the Multi-layer with coordination, the local MPCs are not directly communicated between them but communicated through the RTO layer (Figure 2.4).

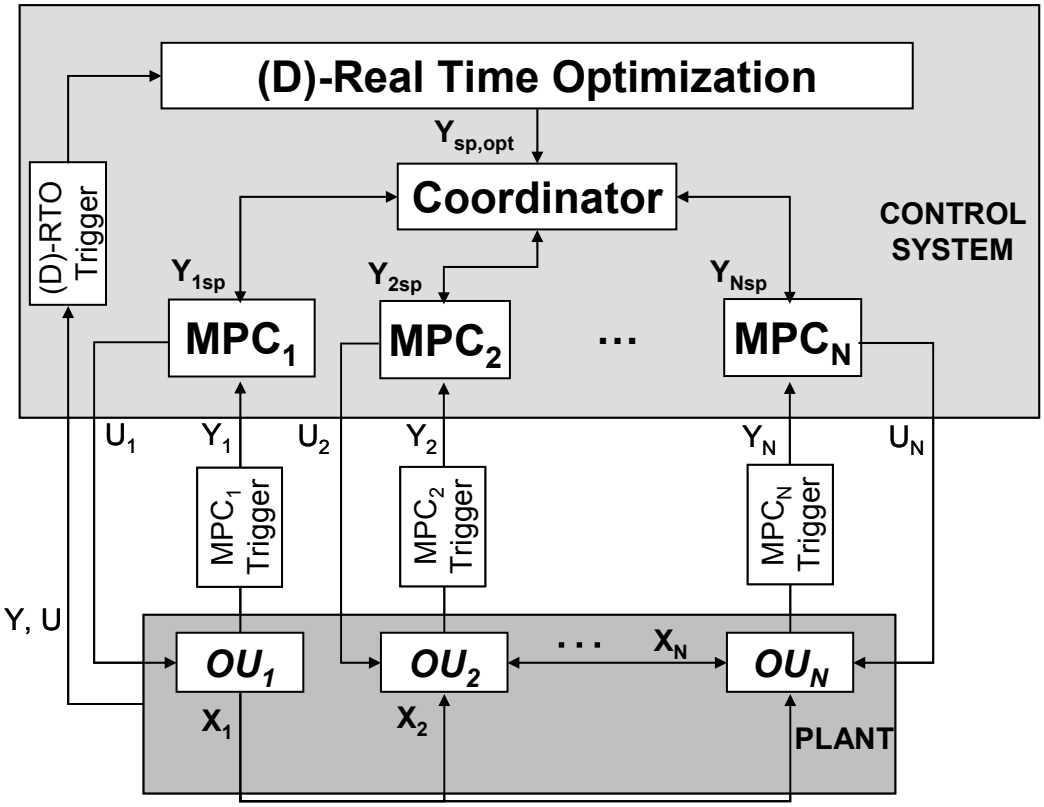

Figure 2.4 Multilayer architecture with Coordination for Plantwide Control **(Ochoa et al., 2009a)**

2.1.3.2 Multilayer without Coordination Architecture

When no coordination is used between the optimization and control layers, the RTO is usually replaced by a D-RTO layer, in order to account for the dynamic nonlinear behavior of the process. The D-RTO layer is in charge of calculating the optimal set point values ($Y_{sp,opt}$) for the process outputs, which are sent directly to the control layer (i.e. NMPC). Then, the control layer calculates the set U of vectors of manipulated variables for being applied in the process, where $U=\{U_1,U_2,\ldots,U_N\}$. **Kadam et al. (2002, 2003)**, **Kadam and Marquardt (2004)** and **Ochoa et al. (2009b)** present examples of PWC using the Multi-layer without Coordination architecture. Finally, the trigger blocks shown in Figure 2.4 and Figure 2.5 are acting as switches for recalling the optimization and control layers, when a certain condition is met. Some typical trigger conditions are presented in Section 5.1.5.

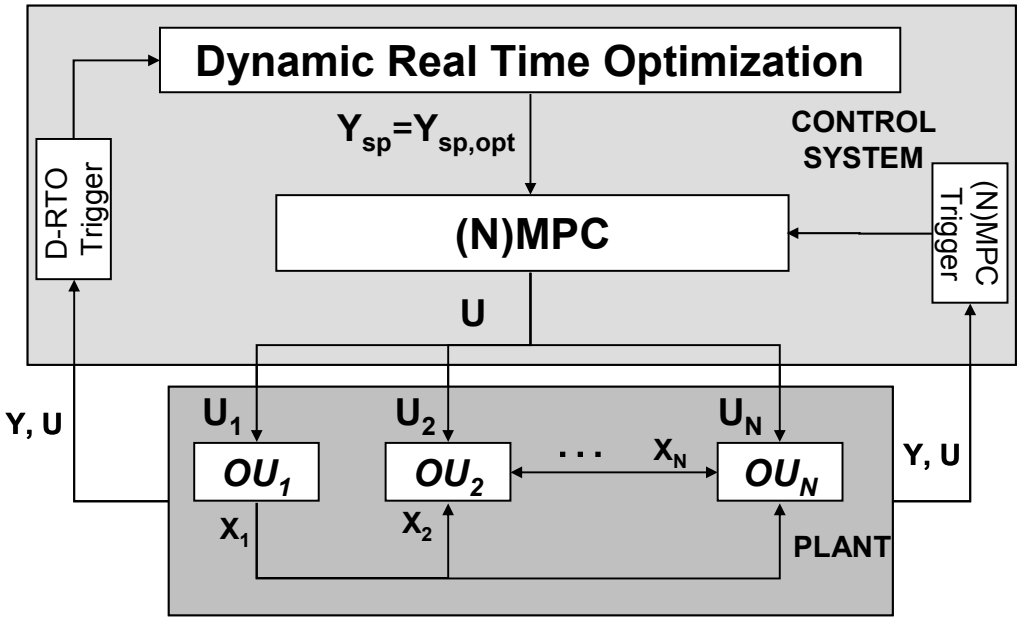

Figure 2.5 Multilayer architecture without Coordination for Plantwide Control **(Ochoa et al., 2009a)**

A final mention should be done regarding the use of a NMPC controller layer instead of a linear MPC in the Multilayer architectures. The use of a nonlinear first principles model of the process is highly desirable in order to have a better predictive capacity of the performance of the process. However, in order to avoid the complexity of developing such a nonlinear model (which also commonly reduces the computational effort for solving the model), most of the works reported in the Multilayer with coordination architecture used a linear MPC. In contrast, works in the Multilayer without coordination architecture used more commonly a Nonlinear MPC.

2.1.4. Single-Layer Architecture

The last PWC architecture in the classification is the Single-layer scheme (Figure 2.6). The single-layer is a centralized structure that has been usually perceived and claimed as intractable for PWC (**Venkat et al., 2007**). In the last years, however, some publications from both industry and academia have shown that such approach is not only possible to implement but also that it provides very good results from an economic point of view (**Bartusiak, 2007**; **Franke and Doppelhamer, 2007**; **Zavala et al., 2007**). Works using this architecture solve online a moving-horizon optimization problem, in which the set of manipulated variables (*U*) corresponds to the set of decision variables that minimizes (or maximizes) a given objective function. Reported works differ in the type of objective function optimized. A first group of works denoted as Performance (N)MPC uses a performance-type

objective function ($J_{(N)MPC}$) in which the tracking of reference values for the controlled and manipulated variables (Y_{ref}, U_{ref}) is penalized as expressed in Equation (2.1).

$$\min_U J_{(N)MPC} = \min_U \left(\int_{t_1}^{t_p} (Y - Y_{ref})^T Q (Y - Y_{ref}) + (U - U_{ref})^T R (U - U_{ref}) + \Delta U^T P \Delta U \; dt \right) \tag{2.1}$$

where Q, R and P are weighting matrices that can be seen as tuning parameters for the (N)MPC.

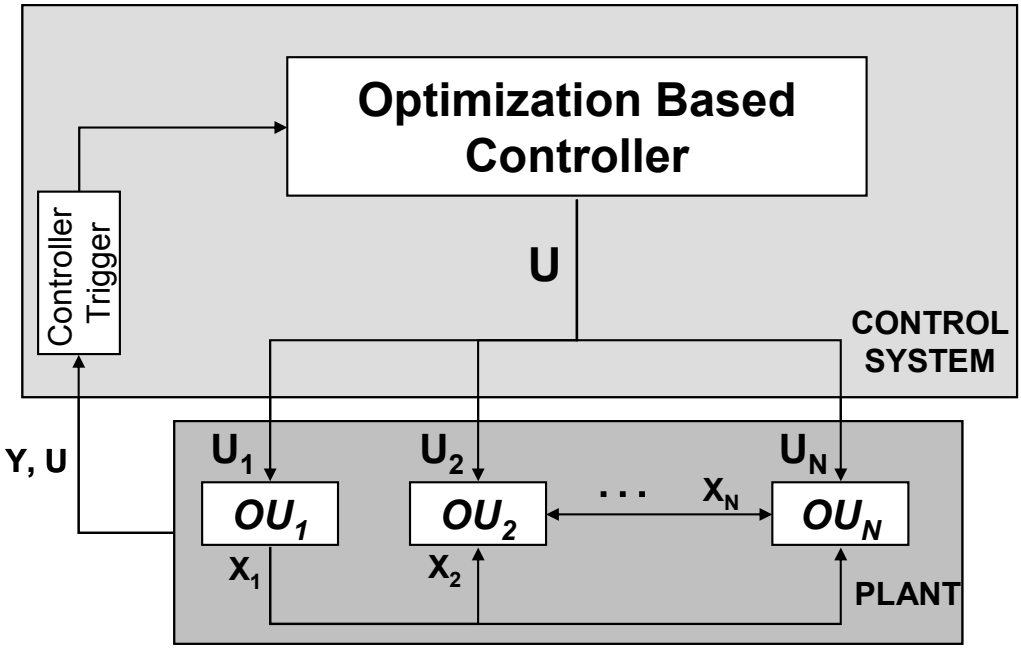

Figure 2.6 Single-layer architecture for Plantwide Control **(Ochoa et al., 2009a)**

A second group of works in the single-layer architecture includes, besides the performance term, an economic penalization term in the formulation of the objective function. It is therefore denoted here as Hybrid (N)MPC and is described by Equation (2.2); where n_y, n_u and n_d are the number of outputs, manipulated variables and measured disturbances respectively, considered relevant for the objective function.

$$\min_U J_{Hybrid} = \min_U \left(J_{(N)MPC} + \left(\sum_{i=1}^{n_y} \int_{t_1}^{t_p} w_{yi} y_i dt + \sum_{m=1}^{n_u} \int_{t_1}^{t_p} w_{um} u_m dt + \sum_{j=1}^{n_d} \int_{t_1}^{t_p} w_{dj} d_j dt \right) \right) \tag{2.2}$$

where w_{yi}, w_{um} and w_{dj} are cost-weighting factors.

The last scheme denoted in the literature as Direct Optimizing Control (Engell, 2007) uses a pure economic objective function (Equation 2.3) in which the usual control specifications enter as constraints and not as set points, and therefore no tracking term is penalized.

$$\min_{U} J_{Econ} = \min_{U} \left(\sum_{i=1}^{n_y} \int_{t_1}^{t_p} w_{yi} y_i dt + \sum_{m=1}^{n_u} \int_{t_1}^{t_p} w_{um} u_m dt + \sum_{j=1}^{n_d} \int_{t_1}^{t_p} w_{dj} d_j dt \right) \tag{2.3}$$

It is important to notice that the Performance (N)MPC (Equation 2.1) as well as the Hybrid (N)MPC (Equation 2.2) differ from the Direct Optimizing Control (Equation 2.3) in that the latter does not consider the use of a Model Predictive Controller (neither linear nor nonlinear) because its objective is a pure economic function and it relies completely in the solution of a dynamic real time optimization problem (D-RTO). Additionally, it is important to mention that in the Performance N(MPC) as well as in the Hybrid case, the use of a nonlinear model of the process would be highly desirable in order to have better model predictions. However the decision about which kind of model to use should be done looking for a good balance between predictive capability and costs (i.e. of developing a complete nonlinear model for the whole process which also complicates the solution strategy resulting in higher computational costs).

Some examples of the application of the Single-layer architecture can be found in **Bartusiak (2007)**, **Biegler and Zavala (2009)**, **Engell (2007)**, **Franke and Doppelhamer (2007)**, **Franke and Vogelbacher (2006)**, **Jockenhövel et al. (2003)**, **Manenti and Rovaglio (2007)**, **Ochoa et al. (2009b)**, **Roman et al. (2006)**, **Toumi and Engell (2004)**, **Zavala et al. (2007)** and the works by **Trvzskâ de Gouvêa and Odloak (1998)** and **Zanin et al. (2000, 2002)**. Most of the reported applications using the Single-layer architecture formulate the optimization-based controller as a D-RTO problem, similar to that included in the Multilayer without coordination architecture. Solving such D-RTO problem is a challenging task that usually is carried out using direct optimization formulations, which can be classified into (**Jockenhövel et al., 2003**): sequential, simultaneous or hybrid approaches (i.e. Multiple shooting). **Srinivasan et al. (2003)** provide a detailed explanation of the mentioned methods. The main features, advantages and disadvantages of the sequential, simultaneous and multiple shooting are summarized in Table 2.1, which have been previously reported by **Jockenhövel et al. (2003)**, **Michalik et al. (2009)**, **Srinivasan et al. (2003)** and **Zavala (2008)**.

Table 2.1 Comparison of direct optimization formulations for solving dynamic optimization problems

Type of Formulation	Sequential (Single shooting)	Simultaneous	Hybrid (Multiple shooting)
Main Features	- Only the input variables are discretized (e.g. using piecewise-constant parameterization over equally spaced time intervals). - The DAE system is solved using standard integration algorithms.	- Requires discretization for both, the inputs and state variables (e.g. using orthogonal collocation). - The discretized DAE model is incorporated as an algebraic constraint in the NLP formulation.	- Requires discretization for both, the inputs and state variables. - The time interval $[0, t_f]$ is divided into n stages. Except for the first stage, the initial conditions of the various stages are considered as decision variables along with continuity constraints stating that the initial states of every stage should match the final ones of the preceding stage, and therefore the size of the problem is increased.
Advantages	- Feasible path approach (i.e. the differential equations are satisfied at each step of the optimization). - High accuracy of the solution. - Easier implementation. - Very suitable for problems with a large number of states.	- Fast Solution - Successfully deals with instabilities of the dynamic model. - Very suitable for problems with a large number of states and degrees of freedom.	- High accuracy of solution. - Parallel computation is possible. - Very suitable for problems with long horizons. - Deals successfully with instabilities of the dynamic model.
Disadvantages	- Requires repeated and expensive solution of the differential equations leading to a slow solution for problems with long time horizons. - Unstable systems are difficult to converge. - Can converge to several local minima due to the usually high nonlinearity of the resulting NLP.	- Infeasible path approach (the differential equations are satisfied only at the optimal solution), therefore results from not converged optimization could be non usable. - In stiff systems, a very fine grid should be used, which increases the size of the problem. - As full discretization usually leads to large-scale NLPs with sparse constraint Jacobian and sparse Hessian, special optimization strategies might be needed.	- Infeasible path method. - Due to the introduction of the additional degrees of freedom the size of the NLP is enlarged. - In systems with a large number of states, the computational load increases highly (e.g. the gradients with respect to the states form large dense blocks inside the NLP solver)

On the other hand, regarding specifically the control issue for the bio-ethanol process it is noticed that despite the rapid growth of the bio-ethanol industry in the last 30 years and the high economic risk that this industry faces (especially in Europe, where the process is claimed to be neither sustainable nor competitive against the oil prices), not much effort has been done in order to improve the efficiency of the process from the optimization and control points of view. Several works have been published regarding mainly the modeling and control of the fermentation unit in the process (including the development of soft sensors for key fermentation variables), but only few works have addressed the control of the process considering more than the fermentation stage. **Costa et al. (2001)** used Dynamic Matrix Control for controlling the substrate or the product concentrations in the fermentor, manipulating the substrate input flow or the cells recycle rate. In a second contribution, **Costa et al. (2002)** proposes a SISO NMPC for controlling the substrate concentration in the fermentor manipulating the substrate input flow. In addition, **Meleiro et al. (2009)** presented a multivariate NMPC to control simultaneously the ethanol, substrate and biomass concentrations in the fermentor. Although the process modeled in these works considers interactions fermentor-cells recycle-flash, the control task is still focused on tracking or regulating the main state variables in the fermentor without considering the optimal economic operation of the whole process. Additionally, the recent work by **Andrade and Lima (2009)** addressed the PWC problem of the purification section (distillation and stripping but without including the fermentation section) of an ethanol production plant, following the guidelines given by **McAvoy and Ye (1993)** and **Price et al. (1994)** for designing decentralized SISO PWC architectures. Besides, **Bartee et al. (2008)** proposed using MPC for controlling the process including milling, cooking, distillation etc.; however, no details about the algorithms or implementation are given. Finally, regarding the optimization point of view, some recent works have been focused on the steady state analysis and optimization for designing the purification section (**Dias et al., 2009a**; **Hoch and Espinosa, 2008**) or a complete bioethanol plant (**Karuppiah et al., 2008**).

Table 2.2 Advantages and disadvantages of the different Plantwide Control schemes

PWC Architecture	Advantages	Disadvantages
Decentralized	- Easy implementation (i.e. does not require the development of a process model). - Stability issues have been theoretically proven. - No extra computational costs.	- Poor disturbance rejection due to that it does not consider the dynamic performance of the process. - Neglects process interactions, and therefore is not suitable for process with many recycle loops. - Does not assure good process profitability (i.e. its aim is to keep the controlled variables at their set points).
Distributed	- Uses MPC controllers, which allowed to introduce a predictive effect in the controller formulation. - Accounts for some degree of interaction between the operating units by exchanging information between the different MPCs.	- Requires the development of a process model (usually linear). - Coordination between the different MPCs is a complex task that could require extra communication and computational costs.
Multi-layer	- Incorporates an optimization layer that pursuits an economical objective, whereas the controller layer accounts for control performance and process stability. - Explicitly accounting of the dynamic performance, when the optimization layer solves a D-RTO problem.	- Computational effort is high, specially if a D-RTO layer is used. - Requires model development, which can be expensive. - Model mismatch between the RTO and controller layers may deteriorate the performance of the PWC architecture. - A good compromise between the economical and the performance control objectives should be achieved, on the contrary, the performance of this PWC architecture may be deteriorated.
Single-layer	- Explicitly accounts an economical objective, which leads the process to maximal profitability. - Considers the process dynamics, which allows having a better capability for facing disturbances of different nature.	- Computational effort is increased. - Relies on a good definition of the economical objective function pursued. - Requires the development of a first principles dynamic model which is a complex task for a PWC context.

Finally, it should be noticed that the Multi-layer and the Single-layer architectures are used as part of the Plantwide optimizing control framework proposed in Chapter 5, due to the following reasons:

- Both formulations include the incorporation of an economical objective function into their formulation, which is necessary if the Plantwide control objective pursued is to maximize the profitability, as stated here.
- The formulations consider the dynamic behavior of the process through the use of a first principles dynamic model, which is used as a tool for predicting the process performance in terms of the objective function value, during the selected optimization horizon. Considering the dynamic behavior of the process is of vital importance in processes where the profitability is at risk when disturbances appear, such the case of the bio-ethanol production process, which is highly vulnerable to raw material quality disturbances, biomass viability, etc.

For concluding this Section, the advantages and disadvantages of the different plantwide control architectures described, are summarized in Table 2.2.

2.2. Stochastic Global Optimization

As it was already explained, the main topic of this work is to propose a Plantwide Control (PWC) strategy for the bio-ethanol process. Such PWC strategy (see Chapter 5) is based on the optimizing control concept, in which a very important step is to solve a large-scale dynamic optimization problem in an efficient way, that is, in short time, without requiring much computational effort and with a high possibility of finding the global optimum. Considering a potential industrial application, the implemented optimization algorithm should be not only reliable, but also easy to understand and to implement. Furthermore, it is important to notice that due to the disturbances appearance and process uncertainties, the global optimum can move, therefore it is important that the optimization algorithm implemented has the capability for finding fast the global optimum. Although the literature in deterministic global optimization presents some powerful methods for solving global optimization problems (as reviewed by **Floudas and Gounaris, 2009**), in general, the main drawback of these methods is the need of gradient information, which becomes a main problem when a complete process is considered, that is, when implementing a plantwide strategy, as the case in this thesis. When deterministic approaches are not suitable for being

applied, stochastic methods appear as an option for solving global optimization problems. Stochastic optimization methods are those involving some kind of randomness or probability, which are useful for solving many global optimization problems either with continuous and/or discrete variables. In general, stochastic methods are simpler to implement from a computational point of view, and easier to use in a particular application because there is no need for derivatives. They are very well suited for highly multimodal problems, for problems involving uncertainties, and for black-box objective functions (**Faber et al., 2005**; **Egea et al., 2009**). Usually those algorithms sacrifice the guarantee of optimality for quickly finding a satisfactory solution (**Zabinsky, 2009**), a very important feature for on-line applications.

Stochastic optimization methods can be classified into evolutionary and non-evolutionary methods, as presented in Figure 2.7. The most important feature of evolutionary methods is that they are inspired in biological systems. A detailed description and explanation of stochastic methods can be found in **Glover and Kochenberger (2003)** and **Schneider and Kirkpatrick (2006)**.

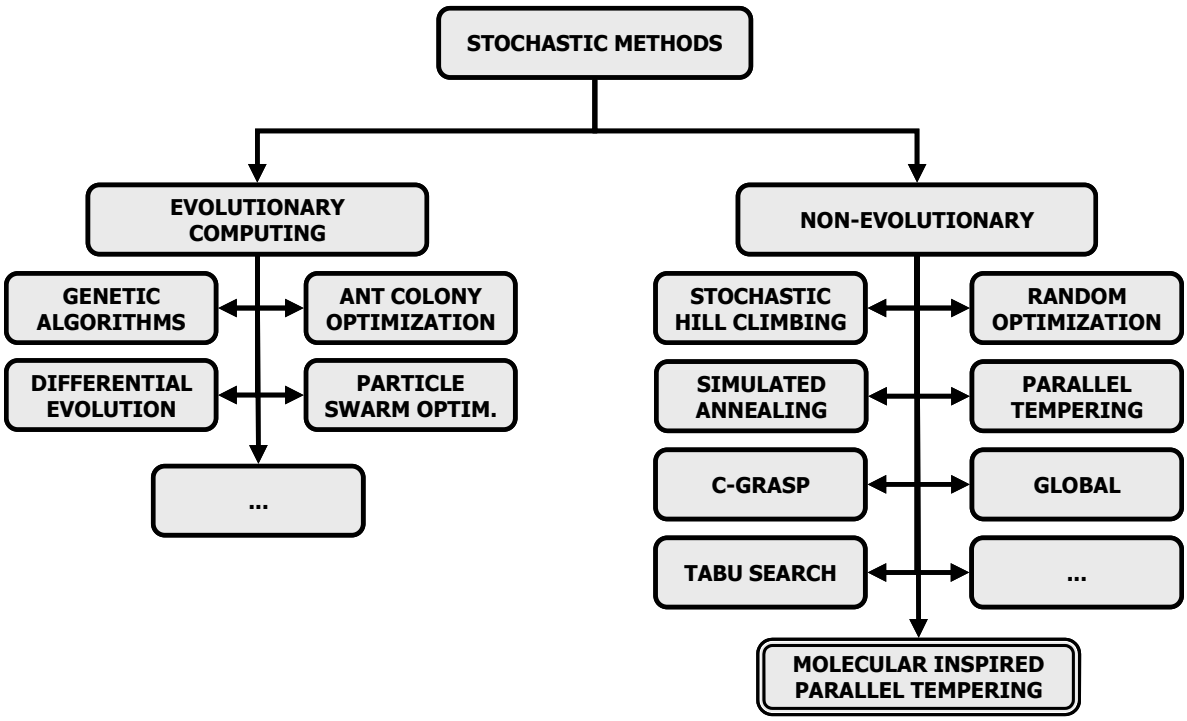

Figure 2.7 Overview of stochastic optimization methods: Evolutionary vs. Non-evolutionary

This section examines several stochastic direct search methods for global optimization, which are direct in the sense that they use no information about derivatives, are simple to implement, and have shown to have a wide applicability in many different disciplines, for successfully solving problems including constrained NLP, MINLP, dynamic optimization and

problems with highly multimodal functions. The general problem to be solved, for which the optimization algorithms are described in this section, is the minimization problem described by Equation (2.4).

$$\begin{aligned} \min_{x} \quad & F_{obj} \\ s.t. \quad & g(x,y) = 0 \\ & h(x,y) \geq 0 \\ & x_{min} \leq x \leq x_{max} \end{aligned} \tag{2.4}$$

where F_{obj} is the objective function to be minimized, x is the set of decision variables, y are the outputs of the process, g represents the set of equality constraints and h represents the set of inequality constraints.

In this work, five stochastic algorithms were used, namely: Localized random search, Simulated Annealing, Particle Swarm Optimization, Parallel Tempering and the Molecular-Inspired Parallel Tempering Algorithm (MIPT) proposed by first time in (**Ochoa et al., 2009c**). In the next chapter, the new MIPT optimization algorithm is presented and tested in a wide range of problems, including constrained NLP, MINLP, dynamic optimization and problems with highly multimodal functions. Results shown in Chapter 3 compare the performance of the new MIPT algorithm, and it is proved that this new stochastic algorithm is a very efficient method for solving global optimization problems, with a high success ratio and with a reasonable computational effort. Therefore, the MIPT algorithm is used in Chapter 6 for solving the dynamic optimization problem that arises during the implementation of the plantwide optimizing control strategy proposed in Chapter 5.

In the following, the theoretical background of the localized random search, simulated annealing, and the particle swarm optimization methods is revised, which were used in Chapter 3 for comparing the performance of the MIPT algorithm developed in this work. On the other hand, the Parallel Tempering and the Molecular Inspired Parallel Tempering are very well described in Chapter 3.

2.2.1. Localized Random Search (LRS)

As it was previously mentioned, random search optimization methods are those employing some kind of randomness or probability in their algorithms. The randomness usually appears in the definition of the new trials and/or in the acceptance criteria at each iteration. In the most simple random search algorithms, the new trials are generated using a probability distribution (e.g. normal, uniform, etc), and the acceptance criteria simply checks if the objective function for the new trial decreases when compared to the previous point. According to **Spall (2004)**, the most popular and simple random search algorithms that contain the most essential of these methods, are: the Blind Random Search and the Localized Random Search (**Baba et al., 1994**; **Jang et al., 1997**; **Solis and Wets, 1981**). The Blind Random Search (BRS) is the simplest version, in which the new trials are randomly generated without taking into account the sampling history. Although the blind search is the simplest algorithm, it is in general a very slow convergence algorithm. On the other hand, the Localized Random Search (LRS) differs from the blind search, in that the new trials are generated randomly around the current position. It is important to clarify that LRS is "local" in the sense that their new trials depend on the local environment near the current estimate, but this is not related with the searching for a local vs. a global solution. In fact, sometimes LRS may also provide global solutions (**Spall, 2004**).

A flow diagram of the localized random search is shown in Figure 2.8. The first step is to pick a starting guess, which can be done randomly or using prior information. At this initial point (x_0), the objective function value is evaluated for further comparison. The algorithm then generates the new trial (x_{i+1}) around the previous sample, depending on a probability distribution ξ, as indicated by Equation (2.5).

$$x_{i+1} = x_i + \xi \tag{2.5}$$

Such a distribution is usually a Gaussian-type (Figure 2.9), whose probability density function (Equation 2.6) is defined by the values of the mean (μ) and the variance (σ^2); however, other distributions can also be used.

$$p(\xi) = \frac{1}{\sqrt{2\pi\sigma^2}} \exp\left(-\frac{(\xi - \mu)^2}{2\sigma^2} \right) \tag{2.6}$$

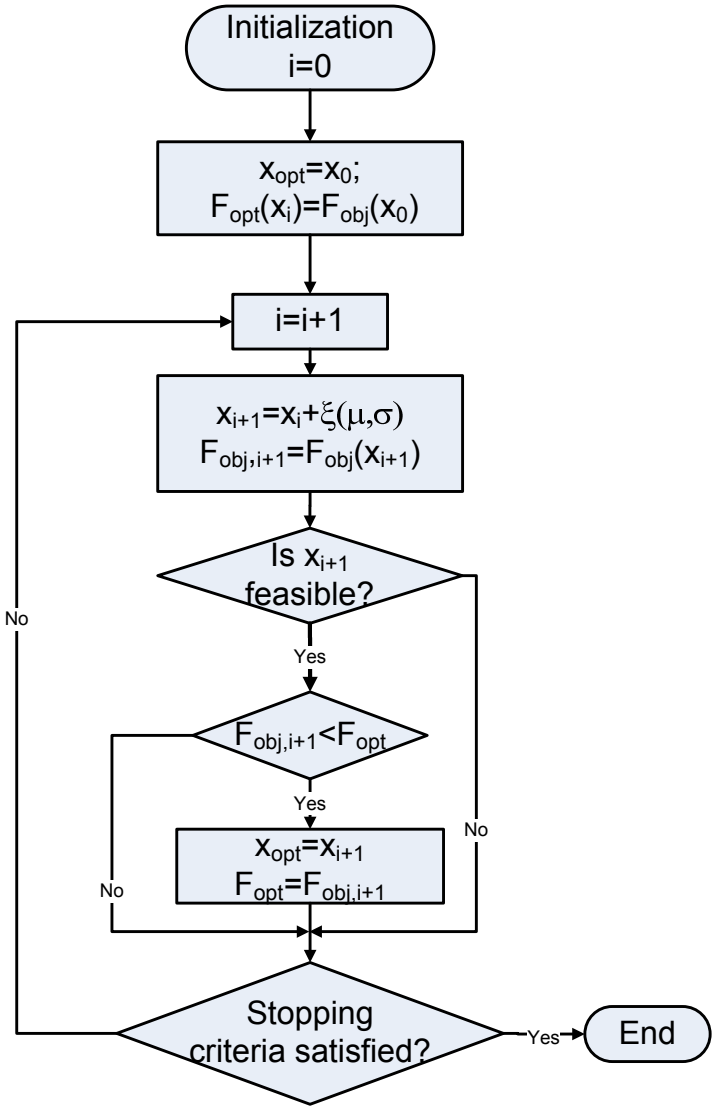

Figure 2.8 Flow diagram of the Localized Random Search (LRS) Algorithm

For the Gaussian distribution, also known as normal or bell distribution, the value of the variance determines the magnitude of the change around the previous sample. As a rule of thumb, almost all random values obtained from a Gaussian distribution are expected to belong to the interval [μ-3σ, μ+3σ]. In addition, in order to make unbiased moves around the current point, the mean value is usually set to zero (μ=0), although some other versions of the algorithm include updating rules for both the mean and variance. The main purpose of such updating rules is to enhance the performance of the pure random search methods, mainly by reducing, in an efficient and reliable way, the search space of the optimization problem at each iteration. **Li and Rhinehart (1996)** propose interesting rules for using the gradient information and the history of success in the calculation of the mean and variance.

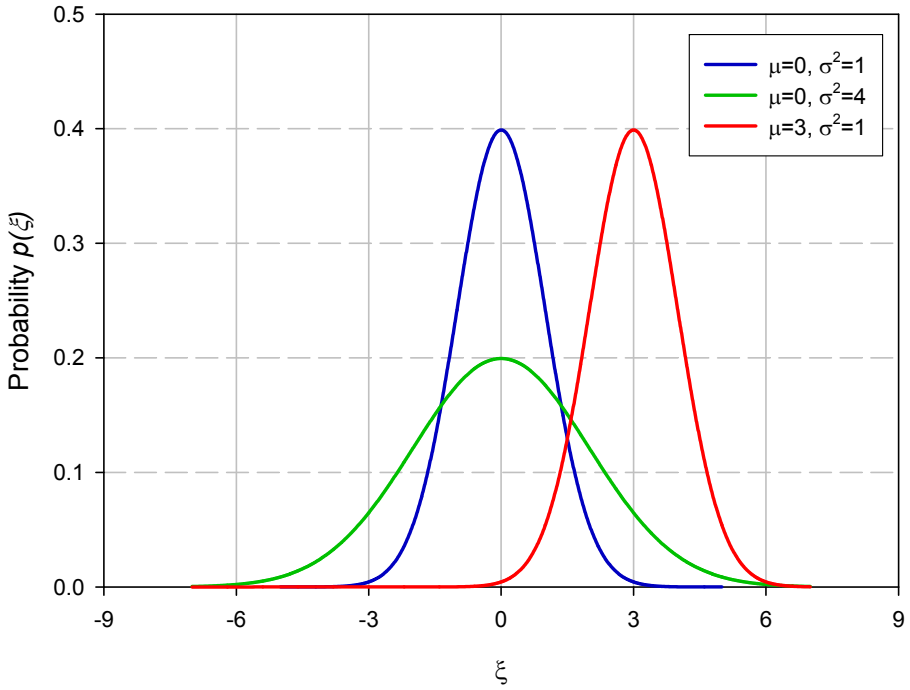

Figure 2.9 Examples of probability density functions for Gaussian distributions

After generating the new trial, the objective function is evaluated, and all constraints are checked. Then, the new trial is accepted only if it is feasible and if $F_{obj}(x_{i+1}) < F_{opt}$, where F_{opt} is the current optimal value of the objective function. Finally, the stopping criteria are checked, and the optimization stops when at least one of them has been satisfied.

Finally, it is important to notice that the localized random search algorithm, as shown in Figure 2.8, is used in Chapter 6 as one of the implemented optimization algorithms for the Plantwide Optimizing Control approach proposed in this work because:

- The algorithm is very simple to implement (i.e. does not need derivative information, requires simple programming), which can be attractive for any potential application at industrial level.
- The algorithm is very intuitive, and the only parameters to be tuned are the mean and variance of the probability distribution.
- The hardware and software requirements for its implementation are not stringent.

Although the LRS algorithm might be convenient for solving local optimization problems, its main drawback is that it lacks of a specific global character which, as it will be shown in Chapter 6, is important for dealing with unknown disturbances that shift the optimal

operating point far away form the current optimal. The implementation of the LRS algorithm (Figure 2.8) was done in MATLAB® (The MathWorks, Inc.).

2.2.2. Simulated Annealing (SA)

The simulated annealing algorithm developed by **Kirkpatrick et al. (1983)** used the concept of annealing in liquids and metals for finding the low energy configurations of disordered magnetic materials. Because of the analogy to the minimization of an objective function in an optimization problem, this algorithm has been extensively used in many other applications in fields like material engineering, electrical engineering, mechanical engineering, bioengineering, structural engineering, computational chemistry, crystallography and many other (**Tan, 2008**). A flow diagram of the algorithm is shown in Figure 2.10.

The algorithm is initialized by defining an initial guess (x_0) as well as the initial annealing parameter β_0 and the annealing policy. The annealing parameter is usually interpreted as the reciprocal of the system temperature (**Frenkel and Smit, 2002**):

$$\beta = \frac{1}{k_B T} \tag{2.7}$$

where k_B is the Boltzmann constant and T is the temperature. After defining an initial point, a new trial (x_{i+1}) is randomly generated (from any random distribution, as in the case of the localized random search method described in the previous section), and the objective function value for this new trial ($F_{obj}(x_{i+1})$) is evaluated. Then, the acceptance probability P_{acc} is calculated from Equation (2.8) and compared against a random number (r) generated from a uniform distribution (e.g. $r \in [0,1]$). Such comparison is called the Metropolis condition (or Metropolis criterion) proposed first by **Metropolis et al. (1953)** in a pioneer work in statistical mechanics. When the Metropolis condition as criteria for accepting or rejecting a new trial is used, most of the trials will be accepted for low values of β (i.e. for high temperature values) providing the method with a global character by allowing the exploration of a wider region of the search space. However, for high values of β (i.e. low temperatures), the majority of the moves that deteriorate the objective function value, causing an increase in the energy of the system in analogy with the minimization of energy landscapes, will be rejected. As can be seen, the definition of the annealing parameter is a determining factor in the success of the method. A simple rule that can be implemented is

that the annealing β-parameter increases linearly with the number of iterations (i.e. $\beta(i)=ci$, where c is a constant representing the rate of annealing and i is the iterations counter).

$$P_{acc} = \min\left\{1, \exp\left(-\beta_{i+1}\left(F_{obj}(x_{i+1}) - F_{opt}\right)\right)\right\} \tag{2.8}$$

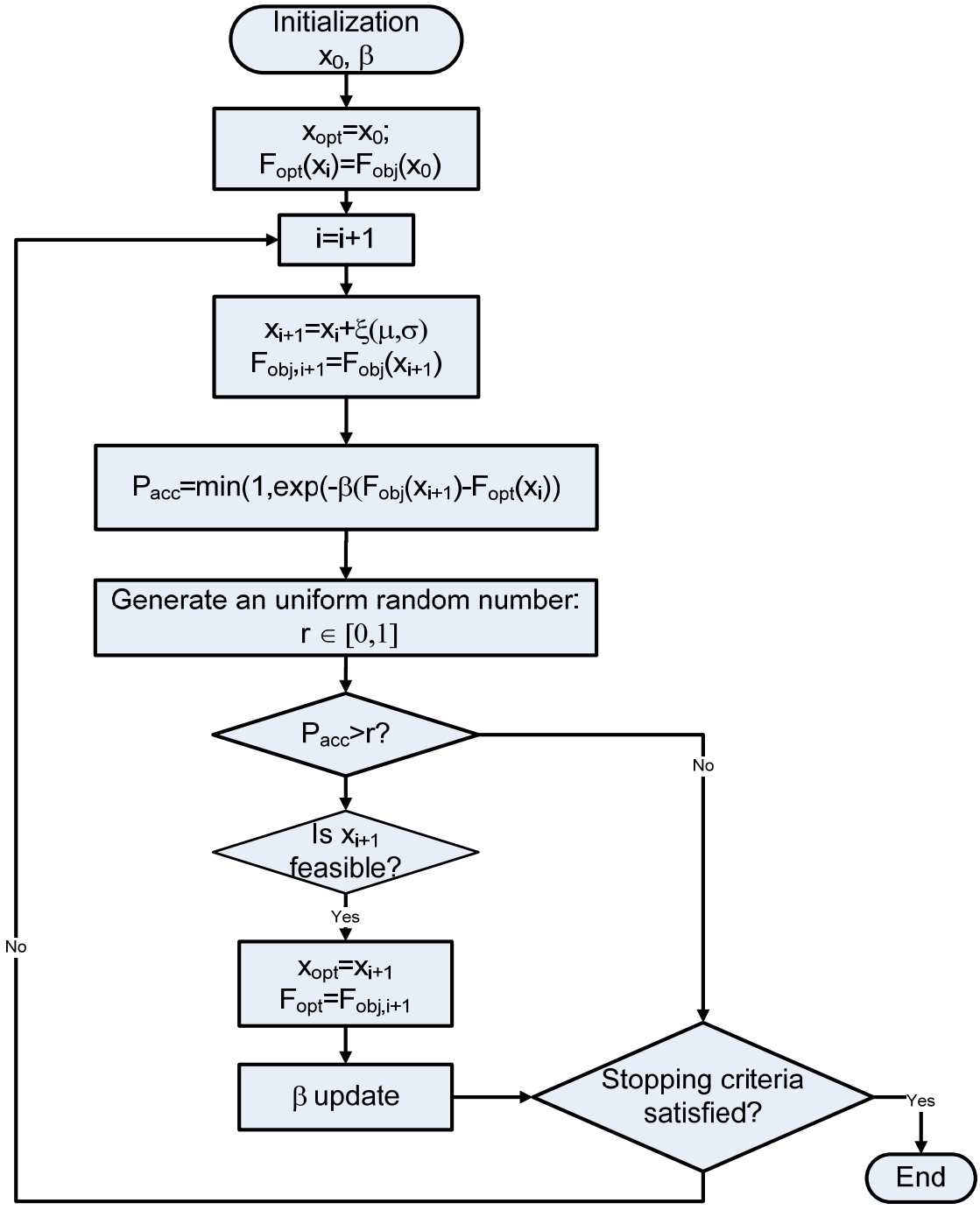

Figure 2.10 Flow diagram of the Simulated Annealing (SA) optimization algorithm.

The simulated annealing algorithm has been widely and successfully applied for solving global optimization problems in many disciplines (**Tan, 2008**), which can be explained due to the main virtues of this Monte Carlo-based method, such as:

- its random nature, which allows the exploration of a much wider region
- the Metropolis condition which avoids getting trapped in a local optimum
- the annealing effect which takes care of the convergence of the method

A detailed explanation of the origins of the method and a discussion of different cooling techniques (i.e. for defining a convenient annealing policy) can be found in the work by **Schneider and Kirkpatrick (2006)**. A recent survey of different simulated annealing algorithms for single and multiobjective optimization is presented by **Suman and Kumar (2006)**. The simulated annealing algorithm (provided by the Optimization Toolbox in MATLAB) is used in this work in Chapter 3 for solving several global optimization problems.

2.2.3. Particle Swarm Optimization (PSO)

The Particle Swarm Optimization (PSO) is a stochastic method based on the movement of swarms, developed by **Kennedy and Eberhart (1995)**. In general terms, the PSO algorithm considers n different particles (k=1,2,…,n) moving in the search space looking for the best solution. At each iteration, a new trial ($x_{i+1,k}$) is generated for each particle according to its current velocity ($v_{i,k}$), its best preceding position ($X_{best,k}$) and the best preceding position for the whole swarm (X_{gbest}). In this way, each particle updates its position using some knowledge from its own experience, but also from the past experiences of the whole swarm. PSO is similar to genetic algorithms in that it uses a population of particles (individuals) for exploring the search space, but it differs in that all particles are kept as members of the population (i.e. there is no selection operation) and they just change its position and velocity during the optimization procedure. The algorithm for the original PSO method is presented in Figure 2.11.

For initializing the algorithm, the number of particles (n) must be defined and the initial position and velocity for each of them is randomly picked. After that, the particle with the best objective function is set as X_{gbest} (best particle in the swarm) with a corresponding objective function value F_{gbest}. Then, before calculating the new position for each particle ($x_{i+1,k}$), a new velocity ($v_{i+1,k}$) is calculated according to three terms (Equation 2.9).

$$v_{i+1,k} = v_{i,k} + \phi_1\left(X_{best,k} - x_{i,k}\right) + \phi_2\left(X_{gbest} - x_{i,k}\right) \quad (2.9)$$

The first term is the velocity of the particle in the previous iteration ($v_{i,k}$), whereas the second and third terms account for the best previous position ($X_{best,k}$) and the best position between all particles in the swarm (X_{gbest}), respectively. It is important to notice that the second and third terms in the calculation for $v_{i+1,k}$ are weighted by some ϕ_1 and ϕ_2 factors, which define how much the individual and the social experience affect the calculation of the new position for each particle. Usually those factors are calculated considering a random component (i.e. $\phi_1=c_1\xi_1$, where c_1 is a constant and ξ_1 is a random number generated from an uniform distribution in which $\xi_1\in[0,1]$). The new velocity $v_{i+1,k}$ is limited by the maximal velocity allowed (v_{max}). According to **Eberhart and Shi (2001)**, v_{max} is a very important parameter determining the resolution at which the regions between the present and the target positions (global optima) are searched. Therefore, if v_{max} is too low, particles will become trapped in local optima, whereas in the opposite case, they might pass good positions without exploring them. Next, the new position $x_{i+1,k}$ is calculated according to Equation (2.10), assuming unit time steps, and the corresponding objective function ($F_{obj}(x_{i+1,k})$) is evaluated.

$$x_{i+1.k} = x_{i,k} + v_{i+1,k} \quad (2.10)$$

If the objective function for the new trial position ($F_{obj}(x_{i+1,k})$) is better than its own best objective function ($F_{best,k}$), the former will be set as $F_{best,k}$. If ($F_{obj}(x_{i+1,k})$) is also better than the best objective function for the whole swarm it is set as F_{gbest}. The procedure is repeated for all particles in the swarm until any of the stopping criteria is met. A more detailed explanation of the algorithm by its developers, including a discussion of many published variants of the algorithm can be found in **Eberhart et al. (2001)**.

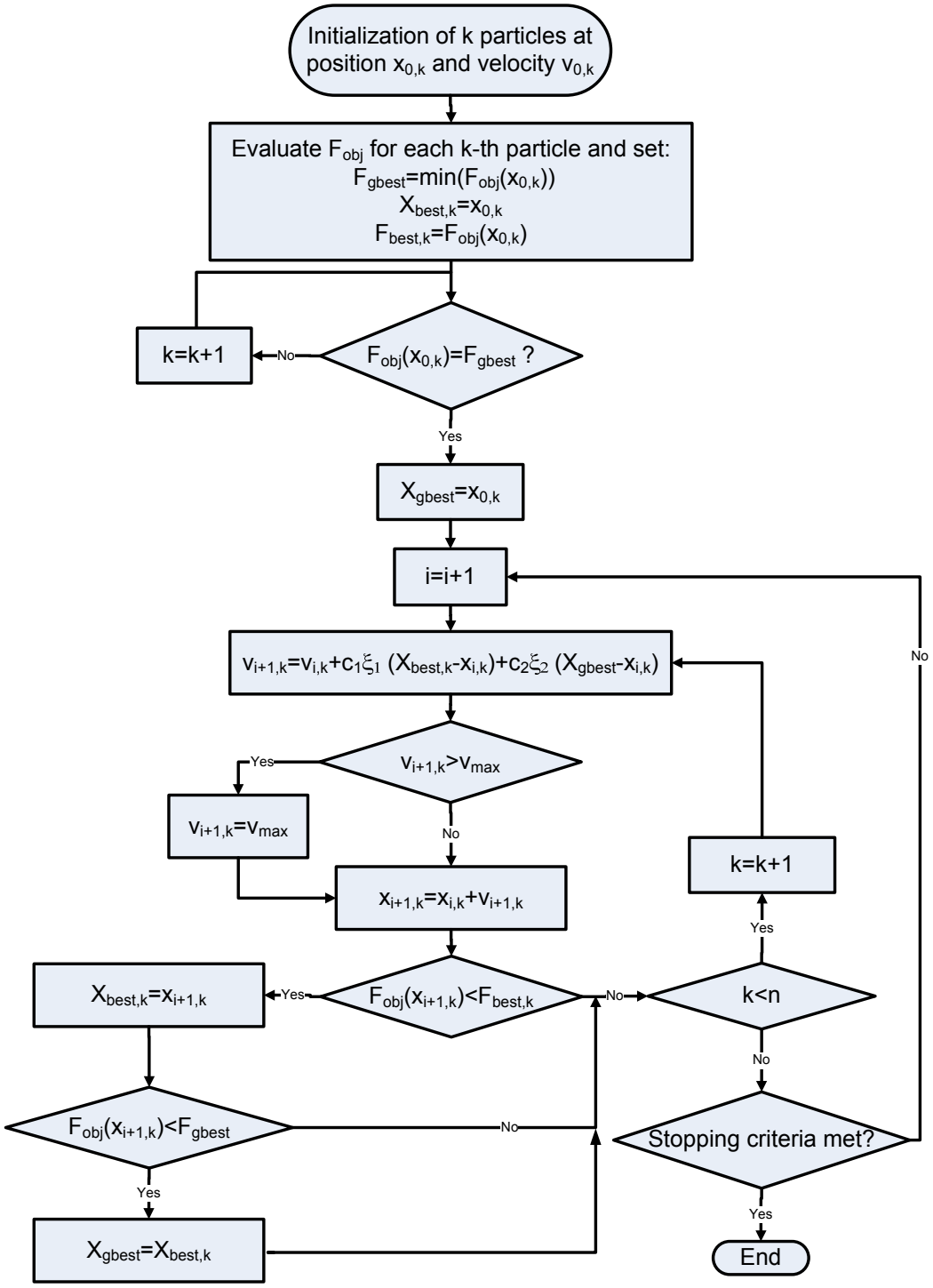

Figure 2.11 Flow diagram of the Particle Swarm Optimization method (PSO)

PSO is used in Chapter 3 for comparing its performance in solving challenging global optimization problems. The algorithm in Figure 2.11 was implemented in MATLAB, following the formulation given by **Clerc and Kennedy (2002)**.

2.2.4. Genetic Algorithms (GA)

Genetic algorithms (GA) is the generic term used to designate evolutionary stochastic search method inspired on the mechanisms of natural selection, mutation and reproduction of living organisms. In analogy to living organisms the individuals simulated in genetic algorithms store genetic information in chromosomes, which can then be totally or partially transmitted to the next generations.

The optimization by means of GA is performed assuming that the objective function to be maximized (or minimized) measures the fitness of the individual to the environment. Thus, by means of the selection operation, only the best fitted individuals in the population (parents) are allowed to breed a new generation of individuals (children), which will eventually substitute the older generations. The reproduction process may take place by different mechanisms, including for example binary cross-over, the random interchange of genetic information between two different parents, or unitary mutation, the replication of the genetic information of the parent incorporating random changes in the genetic sequence. Once a new generation of individuals has been generated, their fitness function (objective function) is evaluated and the whole process of natural selection and reproduction is repeated until any stopping criterion is met. This mechanism of successive cycles of selection and genetic information interchange is expected to lead to the rise of a population of very well-fitted individuals, and eventually, reaching the highest possible fitness value for the system.

Since it is possible to consider many different types of selection rules as well as reproduction operations, there are many possible alternatives for implementing genetic algorithms. Chapter 3 of the book by **Dréo et al. (2006)** presents an excellent description of the different selection operations. A generalized flow diagram of the GA optimization is presented in Figure 2.12.

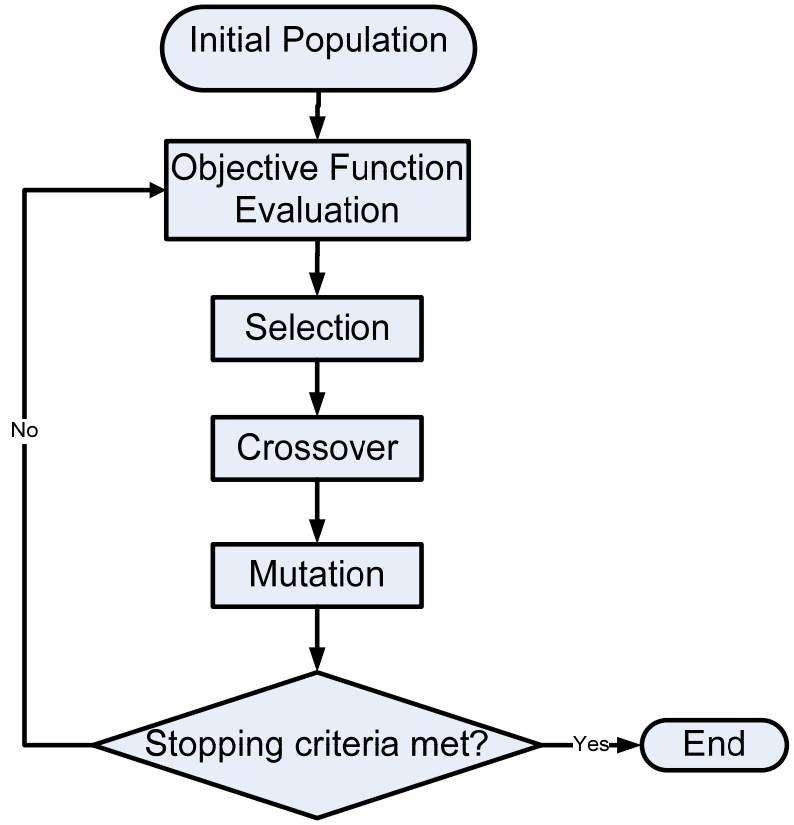

Figure 2.12. Flow diagram of the Genetic Algorithms (GA) optimization method

During the initialization of the GA method, the number of individuals in the population (n) as well as the length of the chromosomes (l) must be defined. Usually, n and l are kept constant during the optimization procedure, but it is also possible to consider varying population sizes and varying chromosome lengths during breeding. Each individual in the population is initially generated by randomly assigning genetic information to its chromosome. This information is usually binary (0 or 1) although other types of information may be used. The advantage of binary genetic information relies on the easier implementation of a wide range of genetic operations during the reproduction stage.

By far, the theoretical background in the core topics addressed in this work, namely, plantwide control and stochastic global optimization has been presented. In the next Chapter, the new algorithm for global optimization denoted as Molecular-Inspired Parallel Tempering, developed in this work, is presented.

2.3. Chapter conclusions

In this chapter, a classification of the different reported architectures for addressing the Plantwide Control (PWC) problem in chemical processes has been proposed, and the theoretical background of those PWC schemes was reviewed, summarizing its main advantages and disadvantages in Table 2.1. After analyzing the different plantwide control architectures, the Multi-layer and the Single-layer schemes were selected to be used as part of the formulation of the Plantwide optimizing control framework proposed in Chapter 5. The main reason for this decision is that both formulations incorporate the statement and solution of a Dynamic Real Time Optimization (D-RTO) problem, which not only takes explicitly into account the dynamic behaviour of the process (which is important when the process is often subject to disturbances), but also allows the formulation of an economical objective function (e.g. maximization of the profitability) to be pursued as the main control objective of the process. In addition, considering that the solution of a D-RTO problem is an important step in the development of the Plantwide Optimizing Control methodology proposed in this work, the theoretical background of some relevant stochastic optimization algorithms was also described.

Finally, it must be noticed that in this work stochastic optimization methods are used instead of deterministic because the former do not require gradient information. The need for the gradient increases the complexity of the problem becoming critical especially when implementing a plantwide strategy. In general, stochastic algorithms have been receiving increasingly attention because of their simplicity and they have been successfully used in several chemical and bio-chemical process applications, showing to be well suited for highly multimodal problems, for problems involving uncertainties, and for black-box-type objective functions. Furthermore, in spite of sacrificing the guarantee of optimality, stochastic methods are able to find quickly a satisfactory solution, which is a very important feature for on-line applications.

3. A New Stochastic Algorithm for Global Optimization: Molecular-Inspired Parallel Tempering

In this Chapter, a new algorithm for stochastic global optimization denoted as Molecular-Inspired Parallel Tempering (MIPT) is presented. In Section 3.1, a brief review of the original Parallel Tempering (PT) algorithm (which is the starting point for the development of the MIPT) is included. The MIPT algorithm is detailed described in Section 3.2, and a comparison of the performance of MIPT with respect to well-established optimization methods is presented in Section 3.3.

3.1. Parallel Tempering

Parallel Tempering (PT), referred also as the Replica Exchange Method (**Swendsen and Wang, 1986**) or the Markov Chain Monte Carlo approach (**Geyer, 1992**), simultaneously simulates multiple non-interacting replicas of a system under different thermodynamic or tempering conditions, e.g. under different temperatures (**Earl and Deem, 2005**; **Li et al., 2009a**). Each replica can be independently cooled or warmed in order to achieve a global exploration effect at higher temperatures (because the replicas are able to escape local minima) and a local refinement effect (annealing effect) at lower temperatures. A key feature of PT is that the method considers two different types of transitions for generating new moves during the optimization algorithm (**Hansmann, 1997**; **Schneider and Kirkpatrick, 2006**). The first is a standard Monte Carlo (MC) move independently applied at each temperature level. The second is a replica transition, in which the configuration or conformation (i.e. set of values of the decision variables) is exchanged between different replicas. It is important to notice that in the standard MC transition the i-th replica is only allowed to change its configuration in a neighborhood around x_i; whereas the replica transition allows to exchange complete configurations usually between adjacent replicas (adjacent in the temperature space, not in the configuration space). Thus, the replica

transition move allows the replica to wander from low temperatures (local refinement) to high temperatures (global exploration) by introducing random walk in the temperature space (**Hansmann, 1997**).

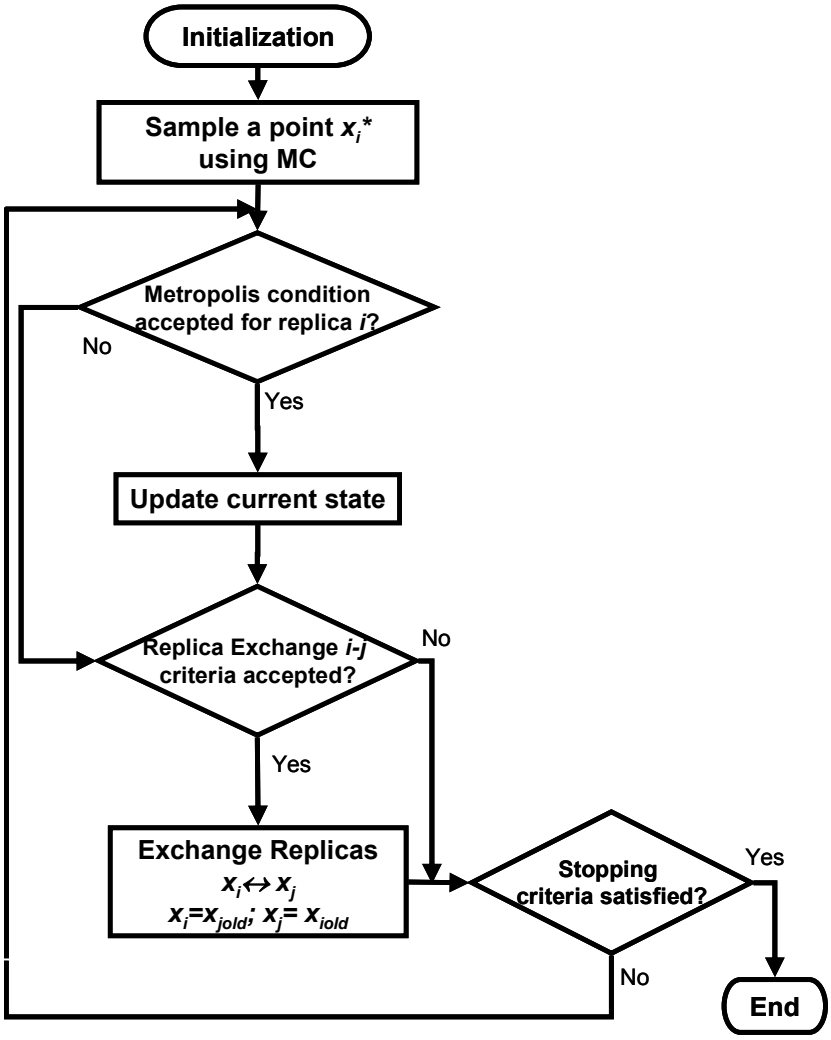

Figure 3.1 Simplified flowchart of the Parallel Tempering Algorithm (**Ochoa et al., 2009c**)

A simplified flowchart of the parallel tempering algorithm is presented in Figure 3.1. The system is initialized by randomly selecting the position x_i (for i=1,2,..,N) of the N replicas in the search space, evaluating their corresponding objective function values ($F_{obj}(x_i)$), and assigning a temperature (T_i) to each replica. It is important to notice, that position x_i is defined by the set of values of decision variables in the optimization problem, which is called in the following the configuration of the i-th replica. Then, the new possible position (x_i*) for each replica is determined using Monte Carlo (MC) random steps (ξ) around its current position (x_i), as shown in Equation (3.1), which is called the MC move:

$$x_i^* = x_i + \xi \qquad (3.1)$$

where ξ represents a random number taken from a given distribution (i.e. uniform, Gaussian, etc.). The new position x_i^* of the replica is only accepted if the Metropolis condition given in Equation (3.2) is satisfied (otherwise the current position of the replica is retained).

$$r < P_{acc} \tag{3.2}$$

where $r \in [0,1)$ is a uniform random number and P_{acc} is the Metropolis acceptance probability given by Equation (3.3):

$$P_{acc} = \min\left(1, \exp(-\beta_i \Delta G_i)\right) \tag{3.3}$$

where β_i is a parameter inversely proportional to T_i, and, in analogy to thermodynamics, the "Gibbs free energy" change ΔG_i is taken as expressed in Equation (3.4):

$$\Delta G_i = F_{obj}(x_i^*) - F_{obj}(x_i) \tag{3.4}$$

After applying a certain number of standard MC movements (Equation 3.1), the replica transition move is proposed (usually between adjacent *i-j* replicas) according to Equation (3.5), in which the replica *i* takes as new position (x_i^*) the current position (x_j) of the replica *j*, and at the same time x_j^* is proposed to take the current configuration of the *i*-th replica (x_i).

$$x_i^* = x_j \,,\; x_j^* = x_i \tag{3.5}$$

The replica exchange transition given by Equation (3.5) is only accepted if the Metropolis-like condition (Equation 3.2) is satisfied. In this case, the acceptance probability criterion *P* is calculated according to Equation (3.6):

$$P_{acc} = \min\left(1, \exp(-(\beta_j - \beta_i)\Delta G_{ij})\right) \tag{3.6}$$

where ΔG_{ij} is given by Equation (3.7):

$$\Delta G_{ij} = F_{obj}(x_j) - F_{obj}(x_i), \quad |j-i| = 1 \tag{3.7}$$

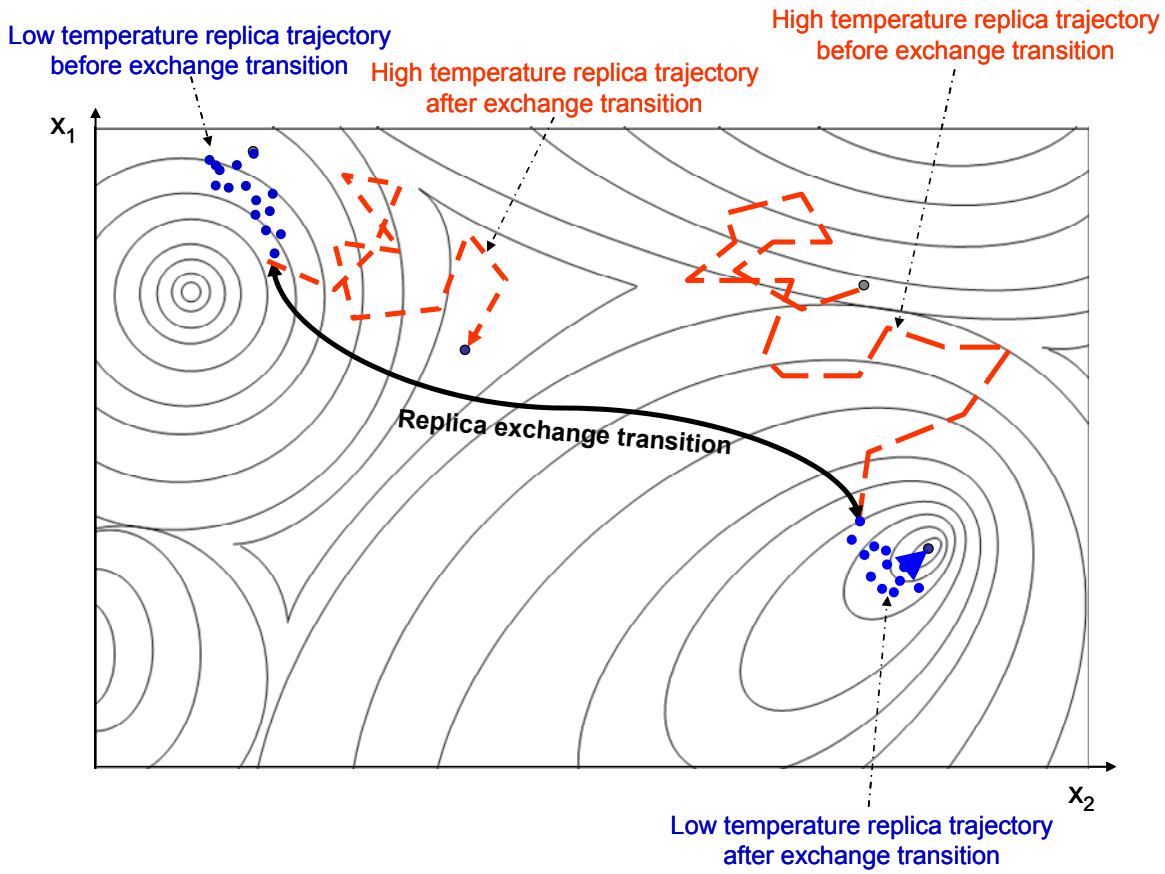

Figure 3.2 Representation of the replica transition in Parallel Tempering

It should be highlighted that during the transition (Equation 3.5), the values of the decision variables of the two replicas involved are completely exchanged. Finally, the procedure is repeated from the generation of the Monte Carlo steps (Equation 3.1) until a certain stopping criterion is met (i.e. a given tolerance, maximum number of iterations, etc). A schematic representation of a replica transition in PT is shown in Figure 3.2. Two replicas (one at high and one at low temperature) are considered in an optimization problem with two decision variables (x_1 and x_2). The low temperature replica moves through the search region in short MC moves (dotted line) with a low probability of accepting worst configurations, whereas the high temperature replica moves in longer MC moves (dashed line) with a higher probability of accepting worst configurations. At a certain point in their trajectories, a replica exchange transition is accepted and the configurations of both replicas are interchanged. Therefore, the low temperature replica continues its search at the position of the high temperature replica and at the same time, the high temperature replica continues at the position of the low temperature replica. This algorithm was implemented in MATLAB following the flowchart presented in Figure 3.1.

Parallel Tempering methods have been successfully applied in different fields during the last 20 years, especially for finding the optimal configuration of polymers (**Sikorski, 2002**), biomolecules (**Calvo, 2009**) and proteins (**Lin et al., 2003**; **Schug and Wenzel, 2004**); for the optimal determination of X-ray structures (**Favre-Nicolin and Cerný, 2002**), for solving benchmark global optimization problems (**Li et al., 2009a**), and many other applications (**Earl and Deem, 2005**). In spite of the successful application of the PT algorithm especially in complex systems with many local minima (complex systems with a rugged energy landscape), there are still some open issues that could be addressed in order to overcome some weaknesses of the algorithm towards improving its performance. For example, it is important to find more efficient strategies for amplifying the global character of the algorithm (improving the barrier-crossing capability, as mentioned by **Li et al., 2009b**). Another issue is the adequate selection of temperatures for each replica. Several authors have pointed out the need of defining not only good temperature values, but also a suitable temperature distribution in order to provide the PT algorithm with a good capability for escaping local minima at a low computational cost. For example, according to **Earl and Deem (2008)**, the highest temperature must be high enough for the simulation to pass over all of the energy barriers in the search space in a manageable computational time. Furthermore, as stated by **Bittner et al. (2008)** after two adjacent replicas have been exchanged, it is more likely than in the next move they change back to the original state than an exchange with another replica, and therefore, the replicas became trapped (they do not move from low to high temperatures at all). In the next section, a new Molecular-Inspired Parallel Tempering algorithm (MIPT) is proposed, which addresses some of these open issues, resulting in a more efficient algorithm very well suited for Global Optimization problems of different nature, as it will be shown through the case studies solved in Section 3.3.

3.2. Molecular-Inspired Parallel Tempering Algorithm (MIPT)

A novel stochastic algorithm for global optimization, denoted as Molecular-Inspired Parallel Tempering (MIPT), is developed in this section. MIPT incorporates some basic features of Molecular Dynamics simulation into the Parallel Tempering formulation. In MIPT, molecules move in the decision-variable-space as the result of different forces: repulsion, friction and

random forces. Two different types of molecules are considered: explorers and refiners. Explorers present lower friction and are subject to repulsion forces causing them to move faster towards low molecular density regions. Refiner molecules can only be feasible and are subject to larger friction forces restricting their motion to a narrow region around their current position. The efficiency of MIPT is tested in Section 3.3 in five challenging case studies.

The Molecular Inspired Parallel Tempering (MIPT) algorithm mimics the behavior of charged molecules in solution. Each molecule is affected by three different forces: repulsion ($\mathbf{F}_{rep}$), random ($\mathbf{F}_{Bm}$), and friction ($\mathbf{F}_{f}$), as depicted in Figure 3.3.

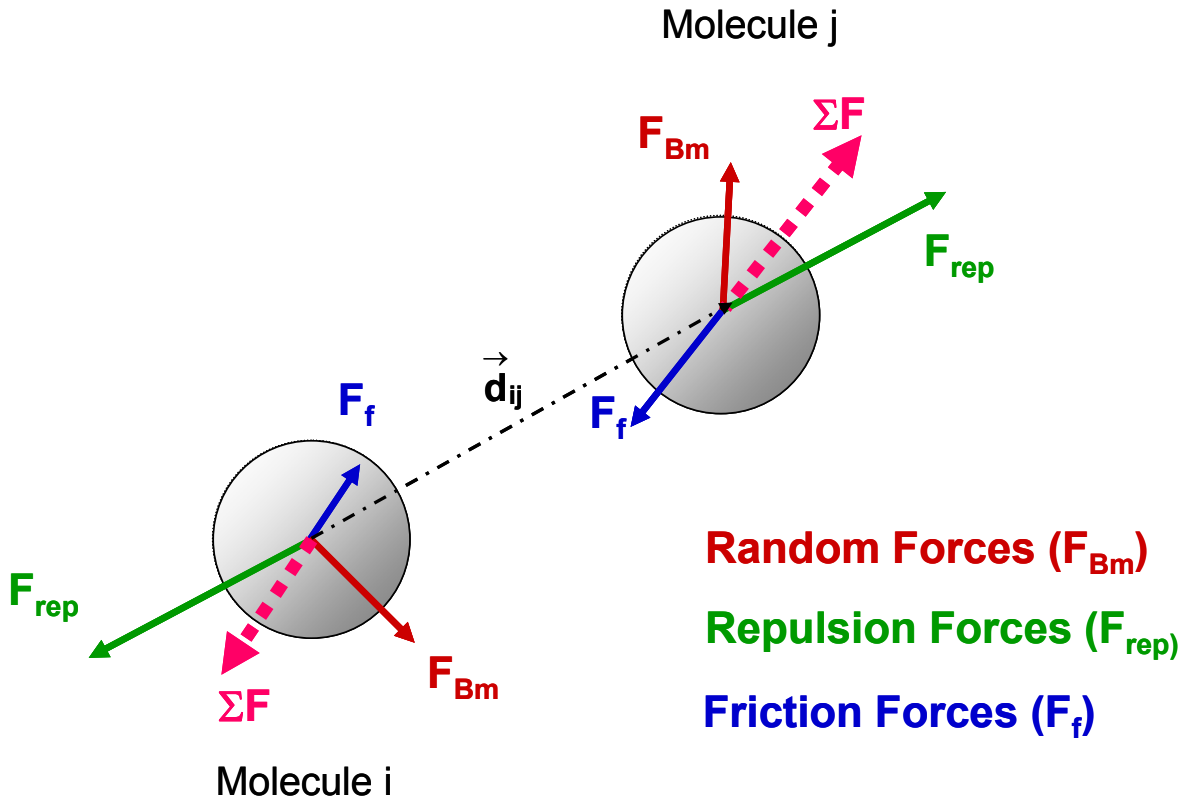

Figure 3.3 Schematic representation of the forces acting on two molecules in solution: Basis of MIPT algorithm. Green arrows: Repulsion forces; Red arrows: Random forces; Blue arrows: Friction forces; Pink dashed arrows: Sum of forces acting on each molecule. Black arrow: Intermolecular distance

The repulsion force exerted by molecule *j* over molecule *i* ($\mathbf{F}_{rep,j}(i)$) is calculated in analogy to Coulomb's law (Equation 3.8), as inversely proportional to the square of the distance (d_{ij}) between them.

$$\mathbf{F}_{rep}(i) = -K_1 \sum_{j \neq i} \frac{\hat{\mathbf{d}}_{ij}}{d_{ij}^2} \tag{3.8}$$

The random force ($\mathbf{F}_{Bm}$), is responsible for the Brownian motion of the molecule and it is expressed by means of a normalized Gaussian distribution vector ξ_G with zero mean and standard deviation one, as given by Equation (3.9).

$$\mathbf{F}_{Bm}(i) = K_2 \xi_{G,i} \tag{3.9}$$

The parameters K_1 and K_2 in Equation (3.8) and Equation (3.9) are the repulsion force and the stochastic force constants, respectively; these force constants can be seen as tuning parameters of the MIPT algorithm. Finally, the friction force ($\mathbf{F}_f$) has an opposite direction to the net external force ($\mathbf{F}_{net}^{ext}=\mathbf{F}_{rep}+\mathbf{F}_{Bm}$) and it is proportional to the velocity $\mathbf{v}_i$ of the molecule by a factor γ_i, as shown in Equation (3.10):

$$\mathbf{F}_f(i) = -\gamma_i \mathbf{v}_i \tag{3.10}$$

where γ_i is a friction coefficient inversely proportional to the temperature associated to each molecule and it is the parameter used in this approach for tempering the algorithm. In general, γ_i may be expressed as a function of the objective function value (F_{obj}) (Equation 3.11) in such a way that the best molecules will be subject to the highest friction coefficients and the worst molecules to the lowest friction coefficients. Any type of distribution of friction coefficients can be used. In this work, a logarithmic distribution of friction coefficients determined by the values of the objective function for each molecule is considered, as given by Equation (3.11).

$$\gamma_i = \exp(\ln(\gamma_{\min}) + ((\ln(\gamma_{\max}) - \ln(\gamma_{\min})) * ((n_m - rank(i)) * Feasible(i)/(n_m - 1)))) \tag{3.11}$$

where γ_{min} and γ_{max} are the minimal and maximal values allowed for the friction coefficient. n_m is the total number of molecules, rank(i) ($1 \leq rank(i) \leq n_m$) is the position of molecule i in a ranking classification according to its objective function value F_{obj} and its feasibility value (0-infeasible, 1-feasible). In this way, if the molecule is in an infeasible position ($Feasible(i)=0$),

then $\gamma(i) = \gamma_{min}$, which results in a larger displacement (Δx(i)) for molecule *i*, in comparison to the displacement of all other molecules.

At the equilibrium condition, the sum of forces acting on each molecule is zero (Equation 3.12) and their velocities become constant ($\mathbf{v}_i = d\mathbf{x}_i/dt = \text{const.}$).

$$\Sigma \mathbf{F}(i) = \mathbf{F}_{rep}(i) + \mathbf{F}_{Bm}(i) + \mathbf{F}_f(i) = \mathbf{0} \tag{3.12}$$

Combining Equation (3.10) and (3.12), and using finite differences to approximate the velocity of the molecules, the friction force ($\mathbf{F}_f$) is found to be:

$$\mathbf{F}_f(i) = -\left(\mathbf{F}_{rep}(i) + \mathbf{F}_{Bm}(i)\right) \approx -\gamma_i \frac{\Delta \mathbf{x}_i}{\Delta t} \tag{3.13}$$

where $\Delta\mathbf{x}(i)$ is the displacement of the *i-th* molecule during a sample time Δt. Considering one optimization step equivalent to one arbitrary unit of time (Δt=1), then the displacement of the molecules at each optimization step, used for generating the new trials of the algorithm, can be calculated using Equation (3.14):

$$\Delta \mathbf{x}_i = \frac{-K_1 \sum_{j \neq i} \frac{\hat{\mathbf{d}}_{ij}}{d_{ij}^2} + K_2 \xi_{G,i}}{\gamma_i} \tag{3.14}$$

On the other hand, one special feature of MIPT that differentiates it from the original PT is that in MIPT the replicas (molecules) are classified in two groups: *refiners* and *explorers*. Refiners-type molecules are always feasible points constrained to higher friction values, forcing the search to a narrow region around their current position and providing a local character to the method. These molecules make shorter displacements in the search region in order to refine the search in a neighborhood that contains local optima. Explorer-type molecules have lower friction values, are allowed to be infeasible and are affected by the repulsive effect ($\mathbf{F}_{rep} \neq \mathbf{0}$), which force them to move towards unexplored zones, providing a global character to the method. In this way, explorers make larger moves escaping from local optima that are already being explored by refiners. It is important to highlight that the inclusion of the repulsion force for the explorer-type molecules allows the MIPT algorithm to

greatly improve the barrier-cross capability of the original PT. A graphical representation of the main characteristics of the refiners and explorers is shown in Figure 3.4.

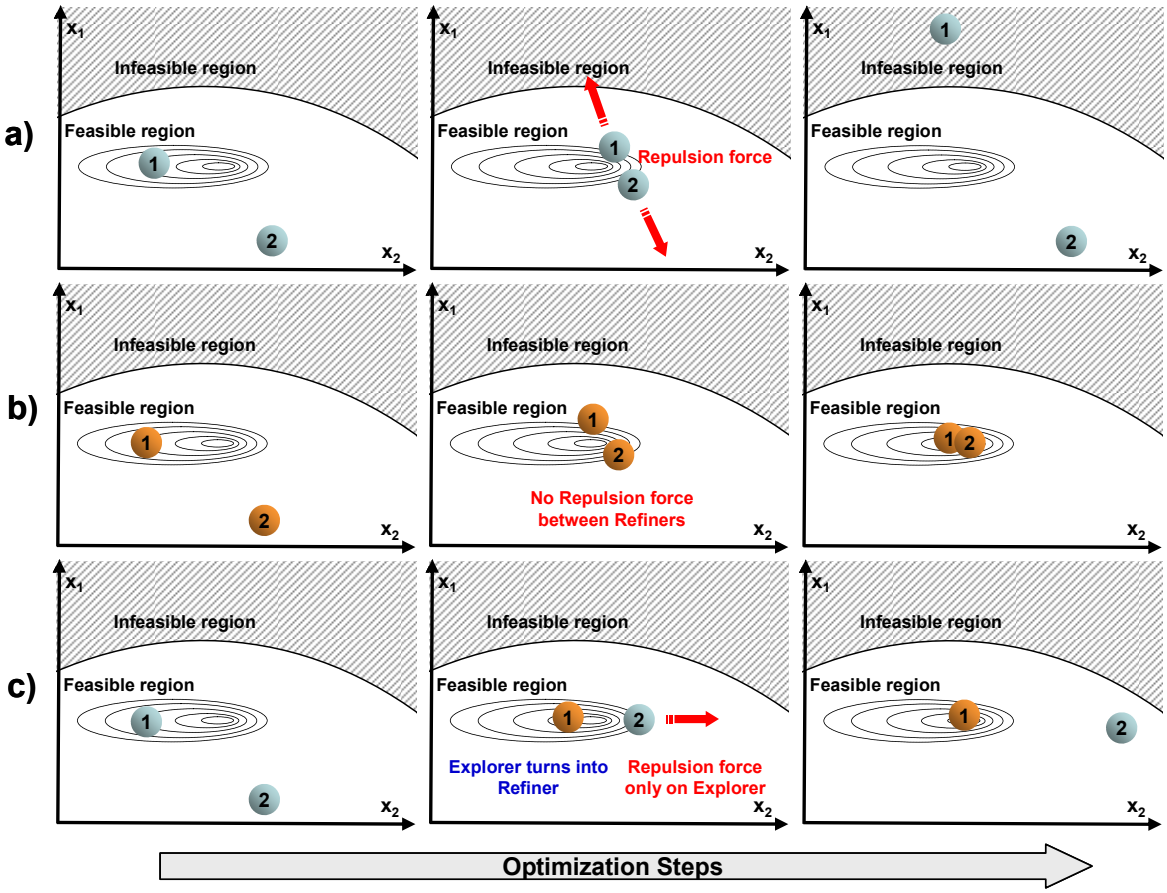

Figure 3.4 Main characteristics of the molecules used in MIPT and their interaction (**Ochoa et al., 2010b**): a) Two explorer-type molecules, both are subject to intermolecular repulsion forces and are allowed to be infeasible, b) Two refiner-type molecules, they do not experience repulsion and must be always feasible, c) Explorer-type molecule (1) turns into a refiner (it found a feasible objective function value better than that of the worst refiner) whereas molecule (2) is kept as a explorer. Only the explorer is subject to repulsion force

So far, the main features of the MIPT algorithm have been introduced, namely: the types of forces acting on each molecule which are responsible for its displacement ($\Delta \mathbf{x}_i$) in the search space at each step of the algorithm, and the type of molecules used in the algorithm in order to improve both the global and the local character of the optimization algorithm. The remaining of this section explains in detail the MIPT algorithm, which is depicted in the flow diagram shown in Figure 3.5. The following description is presented taking into account the problem of minimizing a given objective function.

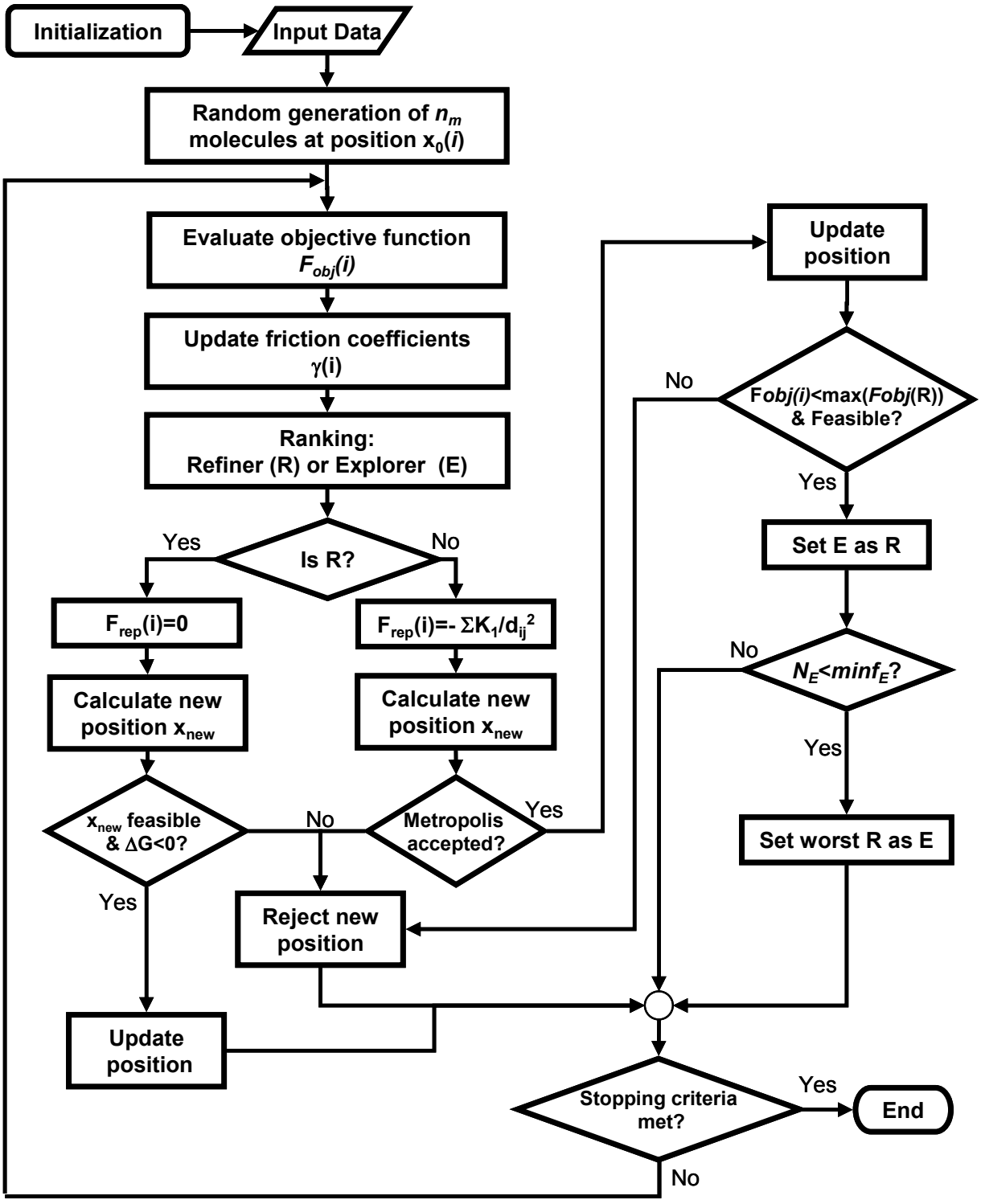

Figure 3.5 Molecular-Inspired Parallel Tempering (MIPT) Algorithm for Global Optimization **(Ochoa et al., 2009c)**

The MIPT optimization algorithm starts with the initialization of the number of molecules (n_m), the stopping criteria and the tuning parameters of the algorithm. MIPT tuning parameters include the range of γ-values used for the friction coefficients of the molecules, the force constants K_1 and K_2, the parameter K_3 included in the calculation of the Metropolis acceptance probability (see Equation (3.17)) and the minimum allowed fraction of explorers

(*minf*$_E$). It is suggested that $n_m \geq 2 \cdot n_{dv}$, in order to achieve an efficient coverage of the search region, taking into account that the probability of finding the global optimum increases with the number of molecules. However, selection of an adequate number of molecules depends on the specific problem addressed (e.g. on the number of local minima and the number of decision variables involved). In general, it is recommended to look for a good compromise between the success of finding the global optimum and the required computational effort. Furthermore, it is suggested that $minf_E \geq n_m/2$ ensuring that at least half of the molecules are exploring the search region looking for the global optimum. The next step is the random generation of the initial n_m molecules (starting positions $\mathbf{x}_{0(i)}$). Then, the objective function (F_{obj}) is evaluated for each molecule and the γ-factors are updated (i.e. calculated as a function of the rank in $F_{obj,}$ see Equation 3.11). Afterwards, the molecules are ranked as Refiners (*R*) or Explorers (*E*), according to their objective function values and feasibility. The ranking criteria must satisfy the condition that the total number of explorers (N_E) should be greater or equal than the minimum number of explorers required, that is $N_E \geq minf_E$ .Then the algorithm is split into two branches depending on whether the molecule is a refiner or an explorer. The refiners' branch begins setting the repulsion force to zero ($\mathbf{F}_{rep} = \mathbf{0}$). The random force $\mathbf{F}_{Bm}(i)$ is calculated from a Gaussian distribution, as given by Equation (3.9). After that, the new position ($\mathbf{x}_{new,i}$) for each molecule is calculated according to Equation (3.15), where the displacement $\Delta\mathbf{x}_i$ is given by Equation (3.14).

$$x_{new,i} = x_i + \Delta \mathbf{x}_i \tag{3.15}$$

Once the new position has been calculated, the objective function value ($F_{obj,new}$) for $\mathbf{x}_{new,i}$ is evaluated, and the normalized "free energy" change ΔG_i with respect to the current objective function value (F_{obj}) is calculated according to Equation (3.16).

$$\Delta G_i = \frac{F_{obj,new}(i) - F_{obj}(i)}{\max(F_{obj}) - \min(F_{obj})} \tag{3.16}$$

After calculating ΔG_i, all constraints are evaluated to check the feasibility of the new position. If the new position is an infeasible point, $\mathbf{x}_{new,i}$ is rejected. On the contrary, if $\mathbf{x}_{new,i}$ is feasible and also $\Delta G_i < 0$, the new position is accepted and the position of molecule *i* is updated to its new value ($\mathbf{x}_i = \mathbf{x}_{new,i}$).

The explorers' branch begins calculating $\mathbf{F}_{rep}(i)$ as a function of the intermolecular distance (Equation 3.8). The calculation of the new point $\mathbf{x}_{new,i}$ and the corresponding ΔG_i is carried out as in the case of the refiners (using Equation 3.15 and Equation 3.16, respectively). After that, the Metropolis criterion given in Equation (3.2) is evaluated in order to reject or accept the new position $\mathbf{x}_{new,i}$. In this case, the Metropolis acceptance probability is given by Equation (3.17):

$$P_{acc} = \min\left(1, \exp\left(-K_3 \gamma_i \Delta G_i\right)\right) \tag{3.17}$$

Equation (3.17) is an equivalent expression to that used in PT (see Equation 3.3) and in general in any formulation based on the Metropolis-Monte Carlo algorithm. In MIPT the tempering parameter used is the friction factor γ.* If the Metropolis criterion is satisfied, the new position will be accepted and updated. In the following step the algorithm checks the feasibility of the new position and if the new position is feasible and also has an objective function value lower than that for the worst refiner (the one with the highest F_{obj}), it would be set as refiner. Then, the total number of explores (N_E) is checked, and if $N_E \leq minf_E$, the worst refiner must be set as an explorer. Finally, the stopping criterion is checked and the algorithm stops if it has been met. The MIPT algorithm was implemented as an Optimization Toolbox in MATLAB according to the procedure shown in Figure 3.5. Instructions for the use of the MIPT Toolbox, as well as a quick overview of the algorithm pseudo-code, are presented in Appendix A. Additional information can be found in **Ochoa et al. (2009c, 2009d, 2010b)**.

Finally, it is important to remark that the main advantage of the MIPT over the original Parallel Tempering (PT) formulation is that the classification of the replicas (molecules) in the MIPT algorithm into two different types (explorers and refiners) provides the method with an improved global character without deteriorating the local search capability. The improved global character of the MIPT over PT is evidenced in Section 3.3.1, where a set of challenging global optimization test problems containing many local minima is solved using both algorithms, and it is show that MIPT surpasses the performance obtained by using PT.

* Actually, γ is related to the β parameter used in Equation (3.3) according to the following expression: $\gamma=\beta/K_3$, and therefore, γ is related to the temperature according to: $\gamma=(K_3 k_B T)^{-1}$, where k_B is the Boltzmann's constant.

3.3. Performance Evaluation of the MIPT Algorithm for Global Optimization

In this section, the capability and efficiency of the MIPT algorithm developed for solving different Global Optimization (GO) problems is tested in six case studies, and compared with other established, well-known optimization methods. The first example tests the performance of different optimization methods (including MIPT) over a set of 8 challenging benchmark GO test problems containing many local minima. The second case study evaluates MIPT performance in Mixed Integer Nonlinear Problems (MINLP). The last four examples are specifically related to bio-ethanol production, testing MIPT performance in the steady state optimization problem of biochemical reaction networks, the parameter identification problem in a 12-parameter unstructured model, the dynamic optimization problem of ethanol fed-batch fermentation, and solving the optimizing control problem for the purification stage of the process (distillation and rectification). Results shown in this Section demonstrate that MIPT is an efficient and very suitable algorithm for global optimization, capable of reaching the global optimum with 100% success ratio in most cases, without requiring much computational effort.

MIPT was implemented in MATLAB, using the MIPT toolbox developed in this work (Appendix A). The results were obtained using a PC with 1.66GHz Intel Core 2 Duo processor and 1 GB RAM. The default set of parameters for MIPT used in all case studies is shown in Table 3.1.

Table 3.1 Default set of parameters of the MIPT algorithm

Parameter	Value
γ_{min}	10^{-3}
γ_{max}	1
K_1	5
K_2	5×10^{-4}
K_3	100
n_m	$2n_{dv}$
$minf_E$	0.1

3.3.1. Dixon-Szegö Set

The first example is a set of 8 standard continuous GO test problems taken from the Dixon-Szegö collection (**Dixon and Szegö, 1978**). This set of functions was chosen because it is diverse enough to cover many kinds of difficulties that arise in global optimization (**Hedar and Fukushima, 2006**). A description of the 8 test problems including the already known global minima values can be found in **Hedar and Fukushima (2003)**, and a brief summary of the test functions used is included in Appendix B.1. A graphical representation of two challenging functions from the set, the Easom and Shubert functions, is shown in Figure 3.6 in order to show graphically the complexity of the GO problems addressed.

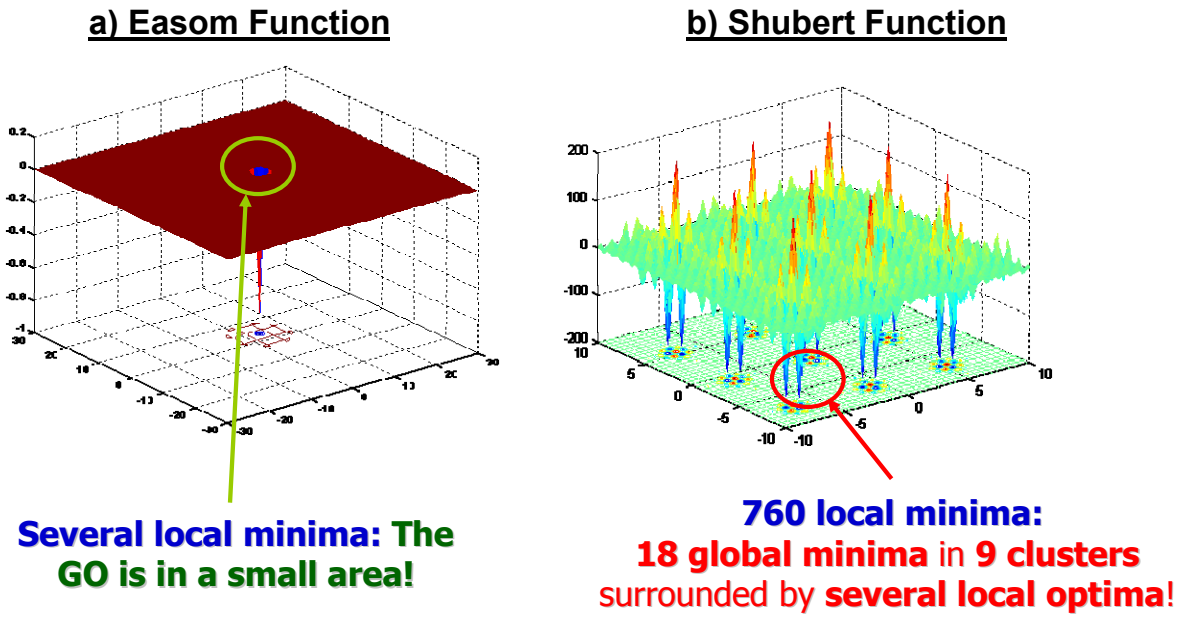

Figure 3.6 Objective function surfaces and main features of the Easom (a) and Shubert (b) benchmark functions.

In this work, each test problem was run 100 times, starting from randomly generated points. Two stopping criteria were implemented. The first one is the criterion reported by **Hirsch et al. (2007)**, which is given in Equation (3.18):

$$\left|F_{global} - F_{obj}\right| \leq \varepsilon_1 \left|F_{global}\right| + \varepsilon_2 \tag{3.18}$$

where F_{global} is the global optimum already known for each test function (see Appendix B.1.), F_{obj} is the current objective function value, and ε_1 and ε_2 are tolerance parameters taken as 10^{-4} and 10^{-6}, respectively. The second criterion was the maximum number of function evaluations, which was set to 100.000 function evaluations.

Table 3.2 shows a comparison between the results obtained using MIPT, Simulated Annealing (SA), Particle Swarm Optimization (PSO), the PT algorithm (which was implemented as described in Section 3.1), a new version of the GLOBAL method (**Csendes et al., 2008**) and the Continuous Grasp (C-GRASP) method (**Hirsch et al., 2007**). Columns in Table 3.2 show the test problems addressed, the number of decision variables in each case, the number of known local minima for each test problem, the average number of function evaluations (*Nfeval*) before reaching any stopping criterion, and the success ratio for the MIPT, SA, PSO, PT, the Global and C-GRASP methods, respectively. It is important to highlight that MIPT algorithm achieved a 100% of success ratio in all cases, as also reported for the GLOBAL method and the C-GRASP[†]. In contrast, the SA and PSO methods stalled in local minima in some of the runs, resulting in a lower success ratio. In the case of SA, the algorithm failed in the Hartman-6 problem, which is a challenging problem involving many local minima and 6 decision variables. In terms of success ratio, the PSO algorithm showed the worst performance, because its success ratio oscillated between 33%-92%, being unable to show complete success in any problem.

According to results shown In Table 3.2, MIPT showed a better performance in solving the Easom, Shubert, Hartman-3 and Hartman-6 problems, whereas the GLOBAL achieved better performance for the remaining problems except for the Goldstein-Price. In conclusion, some facts are remarkable:

1. The MIPT method was able to significantly improve PT results especially in larger problems involving many local minima. This is mainly a result of the improved global character of the MIPT algorithm, over the original PT formulation.
2. The MIPT algorithm outperforms the SA and PSO methods, not only requiring a lower number of function evaluations in all the problems, but also achieving a 100% success ratio in all cases.
3. In general the performance of the MIPT method lies below the range of average values of all other methods, showing to be competitive in solving global unconstrained highly multimodal problems. It should also be noticed that MIPT is the best algorithm for the most challenging problems, including the Shubert, and Easom functions (Figure 3.6), even though they have completely different characteristics. These results show that the MIPT is a versatile algorithm, suitable for a wide range of global optimization problems.

[†] Results for the GLOBAL and C-GRASP methods were taken from the corresponding reported literature, where the stopping criterion was only the one given by Equation (3.18). The second stopping criterion was only implemented for the algorithms run in this work, namely, MIPT, PT, SA and PSO.

Table 3.2 Comparative Results for case study 1: MIPT vs. SA, PSO, PT, GLOBAL and C-GRASP. Values in bold correspond to the lowest average number of function evaluations for each case study.

Test Function	**# Decision Variables**	**#Local Minima**	***Average number of function evaluations (%Success)***					
			MIPT	**SA**	**PSO**	**PT**	**GLOBAL**	**C-GRASP**
Easom	2	Several	**259 (100%)**	749 (100%)	2012 (81%)	703 (100%)	1600 (100%)	89600 (100%)
Goldstein-Price	2	4	466 (100%)	240 (100%)	1808 (84%)	14900 (100%)	923 (100%)	**29 (100%)**
Hartman-3	3	Many	**1414 (100%)**	1631 (100%)	2431 (85%)	4980 (100%)	3610 (100%)	20700 (100%)
Hartman-6	6	Many	**3231 (100%)**	12711 (6%)	10251 (67%)	>1E5 (0%)	16900 (100%)	79700 (100%)
Shekel-5	4	5	2955 (100%)	3490 (100%)	12970 (38%)	20500 (100%)	**1490 (100%)**	5550000 (100%)
Shekel-7	4	7	2830 (100%)	2873 (100%)	13659 (33%)	6280 (100%)	**1680 (100%)**	4050000 (100%)
Shekel-10	4	10	3358 (100%)	3435 (100%)	11809 (43%)	5880 (100%)	**1820 (100%)**	4700000 (100%)
Shubert	2	760	**401 (100%)**	403 (100%)	1162 (92%)	554 (100%)	1400 (100%)	82400 (100%)

3.3.2. Mixed Integer Nonlinear Problem (MINLP)

In this section, a case study consisting in a Mixed Integer Nonlinear Problem (MINLP) that involves 7 decision variables is addressed, which is formulated in Equation (3.19). **Yiqing et al. (2007)** have recently reported results for this problem, comparing Genetic Algorithms (GA), a Simulated Annealing based algorithm (M-SIMPSA), the original PSO algorithm, and an improved PSO algorithm denoted as R-PSO. Furthermore, R-PSO algorithm was used in two variants: R-PSO_unc which updates continuous and discrete variables simultaneously, and the other, denoted as R-PSO_c that updates the different types of variables at difference pace.

$$
\begin{aligned}
&\min \left[(y_1-1)^2+(y_2-2)^2+(y_3-1)^2-\ln(y_4+1)+(x_1-1)^2+(x_2-2)^2+(x_3-3)^2\right] \\
&s.t. \quad y_1+y_2+y_3+x_1+x_2+x_3 \le 5 \\
&\quad y_3^2+x_1^2+x_2^2+x_3^2 \le 5.5 \\
&\quad y_1+x_1 \le 1.2;\ y_2+x_2 \le 1.8; \\
&\quad y_3+x_3 \le 2.5;\ y_4+x_1 \le 1.2; \\
&\quad y_2^2+x_2^2 \le 1.64;\ y_3^2+x_3^2 \le 4.25 \\
&\quad y_2^2+x_3^2 \le 4.64;\ \ x \le 0;\ \ y \in \{0,1\}^4
\end{aligned}
\tag{3.19}
$$

Figure 3.7 shows the comparison between the mentioned stochastic algorithms and MIPT, in terms of the average number of function evaluations (*Nfeval*) and the success ratio (*NRC*), which is the percentage of runs that converged to the global optimum (F_{obj}=4.579582), in 100 executions randomly initialized. As shown in Figure 3.7, MIPT algorithm has reached the global optimum in all the runs, having a success ratio NRC=100%. Furthermore, MIPT has also required by far the fewest number of function evaluations for reaching the global optimum, which demonstrates its capability for dealing successfully with MINLP problems.

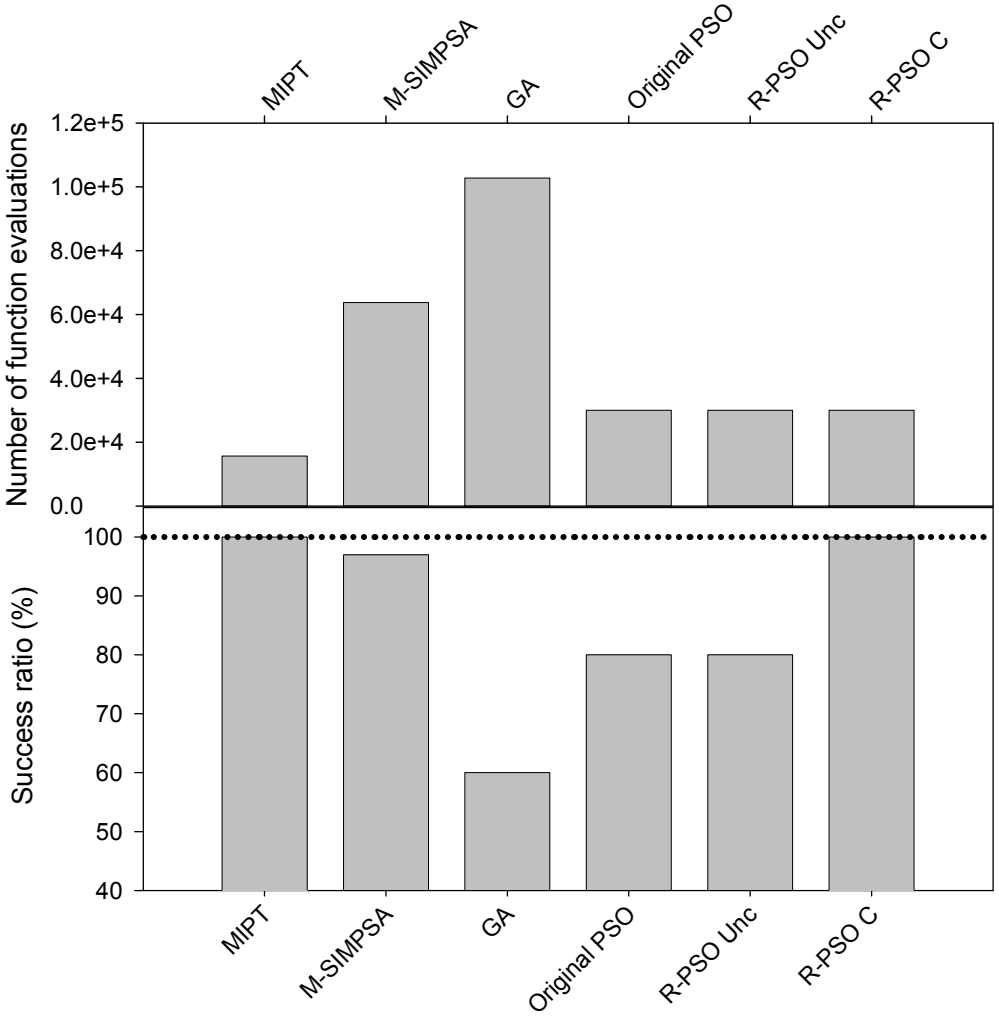

Figure 3.7 Comparative results for the mixed-integer nonlinear optimization problem presented by **Yiqing et al. (2007)**: Number of function evaluations and success ratio for MIPT, M-SIMPSA, GA, Original PSO, R-PSO Unc, R-PSO C, for 100 different runs randomly initialized.

3.3.3. Nonlinear Constrained Optimization Problem

The third case study is an example of the steady state optimization problem of biochemical reaction networks, which addresses the maximization of the flux of Piruvate Kinase (V_{PK}), the enzyme directly responsible for ethanol production in the *Saccharomyces cerevisiae* pathway (**Xu et al., 2008**). This case study consists on a nonlinear constrained optimization problem, given in Equation (3.20):

$$
\begin{aligned}
&\max\ V_{PK}(X_1, X_2, X_3, X_4, X_5, Y_1) \\
&s.t.\quad f(X,Y) = 0 \\
&\qquad V_{in} - V_{HK} = 0;\ V_{HK} - V_{PFK} - V_{Pol} = 0 \\
&\qquad V_{PKF} - V_{GAPD} - 0.5V_{Gol} = 0;\ 2V_{GAPD} - V_{PK} = 0 \\
&\qquad 2V_{GAPD} + V_{PK} - V_{HK} - V_{Pol} - V_{PFK} - V_{ATPase} = 0 \\
&\qquad V_{PK} \le 2V_{in};\ Y_{k0} \le Y_k \le 50Y_{k0};\ k = 1,2,3,4,5,8
\end{aligned}
\tag{3.20}
$$

where f represents the nonlinear steady-state model of the process (which is presented in detail in Appendix B.2), X_i the metabolites concentrations, Y_k the enzymes activities, and X_{i0} and Y_{i0} are the basal steady-state values (corresponding to an objective function value V_{Pk0}=30.1124). **Xu et al. (2008)** solved the problem by applying a standard iterative Indirect Optimization Method (IOM) and a modified iterative IOM approaches, finding an objective function value of V_{PK}=64.828 V_{PK0} and V_{PK}=64.829 V_{PK0}, respectively. The same problem was solved in this work using MIPT, Simulated Annealing (SA) and Particle Swarm Optimization (PSO). SA results were obtained using the MATLAB Optimization Toolbox whereas PSO was also implemented in MATLAB following the formulation given by **Clerc and Kennedy (2002)**. These three methods reached the same objective function value, V_{PK}= 65.022 V_{PK0}, better than that obtained by the IOM approaches. A comparison on the performance for MIPT, SA and PSO in terms of number of function evaluations (*Nfeval*) and *CPU* time for the average, best and worst cases from 100 different runs randomly initialized, is presented in Figure 3.8. Values for the IOM approaches are not reported in the original work, and therefore are not included in the comparison. As it can be seen, MIPT has the best performance in terms of CPU time, whereas the number of function evaluations required for reaching the global optimum lies between those needed by SA and PSO, which confirms that MIPT provides a good performance also in constrained optimization problems.

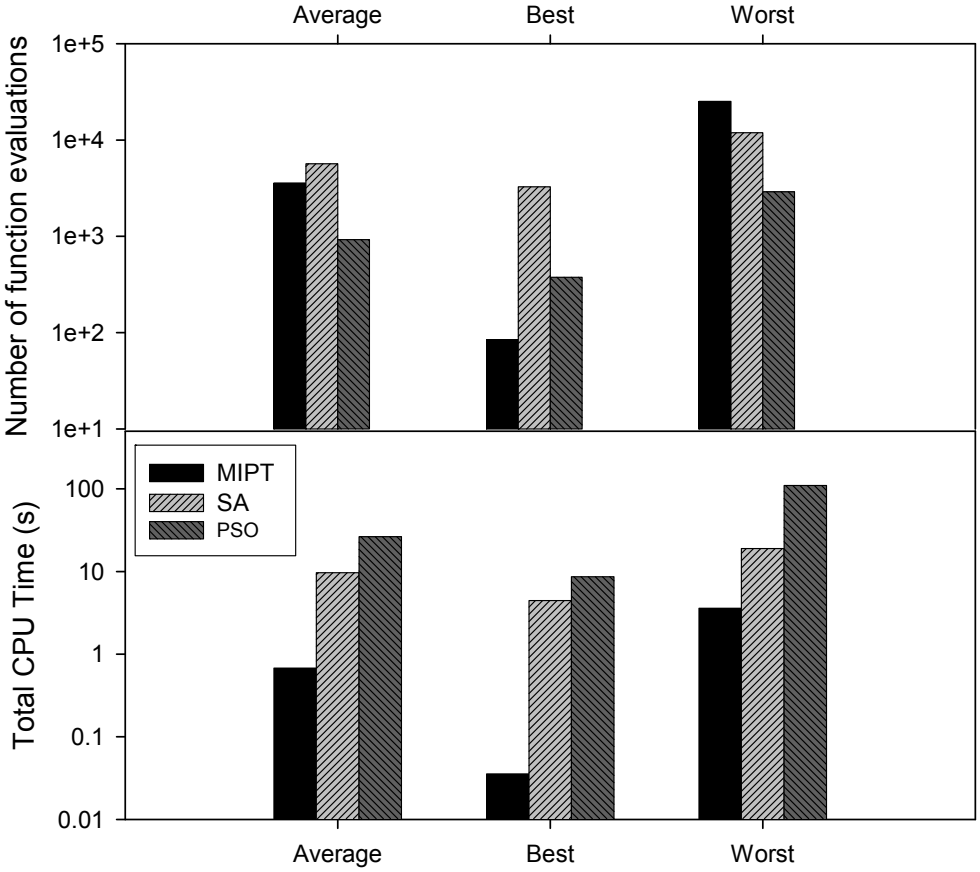

Figure 3.8 Comparative results for the nonlinear constrained optimization problem presented by **Xu et al. (2008)**: Number of function evaluations and total CPU time for MIPT, SA and PSO for 100 different runs randomly initialized.

3.3.4. Nonlinear parameter identification

The fourth case study addresses the parameter identification of an unstructured model of ethanol production. The model includes 12 parameters to be identified by minimizing the normalized squared error between the predictions of the model and experimental data. The model and the experimental data for identification have been reported by **Phisalaphong et al. (2006)**, and are summarized in Appendix B.3. In order to compare MIPT performance, the identification problem was also solved using Simulated Annealing (SA), Genetic Algorithms (GA) and a gradient-based (GRAD) method (i.e SQP), incorporated into the MATLAB Optimization Toolbox. The values of the objective function (normalized squared error) and computation time for the average, best and worst cases of ten different independent runs (randomly initialized) are presented in Figure 3.9. The stopping criterion was 1000 iterations for each algorithm. It can be observed that the best results (corresponding to the minimal objective function values) in all cases (average, best and

worst) have been obtained using the MIPT algorithm proposed in the present work. It can also be observed that the average CPU time of the MIPT method lies within the range of average values of the other methods. Therefore, it is possible to conclude that a significant improvement towards finding the global optimum is achieved using the MIPT method without increasing the computational effort.

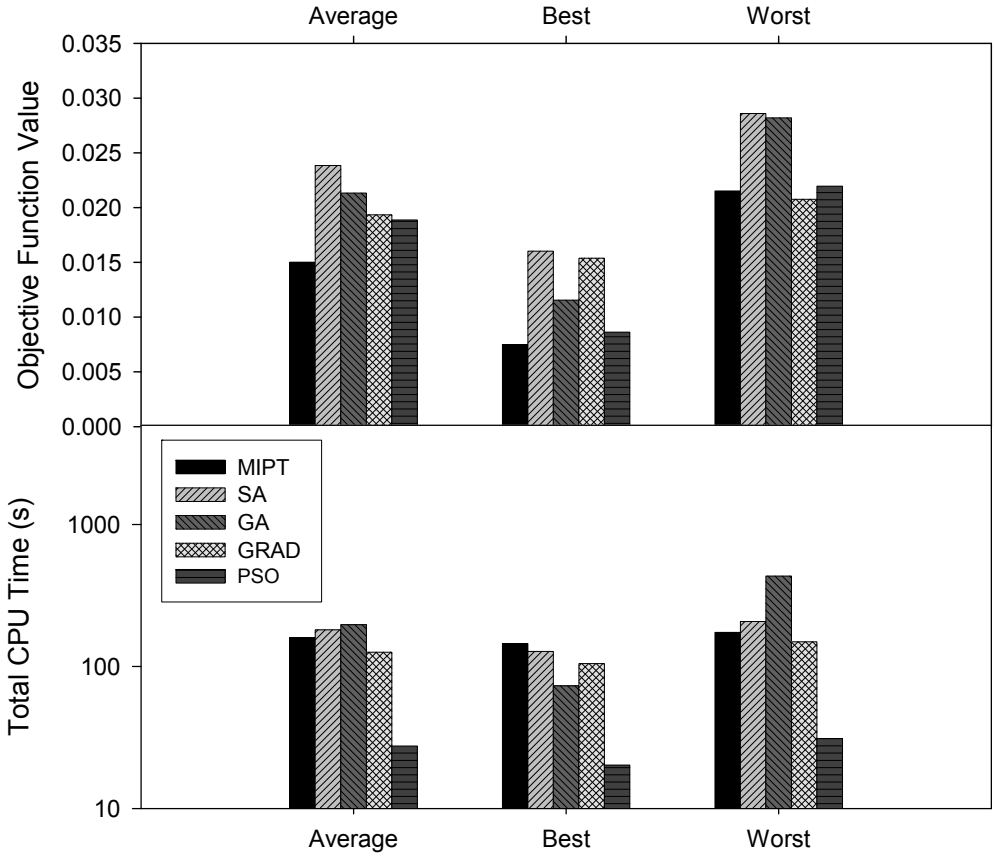

Figure 3.9 Comparative results for the nonlinear parameter identification problem of the model presented in **Phisalaphong et al. (2006)**: Values of the objective function and total CPU time for MIPT, SA, GA and GRAD, for 10 different runs randomly initialized.

3.3.5. Dynamic optimization of ethanol fed-batch fermentation

Solving the dynamic optimization problem for a fed-batch bioreactor allows finding optimal feeding profiles that should be applied to the process in order to maximize a given productivity objective function. This problem is usually solved using direct dynamic optimization methods, which parameterize the control profile as piecewise polynomial functions. However, in this work, parameterization of the control profile is done using cosine functions which are nonlinear and have the advantage of being non-monotonic, allowing to find control profiles that increase and decrease smoothly and continuously. Such

parameterization can be especially suitable for bioprocesses applications. The dynamic optimization problem for the fed-batch ethanol production has been previously studied in different works and the model of the process can be found in **Banga et al. (1997)** and it is also included in Appendix B.4. Equation (3.21) summarizes the optimization problem solved in this section. The state variables on the process are Volume (*V*), Biomass (*X*), Glucose (*S*) and Ethanol (*E*) concentrations. The manipulated variable whose profile is found by solving the dynamic optimization problem is the input flow of glucose (*F*). The productivity of the process has been maximized using different optimization algorithms, taking the parameters of the cosine profile as decision variables, using as stopping criterion the maximum number of function evaluations (i.e. 1000). All the optimization algorithms were randomly initialized, that is, the starting points were randomly selected from the set of values bounded by the upper and lower limits of the decision variable(s). The results of ten different independent runs are summarized in Figure 3.10. It is observed that the best results were obtained using the MIPT algorithm proposed in this work, compared to the Simulated Annealing algorithm (SA), the Genetic Algorithm (GA) and the gradient-based (GRAD) method (i.e. SQP). It is important to notice that the highest productivity values of individual runs were obtained for both the MIPT algorithm and the gradient based (GRAD) method, but the average performance of the MIPT is consistently high while the performance of the gradient method is strongly dependent on the starting conditions of the optimization. In the graph of Figure 3.10, the best cosine feeding profile obtained from MIPT optimization is compared to the best feeding profile obtained by **Banga et al. (1997)** using a piecewise linear approximation. The use of a smooth non-linear profile, although similarly shaped, allows improving significantly the productivity of the ethanol fermentation process.

$$
\begin{aligned}
&\max_{F(t)} \; Productivity = E(t_f)V(t_f) \\
&s.t. \quad f(\dot{x},x,u,d,t) = 0 \\
&\qquad x(t_0) = x_0 \\
&\qquad x^l \le x(t) \le x^u \\
&\qquad F(t) = a_0 + a_1 \cos\left(w_1 \left(\frac{t-t_0}{t_f - t_0} \right) + \phi_1 \right) + a_2 \cos\left(w_2 \left(\frac{t-t_0}{t_f - t_0} \right) + \phi_2 \right) \\
&\qquad 0 \le F(t) \le 12
\end{aligned}
\tag{3.21}
$$

Opt. Method	Productivity (g)		
	Average	Worst	Best
MIPT	**20557.8**	**20556.1**	**20559.3**
SA	20554.5	20551.3	20557.7
GA	18876.9	17751.9	20555.2
GRAD	19104.8	17643.8	**20559.3**

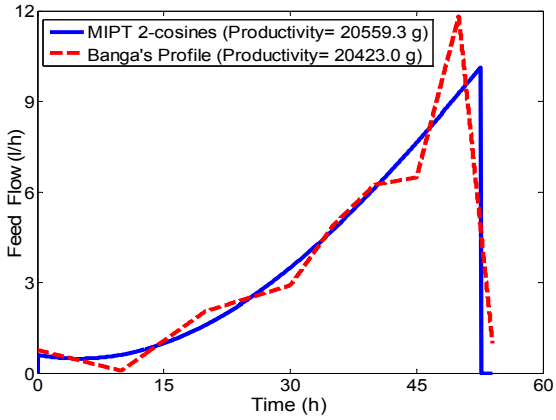

Figure 3.10 Dynamic optimization of ethanol fed-batch fermentation. MIPT vs. Simulated Annealing (SA), Genetic Algorithms (GA) and gradient-based (GRAD). In the right, the best smooth non-linear feeding profile obtained with MIPT vs. the best piecewise linear profile by **Banga et al. (1997)**.

3.3.6. Optimizing control of a Purification stage in Bio-ethanol production

The last case study addresses the optimizing control problem of a two-distillation-column system for purification of a beer stream in an ethanol production process, which is shown in Figure 3.11.

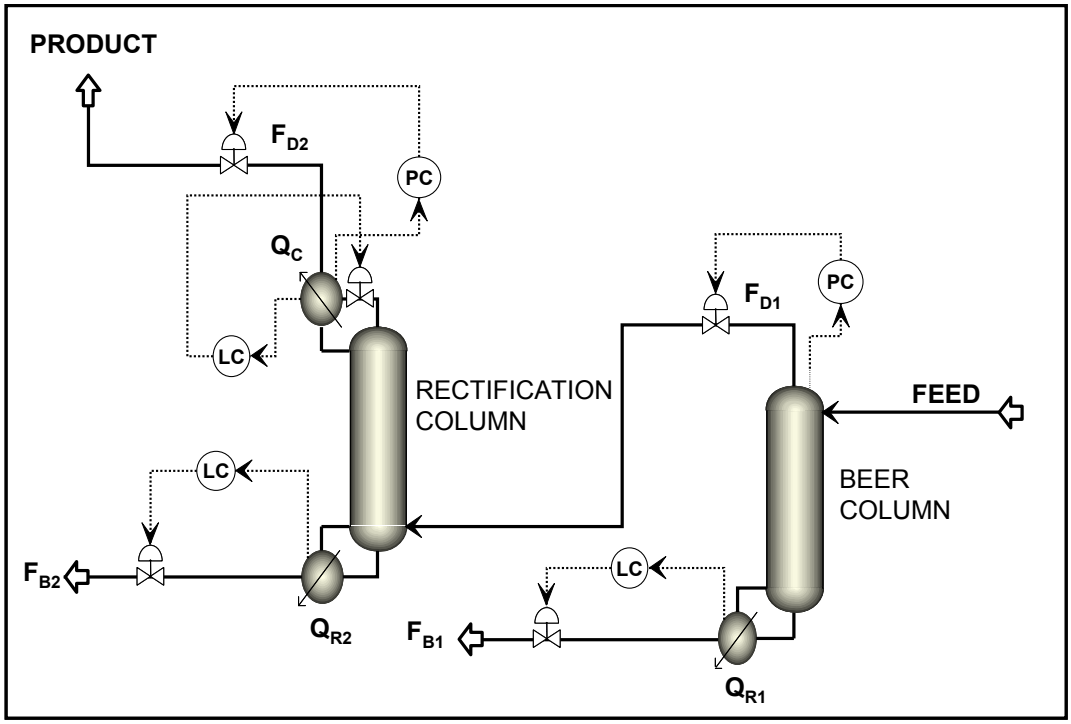

Figure 3.11 Flow diagram of a two-distillation column system for ethanol purification. Beer column: no condenser. Rectification column: partial condenser.

The steady state model of the process (taken from the Aspen Plus Library) was exported to AspenTech's Aspen Dynamics for obtaining the dynamic model comprising a total of 2411 equations, involving 241 state variables. Five control loops for controlling the pressure in both columns, the level in the reboilers and in the partial condenser of the rectification column were included. The initial conditions for the dynamic model are the original steady state values. In case of disturbance, the heat duty of both reboilers (Q_{R1} and Q_{R2}) and the heat duty of the partial condenser (Q_{C2}) can be used as manipulated variables in order to optimize the economic operation of the process (i.e. minimizing a cost function by varying the decision variables of an Optimizing Control problem). The cost function (F_{obj}) to be minimized is given by Equation (3.22), where Δt_{opt} is the optimization horizon, F_{B1}, F_{B2}, F_{D2} are the mass flow rates in the bottoms of the distillation and the rectification columns, and the distillate mass flow rate at the top of the rectification column. x_{EB1}, x_{EB2}, x_{WD2} are the ethanol mass fractions at the bottom of the distillation and rectification, and the water mass fraction at the top of the rectification column. The factors that multiply each term of Equation (3.22) are penalization terms related to the ethanol price, the cost of steam to the reboilers and the cost of cooling water in the partial condenser. f represents the nonlinear dynamic model of the process, u_{min} and u_{max} are the upper and lower bounds for the decision variables in Equation (3.22) and x_{ED2} is the mass fraction of ethanol in the distillate of the second column.

$$\min_{Q_{R1},Q_{R2},Q_C} \int_{t_{opt}}^{t_{opt}+\Delta t_{opt}} \left(0.63\left(x_{EB1}F_{B1} + x_{EB2}F_{B2} + x_{WD2}F_{D2}\right) + 6.33\left(Q_{R1} + Q_{R2}\right) + 0.31Q_C\right)dt$$

$$\begin{aligned} s.t.\quad & f(\dot{x}, x, u, d, t) = 0 \\ & x_i(t_0) = x_{0i} \\ & u_{\min} \le u \le u_{\max} \\ & x_{ED2} \ge 0.9 \end{aligned} \tag{3.22}$$

In order to discuss the performance of different optimization algorithms in optimizing the economic operation of this large scale system, a step disturbance corresponding to a 25% increase of the feed flow rate to the system was done. An optimization horizon of two hours was considered. The maximum number of function evaluations used as stopping criteria was 200. In the scope of comparison, MIPT, SA, PSO and a Gradient based method (GRAD) were

tested. SA and GRAD were run using the MATLAB Optimization Toolbox (in the case of GRAD, a SQP method was used).

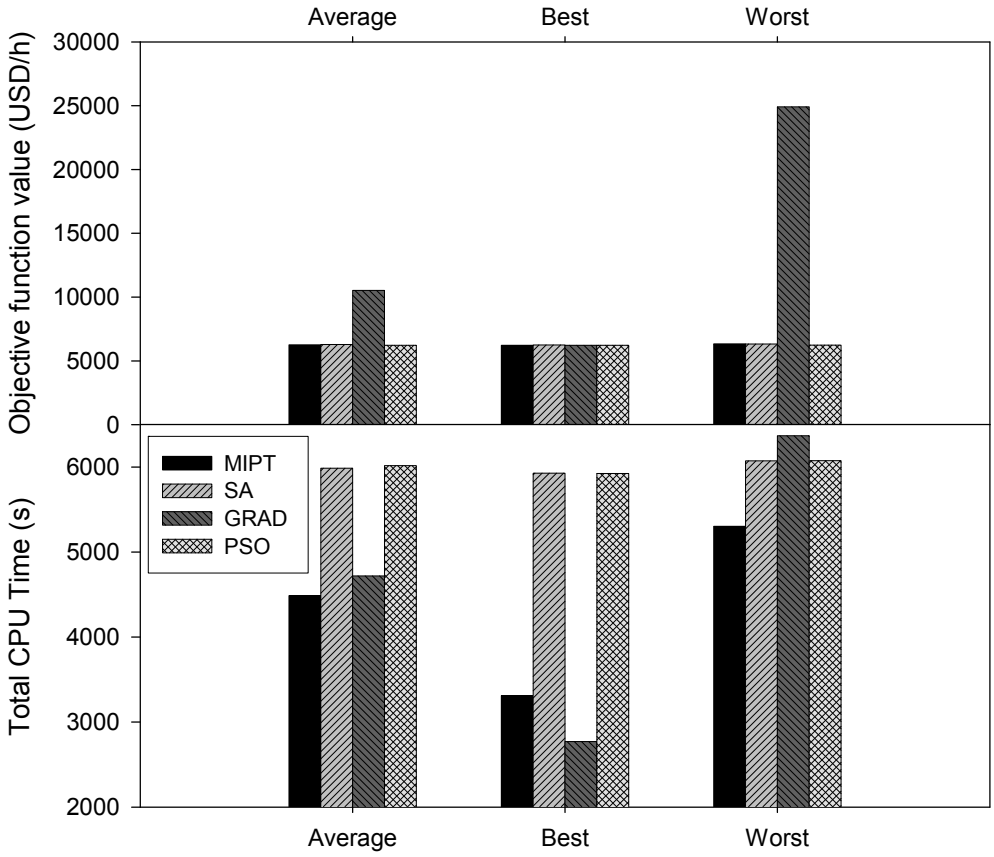

Figure 3.12 Comparative results for the dynamic optimization of a two-distillation column system for ethanol purification: Values of the objective function and total CPU time for MIPT, SA, GRAD and PSO, for five different runs randomly initialized.

Figure 3.12 shows the comparison results for the average, best and worst cases of 5 randomly initialized runs for each method, in terms of the objective function value reached after satisfying the stopping criteria (e.g. the maximal number of functions evaluations allowed was 200) and the total CPU time, respectively. It can be seen that MIPT algorithm has reached the same average and best optimal values than SA and PSO, but requiring less CPU Time in average. In contrast, the GRAD method had the worse performance for the average and worst cases, which is due to the fact that the method got trapped into local minima, probably because of the random initialization that was done in order to provide a faire comparison. In this example, it has been shown that MIPT is also suitable for large-scale global dynamic optimization problems, which makes it a promising alternative for on-line optimizing control applications.

3.4. Chapter conclusion

In this chapter, a new stochastic algorithm for Global Optimization, denoted as Molecular-Inspired Parallel Tempering (MIPT) has been proposed combining the advantages of Monte Carlo methods (taking as a base the PT algorithm) and the basic principles of Molecular dynamics. It was shown that MIPT was capable to reach the global optima with a high success rate and a reasonable number of function evaluations for a wide range of problems, including constrained NLP, MINLP, dynamic optimization and problems with highly multimodal functions. Through six challenging case studies, the performance of MIPT was compared to well-established optimization algorithms, reaching the best performance in most of the cases and showing to be a very well suited method for solving global optimization problems. In fact, the excellent results in terms of number of function evaluations and in success rate for finding the global optimum, especially in the set of benchmark test functions with many local minima and in the dynamic optimization related case studies, are the main reasons why the MIPT is the algorithm used for solving the Dynamic Real-Time optimization problem that arises in the formulation of the Plantwide Optimizing Control procedure proposed in Chapter 5. Finally, it was also shown that the MIPT method was able to significantly improve the performance of the Parallel Tempering algorithm, especially in larger problems involving many local minima. This is mainly a result of the improved global character of MIPT over the original PT formulation, resulting in a more efficient algorithm very well suited for different types of Global Optimization problems.

4. Case Study: Continuous Bio-ethanol Production Process from Starch

In this chapter, a detailed description of the continuous bio-ethanol process form starchy raw materials is presented, including the dynamic model for each operating unit involved in the process. The dynamic model presented in Section 4.1 was implemented using Simulink as described in Section 4.2. It is important to mention that despite the fact that different steady state models and simulations for the bio-ethanol process have been already reported in the literature (**Kwiatkowski et al., 2006**; **Alvarado-Morales et al., 2009**), this is the first time that a completely rigorous dynamic model for the whole process is presented. The basic control loops in the process are also included in the model.

4.1. Process Description and Modeling

In this Section, the generalities and the dynamic model for the main operating units involved in the Bio-ethanol production process, namely the enzymatic hydrolysis, fermentation and the purification sections, are described.

4.1.1. Generalities

The purpose of this section is to present a complete description of the bio-ethanol process from starch-containing raw materials, which is the case study addressed in this work. In general the complete process involves five main unit operations: Milling, Enzymatic Hydrolysis, Fermentation, Ethanol Purification and DDGs (Distilled Dried Grains) drying, as shown in Figure 1.4. The purpose of milling is to break up the starchy raw material to an appropriate particle size, in order to facilitate the penetration of water during the hydrolysis stage. By means of the enzymatic hydrolysis, starch is depolymerized into its basic monosaccharide building blocks (glucose). During fermentation, certain microorganisms successfully transform glucose into ethanol as part of their metabolism. In the purification

section, ethanol is separated from all other components present in the fermentation broth, reaching a purity ≥ 99.8% wt (≥ 99.5% mol). The DDGs drying section removes water from the ethanol-free stream obtained at the bottom of the distillation column, producing a by-product that can be used as animal feed due to its high protein content (up to 30%). In this work, the milling and DDGs drying sections are not considered for plantwide control, because milling is only a grinding process that does not change the chemical structure of the raw materials (although the grain size may influence the efficiency of enzymatic hydrolysis of the raw material), and the DDGs unit is devoted to the post-processing of a byproduct (i.e. stillage), which is not taken into account in the profitability analysis in this work.

Figure 4.1 presents a flowsheet of the process considered, in which the feed to the process is a starch slurry stream (F_0) coming from the milling unit, and the end-product is fuel-grade ethanol (F_{20}). The by-products of the process are the *stillage* (B_1), which is a mixture of non-fermentable matter leaving the process at the bottom of the distillation column for being sent to the DDGs unit; and CO_2 (produced at the fermentation stage), which should be sent to a scrubber (via stream F_{18}). For simplicity, the local control loops are not shown in Figure 4.1, as they will be described in Section 6.1.1. It is possible to distinguish three main sections in the process, which correspond to the starch hydrolysis, fermentation, and purification sections. For the specific example addressed in Chapter 6, a nominal production of 100.000 ton ethanol/year (12.6 Ton/h for 330 days of operation during 24h/day) is considered, using a mash of starchy material as feed. The process design procedure, which is based on a sensitivity analysis, is described in detail in Appendix D.

As it can be seen in Figure 4.1, the process consists on the following main equipment:

- A liquefaction tank (R-101) and a saccharification tank (R-102), where the enzymatic conversion of the starch polysaccharide into glucose (monosaccharide) is carried out. These tanks belong to the section denoted as **Starch hydrolysis**.
- A fermentation tank (R-201), a biomass filter (F-201), a cells treatment tank (V-201) and a flash vessel (V-202), where the glucose fermentation to ethanol, as well as yeast separation, treatment and posterior recycle is carried out, and also CO_2 separation is done. These equipments correspond to the **Fermentation** section.
- A distillation column with reboiler and total condenser (T-301), a rectification column with reboiler and partial condenser (T-302) and the molecular sieves beds (T-303/ T-304), where ethanol purification and dehydration for reaching the fuel-grade ethanol is carried out. These equipments make up the **Purification** section.

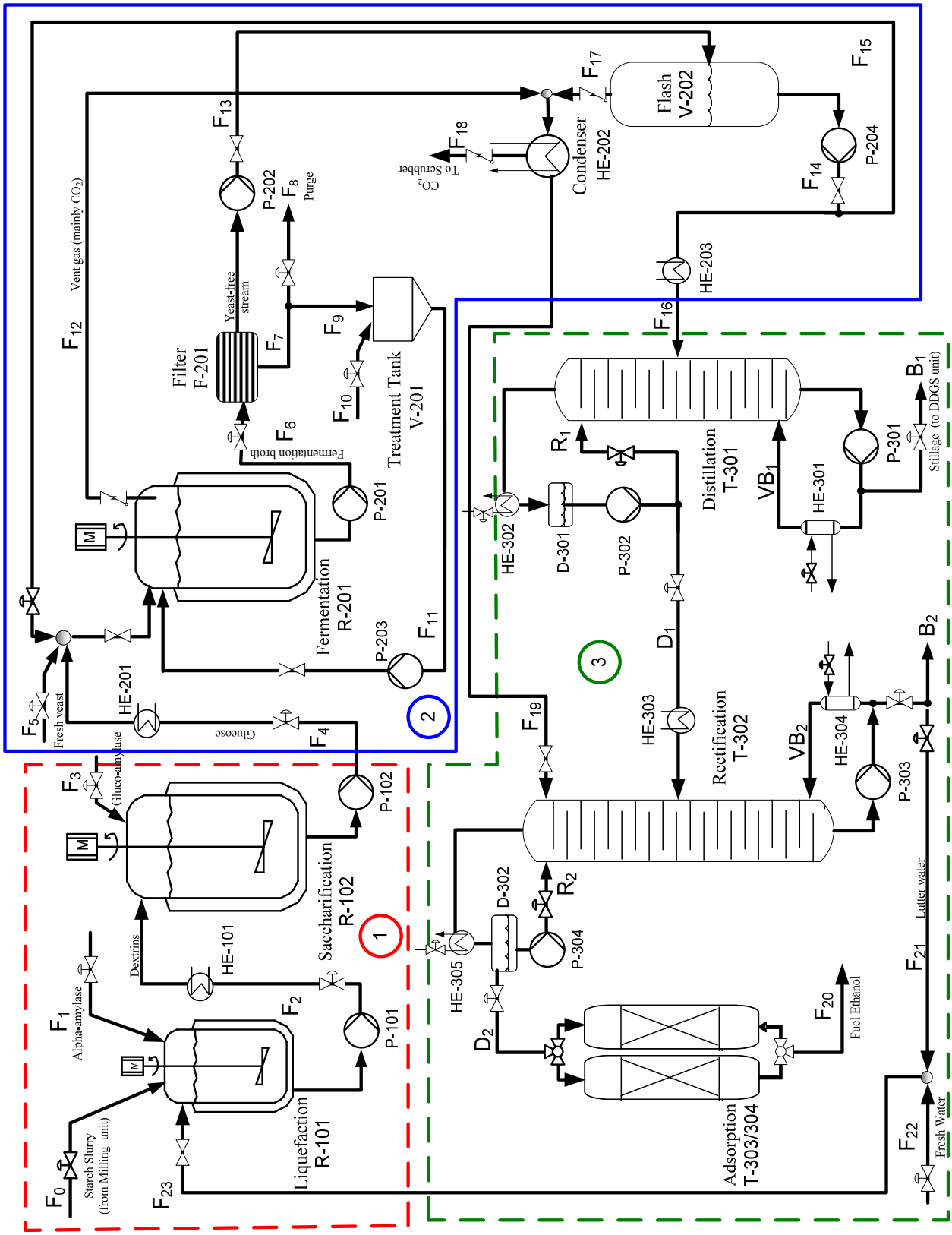

Figure 4.1 Flowsheet diagram for the continuous bio-ethanol production process from starch considered for plantwide control (control loops are not shown). 1- Enzymatic Starch hydrolysis (red region); 2- Fermentation (blue region), and 3-Purification (green region) Section.

Some of the most relevant characteristics of the bio-ethanol production process, that constitute a challenge when addressing the plantwide control problem, include:

- There is a high variability in the quality of the raw material.
- The main state variables in the process present a highly nonlinear behavior.
- The process may contain recycle loops. In the particular process flowsheet considered in this work, three different recycle loops are present. The first loop is the recycle of cells from the filter to the fermentor (F_{11}). The second loop is the recycle of the yeast-free stream from the bottom of the flash to the fermentor (F_{15}). Finally, the third loop is the recycle of lutter water from the bottom of the rectification column to the liquefaction tank (F_{21}). Due to the presence of these recycle loops the process has strong interactions between different units that makes difficult the control task.
- The biomass concentration in the fermentor must track its optimal value (as it will be explained in Section 6.1.1), which is a dynamic variable whose optimal value depends on the behavior of other state variables in the process.

In the following, a description of each stage involve in the continuous bio-ethanol production process is given, and the corresponding dynamic model is presented.

4.1.2. Starch Hydrolysis

4.1.2.1. Description

Starch is a combination of two polymeric carbohydrates called amylose and amylopectin. Amylose (Figure 4.2a) is constituted by glucose monomer units which are linked by $\alpha-1,4$ linkages. Amylopectin (Figure 4.2b) has a branched structure comprising the $\alpha-1,4$ glucosidic linkages as in the amylase, but also branches connected by $\alpha-1,6$ linkages. The ratio of amylose to amylopectin is characteristic for each starch source and has an impact on its gelatinization properties (e.g. gelatinization temperature range). Starches have the general formula $(C_6H_{10}O_5)_n$, where *n* is the total number of glucose monomer units (**Jacques et al., 2003**).

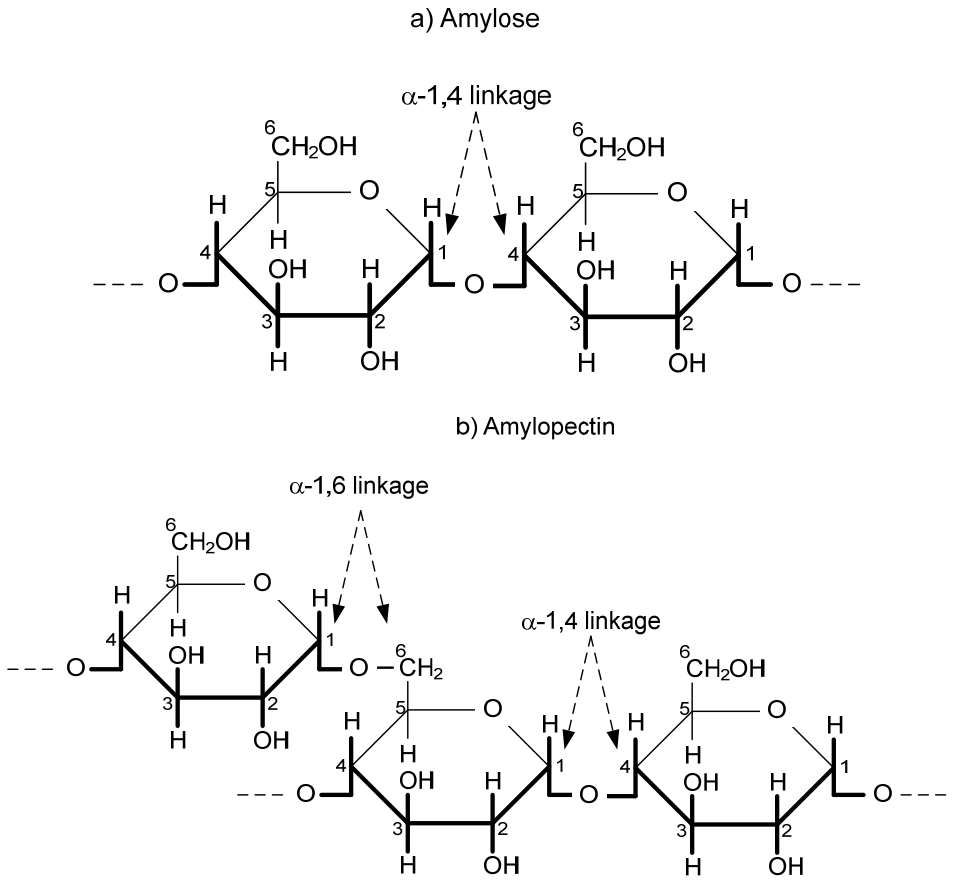

Figure 4.2 Polymeric components of starch: a) Amylose, b) Amylopectin.

In order to achieve the hydrolysis of the starch into fermentable sugars, the enzymatic hydrolysis of the starchy material is carried out in three stages, as follows:

- Gelatinization: The conversion of starch into fermentable sugars is accomplished by the action of the enzymes α-amylase and glucoamylase. However, in order for the α-amylase to access the starch molecules, the starch should be gelatinized. Gelatinization is a physical process in which a slurry of starch meal is solubilized in water by heating. This is sometimes referred as "cooking", and occurs at the gelatinization temperature, which can range from between 50°C – 120°C, depending on the starch source. In general, gelatinization temperatures for starch cereals are higher than those for root-starches (**Thomas and Atwell, 1999**). During this "cooking", the starch adsorbs water and swells, losing gradually its crystalline structure, making it susceptible to enzymatic attack. The starch gelatinization process is described by Equation (4.1).

$$\left[\left(C_6H_{10}O_5\right)_n\right]_{ungelatinized} \xrightarrow[H_2O]{\Delta} \left[\left(C_6H_{10}O_5\right)_n\right]_{gelatinized} \qquad (4.1)$$

- Liquefaction: During liquefaction, the α-1,4 linkages in amylose and amylopectin of the exposed starch molecules are broken down by the action of the endoenzyme α-amylase, resulting in shorter chains (oligosaccharides) called dextrins. Usually, maltose ($C_{12}H_{22}O_{11}$) is produced during this stage (as shown in Equation 4.2), but other dextrins such as maltotriose ($C_{18}H_{32}O_{16}$) can also be produced (see Equation 4.3).

$$2\left(C_6H_{10}O_5\right)_n + nH_2O \xrightarrow{\alpha-amylase} nC_{12}H_{22}O_{11} \quad (4.2)$$

$$3\left(C_6H_{10}O_5\right)_n + nH_2O \xrightarrow{\alpha-amylase} nC_{18}H_{32}O_{16} \quad (4.3)$$

  In the model developed in this work, the gelatinization and liquefaction stages are considered to be carried out in the same reactor, which corresponds to the liquefaction tank denoted as R-101 in Figure 4.1.

- Saccharification: In the saccharification stage (R-102 in Figure 4.1), the release of monosaccharides (individual glucose molecules) from the liquefied mixture of dextrins occurs. Saccharification is carried out by the action of the exoenzyme glucoamylase, which releases the single glucose ($C_6H_{12}O_6$) molecules by hydrolyzing both (although at different rate), the remaining α-1,4 linkages and the α-1,6 branch linkages. Dextrins (e.g. maltose or maltotriose) conversion to glucose during saccharification can be expressed by means of Equation (4.4) and (4.5):

$$C_{12}H_{22}O_{11} + H_2O \xrightarrow{Glucoamylase} 2C_6H_{12}O_6 \quad (4.4)$$

$$C_{18}H_{32}O_{16} + 2H_2O \xrightarrow{Glucoamylase} 3C_6H_{12}O_6 \quad (4.5)$$

  In general, depolymerization of starch into glucose (involving gelatinization-liquefaction-saccharification) can be expressed by Equation (4.6). Figure 4.3 shows typical operating conditions for the three main stages of starch hydrolysis (**Jacques et al., 2003**).

$$\underset{Starch}{(C_6H_{10}O_5)_n} + nH_2O \xrightarrow{Enzymes} n\underset{Glucose}{(C_6H_{12}O_6)} \tag{4.6}$$

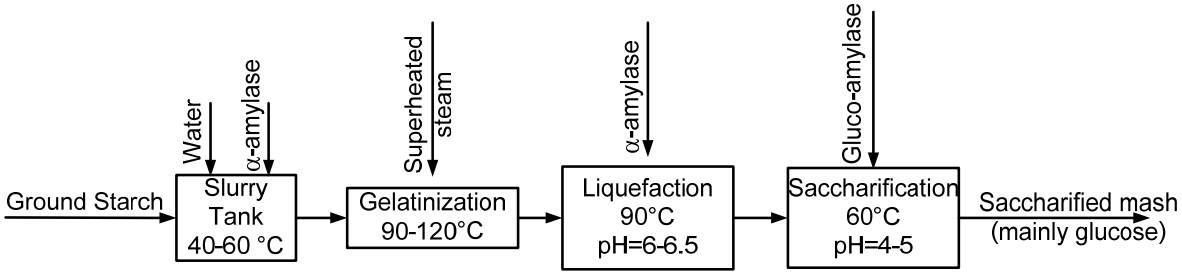

Figure 4.3 Typical block diagram and operating conditions of starch hydrolysis

Now that the generalities of the starch hydrolysis stage have been explained, in the next section, the dynamic model for this stage is presented.

4.1.2.2. Model

The model of the hydrolysis stage was developed according to the sketch shown in Figure 4.4 under the following assumptions:

- Gelatinization and liquefaction take place simultaneously in the liquefaction tank R-101.
- Saccharification takes place only in the saccharification tank R-102.
- The density is assumed to be constant and the same for all the streams.
- There is no thermal degradation of glucoamylase.
- Enzymatic action on gelatinized starch leads to the production of dextrins with a general formula $C_{18}H_{32}O_{16}$.
- Enzymatic action on dextrins leads only to the production of glucose.
- Temperatures in both vessels are assumed to be kept constant at their optimal values by using external heating and/or by manipulation of the cooling fluid passing through the jacket.
- Each vessel is considered to be ideally mixed.

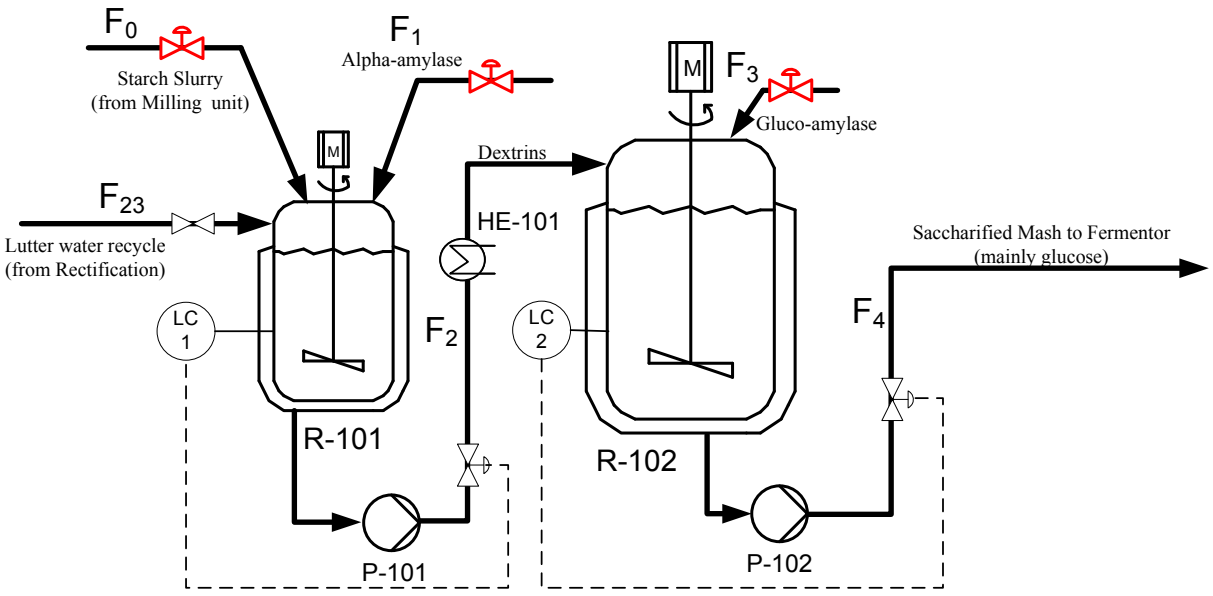

Figure 4.4 Starch hydrolysis section including level control loops (red valves indicate potential manipulated variables available).

Starch slurry containing ungelatinized starch (S_{ung}), water (w) and non-fermentable material (n_f), is fed into the liquefaction tank (through the feed stream F_0), in which gelatinization of S_{ung} into gelatinized starch (S_g) occurs simultaneously with the liquefaction of S_g into dextrins (m_{lt}) by the action of α-amylase (e_1). The model is derived from the mass balances for each state variable (S_{ung}, S_g, m_{lt}, e_1, w and n_f) in the liquefaction tank (represented by the sub-index L) as follows:

The mass balance for the ungelatinazed starch in the liquefaction tank ($S_{ung,L}$) is:

$$\frac{dS_{ung,L}}{dt} = \frac{F_0 S_{ung,0} - r_g V_L - F_2 S_{ung,L}}{V_L} - \frac{S_{ung,L}}{V_L}\frac{dV_L}{dt} \tag{4.7}$$

where F_0 is the starch slurry feed flow from the milling unit, $S_{ung,0}$ is the ungelatinized starch concentration coming on the feed stream, r_g is the gelatinization rate, V_L is the liquid volume in the Liquefaction tank, F_1 is the alpha-amylase feed flow rate and F_{23} is a recycle flow from the bottom of the rectification. F_2 is the output volumetric flow from the liquefaction tank, which is calculated according to the control law given by Equation (4.8).

$$F_2 = F_{2,ss} + K_c (H_L - H_{L,sp}) \tag{4.8}$$

$F_{2,ss}$ is the steady state value for F_2, K_c is the controller gain, and H_L and $H_{L,sp}$ are the measured level and level set point values, respectively.

A mass balance for the gelatinized starch in the liquefaction tank ($S_{g,L}$) is given by

$$\frac{dS_{g,L}}{dt} = \frac{r_g V_L - 0.9643 r_{mlt} V_L - F_2 S_{g,L}}{V_L} - \frac{S_{g,L}}{V_L}\frac{dV_L}{dt} \tag{4.9}$$

where the 0.9643 factor corresponds to the mass stoichiometric factor for gelatinized starch conversion into dextrins (kg dextrins/kg gelatinized starch), and r_{mlt} is the rate for dextrins production.

A mass balance for dextrins ($m_{lt,L}$) results in:

$$\frac{dm_{lt,L}}{dt} = \frac{r_{mlt} V_L - F_2 m_{lt,L}}{V_L} - \frac{m_{lt,L}}{V_L}\frac{dV_L}{dt} \tag{4.10}$$

From a mass balance for alpha-amylase ($e_{1,L}$),

$$\frac{de_{1,L}}{dt} = \frac{F_1 e_{1,1} - r_{de} V_L - F_2 e_{1,L}}{V_L} - \frac{e_{1,L}}{V_L}\frac{dV_L}{dt} \tag{4.11}$$

where $e_{1,1}$ is the alpha-amylase concentration in the diluted enzyme-feed stream F_1; and r_{de} is the enzyme deactivation rate.

A water mass balance is given by;

$$\frac{dw_L}{dt} = \frac{F_0 w_0 + F_{23} w_{23} + F_1 w_1 - F_2 w_L - 0.0357 r_{mlt} V_L}{V_L} - \frac{w_L}{V_L}\frac{dV_L}{dt} \tag{4.12}$$

where w_0 is the water content in the feed flow stream F_0, F_{23} is a mainly water content flow (i.e. it contains some ethanol traces), which results from a mixture of the recycle stream F_{21} (from the rectification bottoms') and a fresh water flow (F_{22}). w_1 is the water content in F_1, and the 0.0357 factor is the stoichiometric mass factor of water consumed (swelled) for

dextrins production (e.g. the amount of water consumed during liquefaction corresponds to a factor of 0.0357 kg water/kg dextrins).

The mass balance for the non-fermentable material ($n_{f,L}$) is given by;

$$\frac{dn_{f,L}}{dt} = \frac{F_0 n_{f,0} - F_2 n_{f,L}}{V_L} - \frac{n_{f,L}}{V_L}\frac{dV_L}{dt} \tag{4.13}$$

where $n_{f,0}$ is the concentration of non- fermentable material in the feed flow F_0.

Finally, Equation (4.14) describes the overall mass balance in the liquefaction tank:

$$\frac{dV_L}{dt} = F_0 + F_1 + F_{23} - F_2 \tag{4.14}$$

In general the volume of liquid in the reactors (V) is related to the level by the following expression:

$$V = A_T H \tag{4.15}$$

where A_T and H represent the cross section area of the tank and the level of liquid in the reactor, respectively.

The mathematical expressions for the reaction rates of starch gelatinization (r_g), dextrins production (r_{mlt}) and enzyme deactivation (r_{de}) involved in Equations (4.7 - 4.13) are given by Equations (4.16 – 4.18) respectively, which were taken from **Brandam et al. (2003)**. The parameters for these expressions are shown in Appendix C.1.

$$r_g = k_g \exp\left(-\frac{E_{ag}}{RT_L}\right) S_{ung,L} \tag{4.16}$$

$$r_{mlt} = k_{mlt}\left(\frac{e_{1,L} a_{act}}{\rho_L}\right) S_{g,L} \tag{4.17}$$

$$r_{de} = k_{de} \exp\left(-\frac{E_{ade}}{RT_L}\right) e_{1,L} \tag{4.18}$$

Parameters k_g, k_{mlt} and k_{de} are the kinetic constant for gelatinization, the kinetic factor for dextrins production, and the kinetic constant for alph-amyalse deactivation. E_{ag} and E_{ade} are the activation energies for gelatinization and enzyme denaturation, respectively. R, T_L, a_{act} and ρ_L are the universal gas constant, the liquefaction temperature, the specific alpha-amylase activity and the density of the liquid mixture in the liquefaction tank.

Next, the model of the saccharification tank is presented. The dextrins-rich stream F_2 is continuously fed to the saccharification tank, in which dextrins are converted into glucose (G) by the action of gluco-amylase (e_2). The mass balances for S_{ung}, S_g, e_1, n_f and e_2, are only affected by a dilution effect. The mass balance for ungelatinized starch in the saccharificator tank ($S_{ung,s}$) is:

$$\frac{dS_{ung,S}}{dt} = \frac{F_2 S_{ung,L} - F_4 S_{ung,S}}{V_S} - \frac{S_{ung,S}}{V_S}\frac{dV_S}{dt} \tag{4.19}$$

where F_4 is the output flow from the saccharification tank, calculated according to the control law given by Equation (4.20) and V_s is the liquid volume in the saccharification tank, which can be calculated from equation (4.21).

$$F_4 = F_{4,ss} + K_c (H_S - H_{S,sp}) \tag{4.20}$$

$$\frac{dV_S}{dt} = F_2 + F_3 - F_4 \tag{4.21}$$

The terms $F_{4,ss}$, H_s and $H_{S.Sp}$ in (4.20) correspond to the steady state value for F_4, the actual liquid level in the saccharification tank and its respective set point.

Mass balances in the saccharification for the gelatinized starch ($S_{g,s}$), alpha-amylase ($e_{1,s}$) and non- fermentables ($n_{f,s}$) are given by Equations (4.22-4.24).

$$\frac{dS_{g,S}}{dt} = \frac{F_2 S_{g,L} - F_4 S_{g,S}}{V_S} - \frac{S_{g,S}}{V_S}\frac{dV_S}{dt} \tag{4.22}$$

$$\frac{de_{1,S}}{dt} = \frac{F_2 e_{1,L} - F_4 e_{1,S}}{V_S} - \frac{e_{1,S}}{V_S}\frac{dV_S}{dt} \tag{4.23}$$

$$\frac{dn_{f,S}}{dt} = \frac{F_2 n_{f,L} - F_4 n_{f,S}}{V_S} - \frac{n_{f,S}}{V_S}\frac{dV_S}{dt} \tag{4.24}$$

The mass balance for glucoamylase in the saccharificator tank ($e_{2,s}$) is

$$\frac{de_{2,S}}{dt} = \frac{F_3 e_{2,3} - F_4 e_{2,S}}{V_S} - \frac{e_{2,S}}{V_S}\frac{dV_S}{dt} \tag{4.25}$$

where F_3 and $e_{2,3}$ are the glucoamylase feed flow and concentration, respectively.

The dynamics of the remaining state variables in the saccharificator tank is also affected by chemical reactions in addition to the dilution effect. The mass balance for the water in the saccharification (w_s) is represented by equation (4.26):

$$\frac{dw_S}{dt} = \frac{F_2 w_L + F_3 w_3 - F_4 w_S - 0.071\, r_{mlt,S}\, V_S}{V_S} - \frac{w_S}{V_S}\frac{dV_S}{dt} \tag{4.26}$$

where w_3 is the water content in stream F_3, and the 0.071 factor represents the water consumed during the saccharification for releasing glucose (0.071 kg water/kg dextrins). Therefore, the total water consumption in liquefaction and saccharification amounts to 0.1111 kg water/kg starch.

The mass balances for dextrins (m_{lts}) and glucose (G_s) in the saccharificator are given by equations (4.27) and (4.28):

$$\frac{dm_{lt,S}}{dt} = \frac{F_2 m_{lt,L} - F_4 m_{lt,S} - r_{mlt,S} V_s}{V_S} - \frac{m_{lt,S}}{V_S}\frac{dV_S}{dt} \tag{4.27}$$

$$\frac{dG_S}{dt} = \frac{1.071 r_{mlt,S} V_S - F_4 G_S}{V_S} - \frac{G_S}{V_S}\frac{dV_S}{dt} \tag{4.28}$$

where the 1.071 factor is the stoichiometric factor for dextrins conversion to glucose (1.071 kg of dextrins /kg glucose). The dextrins reaction rate in the saccharificator ($r_{mlt,S}$) is expressed by Equation (4.29) as reported by **Gonçalves et al. (2001)**:

$$r_{mlt,S} = \frac{k_3 e_{2,S} g_{act} m_{lt,S}}{k_m\left(1+\frac{G_S}{k_i}\right)+m_{lt,S}} \tag{4.29}$$

where g_{act} is the specific glucoamylase activity. k_3, k_m and k_i are the kinetic constant, Michaelis- Menten constant and product inhibition constant for dextrins consumption, respectively.

A final remark should be made regarding the saccharification step. Alternatively, the saccharification can be carried out simultaneously with the fermentation in the Simultaneous Saccharification Fermentation (SSF) process, whose main advantage is the reduction of the inhibition effect by high sugar concentration by adding the glucoamylase directly to the fermentor tank. **Ochoa et al. (2007, 2008)** developed and compared two different models (an unstructured and a cybernetic model) of the SSF process for ethanol production.

The next section to be described and modeled is the fermentation stage, which is composed of: the fermentation tank, a yeast filter, a yeast treatment tank and a flash vessel for carrying out a first purification stage for releasing the CO_2 produced in the fermentation, which was dissolved with the fermentation broth. Additionally, in Section 4.1.5 a degrees-of-freedom analysis for the whole process is presented.

4.1.3. Fermentation

4.1.3.1. Description

Conversion of glucose to ethanol is an exothermic reaction (enthalpy of reaction ~ -550 J/g glucose according to **Riva et al., 1998**) carried out by many types of yeast and by few bacteria. Yeasts are capable of using a wide variety of substrates (although most of these substrates belong to the hexoses family). In general they are able to grow and efficiently ferment ethanol at pH values of 3.5-6.0 and temperatures of 28-35°C. Yeasts, under anaerobic conditions, metabolize glucose to ethanol following the Embden – Merhof pathway (Figure 4.5). Yeasts in the genus *Saccharomyces* are responsible for almost all the current industrial production of alcohol by fermentation (**Roehr, 2001**). As a result of the fermentation process, 2 moles of Adenosine Triphosphate (ATP) are produced per mole of glucose metabolized, and the yeast cells use them mainly for growth. Although fermentation by *Saccharomyces* is an anaerobic process, a small concentration of oxygen must be

provided to the fermentation tank, as it is a necessary component in the biosynthesis of polyunsaturated fats and lipids. However, an excess in O_2 concentration will promote the use of ethanol as an additional substrate for the cells, further increasing cell growth but decreasing ethanol productivity. Besides the addition of a small amount of O_2, other components are required for an efficient fermentation, including some nutrients (i.e. compounds containing nitrogen, hydrogen and small quantities of phosphorus and potassium, between others) and vitamins like biotin.

Since the separation of ethanol from water accounts for much of the energy used in the overall production process, the higher the concentration of ethanol in the fermentor, the lower the purification costs per liter of product. However, there is a practical limit because ethanol is toxic to yeast cells at concentrations ranging between 8 and 18% by weight, depending on the strain of the yeast (**Glazer and Nikaido, 1994**). This phenomenon caused by an adverse effect of ethanol on the cell membranes is denoted as product inhibition. Above the inhibition concentration, a large number of ethanol molecules pass through the cell membrane and once inside the cell, they weaken the cell membrane structure allowing vital molecules, such as glucose, to leak out of the cells back into the medium. This effect is translated into a lower glucose metabolic rate and therefore, in a lower rate of ethanol production.

Fermentation is a very complex process in which many byproducts can be produced. In the case of fermentation by yeast (see Figure 4.5), in addition to ethanol and CO_2, it is possible to obtain glycerol, lactic acid, and fusel oil (higher alcohols). However, those components are not considered in this work, because its presence depends on the raw material used, the fermentation conditions (i.e. operating conditions and microorganism used, etc.) and, because usually their proportion to the other main components is minimal (**Reimelt et al., 2002**). For modeling purposes, in this work it is considered that the main reactions occurring during glucose fermentation by the action of the yeast *Saccharomyces cerevisiae* lead to the production of ethanol, CO_2 and also yeast growth, as follows:

$$C_6H_{12}O_6 \longrightarrow 2C_2H_5OH + 2CO_2 \tag{4.30}$$

$$C_6H_{12}O_6 \longrightarrow yeast \tag{4.31}$$

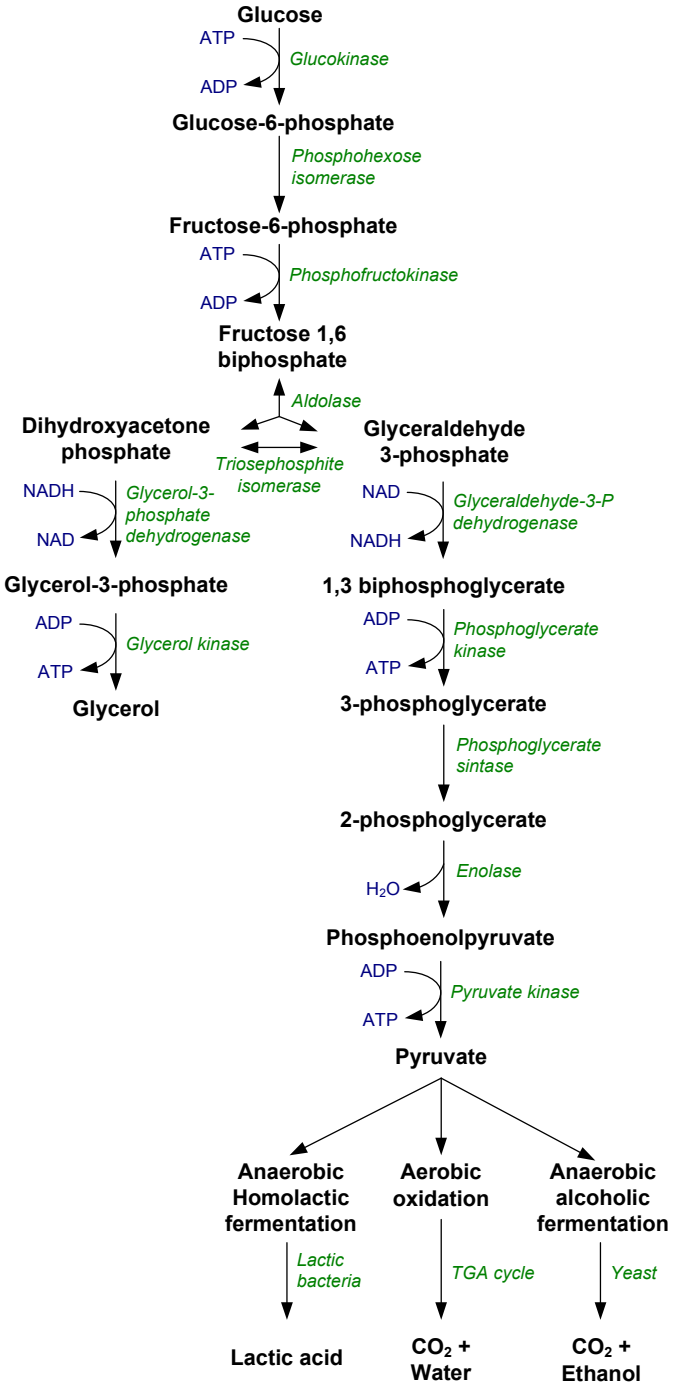

Figure 4.5 Embden-Meyerhof yeast metabolic pathway from glucose (**Jacques et al., 2003**; **Roehr, 2001**)

Equation (4.30) shows the stoichiometric reaction for the production of ethanol (C_2H_5OH) and CO_2, where the theoretical yield of ethanol from glucose ($C_6H_{12}O_6$) is 51.1%. On the other hand, Equation (4.31) represents the anaerobic production of yeast.

Over the years, several configurations of the fermentation stage have been tested for the production of ethanol in order to increase the productivity of the process. A review on the

different fermentation schemes was presented by **Maiorella et al. (1981, 1984)**, including batch, simple CSTR, CSTR with cells recycle, and schemes with selective ethanol removal (as the flash fermentation, extractive fermentation and selective membranes). The main disadvantages of the batch fermentation are its lower productivity, longer fermentation times and higher capital investment (**Reimelt, 2002**) when compared to the continuous schemes. In spite of the advantages of the continuous fermentation configurations in terms of productivity, some new plants are still being designed for batch production, especially due to the high risk of contamination. This main disadvantage of the continuous process can be overcome using a CSTR with cells recycle configuration, such as the technology used in the industrial Biostil® process (Chematur engineering, Sweden) (**Ehnström et al., 1991**). Yeast recycle increases the cell density, leading to a higher ethanol concentration and low substrate concentration in the fermentor (**Ehnström et al., 1991**; **Maiorella et al., 1984**). Another continuous fermentation technology of industrial use is the MULTICONT® process (Vogelbusch, Switzerland), in which a train of CSTR fermentors is employed.

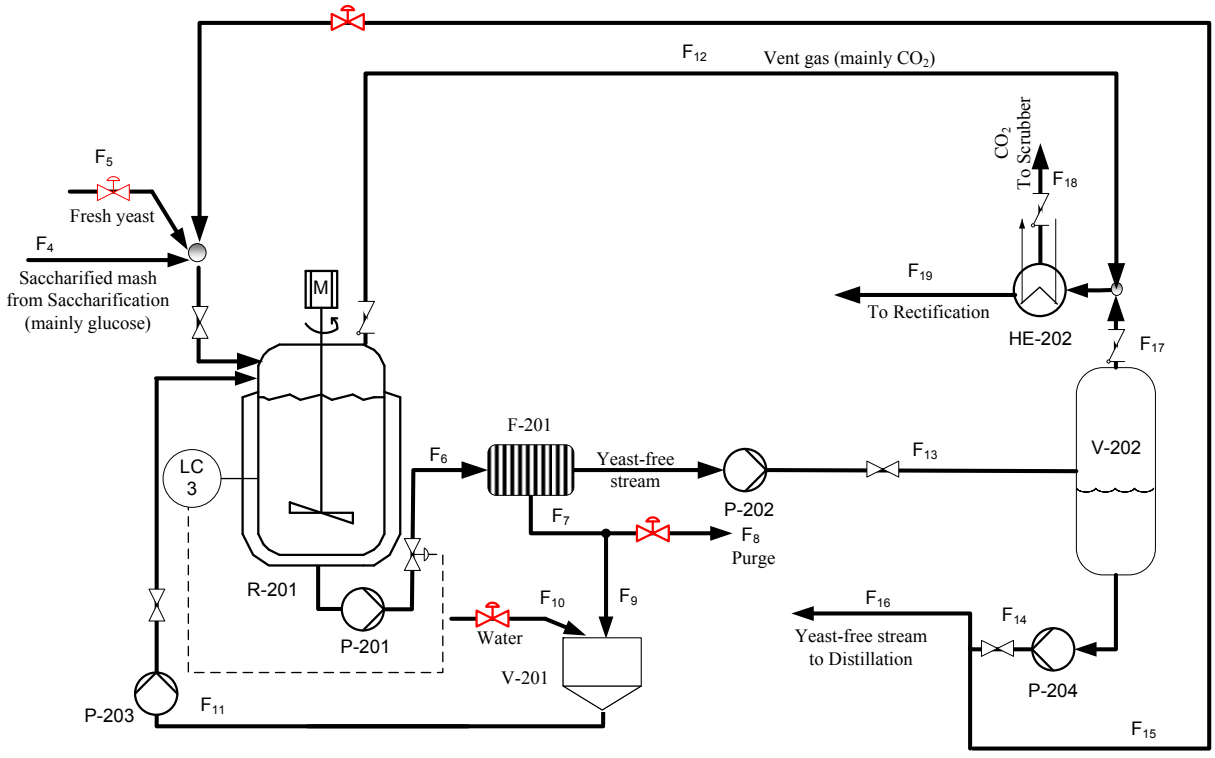

Figure 4.6 Continuous fermentation with cells recycle configuration: fermentor-yeast filter-yeast treatment tank-flash vessel. Valves in red correspond to potential manipulated variables. The dynamics of the filter, treatment tank, flash and condenser are neglected in the model (steady state).

The bio-ethanol process considered in this work is based on the continuous fermentation with cells recycle configuration, as shown in Figure 4.6. As it can be seen, a flash vessel is

also considered as part of the fermentation stage, which has two different tasks: first, the rapid extraction of ethanol for avoiding product inhibition, and second, the removal of the CO_2 still present in the process. Such scheme has been often denoted in the literature as extractive fermentation (**Da Silva et al., 1999**; **Costa et al., 2001**; **Meleiro et al., 2009**), but it should be noticed that it is not related to solvent extractive fermentation, which uses a liquid extractant for improving the removal of ethanol from the fermentation broth.

4.1.3.2. Model

The model was developed according the process shown in Figure 4.6, considering the following assumptions:

- The effect of nutrients and vitamins on the fermentation kinetics is neglected.
- The dynamics of the filter, treatment tank, flash and condenser are neglected as their dynamics are much faster than the dynamics in the fermentor (and also than the dynamics in other equipment involved in the whole process). Therefore those units were modeled at steady state.
- Although a typical yeast treatment tank includes the addition of sulfuric acid for adjusting pH, this is neglected in the model, and the treatment tank is just considered as a mixing tank for yeast recycle.
- The temperature in the fermentor is assumed to be kept constant at the optimal set point value (i.e. 32°C for the yeast to be used in the process[‡]). A typical control scheme uses the cooling flow rate through the jacket as manipulated variable for regulating the temperature.
- pH is assumed to be kept constant at the optimal set point value for the particular yeast strain.
- The density is assumed to be constant and the same for all the streams.
- The fermentor is an ideal continuous stirred tank reactor (CSTR).
- Ideal vapor-liquid equilibrium is assumed in the fermentor.
- For the operating conditions in the flash vessel, only ethanol, CO_2 and water are evaporated from the liquid feed stream.
- The filter involved in the yeast recycle loop, which in a real process consists on a bent-sieve for separation of the fiber, and a centrifuge for separating the yeast to be recycled, is assumed here as a filter in which only the yeast is retained to be

[‡] Optimal temperature and pH are factors that depend on the yeast strain and should be investigated for each particular case.

recycled, whereas all other components pass through the filter to the downstream section of the process.

The feed to the fermentation stage (stream F_4) is a saccharified mash containing mainly glucose (G), which is the only fermentable sugar considered. Fermentation is carried out by the action of the yeast *Saccharomyces cerevisiae* which can be fed to the fermentor through the fresh yeast stream (F_5) and/or the recycle stream (F_{11}). Total Biomass (X_t) comprises a viable (X_v) as well as a dead phase (X_d). The output stream of the bioreactor (F_6) is filtered for retaining all the yeast (viable and dead), which is then sent to the yeast treatment tank (F_9) and recirculated to the fermentor (F_{11}). The yeast-free stream (F_{13}) is fed to the flash vessel, where the remaining CO_2 is released. The stream from the bottom of the flash (F_{14}) is then sent to the distillation unit, with the possibility of being partially recirculated to the fermentor as stream F_{15}. The stream from the top of the flash (F_{17}) is mixed with the vapor output from the fermentor (F_{12}), and passed through a condenser, where water and ethanol are condensed and sent to the top of the rectification column (F_{19}), in the purification Section. The relevant state variables at this stage of the process are $X_{v,F}$,$X_{d,F}$, G_F, E_F and $CO_{2,F}$. The mass balances for the other variables (e.g. $S_{ung,F}$, $S_{g,F}$, $m_{lt,F}$, $n_{f,F}$, $w_{,F}$, $e_{1,F}$, $e_{2,F}$) are only influenced by the dilution effect and for that reason they are not shown here.

The mass balances for the viable ($X_{v,F}$), death ($X_{d,F}$) and total ($X_{t,F}$) biomass are presented in Equations (4.32) – (4.34).

$$\frac{dX_{v,F}}{dt} = \frac{F_{15}X_{v,15} + F_{11}X_{v,11} + F_5X_{v,5} - F_6X_{v,F} + r_XV_F - r_dV_F}{V_F} - \frac{X_{v,F}}{V_F}\frac{dV_F}{dt} \tag{4.32}$$

$$\frac{dX_{d,F}}{dt} = \frac{F_{15}X_{d,15} + F_{11}X_{d,11} - F_6X_{d,F} + r_dV_F}{V_F} - \frac{X_{d,F}}{V_F}\frac{dV_F}{dt} \tag{4.33}$$

$$\frac{dX_{t,F}}{dt} = \frac{dX_{v,F}}{dt} + \frac{dX_{d,F}}{dt} \tag{4.34}$$

where F_{15} is the recycle flow from the bottom of the flash, $X_{v,15}$ and $X_{d,15}$ are the viable and dead yeast concentrations in the recycle stream 15. F_{11} is the recycle flow from the yeast treatment tank and F_5 is the fresh yeast feed flow (which only contains viable yeast). F_6 is the output flow from the fermentor calculated according to the control law (4.35), where the

$F_{6,ss}$, H_F and $H_{F.Sp}$ terms correspond to the steady state value for F_6, the actual liquid level in the fermentor and its corresponding set point.

$$F_6 = F_{6,ss} + K_c\,(H_F - H_{F,sp}) \tag{4.35}$$

The liquid volume in the fermentor (V_F) can be calculated from the overall balance in the liquid phase given by Equation (4.36),

$$\frac{dV_F}{dt} = F_4 + F_5 + F_{11} + F_{15} - F_{12} - F_6 \tag{4.36}$$

The r_X and r_d variables in equations (4.32-4.34) are the biomass growth and death rates respectively, given by equations (4.37) and (4.38), as reported by **Costa et al. (2002)**:

$$r_X = \mu_{\max}\left(1-\left(\frac{E_F}{E_m}\right)^{A_1}\right)\left(1-\left(\frac{X_{t,F}}{X_m}\right)^{A_2}\right)\left(\frac{G_F X_{v,F}}{K_S + G_F}\right)\exp\left(-K_i G_F\right) \tag{4.37}$$

$$r_d = k_{dT}\exp\left(k_{dP}E_F\right)X_{v,F} \tag{4.38}$$

It is important to notice that although kinetic expressions (4.37) and (4.38) were taken from **Costa et al (2002)**, the parameters values used in this work (summarized in Appendix C.1) were identified as described in the Appendix C.2.

According to **Monbouquette (1987)**, when high-biomass-density fermentations with cell recycle processes are considered, it is necessary to take into account that the biomass volume fraction is not part of the reaction volume. Models including this effect are called intrinsic and have shown to provide a more accurate prediction of the substrate and product concentrations. Following the guidelines by Monbouquette, the balances for Glucose and Ethanol take into account the reaction volume correction $X_{t,F}/\gamma_x$, where γ_x is the ratio of dry weight cell per wet cell volume. Therefore, the Glucose (G_F) and Ethanol (E_F) mass balances in the bioreactor are given by:

$$\frac{dG_F}{dt} = \frac{\gamma_X \left(F_4 G_S + F_{15} G_{15} + F_{11} G_{11} - F_6 G_F - r_S V_F\right) + G_F \dfrac{dX_{t,F}}{dt} V_F}{V_F \left(\gamma_X - X_{t,F}\right)} - \frac{G_F}{V_F} \frac{dV_F}{dt} \tag{4.39}$$

$$\frac{dE_F}{dt} = \frac{\gamma_X \left(F_4 E_S + F_{15} E_{15} + F_{11} E_{11} - F_6 E_F - F_{12} E_{12} + r_P V_F\right) + E_F \dfrac{dX_{t,F}}{dt} V_F}{V_F \left(\gamma_X - X_{t,F}\right)} - \frac{E_F}{V_F} \frac{dV_F}{dt} \tag{4.40}$$

where G_{15}, E_{15}, G_{11} and E_{11} are the glucose and ethanol concentrations in the recycle streams 15 and 11 (G_{11}=0 and E_{11}=0, if a yeast filter with a 100% separation efficiency is assumed), respectively. r_S and r_p are the substrate consumption and ethanol production rates respectively, which according to **Costa et al. (2002)**, are given by equations (4.41) and (4.42).

$$r_S = \frac{r_X}{Y_{XS}} + m_X X_{v,F} \tag{4.41}$$

$$r_p = Y_{PX} r_X + m_P X_{v,F} \tag{4.42}$$

Finally, the mass balance for the CO_2 is given by (4.43).

$$\frac{dCO_{2,F}}{dt} = \frac{\dfrac{r_p w_{CO2} V_F}{w_E} + F_{15} CO_{2,15} + F_{11} CO_{2,11} - F_6 CO_{2,F} - F_{12} CO_{2,12}}{V_F} - \frac{CO_{2,F}}{V_F} \frac{dV_F}{dt} \tag{4.43}$$

where w_{CO2} and w_E are the CO_2 and ethanol molecular weight, respectively. F_{12} and $CO_{2,12}$ are the vent gas flow and carbon dioxide concentration in the vent gas from the fermentor.

Fermentation is a complex process involving living microorganisms which is still not completely understood. This makes modeling a challenging task, especially regarding the description of the reaction rates (r_X, r_p, r_S and r_d). Several kinetic models have been proposed in the literature but there is still no consensus on which of them is the best. In any case, a key factor for improving the modeling of the process has been the incorporation of substrate

and product inhibition effects into the growth kinetics (r_X). A comparison of different kinetic models proposed for the continuous ethanol production with cell recycle was presented by **Nishiwaki and Dunn (1999)**. In this work, the kinetic expressions (Equations 4.37, 4.38, 4.41, 4.42) used were taken from the model presented by **Costa et al (2002)**. The kinetic parameters were identified (see Appendix C.2) using experimental data reported by **Jarzebski et al. (1989)**.

Before concluding this section, a brief mention about the filter, yeast treatment tank and flash models should be done. First, since the dynamics of these equipments are much faster than the dynamics of the saccharificator, fermentor, distillation and rectification columns, they were simulated using steady-state models. In the case of the filter, the model used assumes a 100% efficiency for yeast separation (i.e. all yeast, including death cells, is retained in the filter). Therefore, yeast is only involved in the recycle loop to the fermentor (F_{11}), and not downstream. Additionally, as recommended by **Maiorella et al. (1984)**, the total biomass concentration in the recycle loop ($X_{t,11}$) should be kept at a convenient fixed value (which is done using a ratio control loop as explained in Section 6.1.1), for avoiding pumping problems if the viscosity of the recycled slurry is too high. A recycle biomass concentration of 180 kg/m^3 is set in order to calculate the ratio set point for keeping the viscosity of the biomass slurry in a suitable value. A purge stream (F_8) is also considered for avoiding accumulation of death cells in the fermentor.

A steady state mass balance for total biomass in the filter leads to

$$F_7 = \frac{F_6 (X_{v,F} + X_{d,F})}{\gamma_X} \tag{4.44}$$

whereas a total mass balance in the filter yields

$$F_{13} = F_6 - F_7 \tag{4.45}$$

Now, taking into account that part of F_7 is purged (through F_8) for avoiding dead biomass accumulation, the input flow to the yeast treatment tank (F_9) is calculated from a mass balance in the splitter

$$F_9 = F_7 - F_8 \tag{4.46}$$

Finally, a total mass balance in the treatment tank allows the calculation of the recycle flow from the treatment tank to the fermentor (F_{11}):

$$F_{11} = F_9 + F_{10} \tag{4.47}$$

where stream F_{10} is the flow of fresh water required to adjust the biomass concentration in the recycle loop. The flowrate F_{10} is determined by a ratio controller as described in Section 6.1.1.

The flash vessel operates under vacuum at the same temperature of the fermentor, separating a vapor mixture of ethanol, CO_2 and water from the liquid feed stream. The flash is modeled assuming non-ideal vapor-liquid equilibrium. The Antoine parameters correspond to those reported by **Gmehling et al. (1990)**, whereas the activity coefficients were taken from **Wang et al. (2007)**.

The steady state balance equations in molar flow rates for the flash vessel (including the condenser) are presented next. From a total balance in the flash

$$F_{14} = F_{13} - F_{17} \tag{4.48}$$

where F_{13} and F_{17} are the flash feed molar flow and the vapor output flow, respectively.

A mass balance for CO_2 in the flash yields the following equation:

$$F_{17} = F_{13} \frac{y_{CO2,13}}{y_{CO2,17}} \tag{4.49}$$

where CO_2 is considered to be the only non-condensable component.

A mass balance for CO_2 in the condenser leads to

$$F_{18} = y_{CO2,12} F_{12} + y_{CO2,17} F_{17} \tag{4.50}$$

Equation (4.51) and (4.52) are obtained from the vapor-liquid equilibrium of ethanol and water in the flash vessel.

$$y_{E,17} = x_{E,14}\gamma_E \frac{P_{vE}}{P_{flash}} \tag{4.51}$$

$$y_{w,17} = x_{w,14}\gamma_w \frac{P_{vw}}{P_{flash}} \tag{4.52}$$

where *y* and *x* represent mole fractions in the vapor and liquid phases of the each stream, respectively. γ_E and γ_w are the activity coefficients for ethanol and water respectively. P_{vE} and P_{vW} are the vapor pressures for ethanol and water, and P_{flash} is the pressure in the flash vessel.

Now, from the summation equation, the molar fraction of CO_2 in the vapor is obtained

$$y_{CO2,17} = 1 - y_{E,17} - y_{w,17} \tag{4.53}$$

Now, from an ethanol mass balance in the flash, Equation (4.54) is obtained,

$$x_{E,14} = \frac{F_{13}x_{E,13} - F_{17}y_{E,17}}{F_{14}} \tag{4.54}$$

and from the summation of fractions in the liquid phase in the flash:

$$x_{w,14} = 1 - x_{E,14} - \sum_{i \neq w,E} \frac{F_{13}x_{i,13}}{F_{14}} \tag{4.55}$$

where *i* accounts for all other components different than ethanol and water (e.g. glucose, starch and non-fermentable material).

Now, from a total balance in the splitter at the flash bottom:

$$F_{16} = F_{14} - F_{15} \tag{4.56}$$

and from a total balance in the condenser:

$$F_{19} = F_{17} + F_{12} - F_{18} \tag{4.57}$$

Finally, the vapor pressure for each component is obtained from Antoine's Equation:

$$P_{vi} = \frac{10^{A_i - \frac{B_i}{T_{flash} + C_i}}}{760} \tag{4.58}$$

4.1.4. Purification Section

In this section, the last stage in the bio-ethanol continuous process from starch is described, namely, the purification section, which comprises distillation, rectification and adsorption by molecular sieves. First a general description is given, and then the dynamic model for the columns and the sieves bed is developed.

4.1.4.1. Description

Over the years, many different downstream purification technologies have been proposed for ethanol dehydration, in order to obtain the desired purity for using it as a fuel (i.e. >99.8% wt.). Since the ethanol-water mixture forms an azeotrope at around 95.5% wt. of ethanol at a pressure of 1.013 bar (with a boiling point of 78.2°C), distillation at reduced pressure is not economically viable for reaching fuel grade purity. In the beginnings of the bio-ethanol industry, the preferred method for separating the ethanol-water mixture was azeotropic distillation (AD) which involves the addition of a third volatile component (usually benzene or cyclohexane) to form a ternary azeotrope at a more convenient composition. The high energy requirements, large capital costs and health and safety concerns of AD have widely reduced the application of this technique in the bio-ethanol industry. Over the years AD has been replaced by extractive distillation (ED) and adsorption technologies. In ED, a third component (solvent) is also involved, which increases the relative volatility of the components to be separated without forming a ternary azeotrope as is the case in AD. Different solvents have been reported in the literature of ethanol purification by ED, ranging from liquid solvents like ethylene glycol, to dissolved salts such as potassium and sodium acetate, to hyperbranched polymers, and many others. On the other hand, adsorption using molecular sieves is the technology most widely used today for ethanol dehydration. In this

case, the ethanol-water mixture at a composition close to the azeotrope is passed through a bed of zeolites in which the water is trapped and adsorbed whereas the ethanol molecules flow around them, as a consequence of the different size of ethanol and water molecules, 4.52 Å and 1.23 Å, respectively (**Daubert et al., 1989**). Other technologies that have been proposed for ethanol purification include membrane pervaporation and Pressure Swing Distillation (PSD). Pervaporation involves the preferential passage of ethanol through a dense membrane matrix. However, systems involving membrane separation have not been industrially applied because they are claimed to have low maximal capacity and high replacement costs, which impact negatively the economy of the process (**Szitkai et al., 2002**). On the other hand, pressure swing distillation has been recently evaluated and reported to result in a 44% of the reduction costs in the downstream process, by taking advantage of heat integration between the high and low pressure columns (**Arifeen et al., 2007**). However, industrial applications of PSD in the bio-ethanol process have not been reported yet. A more detailed description of these technologies can be found in the works by **Huang et al. (2008)** and **Vane (2008)**. Independently of the technology used, a typical purification section in a bio-ethanol production plant includes a first distillation step (usually two or more columns, including rectification) obtaining an ethanol concentration below the azeotrope. In this work, the configuration of the purification stage (which is currently the preferred configuration in Europe) includes: distillation, rectification and molecular sieves adsorption, as shown in Figure 4.7.

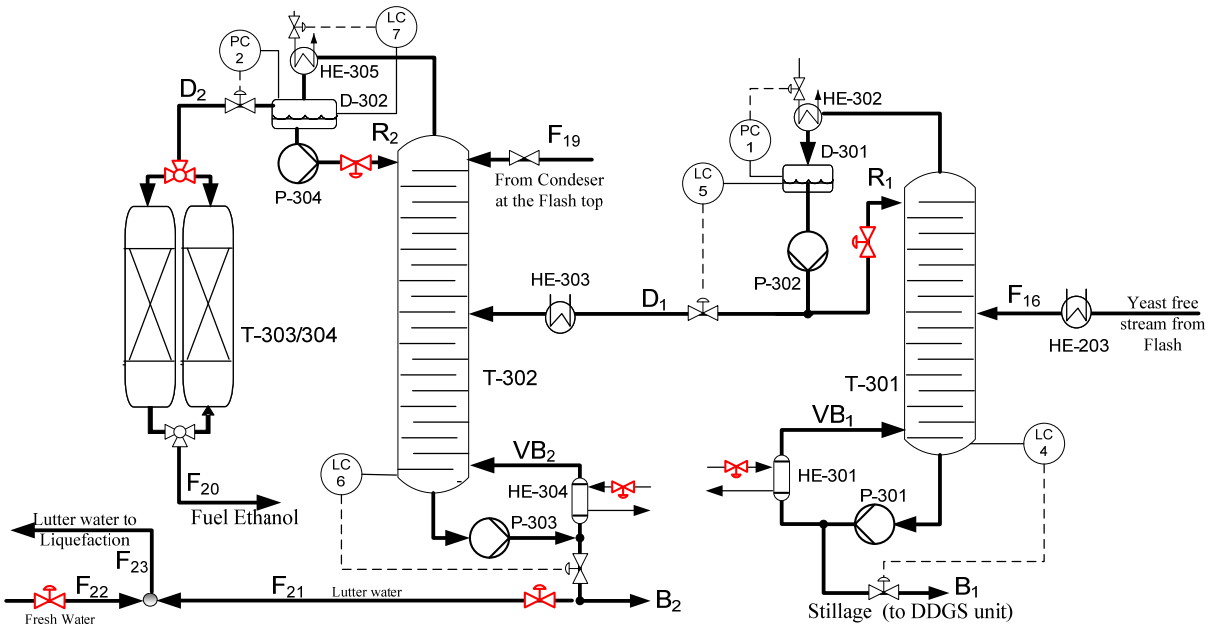

Figure 4.7 Purification section configuration including level and pressure control loops for the distillation and rectification columns (red valves indicate potential manipulated variables)

The feed to the purification stage comes from the flash through two different streams. The main stream (F_{16}), fed to the distillation (beer) column, is a liquid phase stream coming from the bottom of the flash with an ethanol purity of around 4% - 8% wt. The second feed stream (F_{19}) enters directly into the top of the rectification column, as this is a higher ethanol concentration stream (>60% wt.) coming from the top of the flash after passing the condenser where the CO_2 is completely released. The purpose of the first distillation column is to separate the heavy components and some water from a volatile water-ethanol mixture vapor stream leaving the column at the top. Depending on the yeast strain used in the fermentation, fusel oil (i.e. a mixture of higher alcohols) may also be produced, which can be separated as a side-stream in the distillation column. The purpose of the rectification column is to obtain an ethanol-water mixture close to the azeotropic composition. The coupling of distillation and rectification at different operating pressures, mainly vacuum-atmospheric (or higher) respectively, has been identified as an excellent alternative for saving steam consumption in the purification section (**Dias et al., 2009b**; **Reimelt et al., 2002**). In this work, the distillation column has been considered to operate under vacuum (0.3 atm) whereas the rectification column operates at atmospheric pressure. Besides the operating pressures, distillation and rectification columns differ mainly in the number of trays and the type of condenser used. In the distillation case, a lower number of trays may be required and a total condenser is used. In the rectification, a partial condenser is used because the feed to the molecular sieves should be a vapor stream. In order to obtain the required fuel-grade ethanol purity, usually two or more zeolite-type molecular sieves beds are used for adsorption of water (one bed is used for adsorbing the water while the others are regenerated). For simulation purposes, in this work only the model for adsorption is considered. Regeneration of the bed is assumed to take place at a predetermined frequency, resulting in a return of the bed to its initial state (i.e. water-free). Finally, the bottom of the rectification column is partially recirculated to the liquefaction section (through stream 23), in order to reduce the fresh water consumption in the process (**Reimelt, et al., 2002**). In the following, the dynamic model of the purification section is presented.

4.1.4.2. Model

The purification Section shown in Figure 4.7 is modeled considering the following assumptions:

- Perfect mixing in the liquid hold-up of each tray.
- Non-ideal vapor-liquid equilibrium in each tray, described by the UNIQUAC model.
- Negligible vapor hold-up.

- No energy losses from the columns.
- Negligible heat capacity of the trays and columns construction material.
- Total condenser without sub-cooling in the distillation column. Partial condenser in the rectification column.
- The distillation column is modeled as a ternary system: water, ethanol and a heavy phase (containing glucose, starch, non-fermentable matter and all other non-volatile components). The rectification column is modeled as binary ethanol-water system.
- Constant pressure drop across the trays.

Distillation Column

The model for the distillation columns comprises the equations for each tray, the reboiler and for condenser. The trays are numbered from the reboiler ($i = 1$) to the condenser ($i = N_t$). At each tray, the compositions for each component ($j = 1$ to N_c) in both phases, temperature, liquid hold-up, and vapor and liquid flows are calculated.

1. Trays model: For any tray in the column (Figure 4.8), different from the reboiler and condenser, the dynamic model is described by the following equations:

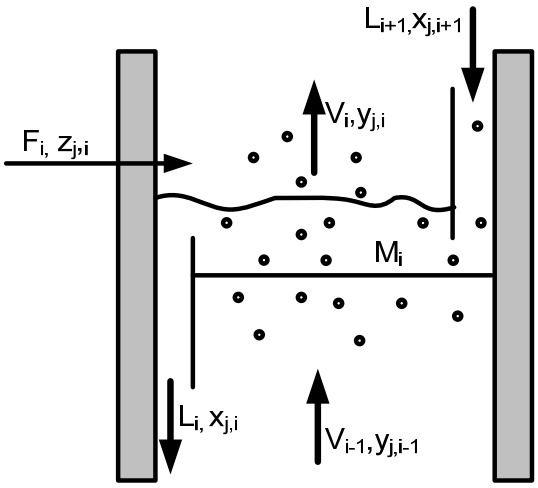

Figure 4.8 Schematic representation of a distillation column tray

Overall mass balance for tray i (for $i \neq 1, N_t$)

$$\left(\frac{dM_i}{dt}\right) = L_{i+1} - L_i + V_{i-1} - V_i + F_i \qquad (4.59)$$

Mass balance for component j (for j =1,2,…,N_c)

$$\left(\frac{d\left(M_i x_{j,i}\right)}{dt}\right) = L_{i+1}x_{j,i+1} - L_i x_{j,i} + V_{i-1}y_{j,i-1} - V_i y_{j,i} + F_i z_{j,i} \qquad (4.60)$$

where the Vapor flow rate (V_i) leaving tray i is given by:

$$V_i = V_{i-1} + F_i(1-q_i) + r_{evap,i} \qquad (4.61)$$

where the first term account for the vapor flow rate coming from below (V_{i-1}), the second term is the vapor coming with the feed stream to the tray where q_i is the liquid fraction in the feed flow, and the last term ($r_{evap,i}$) represents the evaporation rate (or vapor absorption rate) on tray i. According to **Beverley et al. (1999)**, the evaporation/absorption rate depends on the pressure and temperature conditions of the system and the molecular weight. For a multicomponent mixture, the evaporation rate on tray i can be expressed as follows:

$$r_{evap,i} = \frac{1}{3600}\cdot\sum_{j=1}^{Nc}\left[\sqrt{\frac{1}{2\pi w_j RT_{t,i}}}A_j\left(P_{vj,i} - P_{t,i}\right)\right] \qquad (4.62)$$

where $r_{evap,i}$ is given in kmol/h, $P_{vj,i}$ is the vapor pressure of pure component j in tray i (in Pa), $P_{t,i}$ is the pressure at tray i (in Pa), w_j is the molecular weight of component j (in kg/kmol), R is the universal gas constant (=8314 in J/kmolK), $T_{t,i}$ is the temperature at tray i and A_j is the tray area covered by component j, which is calculated according to Equation (4.63). If $P_{v,ji} > P_{t,i}$, evaporation of component j occurs whereas, in the contrary case, component j is absorbed by the liquid phase.

$$A_j = A_{tray}\cdot\frac{a_j x_j}{\sum_{k=1}^{Nc} a_k x_k} \qquad (4.63)$$

where A_{tray} is the tray wet area, a_j is the molecular area of component j, x_j is the mole fraction of component j in the liquid phase.

The liquid flow rate leaving each tray in kmol/h, neglecting the contribution of weeping, is calculated according to the Francis-weir formula (**Vora and Daoutidis, 2001**):

$$L_i = \frac{774\rho_{l,i}\left(v_{l,i} - v_{weir,i}\right)^{1.5}}{w_{l,i}} \tag{4.64}$$

where $v_{l,i}$ and $v_{weir,i}$ are the volume of liquid (in m^3) and the weir volume (in m^3) in tray *i*, respectively. Therefore, $v_{l,i}$ - $v_{weir,i}$ represents the volume of liquid over the weir. $\rho_{l,i}$ is the density of the liquid mixture in tray *i* in kg/m^3, and $w_{l,i}$ is the average molecular weight of the liquid in tray *i* in kmol/kg.

Assuming thermodynamic equilibrium between the liquid and vapor phases, the vapor compositions $y_{j,i}$ (component *j* on tray *i*) are calculated as:

$$y_{j,i} = x_{j,i} \cdot \left(\frac{\gamma_j P_{v,j}}{\sum_{k=1}^{Nc} x_k \gamma_k P_{v,k}} \right)_i \tag{4.65}$$

The activity coefficients γ_j and the vapor pressures were calculated using the UNIQUAC model and the Antoine Equation, respectively. The equations and parameters used in the VLE model are shown in the Appendix C.3.

Finally, the sum of fractions in both phases must be equal to unity:

$$\sum_{j=1}^{Nc} x_{j,i} = 1; \ \sum_{j=1}^{Nc} y_{j,i} = 1; \tag{4.66}$$

The energy balance at tray *i* is given by:

$$\left(\frac{d\left(M_i h_{l,i}\right)}{dt} \right) = L_{i+1}h_{l,i+1} - L_i h_{l,i} + V_{i-1}h_{v,i-1} - V_i h_{v,i} + F_i q h_{l,i} + F_i(1-q)h_{v,i}$$

(4.67)

where h_l and h_v are the enthalpies for the liquid and vapor on tray i, given by Equations (4.68) and (4.69), respectively.

$$h_{l,i} = \sum_{j=1}^{Nc} x_j h_{lj,ref} + \sum_{j=1}^{Nc} x_j \int_{T_{ref}}^{T_{t,i}} C_{pl,j} dT \tag{4.68}$$

$$h_{v,i} = \sum_{j=1}^{Nc} y_j h_{lj,ref} + \sum_{j=1}^{Nc} y_j \int_{T_{ref}}^{T_{t,i}} C_{pl,j} dT + \sum_{j=1}^{Nc} y_j \lambda_j^{T_{t,i}} \tag{4.69}$$

where $h_{lj,ref}$ is the enthalpy of liquid of component j at the reference temperature, $C_{pl,j}$ is the molar heat capacity of component j in the liquid phase, and $\lambda_j^{Tt,i}$ is the molar enthalpy of evaporation of component j at temperature $T_{t,i}$. The expressions for calculating the molar heat capacity and the molar enthalpy of evaporation for each pure component as a function of temperature are given in Appendix C.3.

Since a constant pressure drop across each tray has been assumed, the pressure at each tray is calculated as:

$$P_{t,i} = P_{top} + (N_t - i)\Delta P_t \tag{4.70}$$

where P_{top} is the pressure at the top of the column (pressure in the condenser) and N_t is the total number of trays in the column. The trays are numbered from the bottom (i = 1) to the top (i = N_t).

2. Reboiler model: The reboiler is modeled as an equilibrium stage, and it is considered to include the bottom of the column, as shown in Figure 4.9.

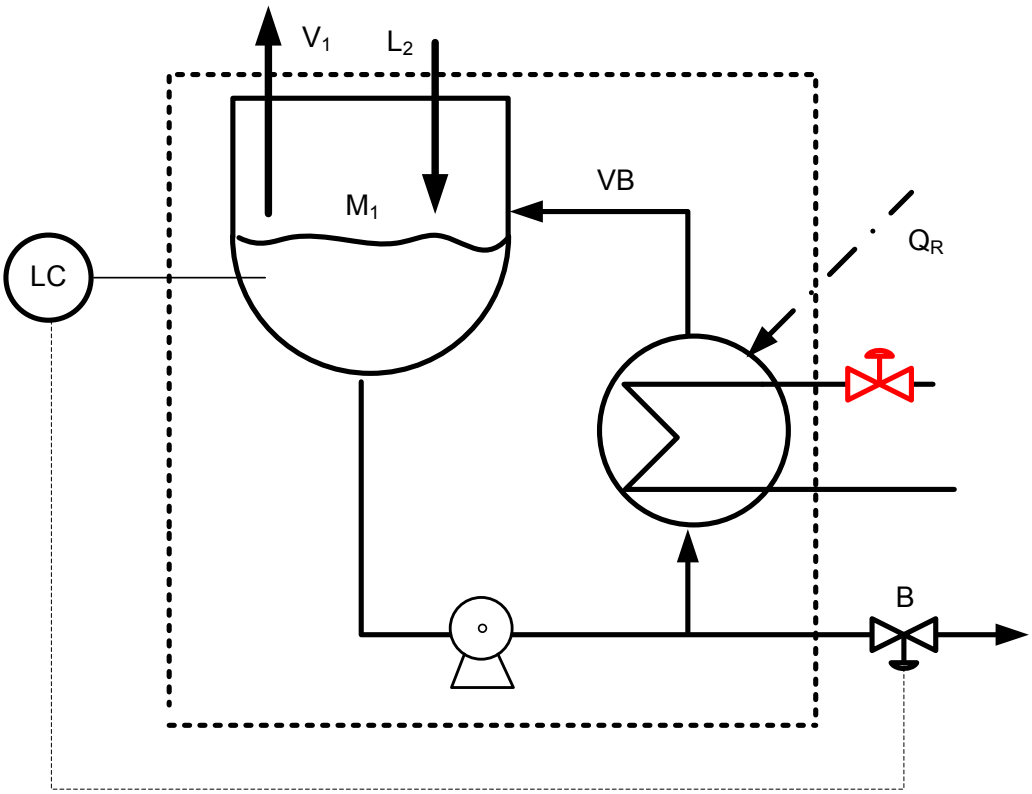

Figure 4.9 Schematic representation of the reboiler section including level control

The reboiler model comprises the mass and energy balances as well as the VLE model described in Appendix C.3. The total mass balance is written as:

$$\frac{dM_1}{dt} = L_2 - V_1 - B \tag{4.71}$$

The balance for component *j* is:

$$\frac{d\left(M_1 x_{j,1}\right)}{dt} = L_2 x_{j,2} - V_1 y_{j,1} - B x_{j,1} \tag{4.72}$$

The calculation of the thermodynamic equilibrium is done using equation (4.65) as in the case for the tray model. Also the summation equation (4.66) is required.

The energy balance is given by:

$$\frac{d\left(M_1 h_{l,1}\right)}{dt} = L_2 h_{l,2} - V_1 h_{v,1} - B h_{l,1} + Q_R \tag{4.73}$$

where heat losses from the column have been neglected.

The reboiler duty (Q_R) is equal to the enthalpy increase of the boil-up as a result of evaporation:

$$Q_R = \lambda_1 \, VB \tag{4.74}$$

where λ_1 is the heat of vaporization of the mixture at the bottom of the column, and is a function of temperature and composition (see Equation C.12 in Appendix C.3)

In addition, the following equality holds:

$$V_1 = VB \tag{4.75}$$

Finally, as shown in Figure 4.9, the level at the bottom of the column (H_B) is controlled by manipulating the bottoms flow rate B, as a function of the error between the measured level (H_B) and the desired set point value ($H_{B,sp}$).

$$B = Kc \left[(H_B - H_{B,sp}) + \frac{1}{\tau_I} \int (H_B - H_{B,sp}) \, dt \right] \tag{4.76}$$

where K_c and τ_I are the gain and integral time of a PI controller.

4. Condenser model: The condenser is modeled as an equilibrium stage, including the reflux drum as depicted in Figure 4.10. For the distillation column, a total condenser without sub-cooling is considered.

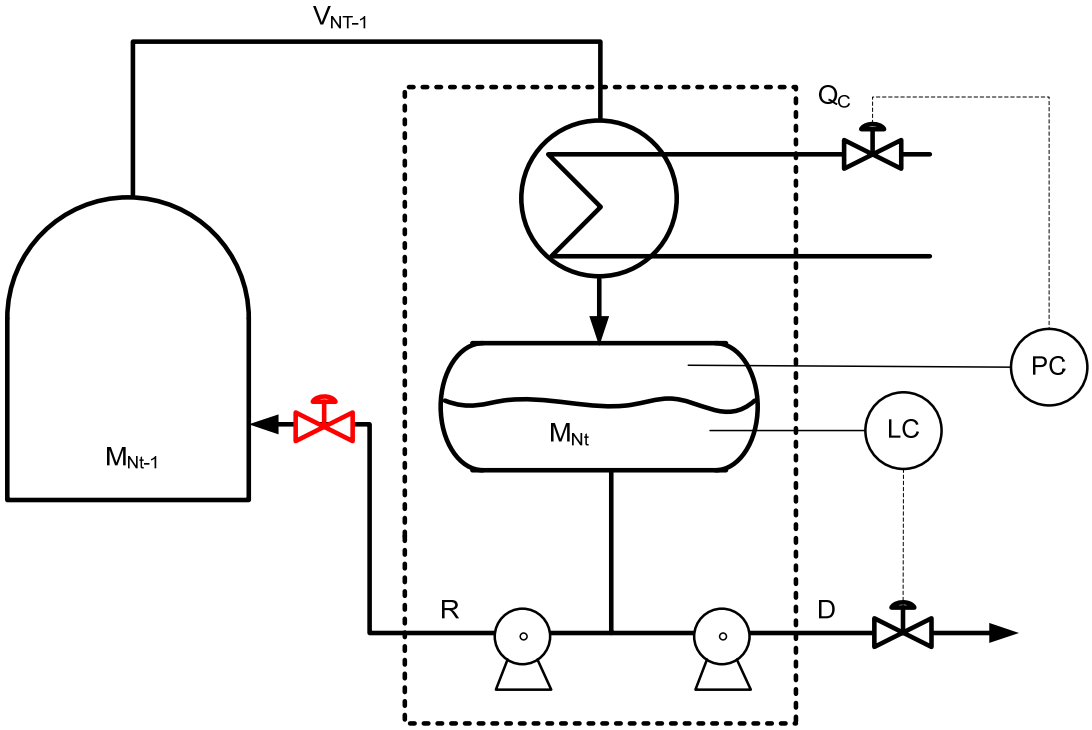

Figure 4.10 Schematic representation of the condenser section for the distillation column including level and pressure control

The mass balance around the condenser is expressed as:

$$\frac{dM_{Nt}}{dt} = V_{Nt-1} - R - D \tag{4.77}$$

The balance for component j in the condenser is:

$$\frac{d\left(M_{Nt}x_{j,Nt}\right)}{dt} = V_{Nt-1}y_{j,Nt-1} - Rx_{j,Nt} - Dx_{j,Nt} \tag{4.78}$$

Again, the calculation of the thermodynamic equilibrium is done using equation (4.65) and the mole fraction summation using equation (4.66) as in the case of the tray model.

The energy balance is given by:

$$\frac{d\left(M_{Nt}h_{j,Nt}\right)}{dt} = V_{Nt-1}h_{v,Nt-1} - Rh_{l,Nt} - Dh_{l,Nt} - Q_c \tag{4.79}$$

where the heat losses were neglected.

Since the condenser duty determines the vapor hold-up at the top of the column, it is possible to control the pressure of the column by manipulating the condenser duty, as it is shown by the pressure loop in Figure 4.10. For the purpose of controlling the pressure, the condenser duty (Q_C) is calculated according to the following control law:

$$Q_c = \lambda_{Nt-1} V_{Nt-1} + Kc \left[(P_{top} - P_{top,sp}) + \frac{1}{\tau_I} \int (P_{top} - P_{top,sp})\, dt \right] \tag{4.80}$$

where the first term in equation (4.80) is a feedforward compensation, whereas the second term is a feedback action calculated as a function of the error between the measured pressure (P_{top}) and its corresponding set point value ($P_{top,\,sp}$).

Finally, level control in the reflux drum can be implemented by manipulating the distillate (D) or reflux (R) rates. In this work, the distillate flow rate is used for controlling the level (H_D) at the reflux drum in the distillation column; therefore, D is calculated as a function of the error between the measured level value (H_D) and its set point ($H_{D,sp}$):

$$D = D_{ss} + Kc \left[(H_D - H_{D,sp}) + \frac{1}{\tau_I} \int (H_D - H_{D,sp})\, dt \right] \tag{4.81}$$

where D_{ss} is the value of the distillate flow at steady state.

Rectification Column

The model for the rectification column is similar to that presented for the distillation column. The basic differences are:

- In the rectification, a second liquid feed stream is fed to the top of the column (tray N_t-1)
- The condenser is partial.
- A different control scheme for the reflux drum is used.

As the main differences are at the top of the column, only the model of the condenser (including reflux drum) will be described. The model is based on the scheme presented in Figure 4.11.

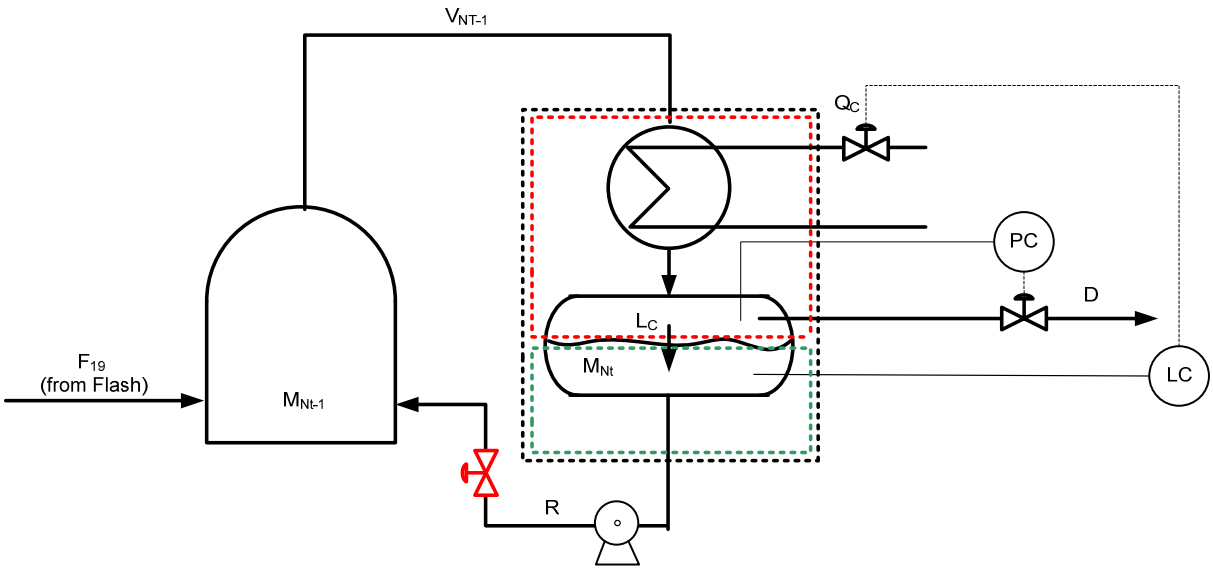

Figure 4.11 Schematic representation of the condenser section for the rectification column including level and pressure control

The balances around the dotted black region in Figure 4.11 are given by:

$$\frac{dM_{Nt}}{dt} = V_{Nt-1} - R - D \tag{4.82}$$

$$\frac{d\left(M_{Nt}x_{j,Nt}\right)}{dt} = V_{Nt-1}y_{j,Nt-1} - Rx_{j,Nt} - Dy_{j,Nt-1} \tag{4.83}$$

$$\frac{d\left(M_{Nt}h_{j,Nt}\right)}{dt} = V_{Nt-1}h_{v,Nt-1} - Rh_{l,Nt} - Dh_{v,Nt-1} \tag{4.84}$$

The thermodynamic equilibrium is calculated according to Equation (4.65). Also the summation Equation (4.66) is required for solving the model.

As in this case the distillate flow rate (D) is a vapor stream, it has no effect on the level (H_D) at the reflux drum. Therefore, the level in the reflux drum can only be controlled by manipulating the reflux rate (R) or the partial condenser duty (Q_c).

From a total molar balance in the liquid zone in the reflux drum (green dotted region),

$$\frac{dM_{Nt}}{dt} = L_C - R \tag{4.85}$$

where L_c is the flowrate of liquid from the condenser to the reflux drum, and is given by

$$L_C = \frac{Q_c}{\lambda_{Nt-1}} \tag{4.86}$$

Replacing Equation (4.86) in Equation (4.85), results:

$$\frac{dM_{Nt}}{dt} = \frac{Q_c}{\lambda_{Nt-1}} - R \tag{4.87}$$

Now, from an overall total mass balance around the vapor space in the reflux drum (red dotted region):

$$\frac{v_{v,Nt}}{R\,T_{Nt}}\left(\frac{dP_{top}}{dt}\right) = V_{Nt-1} - L_C - D = 0 \tag{4.88}$$

where T_{Nt} and $v_{v,Nt}$ are the temperature and the volume occupied by the vapor in the reflux drum respectively. Notice that in Equation (4.88), constant pressure P_{top} in the reflux drum was assumed, thus, from Equation (4.86) and Equation (4.88) results:

$$\lambda_{Nt-1}\left(V_{Nt-1} - D\right) - Q_c = 0 \tag{4.89}$$

Therefore, from a theoretical point of view, pressure can be kept constant by calculating the condenser duty or the distillate flowrate from equation (4.89). Thus, for controlling level and pressure at the top of the column, we have three possible manipulated variables, *R*, *D* and Q_c. That means that there is only one degree of freedom, which in this work (unless otherwise is stated) is the reflux rate *R*. As it has been shown in Figure 4.11, in this work, the pressure P_{top} is controlled by manipulating the distillate flow rate D, which is done according to the control law:

$$D = \left[V_{Nt-1} - \frac{Q_c}{\lambda_{Nt-1}} \right] + Kc \left[(P_{top} - P_{top,sp}) + \frac{1}{\tau_I} \int (P_{top} - P_{top,sp})\, dt \right] \tag{4.90}$$

where the first term accounts for a feedforward compensation which is derived from equation (4.89). The second term is a feedback control action calculated as a function of the error between the measured pressure (P_{top}) and its corresponding set point value ($P_{top,\ sp}$). On the other hand, the level H_D is controlled by manipulating the condenser duty, as a function of the error between the measured level (H_D) and its corresponding set point ($H_{D,sp}$), according to the following control law:

$$Q_C = Q_{Css} + Kc \left[(H_D - H_{D,sp}) + \frac{1}{\tau_I} \int (H_D - H_{D,sp})\, dt \right] \tag{4.91}$$

where Q_{Css} is the condenser duty at steady state.

Finally, for concluding the modeling of the purification Section, the molecular sieves model is presented in the following section.

Molecular sieves

The last step in the purification stage of the bio-ethanol process corresponds to the molecular sieves unit (Figure 4.12).

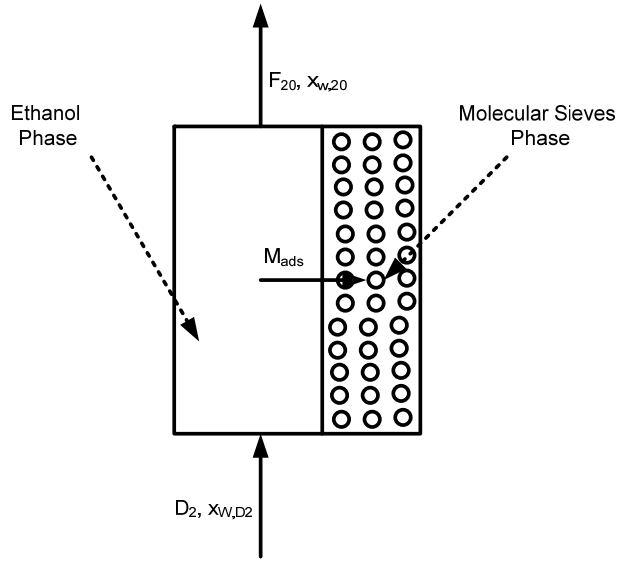

Figure 4.12 Schematic representation of a molecular sieves unit

In this work, a simple model is used in the sieves unit. A single bed unit has been simulated, assuming that the mass of water adsorbed per hour of sieve operation (M_{ads}) is given by (**Karuppiah et al., 2008**):

$$M_{ads} = \frac{ads \cdot m_{MS}}{t_{reg}} \tag{4.92}$$

where m_{Ms} is the mass (in kg) of molecular sieves in the bed, *ads* (kg water/kg molecular sieves) is the adsorption potential of the sieves and t_{reg} is the time of sieve operation without need for regeneration. However, the maximum rate of water adsorption is determined by the equilibrium separation efficiency of the sieves (η_{ads}), as given by:

$$\eta_{ads} = 1 - \left(\frac{x_{w,20}^{*}}{x_{w,D2}} \right) \tag{4.93}$$

where $x_{w,20}$* is the equilibrium mass fraction of water in the ethanol-phase.

From a steady-state mass balance in the ethanol-phase,

$$F_{20} = D_2 - M_{ads} \tag{4.94}$$

where D_2 is the mass flow rate of distillate in the rectification column and F_{20} is the outlet mass flow rate of dehydrated ethanol. From a balance of water in the ethanol-phase,

$$M_{ads} = D_2 x_{w,D2} - F_{20} x_{w,20} \tag{4.95}$$

Combining equations (4.94) and (4.95) and rearranging, the following expression is obtained:

$$M_{ads} = D_2 \left[\frac{x_{w,D2} - x_{w,20}}{1 - x_{w,20}} \right] \tag{4.96}$$

At equilibrium, the mass fraction of water in the outlet flow is $x_{w,20}$*. Now, considering that $x_{w,20}$*<<1, equation (4.96) becomes

$$M_{ads,\max} = D_2 (x_{w,D2} - x_{w,20}^*) \tag{4.97}$$

From the definition of the separation efficiency (4.93), the following expression is obtained:

$$M_{ads,\max} = D_2 x_{w,D2} \eta_{ads} \tag{4.98}$$

Finally, the mass fraction of ethanol in the product stream F_{20} can be calculated as:

$$x_{E20} = 1 - \frac{D_2 x_{wD2} - \min(M_{ads}, M_{ads,\max})}{F_{20}} \tag{4.99}$$

The main operating conditions and design parameters used in the model of the purification section are presented in Appendix C.1. The design parameters for the distillation and rectification columns were obtained using a sensitivity analysis as it is shown in Appendix D, whereas those for the molecular sieves were taken from **Karuppiah et al. (2008)**.

Finally, it is important to consider the overall and component mass balance in a splitter and a mixer located after the bottom of the rectification column, which are used for recycling a fraction of the lutter water, mixed with fresh water for maintaining a constant flow of water to the liquefaction tank.

$$F_{21} + B_2 + VB_2 = L_{1,rect} \tag{4.100}$$

$$x_{i,21} = x_{i,B2} \tag{4.101}$$

$$F_{23} = F_{21} + F_{22} \tag{4.102}$$

$$F_{23} x_{i,23} = F_{21} x_{i,21} + F_{22} x_{i,22} \tag{4.103}$$

4.1.5. Plantwide degrees-of-freedom analysis

In this section, a degrees-of-freedom analysis is carried out in order to check the consistency of the model for the whole plant. This analysis, indicating the dependent variables, the equations of the model and the degrees of freedom, is presented in Table 4.1.

Table 4.1 Plantwide analysis of degrees of freedom for the ethanol production process

Dependent Variables	**Quantity**	**Equation**	**Quantity**
Composition in liquefaction tank (R-101)	n_c	Component mass balances in liquefaction R-101 (4.7, 4.9-4.13)	n_c
Composition in saccharification tank (R-102)	n_c	Component mass balances in saccharification R-102 (4.19, 4.22-4.28)	n_c
Composition in fermentation tank (R-201)	n_c	Component mass balances in fermentation R-201 (4.32-4.34,4.39,4.40,4.43)	n_c
Composition in trays of distillation column (T-301) - 2 phases	$2*N_{T1}*n_c$	Component mass balances in trays of columns (4.60, 4.72, 4.78, 4.83)	$(N_{T1}+N_{T2})*(n_c-1)$
Composition in trays of rectification column (T-302) - 2 phases	$2*N_{T2}*n_c$	Overall mass balances in trays of columns (4.59, 4.71, 4.77, 4.82)	$N_{T1} + N_{T2}$
Temperature in trays of distillation and rectification columns	$N_{T1} + N_{T2}$	Energy balances in trays of columns (4.67, 4.73, 4.79, 4.84)	$N_{T1} + N_{T2}$
Liquid hold-up in trays of distillation and rectification columns	$N_{T1} + N_{T2}$	Vapor-liquid equilibrium in trays of columns (4.65)	$(N_{T1}+N_{T2})*n_c$
Volume of reactors (V_L, V_S, V_F)	3	Overall mass balance in reactors (4.14, 4.21, 4.36)	3
Level of reactors (H_L, H_S, H_F), reflux drums (H_{D1}, H_{D2}) and reboilers (H_{B1}, H_{B2})	7	Geometric relations (4.15)	7
Rates of reaction (r_g, r_{mlt}, r_{de}, $r_{mlt,S}$, r_X, r_d, r_S, r_p)	8	Kinetic expressions (4.16-4.18, 4.29, 4.37, 4.38, 4.41, 4.42)	8
Input flows of starch slurry, enzymes, yeast and water (F_0, F_1, F_3, F_5, F_{10}, F_{22})	6	Summation equations (4.66)	$N_{T1} + N_{T2}$
Liquid output flows from reactors (F_2, F_4, F_6)	3	Level control laws (4.8, 4.20, 4.35, 4.76, 4.81, 4.91)	7

Table 4.1 (cont.) Plantwide analysis of degrees of freedom for the ethanol production process

Dependent Variables	**Quantity**	**Equation**	**Quantity**
Output flows from distillation and rectification columns (B_1, D_1, B_2, D_2)	4	Pressure control laws (4.80, 4.90)	2
Flow and composition of purge stream (stream 8)	$n_c + 1$	Equilibrium separation in filter (4.44)	n_c
Flow and composition of cell recycle stream (stream 11)	$n_c + 1$	Overall and component mass balance in flash V-202 and condenser HE-202 (4.48-4.50, 4.54, 4.56-4.57)	$2n_c + 2$
Flow and composition of vent gas (stream 12)	$n_c + 1$	Vapor-liquid equilibrium in flash, fermentor and condenser HE-202 (4.51-4.52)	$3n_c$
Flow and composition of yeast-free stream (stream 13)	$n_c + 1$	Overall and component mass balances in filter F-201 and yeast treatment tank V-201 (4.45-4.47)	$2n_c + 2$
Flow and composition of recycle stream from flash to fermentor (stream 15)	$n_c + 1$	Equilibrium separation in molecular sieves (4.93)	n_c
Flow and composition of stream from flash to distillation (stream 16)	$n_c + 1$	Overall balance in molecular sieves units (4.94)	1
Flow and composition of stream from flash to scrubber (stream 18)	$n_c + 1$	Vapor mass balance in top of the columns (4.88)	2
Flow and composition of stream from flash to rectification (stream 19)	$n_c + 1$	Reboiler duty (4.74)	2
Flow and composition of product (stream 20)	$n_c + 1$	Liquid and Vapor flow rates from trays of columns (4.61, 4.64)	$2*(N_{T1}+N_{T2})$
Flow and composition of lutter water (stream 21)	$n_c + 1$	Overall and component mass balance in rectification bottoms splitter and lutter water mixer (4.100 - 4.103)	$2n_c + 2$

Table 4.1 (cont.) Plantwide analysis of degrees of freedom for the ethanol production process

Dependent Variables	**Quantity**	**Equation**	**Quantity**
Flow and composition of water to liquefaction (stream 23)	$n_c + 1$	Water adsorption in molecular sieves units (4.92)	1
Pressure in the top of distillation and rectification columns (P_{t1}, P_{t2})	2		
Condenser and reboiler duties in distillation and rectification (Q_{c1}, Q_{c2}, Q_{r1}, Q_{r2})	4		
Reflux and boilup streams in distillation and rectification (R_1, VB_1, R_2, VB_2)	4		
Liquid and vapor flows from the trays of the distillation and rectification columns (L, V)	$2*(N_{T1} + N_{T2})$		
Operation time of molecular sieves unit before regeneration (t_{reg})	1		
TOTAL VARIABLES	$\mathbf{14*n_c + 2*(N_{T1}+N_{T2})*n_c + 4*(N_{T1}+N_{T2})+53}$	**TOTAL EQUATIONS**	$\mathbf{14*n_c + 2*(N_{T1}+N_{T2})*n_c + 4*(N_{T1}+N_{T2})+39}$
For n_c=10 and $N_{T1}+N_{T2}$=80	**2113**	For n_c=10 and $N_{T1}+N_{T2}$=80	**2099**
DEGREES OF FREEDOM = 14			

According to Table 4.1, there are 14 degrees of freedom in the whole process, a result consistent with the number of available manipulated variables after closing the local level and pressure loops. This set of available manipulated variables includes: F_0, F_1, F_3, F_5, F_8, F_{10}, F_{15}, F_{21}, F_{22}, R_1, VB_1, R_2, VB_2 and t_{reg}.

By far, a complete model of the continuous bio-ethanol production from starchy raw materials has been presented. The complete dynamic model has been implemented using MATLAB's Simulink as described in Section 4.2. The validation of the fermentation, distillation and rectification sections is presented in Appendix C. In contrast to those models which are part of the state of the art in the (bio)-chemical engineering field, the model developed in this work for the molecular sieves unit is a new approach. For this reason, in the next section the validation of the molecular sieves model described by Equations (4.92) – (4.99) is presented.

Molecular Sieves model validation

The molecular sieves model described by Equations (4.92) – (4.99) is validated in this section. Initially, the model was developed assuming a constant adsorption capacity *ads*; however, during validation it was observed that a best fit to the experimental data was attained considering a variable adsorption capacity as a function of the sieve operation time (t_{reg}), as described by Equation (4.104):

$$ads = \frac{ads_0}{t_{reg}^{\ 2}} \tag{4.104}$$

Figure 4.13 shows a comparison between experimental data reported by **Al-Asheh et al. (2004)** for 3A-type molecular sieves (green points), the model predictions using a constant adsorption capacity (red line) and model predictions using a variable adsorption capacity (blue line) described by Equation (4.104). The data are plotted as water content in the effluent stream (x_{w20}) divided by the inlet water content (x_{wD2}), versus time. In this particular case, the data correspond to an inlet water content of 5% wt. As it can be seen, the model using a variable adsorption capacity fits very well the experimental data, in contrast to the model assuming a constant adsorption capacity. Therefore, it was decided to include in the molecular sieves model the expression given by Equation (4.104) for taking into account a variable adsorption capacity. The new model was validated by using a different set of experimental data, this time for 4A- type molecular sieves, which is shown in Figure 4.14.

As it can be observed in Figure 4.14, the new model considering the variable adsorption capacity also fits very well the new set of experimental data for the molecular sieves 4A-type. Finally, from the validation results presented in this section and in Appendix C, it can be concluded that the dynamic model developed in this work, based on the mass and energy balances presented in Section 4.1, provides a good approximation for predicting the behavior of the process variables in the fermentation and purification steps (distillation, rectification and adsorption) of an ethanol production process, which are the core units of the process.

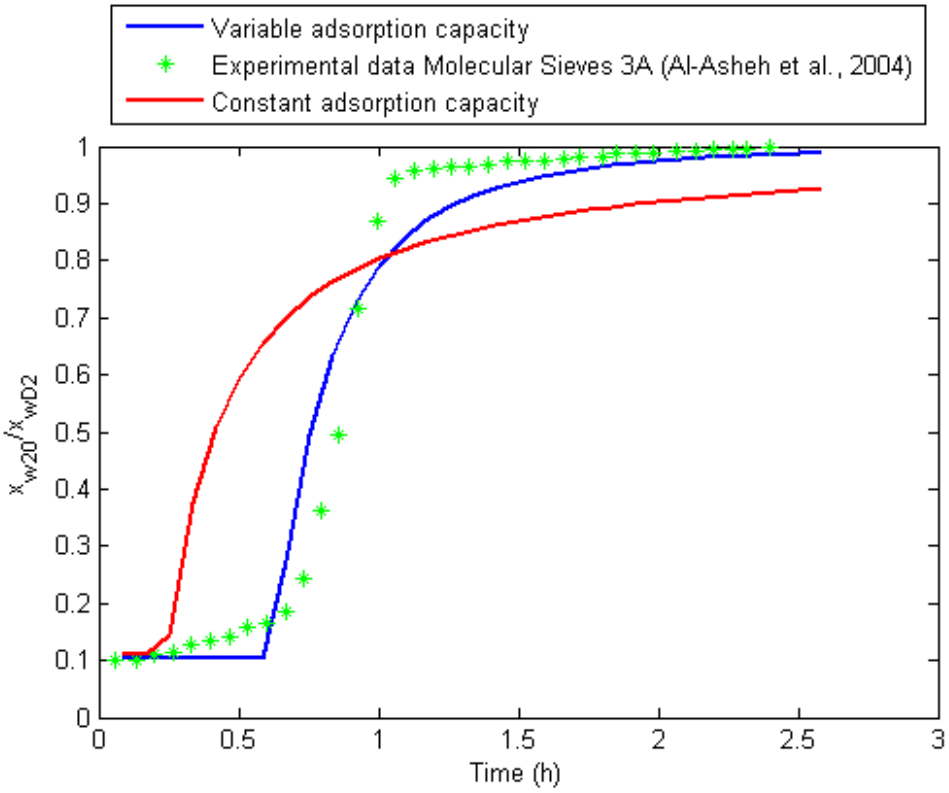

Figure 4.13 Model validation for 3A-type Molecular sieves: Experimental data for 3A. (green points), Simulink model predictions considering a constant adsorption capacity (red line), and Simulink model predictions considering a variable adsorption capacity (blue line).

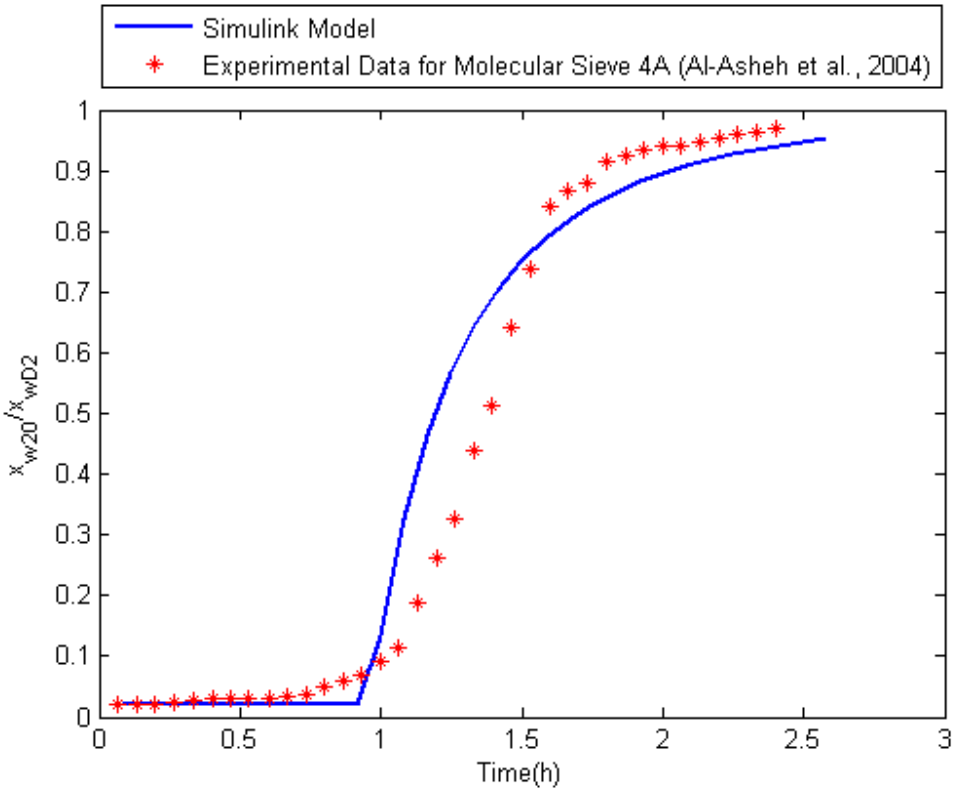

Figure 4.14 Model validation for 4A-type Molecular sieves: Experimental data for 4A (red points), and Simulink model predictions considering a variable adsorption capacity (blue line).

4.2. Simulink Dynamic Model for the Bio-ethanol Process

The case study addressed in this work is based on the continuous alcoholic fermentation of glucose to ethanol, sometimes referred in the literature as extractive fermentation (**Costa et al., 2001**; **Meleiro et al., 2009**) in which fermentation, cells recycle and a flash separation are considered as part of the fermentation stage. As one of the main purposes of this work is to propose a Plantwide Control (PWC) strategy for the ethanol continuous process from starch (typical raw material in the European countries) towards reaching maximal profitability, the process considered in this work (as described in Section 4.1) also includes liquefaction, saccharification and purification sections, similar to those of the Biostil® 2000 process (Chematur Enginering AB, Karlskoga, Sweden). The nonlinear dynamic model of the process, consisting of a nonlinear DAE system comprising 311 differential states and approximately 1800 algebraic equations, was simulated using Mathwork's Simulink®. The scheme of the Simulink model developed is shown in Figure 4.15.

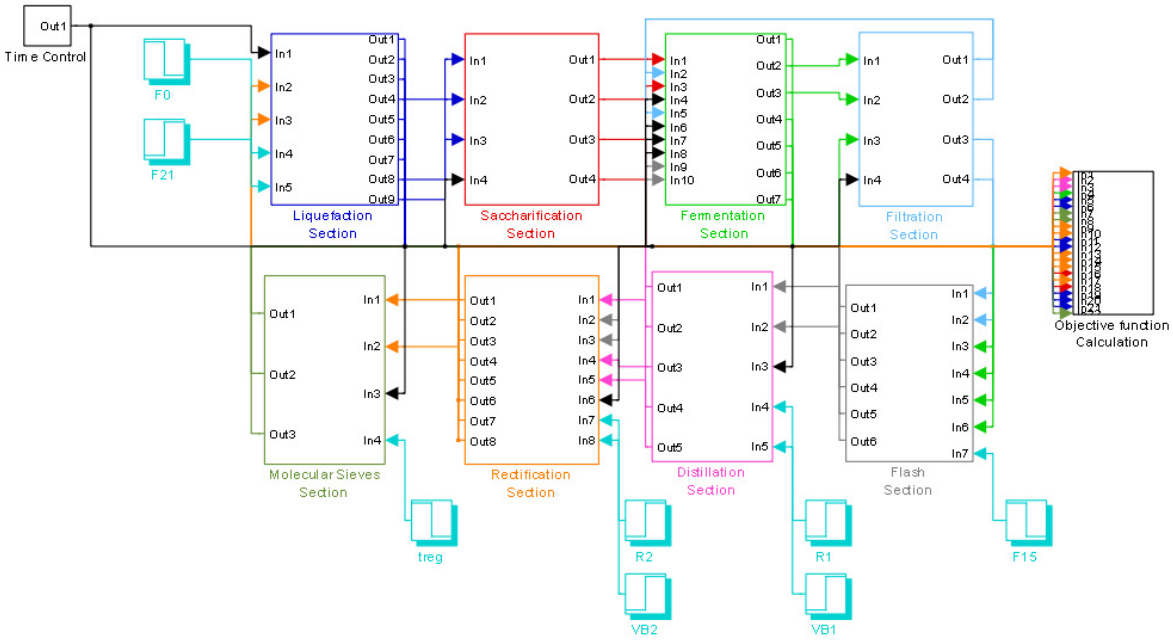

Figure 4.15 Scheme of the Simulink model: The model for each section is included as an embedded MATLAB function block. Cyan step blocks are the manipulated variables denoted as plantwide manipulated in Chapter 6.

In the developed Simulink model, each section of the process, namely, liquefaction, saccharification, fermentation, distillation, rectification and molecular sieves, corresponds to an embedded MATLAB function block. In total, the Simulink model considers 26 input variables that are described and pre-classified in Table 4.2. As a rule, the variables that cannot be manipulated by any means in the process are considered as disturbances, as it is the case of the feed concentrations of starchy slurry and enzymes, whose concentrations correspond to those provided by the suppliers of the raw materials. As it can be seen, 23 of the input variables are considered as potential manipulated variables, which in Chapter 6 (Section 6.1.1) will be classified into local manipulated and plantwide manipulated variables. The remaining three inputs on Table 4.2 are considered as disturbances.

In order to test the plantwide control methodology from an optimization perspective, an important step is the development of an optimal process design for the case study addressed. The design procedure based on a sensitivity analysis of a cost design function with respect to the main process design parameters is presented in Appendix D, considering a nominal production of 100.000 Ton ethanol/year (12.63 Ton/h for 330 days of operation during 24h/day) using a mash of starchy material as feed. After the process design, the Simulink model was used for studying the sensitivity of the process with respect to the main input variables. Such sensitivity analysis is an important tool for understanding the effect of the inputs on the process, which provides highly valuable information for implementing a suitable control system in the process.

Table 4.2 Input variables considered in the Simulink Dynamic Model for Bio-ethanol production: Potential manipulated vs. disturbances[§]

Input Variable	Classification	Meaning
F_0	Potential manipulated	Starch slurry feed flow to the process (m^3/h)
F_1	Potential manipulated	Alpha-amylase input flow to Liquefaction (m^3/h).
F_2	Potential manipulated	Output flow form Liquefaction (m^3/h).
F_3	Potential manipulated	Glucoamylase input flow to Saccharification (m^3/h).

[§] A sensitivity analysis is presented in this section for the variables in bold face.

Table 4.2 (cont.) Input variables considered in the Simulink Dynamic Model for Bio-ethanol production: Potential manipulated vs. disturbances

Input Variable	Classification	Meaning
F_4	Potential manipulated	Output flow from Saccharification (m^3/h).
F_5	Potential manipulated	Fresh yeast flow (m^3/h).
F_6	Potential manipulated	Output flow from Fermentation (m^3/h).
F_8	Potential manipulated	Cells purge flow (m^3/h).
F_{10}	Potential manipulated	Water input flow to the mixing tank (m^3/h).
F_{15}	Potential manipulated	Recycle flow from the flash to the fermentor (m^3/h).
F_{22}	Potential manipulated	Fresh Water input flow to the process(m^3/h)
F_{21}	Potential manipulated	Stillage Recycle from the bottom of the rectification (m^3/h).
R_1	Potential manipulated	Reflux rate in the distillation (kmol/h).
VB_1	Potential manipulated	Boilup rate in the distillation (kmol/h).
B_1	Potential manipulated	Bottoms flow rate in the distillation (kmol/h).
Qc_1	Potential manipulated	Condenser heat flux in the distillation (J/h).
D_1	Potential manipulated	Distillate flow rate in the distillation (kmol/h).
R_2	Potential manipulated	Reflux rate in the rectification (kmol/h).
VB_2	Potential manipulated	Boilup rate in the rectification (kmol/h).
B_2	Potential manipulated	Bottoms flow rate in the rectification (kmol/h).
Qc_2	Potential manipulated	Condenser heat flux in the rectification (J/h).
D_2	Potential manipulated	Distillate flow rate in the rectification (kmol/h).

Table 4.2 (cont.) Input variables considered in the Simulink Dynamic Model for Bio-ethanol production: Potential manipulated vs. disturbances

Input Variable	Classification	Meaning
t_{reg}	Potential manipulated	Regeneration cycle period (h)
$S_{ung,0}$	Disturbance	Starch content on the feed (kg/m^3)
$e_{1,1}$	Disturbance	Alpha-amylase concentration (kg/m^3)
$e_{2,3}$	Disturbance	Gluco-amylase concentration (kg/m^3)

In this section, the Simulink model (Figure 4.15) is used for carrying out the sensitivity analysis of the process with respect to the main input variables. This analysis is done after closing some basic local control loops for the process, including: the level loops for the liquefaction, saccharification and fermentation tanks; the levels in reboiler and condenser in the distillation and rectification columns, as well as the pressure in each column. After closing these basic local loops, there are still 14 potential manipulated variables available in the process, for control purposes. These variables are shown in bold in Table 4.2, and in the following, their impact on the process profitability is studied through a sensitivity analysis. For this purpose, the profitability function presented in Equation (4.105) is used.

$$\begin{aligned}\Phi = w_1 \int_{t_0}^{t_0+\Delta t} F_{20}\,dt - w_2 \int_{t_0}^{t_0+\Delta t} F_0 S_{ung,0}\,dt + w_3 \int_{t_0}^{t_0+\Delta t} x_{ED_2}\,dt - w_4 \int_{t_0}^{t_0+\Delta t} F_6\,dt - w_5 \int_{t_0}^{t_0+\Delta t} VB_1\,dt \\ - w_6 \int_{t_0}^{t_0+\Delta t} VB_2\,dt - w_7 \int_{t_0}^{t_0+\Delta t} x_{EB_1} B_1\,dt - w_8 \int_{t_0}^{t_0+\Delta t} x_{EB_2} B_2\,dt - w_9 \int_{t_0}^{t_0+\Delta t} e_{1,1} F_1\,dt \\ - w_{10} \int_{t_0}^{t_0+\Delta t} e_{2,3} F_3\,dt - w_{11} \int_{t_0}^{t_0+\Delta t} \rho_w F_{22}\,dt - w_{12} \int_{t_0}^{t_0+\Delta t} (1/t_{reg})\,dt\end{aligned} \quad (4.105)$$

The first term in the objective function (4.105) accounts for the incomes obtained from selling the ethanol produced; the second term penalizes the raw material consumption; the third term is a quality soft constraint included for promoting a high ethanol concentration at the top of the rectification column (x_{ED2}) and reducing the risk of production of ethanol out of specifications; the following three terms are used for penalizing the energy consumption in the process (pumping power and steam consumption). The terms weighted by w_7 and w_8

penalize the economic losses due to the presence of ethanol in the streams leaving the process at the bottom of the columns. The next three terms penalize consumption of enzymes (alpha-amylase and glucoamylase) and fresh water, whereas the last term accounts for regeneration costs in the molecular sieves. The Δt is the optimization horizon, which in the case study addressed here was taken as 25 hours.

Table 4.3 Sensitivity analysis of the main process inputs

Input Variable[**]	**Nominal value**	**Variation Interval**	**Sub-optimal initial value from sensitivity analysis**	**Optimal operating point**[††]
F_0 (m^3/h)	30	15 – 45	33	27.3
F_1 (L/h)	20	0.2 – 23	1.3	1.55
F_{22} (m^3/h)	35	28 – 49	42	44.4
F_3 (L/h)	45	22 – 67	45	38.2
$F_{21}/L_{1,rect}$	0.8	0 – 1	0.8	0.933
F_8/F_7	0.015	0 – 0.05	0.02	0.025
F_5 (m^3/h)	0	0 – 1	0	0
F_{15}/F_{14}	0	0 – 0.09	0	0.011
R_1 (kmol/h)	4170	3760 – 4600	4100	3907.1
VB_1 (kmol/h)	5250	4720 – 5770	5250	4987.3
R_2 (kmol/h)	1845	1750 – 1880	1845	1854.7
VB_2 (kmol/h)	2100	2015 – 2120	2070	2047.6
t_{reg} (h)	0.1	0.05 – 1	0.4	0.466

The sensitivity analysis was carried out as follows. After identifying the design parameters as described in Appendix D, the Simulink process model was run setting the inputs at their

[**] The analysis of recycle and purge flows (F_{23}, F_{15} and F_8) was performed considering the corresponding flow ratios, in order to gain a better understanding of the process.

[††] The optimal operating point was determined by solving the optimization problem stated in Equation (4.106) using the MIPT algorithm described in Chapter 3.

nominal values until a steady state was found. Then, each process input was changed between the allowed variation intervals around the nominal point, and the process was simulated starting from the steady state condition previously found.

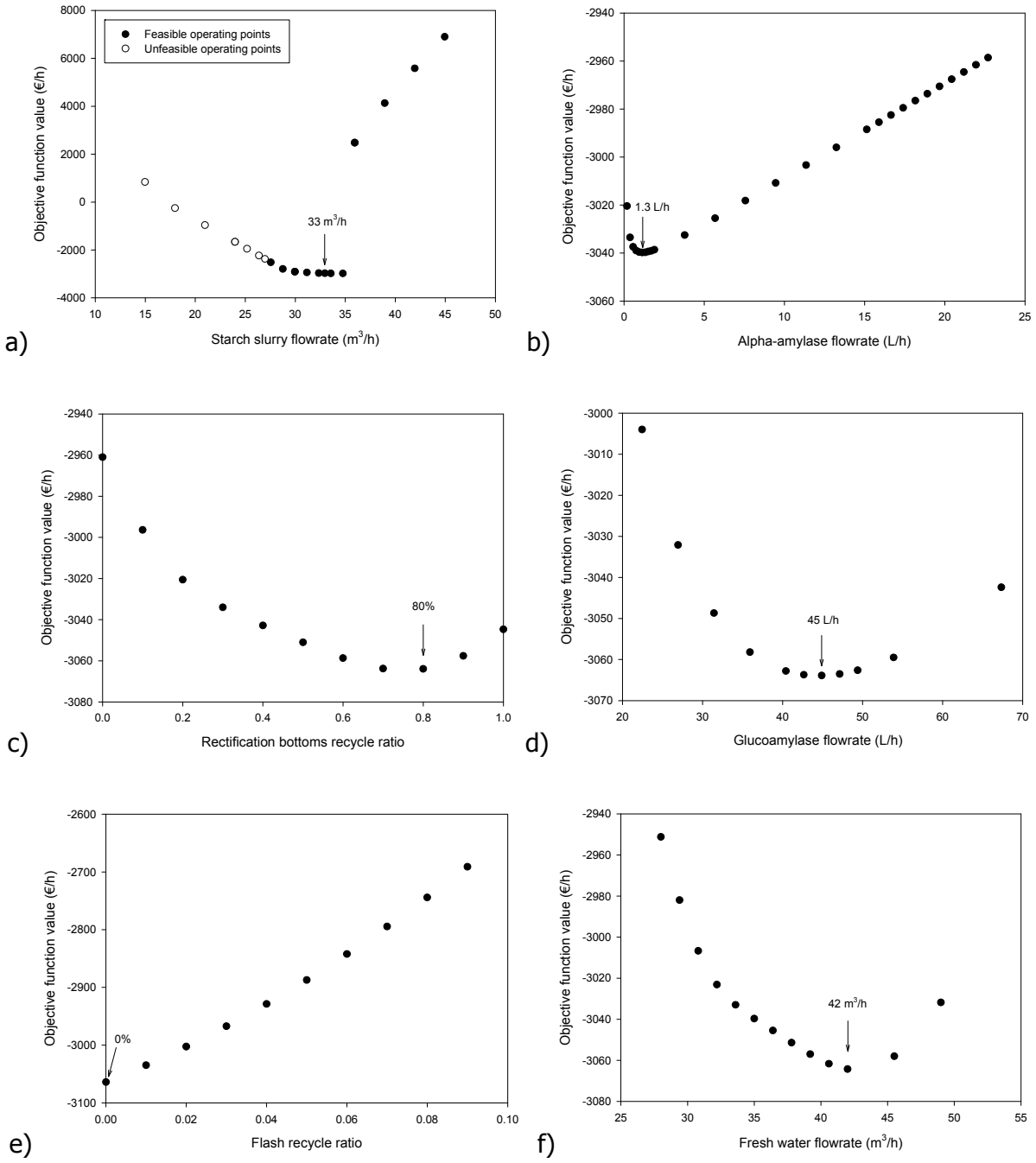

Figure 4.16 Sensitivity analysis of the main input variables of the process. a) Starch slurry flowrate, b) alpha-amylase flowrate, c) Rectification bottoms recycle ratio, d) Glucoamylase flowrate, e) Flash recycle ratio, f) Fresh water flowrate

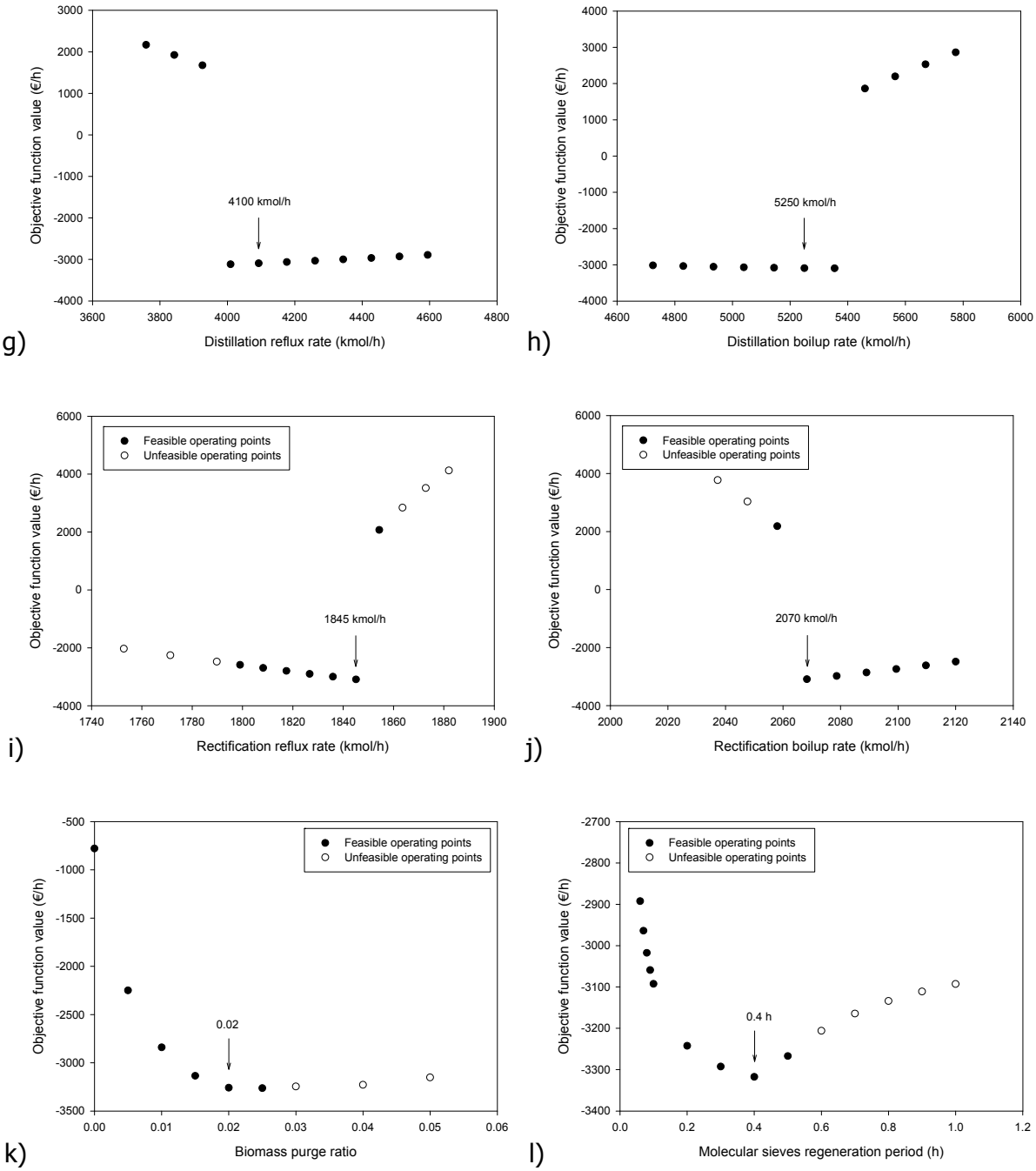

Figure 4.16 (cont.) Sensitivity analysis of the main input variables of the process. g) Distillation reflux rate, h) Distillation boilup rate, i) Rectification reflux rate, j) Rectification boilup rate, k) Biomass purge ratio, l) Molecular sieves regeneration period.

The optimal value selected for each input was the one returning the highest profitability while at the same time satisfying the following constraints:

- Ethanol production rate ≥ 80.000 Ton ethanol/year. The process was designed for a 100.000 ton ethanol/year capacity, and in order to operate a profitable process, the production rate should be higher than the 80% of the total capacity.
- Ethanol purity ≥ 99.8% wt.

After finding the optimal value for the first input, this was taken as the new nominal value, and the procedure was sequentially repeated for the other inputs. Table 4.3 shows the variation interval used for each input variable, and the sub-optimal value obtained after performing the sensitivity analysis. The detailed results of the sensitivity analysis are shown in Figure 4.16. For some variables, infeasible points are sometimes found, corresponding to operating conditions that do no satisfy the minimum production rate and/or the minimum ethanol concentration in the final product.

From the sensitivity analysis results shown in Figure 4.16 it is possible to conclude that the potential manipulated variables with a minimal effect on the profitability function (for the range analyzed) are the input flows of alpha-amylase and glucoamylase, the fresh yeast flow (F_5) and the fresh water flow (F_{22}). Therefore, those variables will not be considered as plantwide manipulated variables (i.e. they are not included as decision variables in the optimization problem that arises in the plantwide optimizing control), but will be considered as part of the local control loops. For the case of alpha-amylase and glucoamlyase flow rates, those will be used for keeping a constant ratio to the starch slurry feed flow rate, as suggested by **Karuppiah (2008)**. On the other hand, the fresh yeast flow will be used together with the biomass purge flow in a local strategy for controlling the viable biomass in the fermentor, and the fresh flow water F_{22} will be calculated for achieving a constant total recycle flow rate to the liquefaction tank (F_{23}). These loops will be presented as part of the local control strategy for the ethanol process in Chapter 6 (see Section 6.1.1).

On the other hand, the values of the manipulated variables denoted as sub-optimal during the sensitivity analysis were taken as starting point for finding the optimal operating point of the process (in terms of the manipulated variables). For this, the model was run until a new steady state was achieved, and then the optimization problem described by Equation (4.106) was solved using the Molecular-Inspired Parallel Tempering (MIPT) optimization algorithm presented in Chapter 3, in order to find the optimal operating point for the process inputs. The optimal values found are listed in the last column of Table 4.3.

$$\begin{aligned} &\min_{U} \ \Phi \\ &s.t. \quad F_{20} \geq 80000 \ ton/year \\ &\qquad x_{E,20} \geq 0.998 \end{aligned} \tag{4.106}$$

U=[F_0, F_1, F_{22}, F_{21}, F_3, F_8, F_5, F_{10}, F_{15}, R_1, VB_1, R_2, VB_2, t_{reg}], F_{20} is the flow of product of the plant (in Ton/year) and $x_{E,20}$ is the mass fraction of ethanol in the final product (stream F_{20}). The constraint used in Equation (4.106) corresponds to a minimum mass fraction of ethanol of 0.998. Notice also that the objective function Φ is the same profitability given by Equation (4.105) evaluated for the same optimization horizon, and that the set of decision variables is constituted by all the inputs catalogued as available potential manipulated variables. Finally, it must be mentioned that the initial conditions of the main state variables in the Simulink model obtained after solving the optimization problem (4.106), are given in Appendix C.5. These conditions constitute the optimal initial steady state of the process.

Until now, the detailed model for the case study addressed in this work has been presented, and the description of the dynamic simulation (including sensitivity analysis to the process inputs) has been given. The dynamic model presented in this section will be used in Chapter 6 for applying the Plantwide Optimizing Control framework developed in this work, which is introduced in the next Chapter.

4.3. Chapter conclusion

In this chapter, a dynamic nonlinear first principles model for the bio-ethanol continuous process from starch has been developed. The model (simulated using Simulink®) comprises the main sections in the bio-ethanol process, namely liquefaction, saccharification, fermentation, distillation, rectification and dehydration (molecular sieves unit). The implemented Simulink model consists of a nonlinear DAE system comprising 311 differential states, approximately 1800 algebraic equations and a total of 14 degrees of freedom (manipulated variables available after closing level and pressure control loops). The developed model was used in this chapter for analyzing the sensitivity of the process profitability with respect to the 14 available degrees of freedom. From this analysis, it was observed that the variables F_1, F_3, F_5 and F_{22}, have a minimal effect on the profitability function (for the range analyzed), and therefore those variables will be considered in Chapter 6 as part of the local control loops of the process, and not as plantwide manipulated variables. Finally, a new, simple but reliable model for the molecular sieves unit was developed and validated, which is adequate for the purpose in this work, i.e. to have a good predictive capability whereas at the same time avoiding a high model complexity.

5. Plantwide Optimizing Control Methodology

In the last 20 years the plantwide control problem in chemical processes has been addressed from different perspectives, some of which were presented already in Chapter 2. Most of the literature in this field is devoted to the formulation of decentralized plantwide control architectures, following either heuristic or mathematical-based procedures. The decentralized architecture can be convenient for processes with a small (or not) degree of interconnection between different operating units, but definitively is not enough for successfully handling dynamic processes that have a high degree of interconnection between different units. The reason for this is that the very first principle of decentralization is to assume that each operating unit is an isolated entity that is not affected by the other units. However, as a rule, and with the purpose of operating with a high profit, industry has to build processes with recycle loops which definitively represent a high degree of interconnection complicating the control task. Despite of this drawback, decentralized architectures are still preferred for solving the problem of controlling a complete process. The main reason for this preference relies on the easiness of implementation and the use of PID controllers, which without doubt are the most commonly used in the process industry. PID controllers are and will be the basis of any control system in an industrial process because of its simplicity (for both, implementation and understanding) and robustness. However, with the emerging of very fast computers and communication tools, a new spectrum of possibilities has been opened for improving the plantwide control strategies in the process industry, of course still using PID controllers as a base but integrating online optimization tools for taking advantage of the available control degrees of freedom using them to push the process towards maximum profitability. Precisely, this is the purpose of this chapter, namely to propose a plantwide control framework that keeps controlled the local control objectives in the process (i.e. safety and environmental specifications, etc) by using SISO control loops (e.g. using PID controllers), whereas at the same time, the available (non-local) control degrees of freedom are used inside a dynamic real time optimization formulation to drive the process towards a maximum profitability at each time. Such approach is denoted in this work as Plantwide Optimizing Control (PWOC) because integrates the Plantwide and the Online optimizing control concepts, as depicted in Figure 5.1.

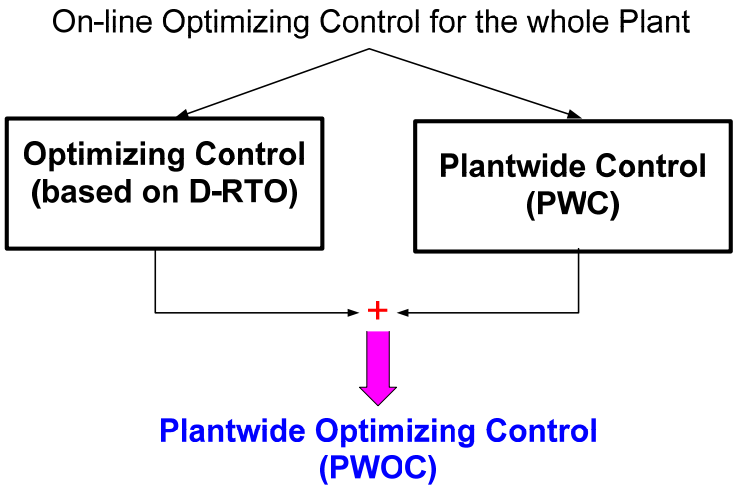

Figure 5.1 Plantwide Optimizing Control Concept (**Ochoa et al., 2010a**)

Online optimizing control optimizes an economic objective function over a finite moving horizon during plant operation based upon a rigorous nonlinear dynamic model (**Küpper and Engell, 2008**). Plant limitations and product specifications are included in the optimization as constraints. This definition is used in this work as a key concept for developing the basic steps of a Plantwide optimizing Control (PWOC) approach. PWOC addresses Plantwide Control (PWC) as a nonlinear dynamic real-time optimization problem, in which the available manipulated variables in the process (i.e. those not used in the local control loops) are used for achieving maximum profitability in the plant in the presence of disturbances. In this way, PWOC calculates optimal values for the set of selected manipulated variables in order to maximize a Plantwide Profitability Objective function (Φ,) instead of maintaining a set of controlled outputs at predefined set points. A key feature of PWOC is that the input-output pairing is avoided (except for the local control loops), because the output actually controlled in the process is the Plantwide Profitability and the available manipulated variables are simultaneously used for satisfying that purpose. Online optimizing control has been receiving increasing attention in the last years in different chemical process applications (**Engell, 2007**). However, not much work has been reported in the open literature about the on-line optimizing control of bioprocesses.

This chapter is organized as follows. In Section 5.1 the Plantwide Optimizing Control (PWOC) methodology is proposed and a detailed description of the stages involved is given. Two different PWOC approaches have been considered: A Single-Layer Direct Optimizing Control approach, denoted in the following as PWOC-one-layer, and a Multi-Layer without

Coordination approach denoted as PWOC-two-layer. Furthermore, as the PWOC framework is based on the solution of a Dynamic Real Time Optimization problem (D-RTO) efficient strategies should be used for solving the problem in real-time. Therefore, in Section 5.2 an approach for shrinking the search region of the optimization problem is proposed, whose main purpose is to reduce the search region of the optimization problem according to the capability of each manipulated variable for rejecting both known and unknown disturbances.

5.1. Stages of the Plantwide optimizing Control (PWOC) Procedure

The proposed PWOC approach comprises six main stages, as shown in Figure 5.2, in which clearly two main different tasks can be identified. The first task (stages 1-3) is a local control-oriented task because it is related to the identification and design of the necessary local control loops. This task can be carried out using the decentralized control framework employing for example PI or PID controllers. The second is a Plantwide control-oriented task (stages 4-6), which can only be implemented after assuring the accomplishment of the objectives established at the local control-task. The main purpose of this Plantwide oriented-task is to use the available control degrees of freedom (i.e. after closing the local loops) for accomplishing a unique objective: maximizing the process profitability. This means that, excluding the local loops, no pre-defined set points will be either regulated or tracked. In the following, a description of each stage considered in Plantwide optimizing Control is presented.

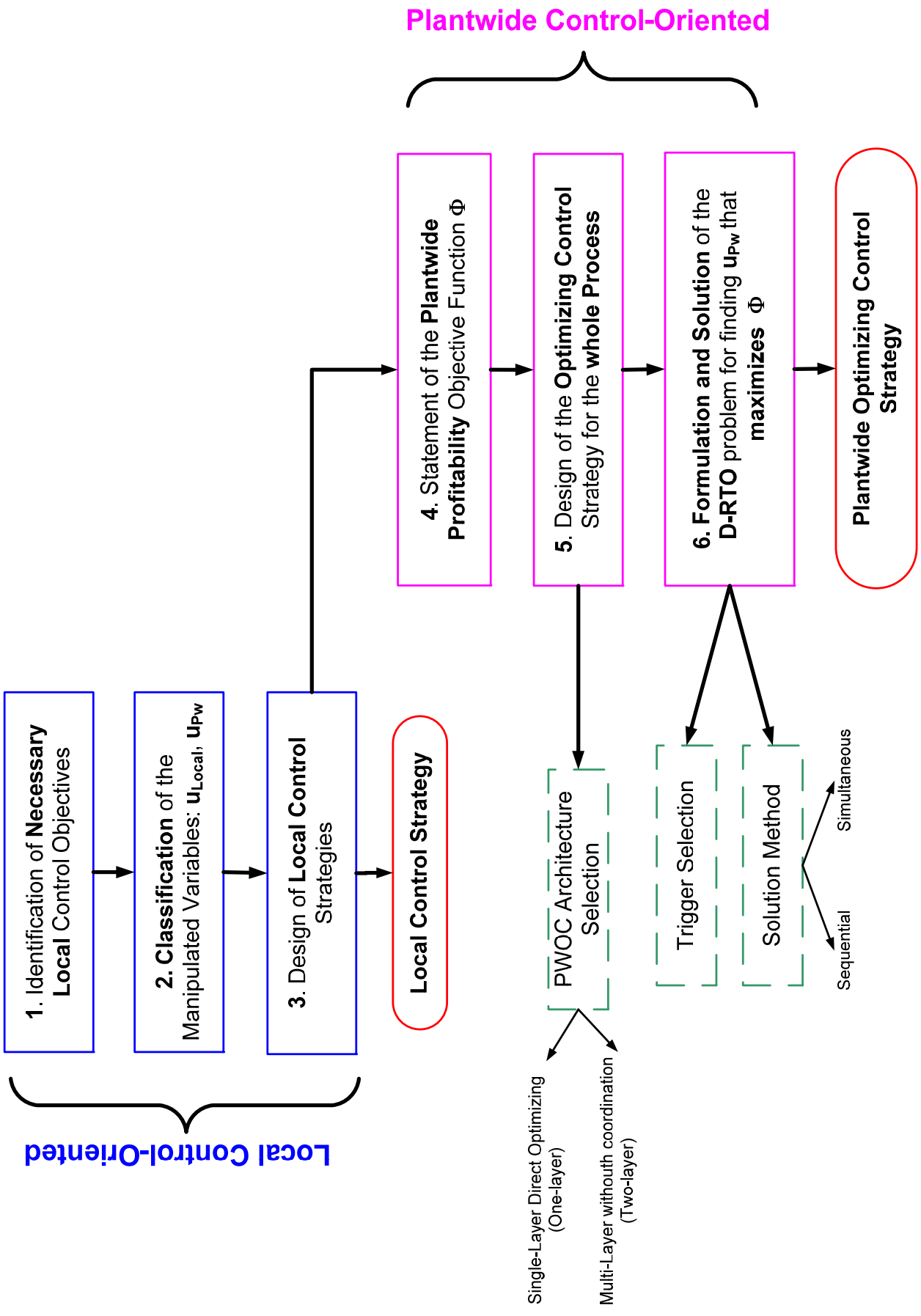

Figure 5.2 Stages of the Plantwide Optimizing Control Procedure

5.1.1. Identification of the necessary Local Control Objectives

Even though the goal of any chemical or biochemical process is the return of maximum profit, there are additional control objectives that must be taken into account before establishing a plantwide control structure for satisfying this economic goal. In this work, the process control objectives are classified in two groups, local-control-oriented and plantwide-oriented, as shown in Figure 5.3. The local control oriented objectives are necessary control loops related to safe operation, environmental and equipment protection, and are recommended to be the primary selected variables that must be locally controlled before establishing the plantwide optimizing control structure, that is, they should be achieved (i.e. kept within pre-defined bounds) independently of the economical performance of the plant, by using local control loops. On the other hand, the Plantwide control-oriented objectives include the maximization of the process profit, while at the same time assuring the product quality and a smooth operation. Such plantwide control objectives should enter directly in the objective function, or as constraints in the optimization problem formulated in step 4 of the Plantwide Optimizing Control (PWOC) framework (Section 5.1.4).

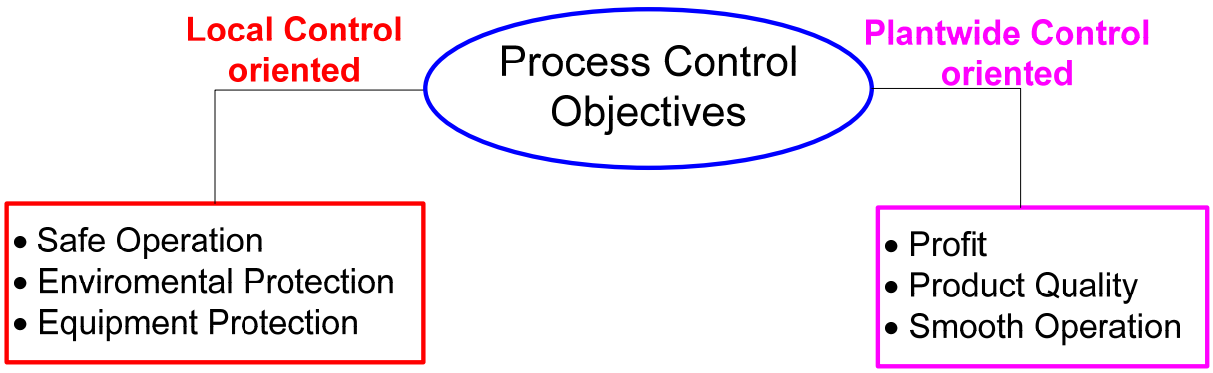

Figure 5.3 Process Control Objectives: Local vs. Plantwide oriented

5.1.2. Classification of the Manipulated variables

The available manipulated variables in the process can be used in the local control loops or for the plantwide optimizing control of the process. Those manipulated variables used for satisfying the local control set points will be denoted as Local manipulated (u_{Loc}), whereas the Plantwide manipulated variables (u_{PW}) are those that remain available after selecting u_{Loc}, and that are used for maximizing the plantwide profitability objective function. Selection of the local manipulated variables involves heuristic knowledge of the causal relationship between the process outputs and inputs, which should be accompanied by simulation studies, especially when highly interacting processes are evaluated. Although in this stage

only a pre-classification of the manipulated variables is done (without taking into account the input-output pairing), in general it is desirable that each input classified as local manipulated variable has a direct effect on only one output variable. Of course, in most situations this is not the case, but it is desirable to select as local manipulated variables those inputs that disturb the less other states in the process.

5.1.3. Design of Local Control Strategies

After identifying the necessary local control objectives in the process and the local manipulated variables (u_{Loc}) required for satisfying those control objectives at the local control loops, it is then necessary to address the design of those local loops. The design of the local control loops includes mainly the pairing of manipulated-controlled variables, the selection of the controller type and the tuning of the controller. Usually at this stage a decentralized plantwide control structure can be used, based on the implementation of multiple PI or PID SISO loops. The pairing problem is often solved by process insight, although for difficult cases a RGA analysis is recommended (**Araujo, 2007**; **Castro and Doyle, 2004**). On the other hand, the tuning of the PI or PID controllers can be addressed in many different ways including the use of controller tuning relations, the use of computer simulation for minimizing a performance objective function, and on-line tuning (**Bequette, 2006**; **Luyben, 1990**; **Marlin, 2000**; **O'Dwyer, 2009**; **Seborg et al., 2003**).

Until now, the stages involved in the local control-oriented part of the plantwide optimizing control framework proposed in Figure 5.2 have been introduced. After designing the necessary local control strategy, the remaining manipulated variables are available degrees of freedom for control. These variables are denoted as Plantwide manipulated variables (u_{PW}), and are used for fulfilling the main objective of the Plantwide-oriented part, namely maximizing the profitability objective function for the whole process.

5.1.4. Objective function Statement

The next step in the Plantwide Optimizing control framework (Figure 5.2) is to establish a plantwide profitability function Φ and its constraints, in order to formulate a D-RTO problem. The objective function Φ depends upon the specific process addressed. However, it may contain terms related to the productivity of the process, raw materials costs, energy consumption, economic losses, etc. Constraints in the optimization problem can be determined by plant and product specifications (e.g. minimal/maximal production rate

according to the demand of the market, required purity of the end-product, etc.), and by limitations in the state and input variables. Equation (5.1) shows a general form of the profitability objective function, which considers a Mayer term (*M*), related to the state of the process at the final time, and a Lagrange term (ℓ) that represents an economical function related to the dynamic behavior of the state variables during the transition from the initial optimization time (t_0) to the final optimization time ($t_0+\Delta t_{opt}$), where Δt_{opt} is the prediction horizon over which the profitability objective function and constraints will be evaluated.

$$\Phi = M(x(t_0 + \Delta t_{opt})) + \int_{t_0}^{t_0+\Delta t_{opt}} \ell(x(t), u(t), t, d)\, dt \qquad (5.1)$$

Since PWOC addresses the optimizing control problem for a complete plant over a finite moving horizon during plant operation, it is very important to determine an adequate prediction horizon Δt_{opt} depending on the specific process analyzed. It is suggested that Δt_{opt} should not be shorter than the characteristic response time of the slowest relevant dynamic in the process (to avoid unexpected long-term performance deterioration), while at the same time it should be as short as possible to minimize computational load.

Once the profitability objective function has been formulated, the next step is to design the optimization-based control strategy to be applied for the whole process. In this work, the Single-layer direct optimizing control and Multilayer without coordination are suggested as the selected architectures for the optimization-based control strategy, due to the fact that they include the formulation of a dynamic real-time optimization problem, allowing the explicit consideration of the process dynamics.

5.1.5. Design of the Optimization-Based Control Strategy

As it was previously mentioned, two different architectures are proposed in this work for implementing the Plantwide Optimizing Control framework: the Single-Layer Direct Optimizing Control and the Multi-Layer Control without Coordination, which have been already introduced in Sections 2.1.4 and 2.1.3.2, respectively. The structures for both approaches are shown in Figure 5.4 and a detailed description of the building blocks for each framework is given in the following.

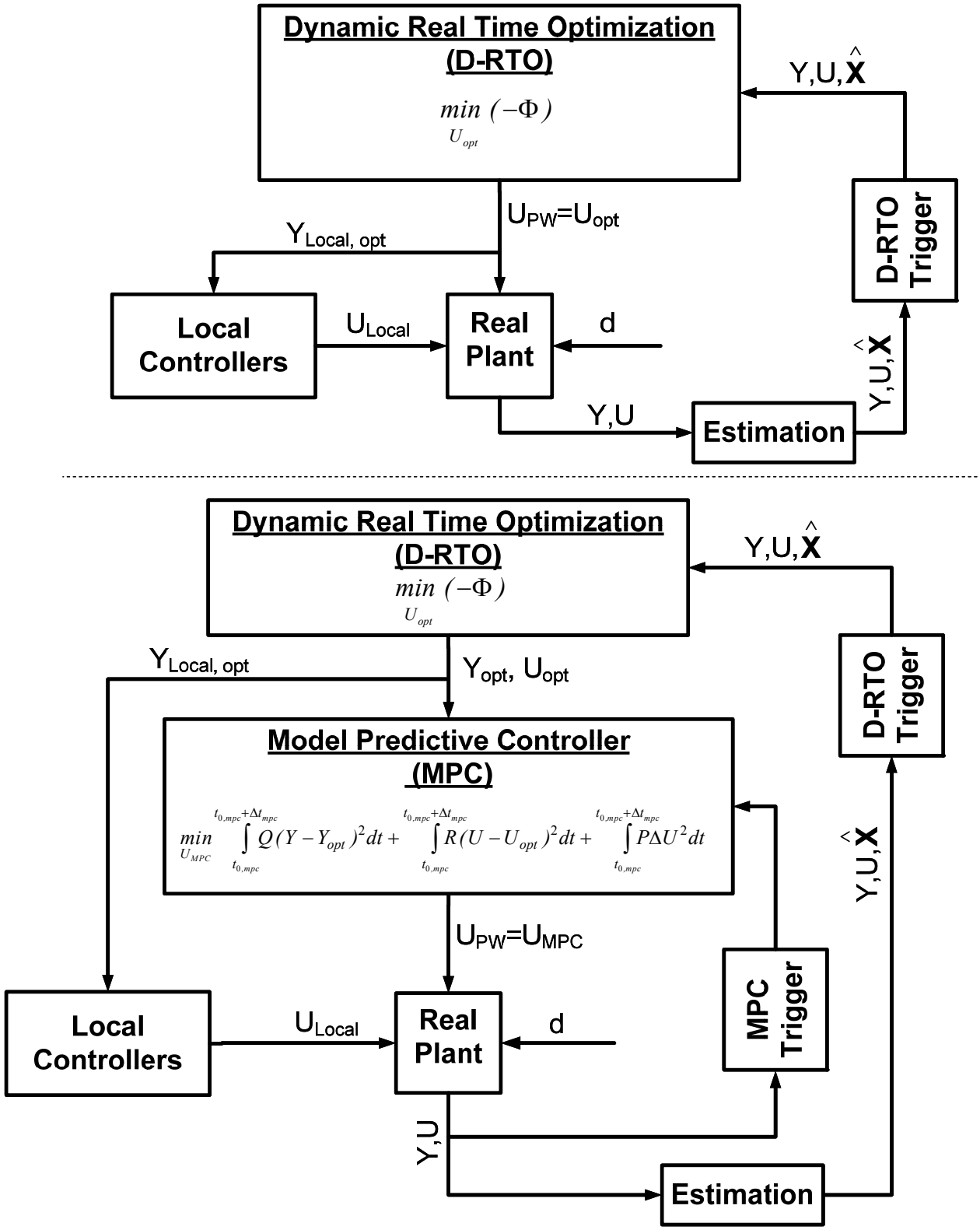

Figure 5.4 General schemes of the Optimization-based Control Strategies for Plantwide optimizing Control. Top: Single Layer Direct Optimizing (PWOC-one-layer). Bottom: Multi-Layer Control without Coordination (PWOC-two-layer).

- Dynamic Real-Time Optimization (D-RTO) layer: This layer consists of a dynamic real-time optimization problem in which the objective function is usually an economical

function that should be maximized over a moving horizon (i.e. profitability described by equation 5.1). Usually the D-RTO problem is subject to equality and inequality constraints defined by restrictions on the states and input variables, purity requirements, throughput, among others. The decision variables of the D-RTO problem are the plantwide manipulated variables ($U_{pw}=U_{opt}$) used for maximizing the economical objective function.

- Real Plant: This block corresponds to the real process for which the Plantwide control problem needs to be solved. In this work, only simulation studies (considering a completely observable process) have been carried out for testing the Plantwide optimizing Control framework (results are presented in Chapter 6). The real plant is represented by the first principles model detailed in Chapter 4, incorporating some noise on key process parameters as described in Chapter 6.
- Estimation Block: In order to find the optimal operating point at each time, it is necessary to estimate the main state variables ($\hat{X}$) that cannot be measured directly in the process; this can be done by using software sensors which employ the information of the available measured variables (Y). In this work, it is assumed that all the state variables are known at every sample time; therefore no estimation block is considered in the simulation studies presented in Chapter 6.
- Trigger: As it can be seen in Figure 5.4, there are two different triggers: an optimization-trigger and a controller-trigger. These trigger blocks act like switches for re-calling the optimization layer (D-RTO trigger) and the control layers (MPC-trigger) when a certain condition is met. An optimization trigger can work based on a time criterion (e.g. the optimization is called periodically at a predetermined frequency), based on the disturbances dynamics (after occurrence of a disturbance) or based on the performance of the plantwide profitability objective function (when Φ decreases below a certain tolerance). On the other hand, the controller trigger can be based on a time criterion or based on the controlled variables deviations from their optimal set points. Figure 5.5 shows schematically the different criteria for activating the optimization and controller triggers.
- Model Predictive Controller (MPC) layer: This layer consists on a MPC (that can be linear or nonlinear), in which the optimal values given by the D-RTO layer are used as set points for the controller. In this work, a Nonlinear Model Predictive Controller (NMPC) is used in the control layer.

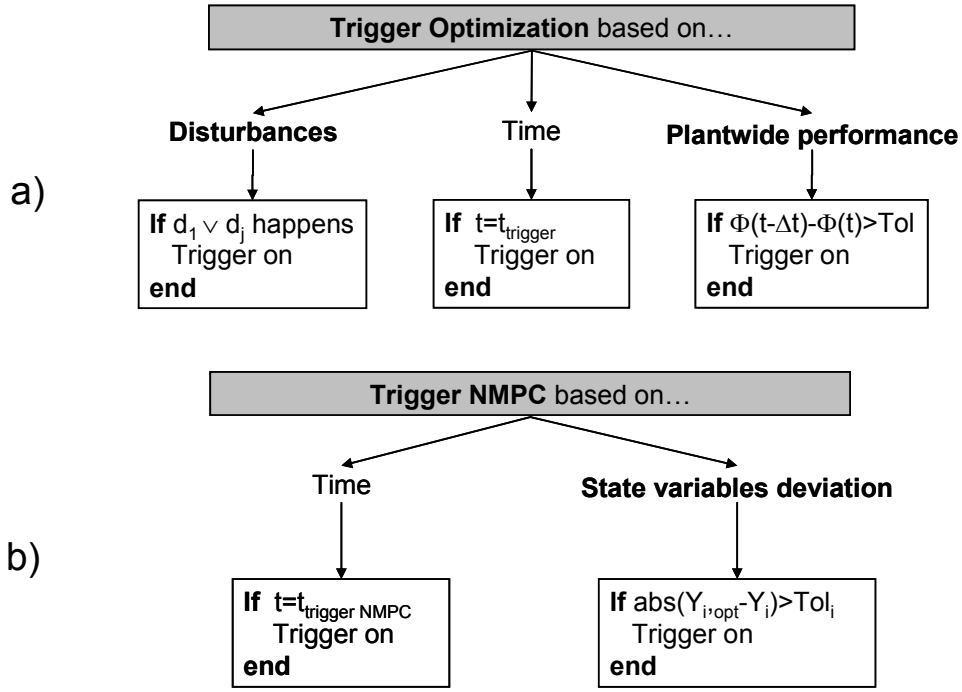

Figure 5.5 Summary of trigger activation conditions: a) Optimization trigger and b) Controller trigger

Comparing the schemes for the one-layer and two-layer frameworks (Figure 5.4), it can be seen that both approaches have very much in common. For example, both approaches are driven by a D-RTO layer, in which the objective function to be maximized is the plantwide profitability Φ. The main difference between the two frameworks is that in the PWOC-one-layer approach, the set of input variables applied to the real plant is given by the optimization layer ($U_{PW}=U_{opt}$), whereas for the PWOC-two-layer, the inputs applied to the real plant are calculated by a control layer ($U_{PW}=U_{MPC}$) that uses as set points, the optimal values (Y_{opt}) of the controlled outputs given by the optimization layer. In both cases, the decision variables of the D-RTO problem are the set of plantwide manipulated variables U_{PW}. However, in the Two-Layer case a second layer (MPC controller) is applied which solves the optimization problem for minimizing a performance-type objective function. This performance-type function may contain three different terms: a penalization of the deviation of the main output variables from their set points (Y_{opt}), a term that constraints the manipulated variables to a small envelope around the reference trajectories (U_{opt}) given by the optimization layer, and a term that prevents large changes in the manipulated variables from one sample time to the next, assuring smooth operation.

In chapter 6, the one-layer and the two-layer optimization-based control strategies will be used inside the Plantwide Optimizing Control framework for the bio-ethanol case study. Furthermore, as these optimization-based control strategies require the solution of a

Dynamic Real-Time Optimization problem, the next stage considered in the Plantwide optimizing control procedure is the solution of such D-RTO problem.

5.1.6. Dynamic Real-Time Optimization

The last stage in the Plantwide Optimizing control framework is to solve the nonlinear dynamic large-scale optimization problem that arises when formulating the optimization based control strategies of stage 5 of the PWOC framework in Figure 5.2, namely the one-layer (Single-Layer Direct Optimizing Control) and the two-layer (Multilayer without coordination). Efficient feasible optimization methods are needed in order to solve the problem in real time. For this purpose, direct optimization formulations are usually employed, which can be classified into sequential, simultaneous or hybrid approaches (e.g. multiple shooting). **Srinivasan et al. (2003)** provide a detailed explanation of the mentioned methods. The main features, advantages and disadvantages of the sequential, simultaneous and multiple shooting formulations have been already presented in Section 2.1 (Table 2.1).

In this work, a sequential formulation using stochastic methods for solving the large scale NLP problem is used. The reason for using the sequential formulation instead of simultaneous or multiple shooting is that the sequential formulation provides a feasible path in which the DAE system is satisfied at each step of the optimization (**Srinivasan et al., 2003**). Ensuring a feasible path during the optimization is a very important fact for real plant applications because in the event of an interruption of the optimization routine (e.g. because the time limit for optimization is reached), it is highly probable that the partial results obtained by an infeasible path approach will not satisfy the optimization constraints, since they are satisfied only at the end of the optimization, posing serious risks to the operation of the plant.

After defining the method for formulating the dynamic optimization problem, an efficient optimization algorithm should be chosen for solving the optimization. In general deterministic or stochastic approaches can be used. In this work, stochastic optimization algorithms are suggested for solving the problem, because they are relatively simple to implement, have a reduced computational load (there is not need of information about derivatives as required by gradient-based methods), and can be easily connected to available simulation packages (**Egea et al., 2009**; **Faber et al., 2005**). In Section 6.3, two different stochastic methods, Localized Random Search (**Spall, 2003**; **Zabinsky, 1998**) and Molecular-Inspired Parallel Tempering (**Ochoa et al. 2009c**, **2009d**, **2010b**) are used for solving a sequential

formulation of the dynamic real time optimization problem that arises in the PWOC for the bio-ethanol case study. According to **Jezowsky et al. (2005)**, random search optimization methods are efficient and robust for solving practical engineering problems although their convergence to the global optimum can not be assured. Independently of the optimization algorithm applied (deterministic or stochastic) or the solution approach (sequential, simultaneous, etc.), the method will search for the optimal solution in the space of the decision variables, i.e. the region bounded by the lower and upper limits of each manipulated variable (which are the decision variables of the optimization problem). Sometimes this search region may be too large, resulting in long computation times and making difficult the solution of the PWOC problem in real time. In order to raise the efficiency of the optimization routine for solving the D-RTO problem, in the following section a novel stochastic-based approach for shrinking the search region of the optimization problem is presented.

5.2. An stochastic approach for shrinking the search region of the optimization problem

When disturbances (known or unknown) occur in a process, the manipulated variables must act in order to reject or compensate their effect. The main idea of new the stochastic-based shrinking approach proposed in this work, is that the changes in each plantwide manipulated variable (Δu_{PWi}) required for rejecting a disturbance can be calculated as a function of the changes in the disturbances (Δd_j) and the profitability objective function ($\Delta \Phi$). Mathematically, this can be written as shown in Equation (5.2).

$$\Delta u_{PWi} = u_{PWi,t+\Delta t} - u_{PWi,t} = f_i(\Delta d_1, \Delta d_2, ..., \Delta d_j, \Delta\Phi) \qquad (5.2)$$

where i is the number of plantwide manipulated variables and j is the number of disturbances that may be present in the process; f_i is a function that represents how much the manipulated variable i should change for rejecting the disturbances. The general expression given in Equation (5.2) considers both a feedforward contribution (that accounts for measured disturbances occurrence) and a feedback contribution (in the sense that the profitability function will decrease or increase after an unknown disturbance has upset the process). Finding an analytical expression for the function f_i (i.e. from the model of the process) is a very complex task in a Plantwide Control context. Therefore, in this work an approximation is proposed, in which a Gaussian distribution is used for describing the

function f_i. This choice of function is made because Gaussian distribution functions are suitable for representing many different real processes as can be evidenced from the Central Limit Theorem (**Gardiner, 1994**). In this way, each plantwide manipulated variable (u_{PW}) is allowed to change only inside a region described by a Gaussian distribution, as expressed by Equation (2.6). Thus, the particular value of the change for each manipulated variable is determined as a random number obtained from the Gaussian distribution as described in Equation (5.3).

$$\Delta u_{PWi} = \xi_i(0, \sigma_{ui}) \tag{5.3}$$

$\xi(0,\sigma_{ui})$ represents a random number obtained from a Gaussian distribution with zero mean and standard deviation σ_{ui}. A zero mean value is fixed in the formulation, because it corresponds to the current value for the plantwide manipulated variables, when the optimization is called (i.e. when the known or unknown disturbances occurs and therefore re-optimization of the plantwide manipulated variables is needed), preventing abrupt changes. On the other hand, the standard deviation σ_{ui} can be calculated as the maximum between different contribution terms, representing the capability of the manipulated variable *i* for rejecting the different known disturbances of the process and/or rejecting a decrease in Φ (that can be caused by both known and unknown disturbances) at time *t*, as shown in Equation (5.4):

$$\sigma_{ui} = \max(w_{i1}\Delta d_1, w_{i2}\Delta d_2, ..., w_{ij}\Delta d_j, w_{i\Phi} z_\Phi \Delta\Phi) \tag{5.4}$$

where w_{ij} are gain factors that express how much a change in the manipulated variable u_{PWi} can reject (or counteract) the occurrence of disturbance d_j, $w_{i\Phi}$ is the gain factor for the manipulated variable *i* rejecting the decrease in the profitability objective function Φ, and z_Φ is a dummy variable that is only activated when the objective function Φ decreases below a given tolerance *Tol*. This is:

$$z_\Phi = \begin{cases} 0, & \Phi(t-\Delta t) - \Phi(t) \le Tol \\ 1, & \Phi(t-\Delta t) - \Phi(t) > Tol \end{cases} \tag{5.5}$$

Regarding the calculation of the gain factors (w_{ij}) used for obtaining the standard deviation σ_{ui}, it would be desirable to calculate these gains from the nonlinear model of the process as expressed in Equation (5.6)

$$w_{ij} = \sum_{k=1}^{n} \left(\frac{\partial u_i}{\partial x_k} \cdot \frac{\partial x_k}{\partial d_j} \right) \tag{5.6}$$

where $\partial u_i/\partial x_k$ represents the inverse of the open loop gain between state variable x_k and input u_i; and $\partial x_k/\partial d_i$ represents the open loop disturbance gain between x_k and disturbance d_j. However, as the complexity of the process model increases, the complexity for calculating the w_{ij} factors analytically also increases. For this reason, it is proposed to estimate these gain factors by using digraphs, which are causal models that can be used to describe the behavior of the process capturing the essential information flow in a cause-effect relationship (**Maurya et al., 2003**). One of the most important advantages of using digraph-based models is that they do not require much quantitative information and therefore have been applied in different fields like hazard and operability analysis and fault diagnosis.

A graphical representation of the shrinking approach for a system with two manipulated variables and two disturbances that occur at the same time is presented in Figure 5.6. The left and right projections show the Gaussian distributions with standard deviation σ_{11} and σ_{22} for describing the probability of change for the manipulated variables u_1 and u_2 respectively, when disturbances occur in the process. The center figure shows the Shrunk Search Region for the optimization problem, formed by the projections of the Gaussian distributions for u_1 and u_2. It is important to notice that even though the maximum standard deviation is selected for each case, a reduction of the search space, and thus a reduction in the computational effort during the optimization, is achieved because the original search region of the optimization problem was only bounded by the upper and lower bounds of u_1 and u_2. The stochastic-based shrinking approach is used in Chapter 6 for reducing the search region of the optimization problem that arises when the PWOC concept is applied to the continuous bio-ethanol production case study. As it will be shown through this example, the PWOC problem has been solved more efficiently by applying the shrinking approach than without shrinking.

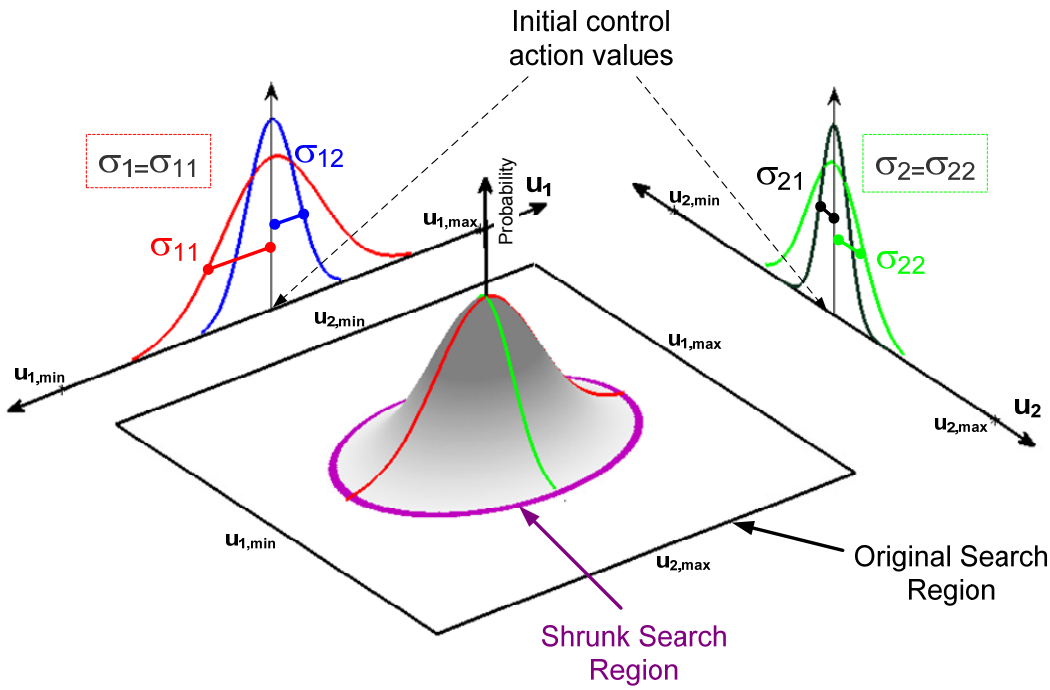

Figure 5.6 Shrinking approach: Probability distribution projections, final shrunk search region and original search region.

5.3. Chapter conclusion

In this chapter, a Plantwide Optimizing Control (PWOC) methodology has been proposed based on the Optimizing Control concept. The PWOC methodology consists on two main tasks: a local control-oriented task, which is usually carried out using typical PID decentralized schemes; and a plantwide control-oriented task, whose main purpose is to maximize the process profitability. Furthermore, a new stochastic-based shrinking approach for reducing the search space of the D-RTO that arises in PWOC has also been developed. The main purpose of the shrinking approach is to use the qualitative relationship between the disturbances and the manipulated variables to constraint the search space of the decision variables according to their capability for rejecting each disturbance. Such shrinking is important for online applications (where very short times are required for finding a solution of the optimization problem), because by reducing the search space, the optimization algorithm does not lose time in changing manipulated variables that are not able to reject a particular disturbance.

6. Plantwide control of the Bio-ethanol Process.

In this chapter, the Plantwide Control (PWC) problem for the continuous bio-ethanol process introduced and described in Chapter 4 is investigated. The organization of this Chapter is as follows. First, the Plantwide Optimizing Control (PWOC) methodology proposed in Chapter 5 is used in Section 6.1 for designing the plantwide control structure of the whole bio-ethanol process using the two different PWOC approaches presented in Section 4.5, namely, the PWOC-one-layer and the PWOC-two-layer. Then, in Section 6.2, a typical decentralized plantwide control scheme for the process is presented, which is a multi-loop formulation that will be used in Section 6.3 for comparing the performance of the Plantwide Optimizing Control architectures. Finally, in Section 6.3, the performance of the PWOC approach is evaluated under three different scenarios. First, a known disturbance in the feed concentration (starch composition) is applied to the process. Second, an unknown disturbance into the kinetic parameters of the fermentation section is introduced in the process (i.e. in the real plant model), which also introduces a model mismatch in the PWOC schemes. And third, a known disturbance in the price of the starch raw material is introduced. The performance of PWOC facing these challenges is compared to the performance when the decentralized Plantwide architecture (i.e. multiple single PID loops) is used, which up to now is the typical configuration in industry.

6.1. Plantwide Optimizing Control (PWOC) for Bio-ethanol production

In this section, the Plantwide optimizing control methodology proposed in Chapter 5 is applied to the case study. First, the steps related to the Local control-oriented task are explained (Section 6.1.1), and then, the steps involved in the Plantwide Control-oriented task are addressed (Section 6.1.2-6.1.4).

6.1.1. Stages 1-3: Identification and design of the Local Control Strategy

According to the guidelines given in Chapter 5, the local-oriented process control objectives are those related mainly to safe operation, environmental and equipment protection. These control objectives must be accomplished, even if they adversely affect the process profitability. From process insight, and in order to assure safe operation, the following loops are identified as necessary local control loops:

- Liquid levels for the liquefaction, saccharification and fermentation tanks.
- Liquid levels for the reflux drum and reboiler in the distillation and rectification columns.
- Pressure control for the distillation and rectification columns.

It must be remarked that in addition to the above-mentioned loops, there are other important loops that should be taken into account as part of the necessary local control strategy (i.e. temperature and pH control for the liquefaction, saccharification and fermentation, and pressure and level control for the flash vessel), due to their unquestionable importance for assuring safe operation and equipment protection. However, in an attempt to reduce the complexity of the simulation task, in this work, the simulation studies were carried out taking into account only the local necessary control loops shown in Figure 6.1. All other local variables were assumed to be constant during the simulation (i.e. ideally regulated at their predefined set point values), either because they have a very fast response and are quickly and easily controlled, or because they do not influence significantly the performance of the plant.

On the other hand, besides the local loops already identified as necessary for safety reasons, five additional control loops are locally implemented (also included in Figure 6.1). The first two loops (blue lines) control the ratio between the flow of enzymes (alpha-amylase and glucoamylase, fed to the liquefaction and saccharification tanks respectively) and the starch slurry feed flow. These control loops have predetermined set points values $R_{F1/F0sp}$ and $R_{F3/F0sp}$, corresponding to the flow ratios F_1/F_0 and F_3/F_0, respectively. The set point values for these local control loops, were calculated according to the recommendations provided by **Karuppiah et al (2008)**, and are listed in Table 6.1, where also the set points for all the other local loops are given. Additionally, after several simulation studies of the dynamics of the fermentation section (including the flash vessel and cells recycle), it was decided to

implement a new local biomass control strategy (**Ochoa et al, 2009b**) for controlling the biomass concentration in the fermentor. This new biomass control strategy comprises two internal control loops as shown in Figure 6.1 (green and purple lines). The first loop corresponds to a split-range controller (green lines), which is used for tracking a viable biomass concentration set point ($X_{V,F\text{-}sp}$) in the fermentor (which may be given by the D-RTO layer as $X_{V,F\text{-}opt}$). In this way, the split range controller is in charge of calculating (e.g. by using a proportional control law) the proper values of the manipulated variables F_5 and F_8 (fresh yeast feed flow to the fermentor and purge flow in the recycle loop respectively) required for tracking the optimal set point for the viable biomass in the fermentor. For example, if the viable biomass concentration in the fermentor ($X_{V,F}$) is above its set point value $X_{V,F\text{-}sp}$, the split range controller should increase the purge flow (F_8). In the opposite case, when $X_{V,F}<X_{V,F\text{-}sp}$, the controller will reduce the purge and open the fresh yeast valve (for feeding fresh yeast) if necessary. The second loop (purple lines in Figure 6.1) corresponds to a ratio controller for achieving a suitable viscosity in the biomass recycle slurry. This controller calculates the actual flow ratio between streams F_9 and F_{10} (which are the free-yeast and water streams fed to the cells treatment tank, respectively) and adjusts F_{10} in order to fulfill the ratio set point ($R_{F10/F9sp}$) required for keeping the biomass concentration in the recycle loop in a suitable value ($X_{t,F}$= 180 kg/m^3, according to the recommendations by **Maiorella et al. 1981**). Finally, it is important to mention that there are two main reasons that motivate the proposal of this biomass control strategy as a local control strategy. The first one is that an optimal biomass concentration in the fermentor should be always guaranteed in order to avoid a misuse of the substrate (which can be quickly consumed for cells maintenance and growth instead of metabolite production) if a higher concentration than the optimal is available. Additionally, if the biomass concentration is below the optimum, a slower metabolite production rate will occur, affecting the productivity of the process. The second reason is that the yeast is only involved in a closed mass-loop comprising fermentation, filtration and cells recycle, and thus, no biomass is found on the streams up the fermentor nor downstream the filter (after F_{13}). Finally, the last control loop considered as local is the flow control of stream F_{23} (by manipulating the fresh water flow F_{22}), which is the recycle of lutter-water to the liquefaction tank (orange lines in Figure 6.1). The main purpose for keeping constant this flow is to reduce the variability introduced by the recycle stream. As already mentioned, the control loops identified as necessary local loops in the bio-ethanol continuous process from starch are shown in Figure 6.1, whereas in Table 6.1 a description for each loop (e.g. controlled and manipulated variables and set point values) is provided. The tuning parameters of these loops can be found in Appendix C.1.

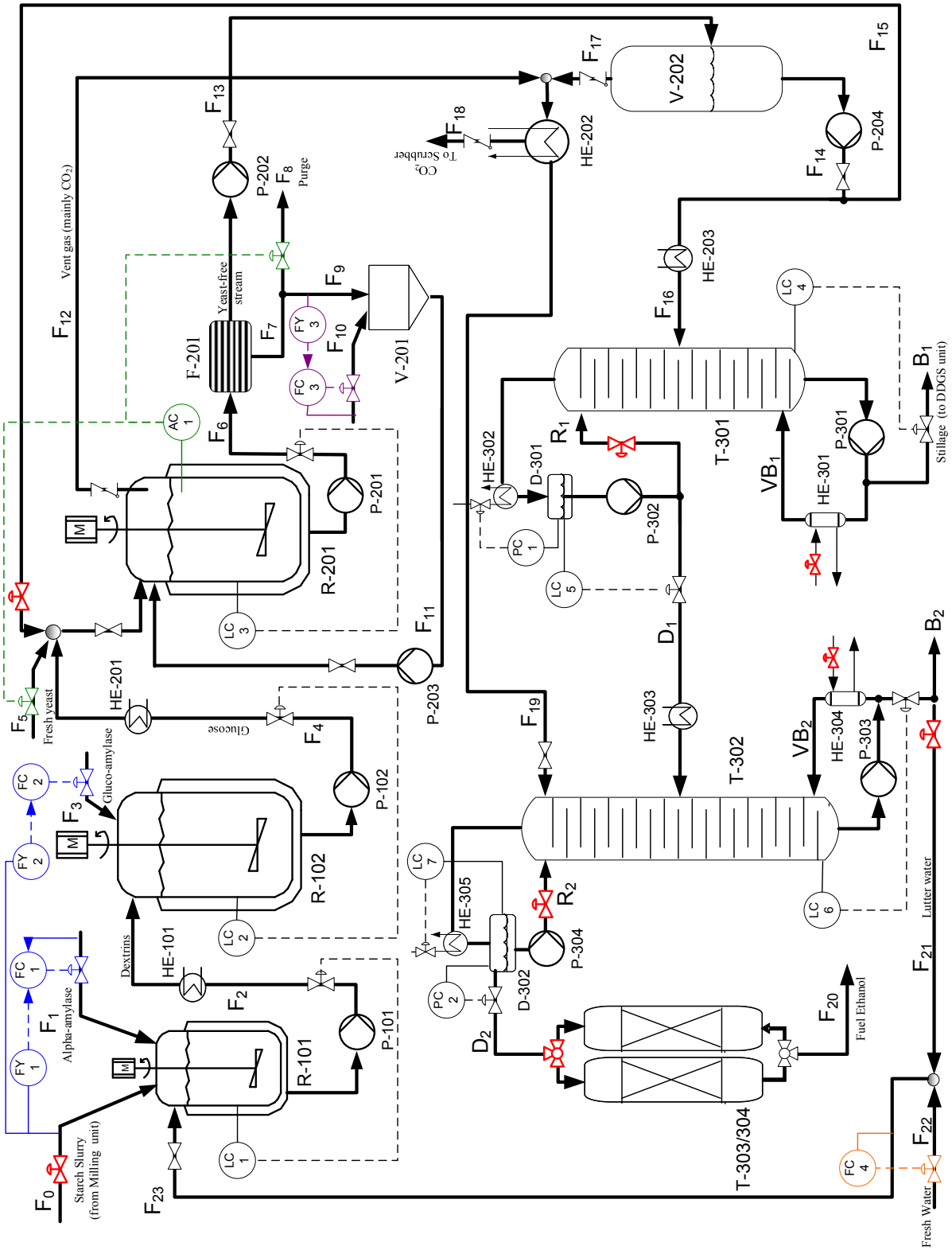

Figure 6.1 Local control loops implemented for the Continuous Bio-ethanol production Process from starch. Level and pressure control loops are shown in black, Enzymes flow ratio control in blue, Viable biomass control in the fermentor in green, Ratio control in the cells recycle loop in purple and lutter water flow control in orange. Available manipulated variables after closing the local loops are shown in red.

Table 6.1 Local control strategy: Variable pairing and set points

Controller ID	**Controlled variable**	**Manipulated variable**	**Set point**
LC-1	H_L	F_2	H_{Lsp}=6 m
LC-2	H_S	F_4	H_{Ssp}=11 m
LC-3	H_F	F_6	H_{Fsp}=12 m
LC-4	H_{B1}	B_1	H_{B1sp}=5 m
LC-5	H_{D1}	D_1	H_{D1sp}=3 m
LC-6	H_{B2}	B_2	H_{B2sp}=3 m
LC-7	H_{D2}	Qc_2	H_{D2sp}=2 m
PC-1	P_{t1}	Qc_1	P_{t1sp}=225 mmHg
PC-2	P_{t2}	D_2	P_{t2sp}=760 mmHg
FC-1	Ratio F_1/F_0	F_1	$R_{F1/F0sp}$= 5.7e-5
FC-2	Ratio F_3/F_0	F_3	$R_{F3/F0sp}$= 0.0014
FC-3	Ratio F_{10}/F_9	F_{10}	$R_{F10/F9sp}$=5.33
FC-4	F_{23}	F_{22}	F_{23sp}=62.86 m^3/h
AC-1	$X_{v,F}$	F_8 and F_5	$X_{v,F\text{-}sp}$= $X_{v,F\text{-}opt}$, is a variable SP given by the D-RTO layer

An important part of the Plantwide Optimizing Control procedure at this stage is to classify the available manipulated variables between local and plantwide manipulated. The classification of the variables for the present case study is given in Table 6.2. Notice that the variables denoted as plantwide manipulated are shown in Figure 6.1 in red, which are the available degrees of freedom for accomplishing the aim of the Plantwide Optimizing Control, to maximize the process profitability.

As it was already mentioned, the process has 23 manipulated variables, and only 15 of them are used as local manipulated variables in the local control strategy described in Figure 6.1. Therefore, the remaining 8 manipulated variables (F_0, F_{15}, VB_1, R_1, VB_2, R_2, t_{reg}, F_{21}) which are the starch input flow, recycle flow from the flash to the fermentor, boilup and reflux rates for each column, the regeneration time of the molecular sieves unit, and the recycle flow from the rectification to the liquefaction, are the manipulated variables denoted in the following as Plantwide manipulated variables (u_{PW}). These variables will be used as decision variables of the D-RTO problem that arises in the Plantwide Optimizing Control formulation, as it will be shown in Section 6.3.

Table 6.2 Description and classification of input variables

#	Input Variable	Classification	Meaning
1	F_0	Plantwide manipulated	Starch slurry feed flow to the process (m^3/h)
2	F_1	Local manipulated	Alpha-amylase input flow to Liquefaction (m^3/h).
3	F_2	Local manipulated	Output flow from Liquefaction (m^3/h).
4	F_3	Local manipulated	Glucoamylase input flow to Saccharification (m^3/h).
5	F_4	Local manipulated	Output flow from Saccharification (m^3/h).
6	F_5	Local manipulated	Fresh yeast flow (m^3/h).
7	F_6	Local manipulated	Output flow from Fermentation (m^3/h).
8	F_8	Local manipulated	Cells purge flow (m^3/h).
9	F_{10}	Local manipulated	Water input flow to the mixing tank (m^3/h).
10	F_{15}	Plantwide manipulated	Recycle flow from the flash to the fermentor (m^3/h).
11	F_{21}	Plantwide manipulated	Stillage Recycle from the bottom of the rectification (m^3/h).
12	F_{22}	Local manipulated	Fresh Water input flow to the process(m^3/h)
13	R_1	Plantwide manipulated	Reflux rate in the distillation (kmol/h).
14	VB_1	Plantwide manipulated	Boilup rate in the distillation (kmol/h).
15	B_1	Local Manipulated	Bottoms flow rate in the distillation (kmol/h).
16	Qc_1	Local Manipulated	Condenser heat flux in the distillation (J/h).

Table 6.2 (cont.) Description and classification of input variables

#	Input Variable	Classification	Meaning
17	D_1	Local Manipulated	Distillate flow rate in the distillation (kmol/h).
18	R_2	Plantwide manipulated	Reflux rate in the rectification (kmol/h).
19	VB_2	Plantwide manipulated	Boilup rate in the rectification (kmol/h).
20	B_2	Local Manipulated	Bottoms flow rate in the rectification (kmol/h).
21	Qc_2	Local Manipulated	Condenser heat flux in the rectification (J/h).
22	D_2	Local Manipulated	Distillate flow rate in the rectification (kmol/h).
23	t_{reg}	Plantwide manipulated	Regeneration cycle period (h)

After designing the local control strategy, the next step in the Plantwide optimizing control procedure is the statement of the plantwide profitability objective function, which is the first step related to the plantwide-oriented task.

6.1.2. Stage 4: Statement of Plantwide Profitability Function (Φ)

The following profitability objective function (Equation 6.1) is formulated as the function to be maximized for the bio-ethanol process studied in this work:

$$\begin{aligned}\Phi = w_1 \int_{t_0}^{t_0+\Delta t_{opt}} F_{20}\,dt - w_2 \int_{t_0}^{t_0+\Delta t_{opt}} F_0 S_{ung,0}\,dt + w_3 \int_{t_0}^{t_0+\Delta t_{opt}} x_{ED_2}\,dt - w_4 \int_{t_0}^{t_0+\Delta t_{opt}} F_6\,dt \\ - w_5 \int_{t_0}^{t_0+\Delta t_{opt}} VB_1\,dt - w_6 \int_{t_0}^{t_0+\Delta t_{opt}} VB_2\,dt - w_7 \int_{t_0}^{t_0+\Delta t_{opt}} x_{EB_1} B_1\,dt - w_8 \int_{t_0}^{t_0+\Delta t_{opt}} x_{EB_2} B_2\,dt \\ - w_9 \int_{t_0}^{t_0+\Delta t_{opt}} e_{1,1} F_1\,dt - w_{10} \int_{t_0}^{t_0+\Delta t_{opt}} e_{2,3} F_3\,dt - w_{11} \int_{t_0}^{t_0+\Delta t_{opt}} \rho_w F_{22}\,dt - w_{12} \int_{t_0}^{t_0+\Delta t_{opt}} (1/t_{reg})\,dt\end{aligned} \quad (6.1)$$

where w_i are pure economical weight factors, which are listed in Table 6.3. The first term in Equation 6.1 is related to the productivity of the process expressed as the product flow rate (i.e. ethanol fuel-grade); the second term penalizes raw material consumption and the third

term is a quality soft constraint used for promoting a high ethanol concentration at the top of the rectification column, before entering the molecular sieves unit. The following three terms (weighted by w_4, w_5 and w_6) are used for penalizing the energy consumption in the process (pumping power and steam consumption). The terms weighted by w_7 and w_8 penalize the economic losses due to the presence of ethanol in the streams leaving the process at the bottom of the columns. The next three terms penalize consumption of enzymes (alpha-amylase and glucoamylase) and fresh water. Finally, the last term penalizes the costs involved in the regeneration of each molecular sieves unit. t_0 is the initial time for the optimization routine and Δt_{opt} is the prediction horizon over which the objective function and constraints are evaluated. Δt_{opt}=25 hours has been selected taking into account the slowest dynamic response of the process to changes in its inputs.

Table 6.3 Weight factors used in the profitability objective function

Weight factor	Value	Description
w_1	33.7 €/kmol	Ethanol selling price
w_2	0.16 €/kg	Starch price (e.g. from corn)
w_3	3000 €/h	Soft constraint
w_4	11.57 €/m^3	Energy cost due to pumping
w_5	0.257 €/kmol	Vapor consumption price
w_6	0.257 €/kmol	Vapor consumption price
w_7	33.7 €/kmol	Ethanol price
w_8	33.7 €/kmol	Ethanol price
w_9	5 €/kg	Alpha-amylase price
w_{10}	3.5 €/kg	Gluco-amylase price
w_{11}	4.1×10^{-5} €/kg	Fresh water price
w_{12}	37 €/regeneration cycle	Price for regenerating a molecular sieves unit.

Most of the weighting factors shown in Table 6.3 are prices taken from **Franceschin et al. (2008)**. w_3 is a soft constraint that was tuned during the preliminary simulation studies. w_4 was assumed to be 2% of the ethanol price and w_7-w_8 were considered to be equal to the ethanol price. Finally, w_{12} was determined considering that the regeneration of a molecular sieves unit consumes 0.84 GJ/m^3 of ethanol dehydrated (source: **NPPBCO**). The nominal production of the plant is 100.000 ton ethanol/year (15.8 m^3/h) and therefore, 13.3 GJ/h are required for dehydrating the product. Assuming a cost of 14.0 €/GJ (source: **NPGA**) and considering a regeneration period of 0.2 h (**Kempe, 2008**), each cycle costs around €37.

6.1.3. Stage 5: Design of the Optimization-Based Control Strategy

In order to compare the one- and two-layer Plantwide Optimizing Control schemes, in this Section, the design of the optimization-based control strategy is carried out using both PWOC schemes, as shown in Figures 6.2 and 6.3.

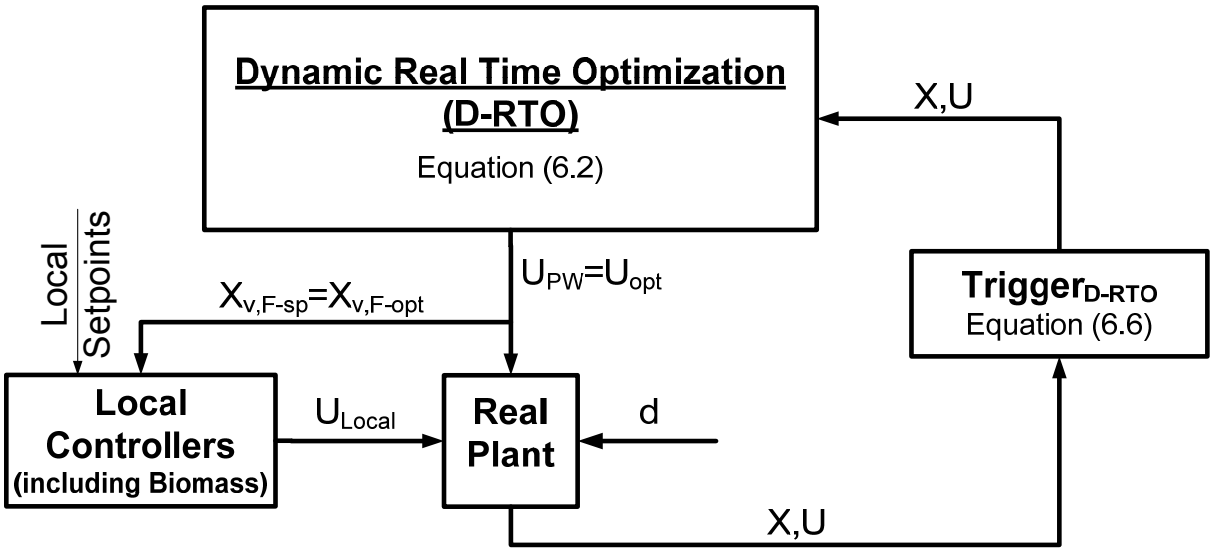

Figure 6.2 Plantwide Optimizing Control-One-Layer scheme

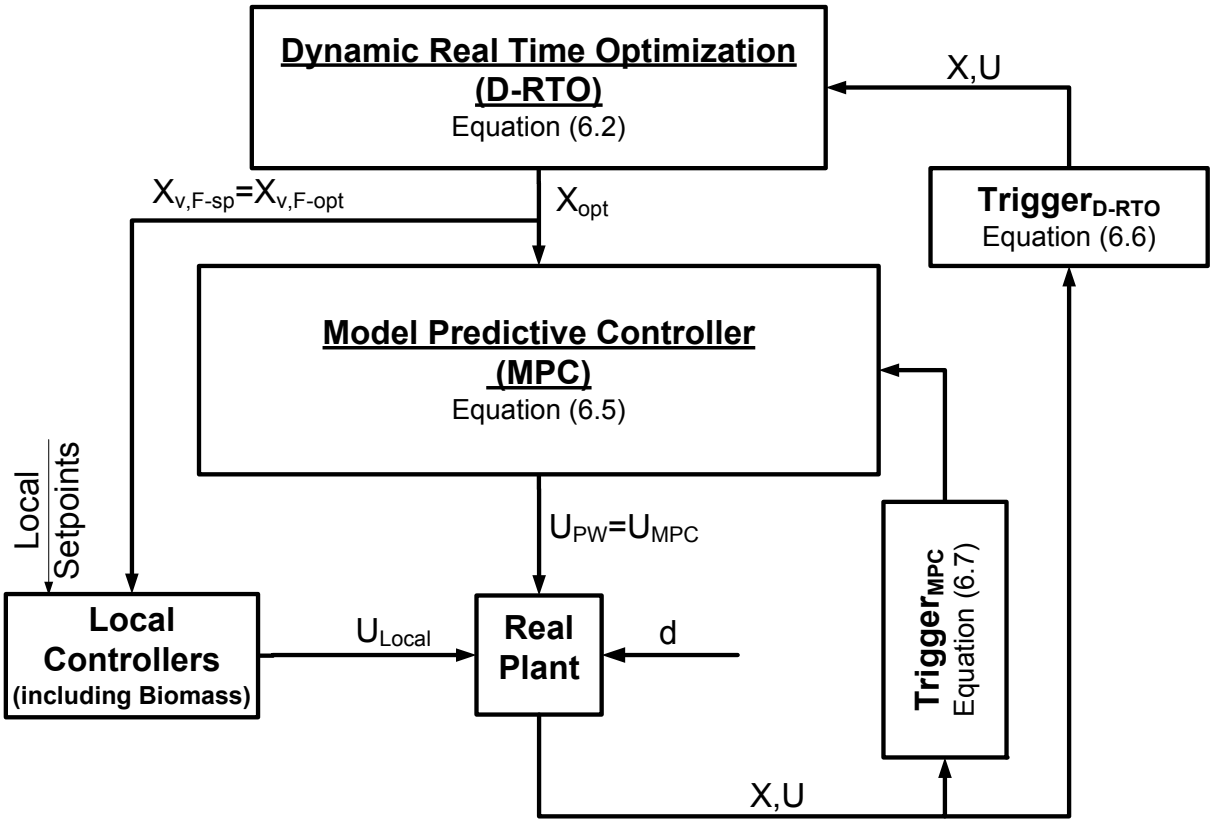

Figure 6.3 Plantwide Optimizing Control-Two-Layer scheme

In the following, the most important features for the two addressed optimization based control plantwide schemes are summarized:

1. The viable biomass control (AC-1 in Figure 6.1) loop is running in cascade with the D-RTO layer (in both frameworks), from which it receives the optimal set point value ($X_{v,F\text{-}opt}$) that should be locally tracked.

2. In both cases, the profitability objective function to be maximized in the D-RTO layer is given by Equation (6.1). The complete formulation of the optimization problem addressed in the D-RTO layers is given in Equation 6.2.

$$
\begin{aligned}
&\min_{u_{PW}=\left[F_0,F_{15},VB_1,R_1,VB_2,R_2,t_{reg},F_{21}\right]} \quad (-\Phi(\dot{x},u,t_0,\Delta t)) \\
&s.t.\ f(\dot{x},x,u,d,t)=0 \\
&\quad x(t_0)=x_0, \\
&\quad u_{\min} \le u_{PW} \le u_{\max} \\
&\quad x_{E20}(t_0+\Delta t_{opt},u_{PW}) \ge 0.998 \\
&\quad F_{20}(t_0+\Delta t_{opt},u_{PW}) \ge 80000 \\
&\quad x_{ED2}(t_0+\Delta t_{opt},u_{PW}) \ge x_{ED2}(t_0+\Delta t_{opt},u^*_{PW})
\end{aligned}
\tag{6.2}
$$

As it can be seen, the decision variables of the optimization problem are the values for the u_{PW} (u_{PW}=[F_0,F_{15},VB_1,R_1,VB_2,R_2,t_{reg},F_{21}]). The first constraint in Equation (6.2) accounts for the fulfillment of the dynamic model. The second constraint assigns the initial conditions of the state variables in the dynamic model. The third constraint bounds the values of the set of plantwide manipulated variables (u_{PW}) between the minimum (u_{min}) and maximum (u_{max}) allowed (which are given by design and operating specifications). The fourth constraint is included for assuring a final product quality equal or higher than the specification for fuel-ethanol (i.e. 0.998 mass fraction of ethanol). The fifth constraint accounts for a product flow rate equal or higher than 80.000 Ton/year (the nominal value is 100.000 Ton/year), in order to assure a minimal throughput for keeping a good profit. Finally, the last inequality constraint is used inside the optimization loop for assuring that the solution of the optimization problem will guarantee a long-term ethanol concentration at the top of the rectification column (x_{ED2}). This is done by forcing the optimization towards values of

x_{ED2} at the end of the optimization horizon equal or greater than the concentration obtained if the plantwide manipulated variables were kept constant at u_{Pw}* (which are the values of the manipulated variables at the time t_0).

3. The performance-type objective function in the NMPC layer of the PWOC-two-layer approach penalizes deviations of the main state variables in each equipment from their optimal set point values given by the D-RTO layer during a prediction horizon Δt_{mpc}=2 hours. As stated in Equation (6.3), the state variables whose performance is penalized are the following: the maltotriose in the liquefaction tank ($m_{lt,L}$), glucose in the saccharification tank (G_S), ethanol in the fermentor (E_F), top and bottoms ethanol concentration in the distillation column (x_{ED1} and x_{EB1}, respectively), top and bottoms ethanol concentration in the rectification column (x_{ED2} and x_{EB2}, respectively), and finally, ethanol concentration at the molecular sieves output, which is the final product concentration (i.e. x_{E20})

$$\Gamma = \int_{t_{0,mpc}}^{t_{0,mpc}+\Delta t_{mpc}} Q\Big[(m_{lt,L} - m_{lt,L\,opt})^2 + (G_S - G_{S\,opt})^2 + (E_F - E_{F\,opt})^2 + (x_{ED_1} - x_{ED_1\,opt})^2 + \\ + (x_{EB1} - x_{EB1_{opt}})^2 + (x_{ED2} - x_{ED2_{opt}})^2 + (x_{EB2} - x_{EB2_{opt}})^2 + (x_{E20} - x_{E20opt})^2\Big] dt \tag{6.3}$$

$$Q = \begin{bmatrix} \frac{1}{m_{lt,Lopt}} & 0 & 0 & 0 & 0 & 0 & 0 & 0 \\ 0 & \frac{1}{G_{S\,opt}} & 0 & 0 & 0 & 0 & 0 & 0 \\ 0 & 0 & \frac{1}{E_{Fopt}} & 0 & 0 & 0 & 0 & 0 \\ 0 & 0 & 0 & \frac{1}{x_{ED1opt}} & 0 & 0 & 0 & 0 \\ 0 & 0 & 0 & 0 & \frac{1}{x_{EB1opt}} & 0 & 0 & 0 \\ 0 & 0 & 0 & 0 & 0 & \frac{1}{x_{ED2opt}} & 0 & 0 \\ 0 & 0 & 0 & 0 & 0 & 0 & \frac{1}{x_{EB2opt}} & 0 \\ 0 & 0 & 0 & 0 & 0 & 0 & 0 & \frac{1}{x_{E20opt}} \end{bmatrix} \tag{6.4}$$

where Q is a diagonal matrix given by Equation (6.4). Q was defined as a normalization factor for each term in the objective function Γ, with the purpose of having the same weight value for each contribution term in the performance-type objective function.

4. The specific optimization problem solved in the NMPC layer of the PWOC-two-layer scheme is given by Equation (6.5).

$$\begin{aligned} &\min_{u_{PW}=\left[F_0,F_{15},VB_1,R_1,VB_2,R_2,t_{reg},F_{21}\right]} \quad (-\Gamma(\dot{x},u,t_{0,mpc},\Delta t_{mpc})) \\ &s.t.\ f(\dot{x},x,u,d,t)=0 \\ &\quad x(t_{0,mpc})=x_0 \\ &\quad u(t_{0,mpc})=u_{opt} \\ &\quad u_{\min}\le u_{PW}\le u_{\max} \end{aligned} \tag{6.5}$$

Constraints given in Equation (6.5) for the MPC-layer have the same meaning that those already explained for the D-RTO problem, except for the third constraint, which assigns the optimal decision variables values found by the D-RTO layer, as initial condition for the decision variables in the NMPC layer.

5. The estimation block has been neglected in both schemes under the assumption of a completely observable system (i.e. all state variables are assumed to be known).

6. The D-RTO layer in both schemes is recalled using a trigger based on the detection of disturbances and on the deterioration of the plantwide performance (detection of a decrease in the profitability objective function). This means that the D-RTO layer will be activated when a known disturbance enters the process or when a decrease in the profitability objective function takes place (e.g. caused by the occurrence of an unknown disturbance). The trigger condition for recalling the D-RTO layer is activated according to Equation (6.6).

$$Trigger\_DRTO=\begin{cases} on, & \max(d_1,d_2,...d_j)\ge d_{threshold}\vee \Phi(t-\Delta t)-\Phi(t)\ge Tol \\ off, & otherwise \end{cases} \tag{6.6}$$

where d_1, d_2,...,d_j are normalized deviation values of known disturbances that enter into the process, Δt is the sampling time and *Tol* is the maximum decrease allowed in the profitability objective function during the sampling time.

Similarly, the trigger condition for the NMPC layer is given by Equation (6.7).

$$Trigger\_NMPC = \begin{cases} on, & \left| x_{SP,i} - x_i(t) \right| > e_{i,threshold} \\ off, & otherwise \end{cases} \tag{6.7}$$

where $x_{SP,i}$ is the set point value of state *i*, $x_i(t)$ is the value of state *i* at time *t*, and $e_{i,threshold}$ is the maximum error allowed for state *i*. The evaluation of the NMPC trigger is performed at a predefined frequency, in this particular example, every 0.2 hours.

7. Finally, the real plant block is represented in this work by the Simulink model (described in Chapter 4). The real plant model incorporates white noise signals for three different kinetic parameters (one for each reaction section). These parameters are the rate constant of maltotriose production in the liquefaction (k_{mlt}), the rate constant of maltotriose consumption in the saccharification (k_3), and the maximum specific growth rate of yeast in the fermentation (μ_{max}). The noise power considered was 10^{-5}, 10^{-5} and 10^{-4}, respectively. On the other hand, the local set points entering to the local controllers block are those given in Table 6.1, with exception of $X_{v,F\text{-}sp}$, which is given by the D-RTO layer.

So far, the five first steps in the plantwide optimizing control methodology have been implemented to the bio-ethanol continuous process from starch, going from the local control loops design up to the design of the optimizing control strategy (using both, the PWOC-one-layer and the PWOC-two-layer). In the final step of the PWOC methodology, the D-RTO problem that arises in PWOC (Equation 6.2) is solved, returning as solution the optimal values for the decision variables of the PWOC problem, that is, the optimal values for the plantwide manipulated variables that lead the process to maximal profitability.

The PWOC strategies were implemented in MATLAB and the models of the process employed in the simulation, named, start-up, real plant, optimization and NMPC, were developed in

Simulink. All these Simulink models are based on the dynamic nonlinear process model developed in Chapter 4. The start-up model is used for loading the nominal steady state values of the state variables, and the corresponding input variables. The real plant model is the one already described, in which white noise signals have been incorporated. The optimization and NMPC models use a prediction horizon of 25 h and 2 h, respectively. The interaction between MATLAB and the different Simulink models for the One-Layer and Two-Layer strategies is schematically represented in Figures 6.4 and 6.5, respectively.

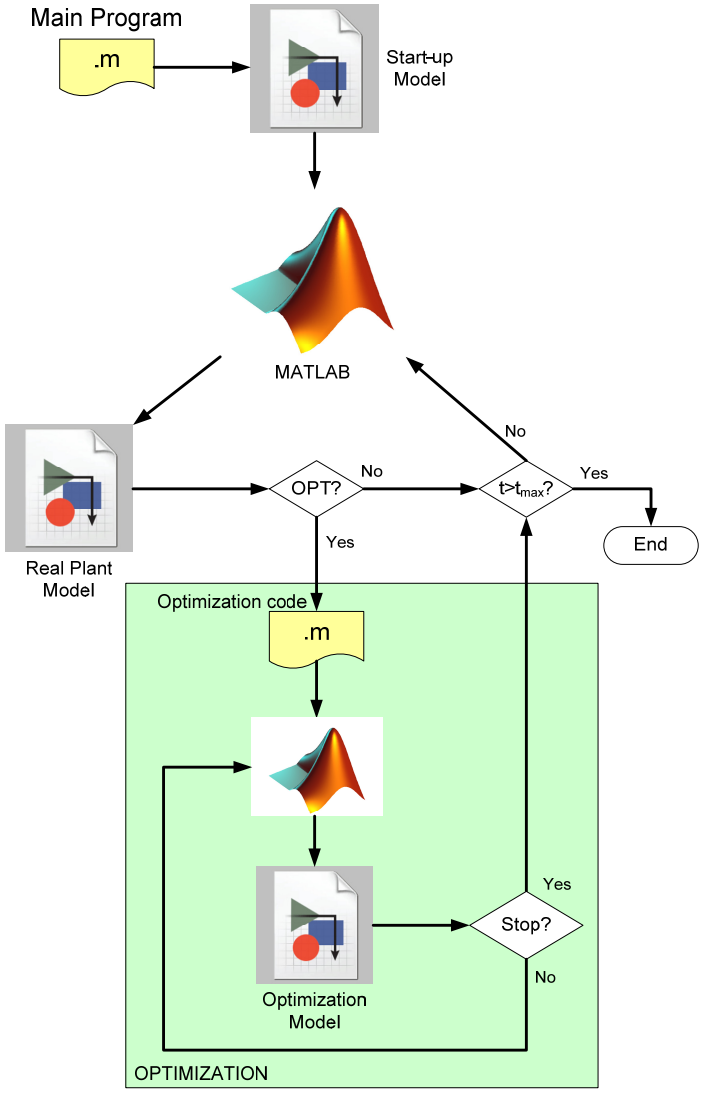

Figure 6.4 PWOC-one-layer implementation in MATLAB and Simulink

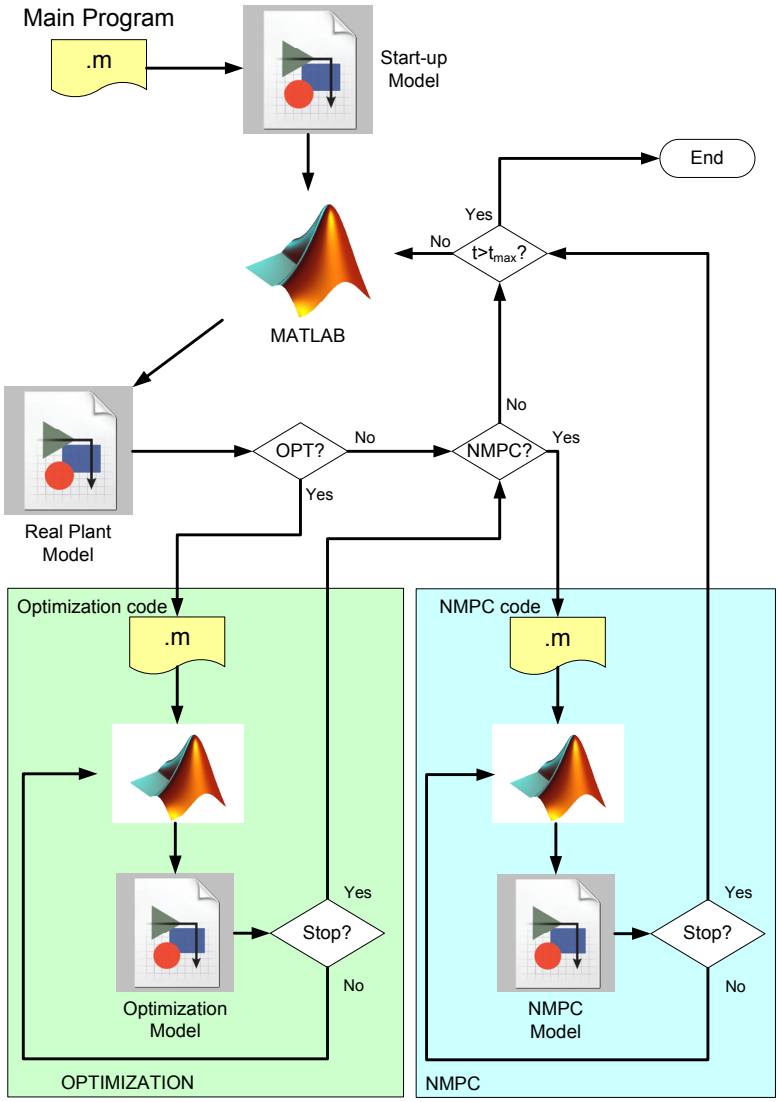

Figure 6.5 PWOC-two-layer implementation in MATLAB and Simulink

6.1.4. Stage 6: Solution of the D-RTO problem

As already mentioned in Section 2.1.4, the D-RTO problem can be solved using different formulations, namely, sequential, simultaneous or multiple shooting. In this work, a sequential formulation using stochastic methods for solving the large scale NLP problem is used. The reasons for implementing the sequential formulation (instead of simultaneous or multiple shooting) and solve it using stochastic algorithms (instead of deterministic), already mentioned in Section 5.1.6, are mainly that the sequential approach is a feasible path formulation, and that stochastic optimization algorithms are simpler to implement, do not require derivative information, usually demand a reduced computational load and can be easily connected with available simulation packages. The D-RTO problem is then solved in this work using two different algorithms, as follows:

1. The Molecular Inspired Parallel Tempering algorithm (MIPT), which was introduced in Section 3.2, and whose performance was evaluated through different case studies in Section 3.3. When compared with other stochastic methods, MIPT proved to be a suitable optimization algorithm for solving specially Dynamic Real Time Optimization problems, and problems involving many local minima. Therefore, the D-RTO problem that arose in the application of the PWOC methodology will be solved using the MIPT algorithm. The MIPT algorithm used in this work is based on follows the flowchart shown in Figure 3.5, and was implemented using the MIPT-toolbox described in Appendix A.
2. The Localized Random Search algorithm introduced in Section 2.2.1, which is a stochastic method with a very simple formulation (i.e. does not need derivative information) and easy to implement, and therefore, it can be attractive for any potential application at industrial level. The Localized Random Search (LRS) algorithm used is based on the flowchart given in Figure 2.8.

Before concluding this section, it should be emphasized that in order to improve the strategy of solution for the D-RTO problem, the shrinking approach introduced in Section 5.2 is used for reducing the search region of the optimization problem, according to the capability of each plantwide manipulated variable for rejecting both, known and unknown disturbances, while keeping a maximum profitability for the whole process. The shrinking approach was then included in the solution of the PWOC-one-layer and the PWOC-two-layer, for reducing the search space of the D-RTO problem in each case. Recalling the basic ideas already exposed in Section 5.2, the implementation of the shrinking approach is carried out as follows. First, the gain factors w_{ij} and $w_{i\Phi}$ in Equation (5.4) –which represent how much a change in the manipulated variable u_{PWi} can reject (or counteract) the occurrence of disturbance d_j, and a decrease in the profitability objective function Φ, respectively– should be calculated for each plantwide manipulated variable (u_{PWi}). Then, the standard deviation σ_{ui} of the Gaussian distribution that will describe the probability of change of each manipulated variable for rejecting the disturbances is calculated as the maximum between different contributions terms (see Equation 5.4). Afterwards, each method explores randomly the shrunk search space according to their respective algorithms. The gain factors for each plantwide manipulated variable with respect to two potential process disturbances ($S_{ung,0}$ and $e_{1,1}$) and the profitability objective function are shown in Table 6.4. Furthermore, as an example, the digraph showing the graphical relationship between $S_{ung,0}$ and each plantwide manipulated variable through the state variables in the process, is shown in Figure 6.6. The values of the weights w_{ij} shown in Table 6.4 for $S_{ung,0}$ were obtained from this digraph.

Table 6.4 Manipulated variable-disturbance gain factors obtained from digraphs

	Gain factor w_{ij} (relationship $u_{PWi} - d_j$)							
	F_0	F_{15}	F_{21}	R_1	VB_1	R_2	VB_2	t_{reg}
$S_{ung,0}$	1/2	1/7	1/11	1/10	1/10	1/11	1/11	1/12
$e_{1,1}$	1/5	1/5	1/3	1/9	1/9	1/10	1/10	1/11
$\Delta\Phi$	1/1	1/2	1/1	1/2	1/1	1/2	1/1	1/1

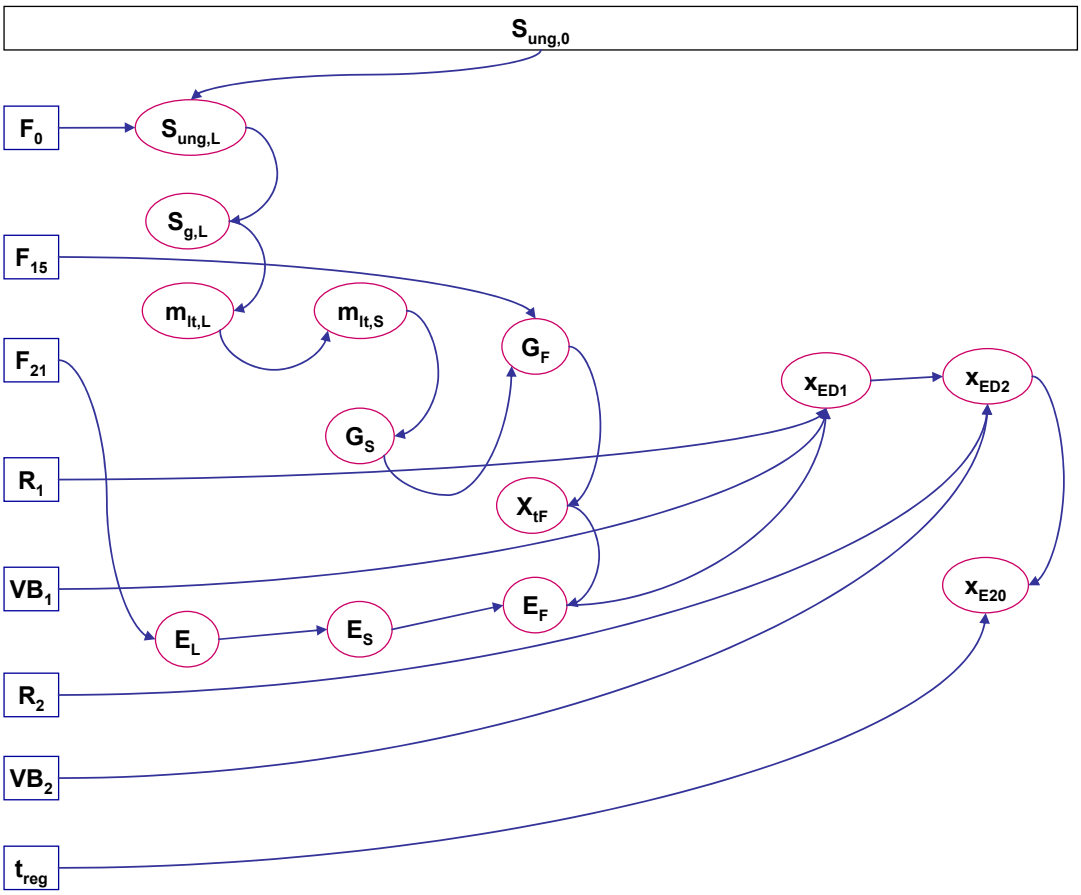

Figure 6.6 Sample digraph showing the relation between the manipulated variables (inside a rectangle) and the disturbance in starch feed concentration. Notice that such relationship comes from the reciprocal of the number of relational steps between the disturbances and manipulated variables through the state variables (in ovals).

So far, the step by step application of the Plantwide Optimizing control methodology proposed in Chapter 5 to the Bio-ethanol continuous process form starch has been carried out. In order to compare the performance of the PWOC methodology, the plantwide control problem for the bio-ethanol case study is also addressed in this work using a decentralized architecture, which is presented in the next section.

6.2. Decentralized Plantwide Control Architecture for the Bio-ethanol process

In this section, a plantwide decentralized control scheme is described, which was implemented for comparison purposes. The decentralized scheme (Figure 6.7) uses seven PI control loops, in addition to the Local Control strategy (Section 6.1.1). This scheme comprises the following loops (pairings controlled-manipulated variable): F_{20}-F_0, G_F-F_{15}, x_{ED1}-R_1, x_{EB1}-V_{B1}, x_{ED2}-R_2, x_{EB2}-V_{B2}, and x_{E20}-t_{reg}. It should be noticed that, following the recommendations given by **Araujo (2007)**, and in order to make an objective comparison of the PWOC results, the selected controlled variables for the distillation and rectification columns in the decentralized scheme are concentrations and not temperatures (or temperature differences), which are usually the real controlled variables used in industry. The corresponding tuning parameters for each loop are reported in Table 6.5.

Table 6.5 Decentralized control strategy: Variable pairing, set points and tuning parameters

Controller ID	Controlled variable	Manipulated variable	Set point	Tuning parameters[‡‡]
FC-5	F_{20} (kg/h)	F_0 (m^3/h)	F_{20sp}=257.94	F_{0ss}=27.3 K=0.2; I=0.5
AC-2	G_F (kg/m^3)	F_{15} (m^3/h)	G_{Fsp} =0.831	F_{15ss}=2.16 K=-0.4; I=0.5
AC-3	x_{ED1}	R_1 (kmol/h)	x_{ED1sp} =0.1885	R_{1ss}=3907.1 K=1500; I=10
AC-4	x_{EB1}	VB_1 (kmol/h)	x_{EB1sp}=8.6E-16	VB_{1ss}=4987.3 K=-7E9; I=10
AC-5	x_{ED2}	R_2 (kmol/h)	x_{ED2sp}=0.8874	R_{2ss}=1854.7 K=2000; I=20
AC-6	x_{EB2}	VB_2 (kmol/h)	x_{EB2sp}=7.3E-15	VB_{2ss}=2047.7 K=-7E9; I=10
AC-7	x_{E20}	t_{reg} (h)	x_{E20sp}=0.999	t_{regss}=0.466 K=-50; I=10

[‡‡] The tuning parameters were determined as follows: First, an initial set of parameters was found according to Shinskey's correlations given in **O'Dwyer (2009)**. Then, each parameter was sequentially fine-tuned by using dynamic simulations of the plant and guidelines given by **McMillan (2005)**.

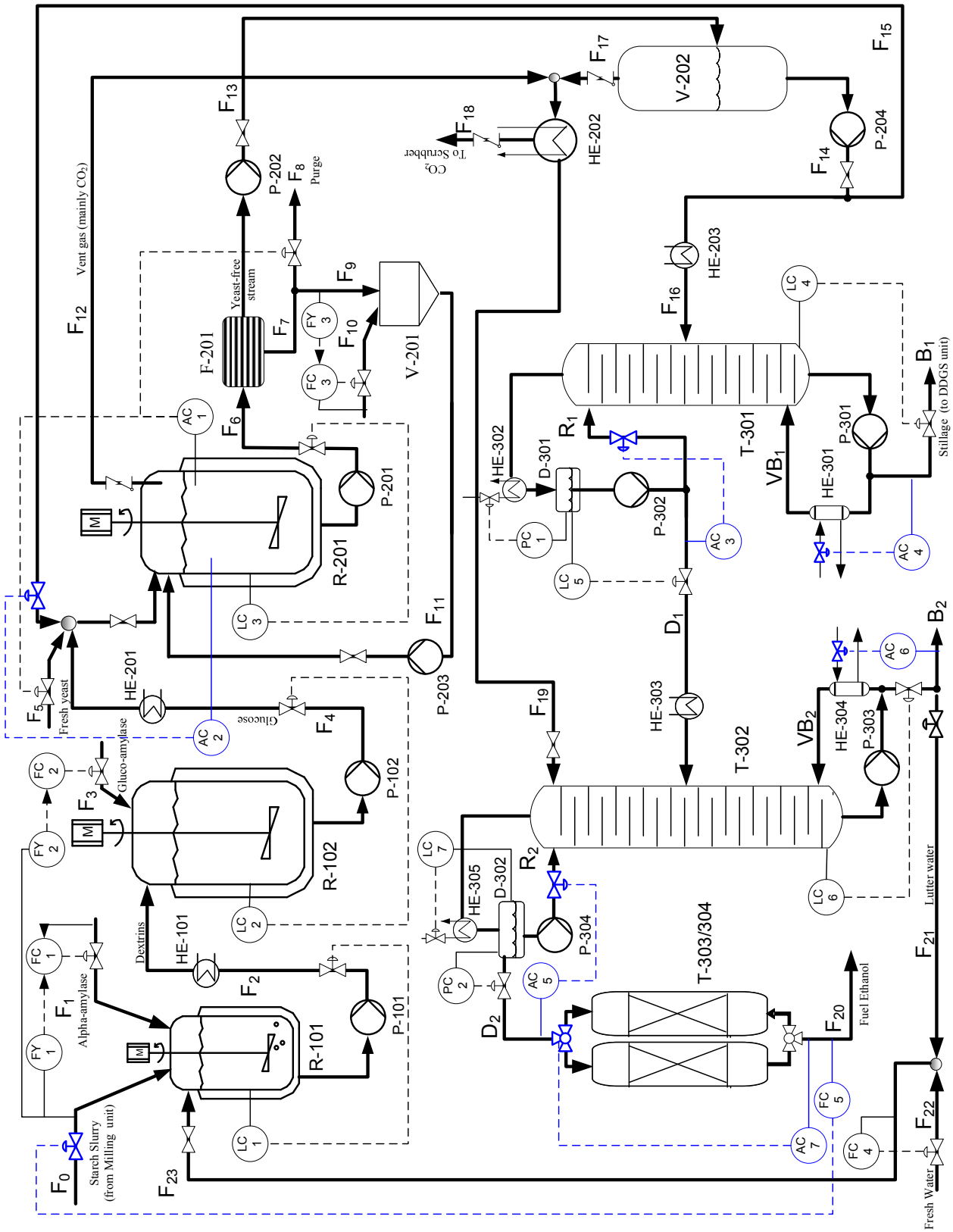

Figure 6.7 Decentralized control scheme (blue) for the ethanol production process (Local control loops described in Section 6.1.1 are also included).

6.3. Results and Discussion: Comparison of Plantwide Optimizing Control Architecture vs. Decentralized

The performance of the Plantwide Optimizing Control methodology proposed in this work is evaluated and compared with the performance of a typical Decentralized scheme, in three different scenarios, as follows:

1. Scenario 1: In this case, a **known disturbance** in the ungelatinized starch feed concentration ($S_{ung,0}$) is applied to the process after 5 hours of continuous steady operation. The disturbance is done as a step change of a 20% decrease, which means that $S_{ung,0}$ changes from 833.17 kg/m^3 to 666.53 kg/m^3 (see Figure 6.8 left). Results obtained for the PWOC-one-layer and the PWOC-two-layer are presented and discussed in Section 6.3.1, where also a comparison with the Decentralized scheme described in Section 6.2 is given.

2. Scenario 2: In this case, the response of the different PWC architectures to an **unknown disturbance** on the fermentation kinetics is investigated. The disturbance consists on a step change introduced into the maximum specific biomass growth rate (μ_{max}), which is a key parameter in the fermentation section of the process. This kind of disturbance can take place, for example, when there is a contamination in the fermentor that causes inhibition of cellular growth. This step-type disturbance is introduced into the "Real plant" block of both PWOC schemes, which represents the real process, but neither the model used by the D-RTO layer nor the model used by the NMPC layer are able to detect such disturbance due to the fact that there is no update of the model parameters. Thus, for both PWOC approaches this unknown disturbance causes a **model mismatch** between the optimization models and the real plant. In order to test the performance of the PWC approaches in a worst-case scenario, the step change applied into the maximum biomass growth rate is a 90% decrease, meaning that μ_{max} changed from 0.423 h^{-1} (at time 5 hours) to 0.0423 h^{-1} (see Figure 6.8 right).

3. Scenario 3: A **raw material price change** is introduced, which tests the performance of the different Plantwide Control architectures for facing a pessimistic scenario with market prices fluctuations. Therefore, the third scenario analyzed considers a worst-case in which the raw material price is increased in a 100% of its

current value. Although such disturbance appears to be exaggerated, in recent years, the corn raw material experienced an increase of around 70% in the period 2005-2007. (**Leibtag, 2008**). Such increase in the price was introduced as a known step disturbance in the PWOC architectures.

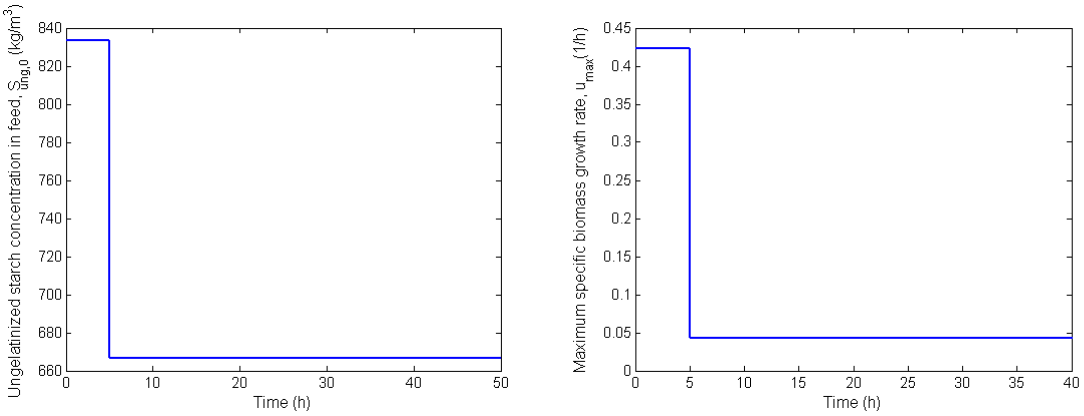

Figure 6.8 Step disturbances considered in Scenarios 1 and 2. Left: Scenario 1 - Known disturbance, 20% decrease in ungelatinized starch concentration in starch slurry feed; Right: Scenario 2 - Unknown disturbance, 90% decrease in maximum specific biomass grow rate. Both disturbances take place at time t=5 h.

The results obtained of applying the Plantwide Optimizing Control schemes for dealing with the three disturbances scenarios already described, are presented in the following sections, where the comparison with the performance obtained using the pure decentralized scheme is also discussed.

6.3.1. PWOC Performance Evaluation: Scenario 1 - Known Disturbance

In this section, results for the PWOC-one-layer and PWOC-two-layer for the case in which a known disturbance enters to the process (Scenario 1) are discussed and compared to those obtained when the typical decentralized scheme described in Section 6.2 is used. Before presenting the results obtained using the different approaches for solving the problem stated in Scenario 1, it is important to remark that all simulation studies in this work were carried out using the nonlinear model of the process (Chapter 4) as the real plant, considering some noise as already mentioned in Section 6.1.3. The results presented in this Section correspond to the simulation of the system starting at an optimal steady state operating point. After 5 hours of operation at this steady state, a known step disturbance in the starch feed concentration enters the process. At this moment, the optimization trigger (in both PWOC

schemes) is switched on and the D-RTO layer is called for first time, in order to calculate the new values of the plantwide manipulated variables that drive the process to optimal operation (maximal profitability). Then, the optimization algorithm (MIPT and/or the LRS) solves the D-RTO problem stated in Equation 6.2. For the PWOC-one-layer case, when a solution is found (i.e. when any stopping criterion is met) the optimal values of the plantwide manipulated variables are applied to the "real plant", and then, the trigger conditions are checked, which if activated, will recall the D-RTO layer. On the other hand, for the PWOC-two-layer, the NMPC layer is also activated after solving the D-RTO problem, which is used and recalled according to the defined NMPC-trigger. The process is run for a total horizon of 50 h.

Figures 6.9 – 6.20 show the simulation results obtained by applying the different Plantwide control schemes to the bio-ethanol process under Scenario 1. The results obtained using the PWOC-one-layer are presented in blue, those for the PWOC-two-layer in green, and the results for the decentralized scheme in red. At this point it is important to remark that all the control approaches compared in this section used the Local Control Strategy described in Section 6.1.1 (see Figure 6.1).

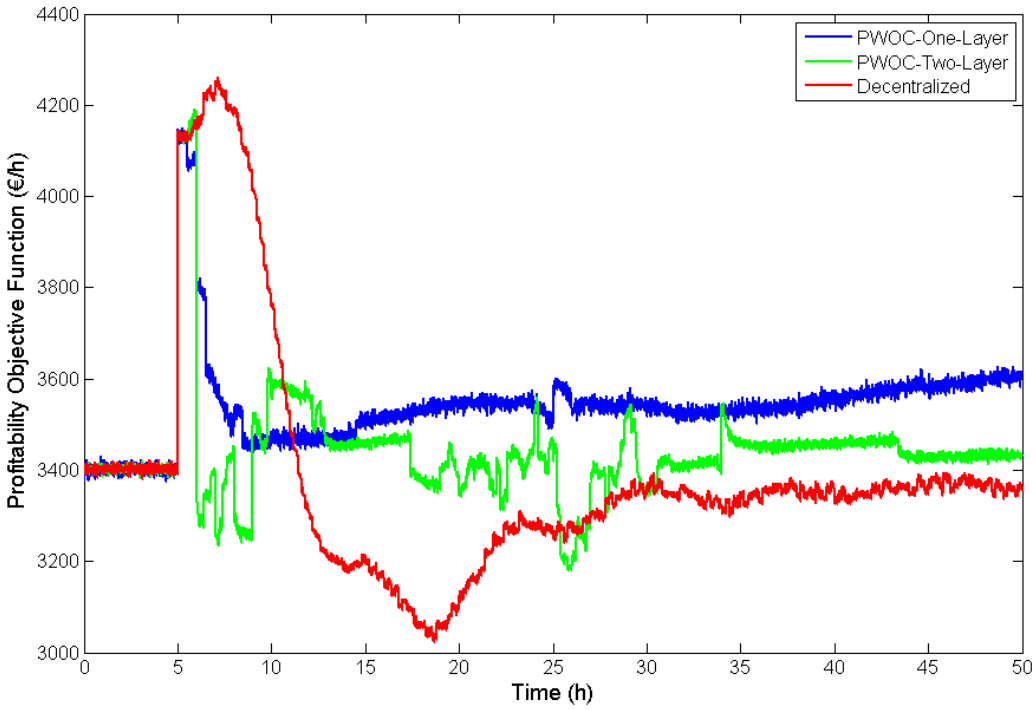

Figure 6.9 Profitability function values for Scenario 1. Blue: PWOC-one-layer. Green: PWOC-two-layer. Red: Decentralized scheme.

Analyzing the results for the profitability objective function (Figure 6.9), it is possible to observe that after the disturbance occurs the PWOC-one-layer (blue) leads the process to higher profitability than the PWOC-two-layer (green) and the decentralized scheme (red). The cumulative profitability achieved by each Plantwide Control scheme is presented in Table 6.6. It can be observed that the PWOC-one-layer has the highest cumulative profitability (1.769×10^5 €), proving to be the best scheme for facing the disturbance in Scenario 1.

Table 6.6 Cumulative Profitability Comparison in Scenario 1: PWOC vs. Decentralized

Plantwide Control Scheme	**Cumulative Profitability (€)**
PWOC-one-layer	1.769×10^5
PWOC-two-layer	1.719×10^5
Decentralized	1.696×10^5

According to Table 6.6, the second best performance is given by the PWOC-two-layer with a cumulative profitability value of 1.719×10^5 €. In contrast, the decentralized architecture resulted in the lowest cumulative profitability and also showed the slowest response to the disturbance. The poor performance (in terms of profitability value) showed by the decentralized plantwide control scheme is due to the fact that the main objective of this decentralized architecture is to maintain the controlled variables at their corresponding set point values, without considering that the disturbance may change the optimal operating point impacting negatively the profitability. In contrast, both PWOC schemes aim to increase the profitability by searching for the best values of the manipulated variables after the disturbance takes place. However, the second layer of the PWOC-two-layer (i.e. the NMPC controller layer) has an additional objective which is to minimize the tracking error of the state variables from their optimal set points given by the optimization layer, neglecting the effect of the manipulated variables on the profitability. In this way, the PWOC-two-layer applies control actions that might differ from the optimal values calculated in the D-RTO layer, which minimize the tracking error but do not maximize the profitability. On the other hand, the PWOC-one-layer has a unique objective, which is the maximization of the process profitability, and as it can be seen in Figure 6.9, it is able not only of rejecting the disturbance, but also of achieving a profitability value much better than the nominal operating point before the disturbance took place. On the other hand, the slow response of the decentralized scheme to the disturbance is caused by the large time delay between the occurrence of the disturbance and its effect on the final product (flow rate and composition).

Figure 6.10 shows the flow rate of anhydrous ethanol leaving the molecular sieves unit. It can be evidenced that for the decentralized scheme the product flow rate (F_{20}) remains almost constant for approximately 4 hours after the disturbance occurred, whereas the change in product flow rate for the PWOC schemes was immediate. This is due to the fact that the PWOC schemes take plantwide decisions against the disturbance immediately after it occurs considering a long-term prediction horizon (25 hours), and thus, the time delay of the process for counteracting the disturbance is significantly reduced.

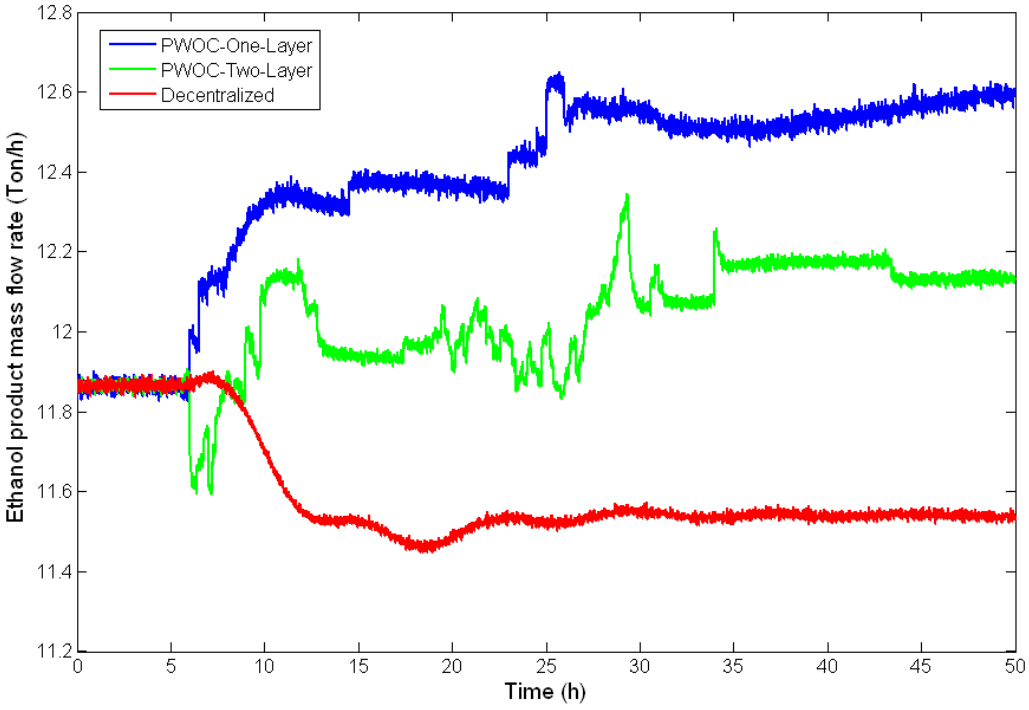

Figure 6.10 Mass flow rate of anhydrous ethanol leaving the molecular sieves units for Scenario 1. Blue: PWOC-one-layer. Green: PWOC-two-layer. Red: Decentralized scheme.

Given that there is a reduction in the concentration of ungelatinized starch in the starch slurry feed, the rate of ethanol production can only be sustained by an increase in the starch feed flow rate, as it is done by all PWC schemes considered. At this point it is important to notice that in the decentralized scheme, the product flow rate is controlled (flow control FC-5 in Figure 6.7) by manipulating the flow rate of starch slurry (Figure 6.11). However, the increase in starch flow rate after the disturbance for the PWOC-one-layer was the largest, whereas for the decentralized scheme it was the smallest. In addition, in Figure 6.10, it is observed that the PWOC approaches increased the product flow rate while the decentralized approach reduced it.

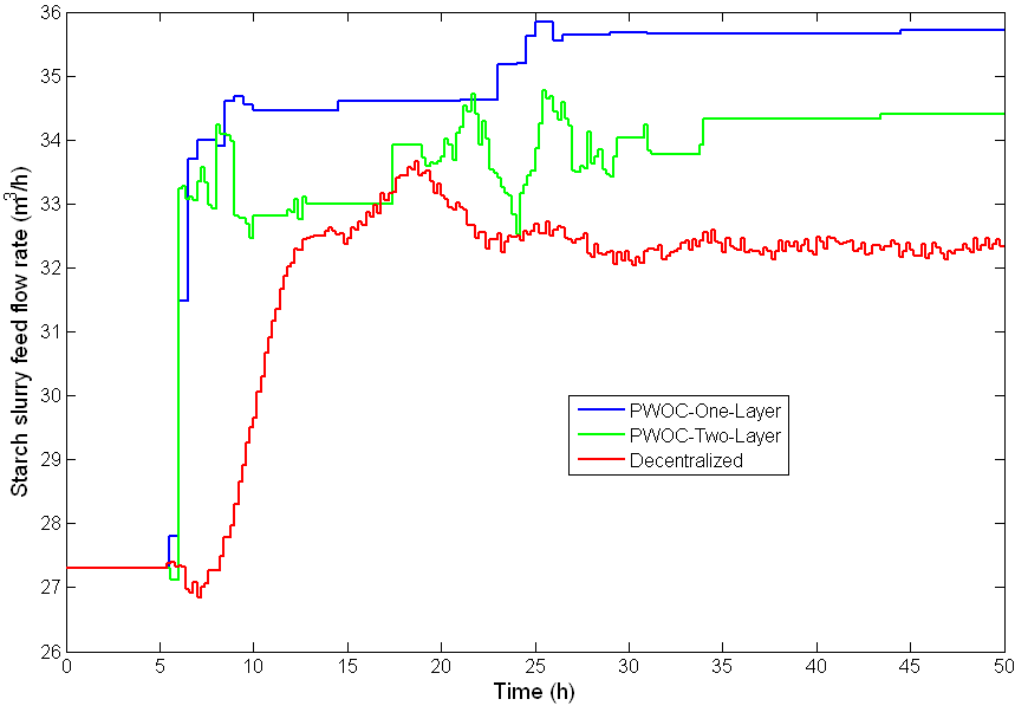

Figure 6.11 Starch slurry volumetric flow rate entering the liquefaction section for Scenario 1. Blue: PWOC-one-layer. Green: PWOC-two-layer. Red: Decentralized scheme.

In general, increasing the flow rate of starch slurry has at least three different effects on the operation of the plant. On one hand there is an increase in the net raw material flow rate for producing ethanol, which can also lead to inhibition of ethanol production by accumulation of ethanol in the fermentor. Second, there is a decrease in residence times in the reactors leading to lower conversion of the raw material (especially in the liquefaction and saccharification stages) and to inhibition of ethanol production if there is an accumulation of unreacted glucose in the fermentor. The third is a dilution effect caused by the additional water and/or non-fermentable compounds entering the system through the starch slurry feed. As a result of the dilution, the inhibition effect by ethanol concentration can be reduced but at the same time, the rate of ethanol production is reduced by the decrease in biomass and glucose concentration in the fermentor. As it can be seen, even without considering additional effects on the separation stage, the simple compensation of raw material for rejecting the disturbance in starch feed composition does not necessarily lead to optimal operation. The advantage of the PWOC-one-layer is that it is able to identify the adequate starch flow rate which maximizes the profitability of the plant, overcoming the compromise imposed by the inhibition and dilution effects. The PWOC-two-layer approach finds a different balance between the profitability and control performance (almost constant product flow rate) objectives. The result is an intermediate behavior between the pure economical

objective (PWOC-one-layer) and the pure control performance objective (decentralized approach). Finally, it is important to mention that the decentralized approach presented a negative offset in ethanol flow rate which can be explained by the slow dynamic response and the long time delays of the plant. For this control configuration, any effort exerted in removing the offset led to controller instability with large and sometimes divergent oscillations.

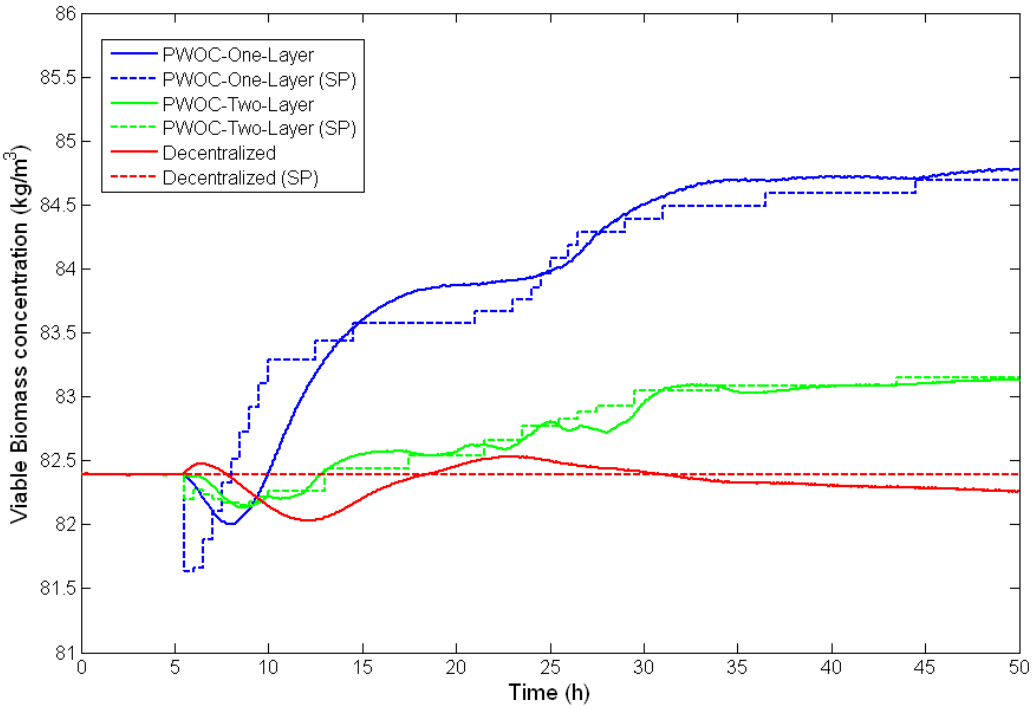

Figure 6.12 Biomass concentration (solid lines) and Biomass concentration setpoint (dashed lines) in the fermentor for Scenario 1. Blue: PWOC-one-layer. Green: PWOC-two-layer. Red: Decentralized scheme.

In the following, an analysis of the main state variables as well as the profiles for the main plantwide manipulated variables in the process is presented. First, the analysis is focused on the fermentation section (Figure 6.12 – 6.14) and then on the purification section, including the rectification and molecular sieves units (Figures 6.15 – 6.20). Figure 6.12 shows the dynamic behavior of the viable biomass concentration in the fermentor. As it can be seen, after the disturbance enters the process, the viable biomass for the PWOC schemes first decreases slightly and then increases reaching values of 84.5 kg/m^3 and 83 kg/m^3 for the PWOC-one-layer and the PWOC-two-layer, respectively, 25 hours after the disturbance occurrence. On the other hand, the decentralized scheme kept the viable biomass at its set point value of 82.4 kg/m^3, which corresponds to the nominal steady state. The optimal

biomass profiles applied by the PWOC schemes drive the ethanol concentration in the fermentor to slightly higher values when compared to the decentralized scheme, as it is shown in Figure 6.13.

Even thought the differences in viable biomass and ethanol concentration in the fermentor may seem small, analyzing Figure 6.14, which is the total ethanol mass flow rate entering to the purification section ($E_F \times F_6$), it is possible to observe that using a combination of higher ethanol concentration and larger starch flow rates (see Figure 6.11), the PWOC-one-layer drives the process operation towards the highest productivity in the fermentation section, contributing very positively to increase increasing the process profitability.

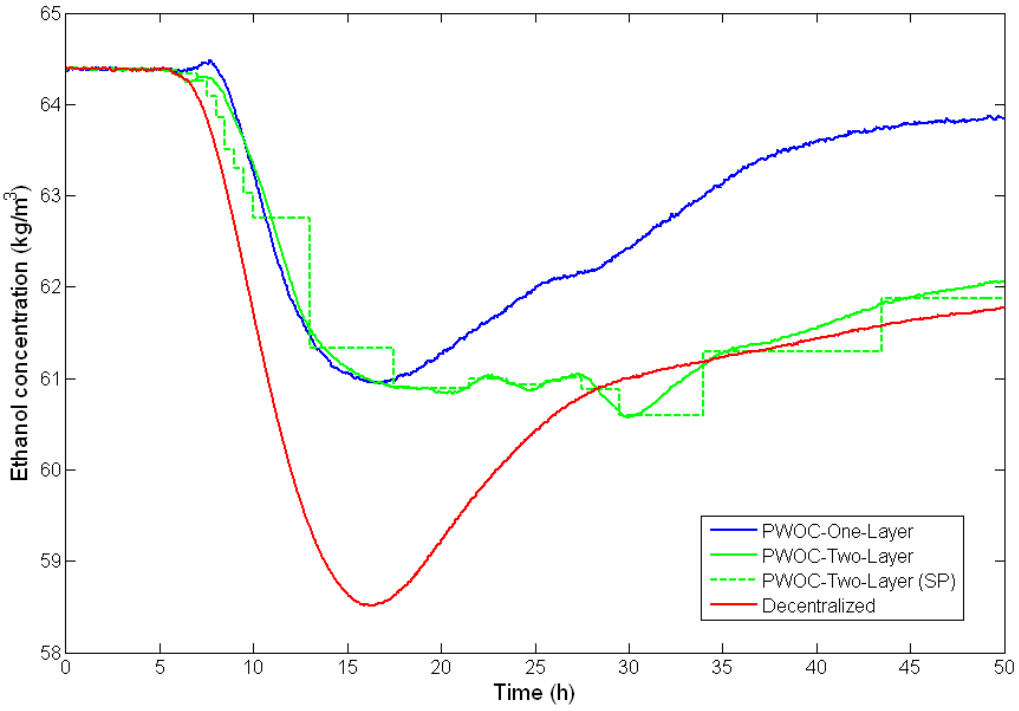

Figure 6.13 Ethanol concentration (solid lines) and ethanol concentration setpoint (dashed line) in the fermentor for Scenario 1. Blue: PWOC-one-layer. Green: PWOC-two-layer. Red: Decentralized scheme.

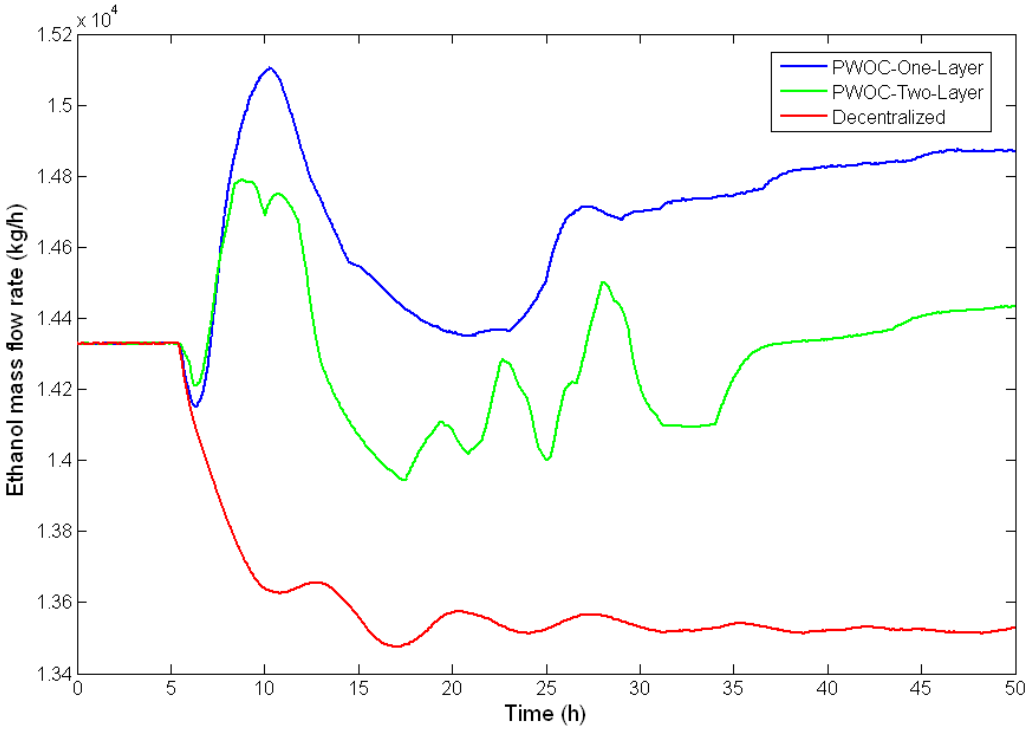

Figure 6.14 Ethanol mass flow rate to the purification section for Scenario 1. Blue: PWOC-one-layer. Green: PWOC-two-layer. Red: Decentralized scheme.

Following the analysis, in the next, the results obtained for the distillation and rectification sections are presented. Figure 6.15 and Figure 6.16 show the results for the ethanol concentration at the top of the distillation (x_{ED1}) and at the top of the rectification (x_{ED2}), respectively. It can be observed that the strategy applied by the PWOC-one-layer (blue line) relies on increasing the purity of the ethanol concentration that leaves the distillation column, whereas allowing a slightly decrease in the ethanol concentration leaving the rectification column. The reason behind this strategy is that, by doing so, the optimizer finds an operating point with lower total energy consumption for the distillation-rectification system, without deteriorating the quality requirements of the final product (Figure 6.19). Such total energy consumption correlated to the sum of the vapour boil-up rates of both columns, is shown in Figure 6.17. At this point, it is important to remark that in this example, the optimum operating conditions for the purification and fermentation sections shifted from their initial nominal values as a consequence of the presence of the disturbance, and this is not considered by the decentralized scheme.

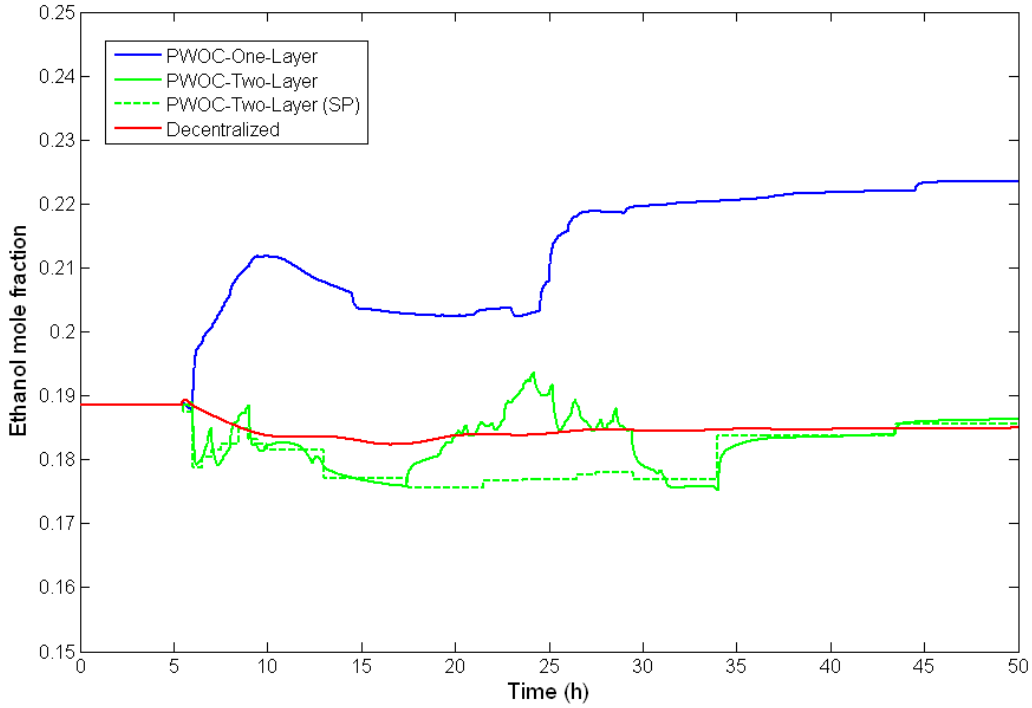

Figure 6.15 Ethanol mole fraction at the top of the distillation column for Scenario 1. Blue: PWOC-one-layer. Green: PWOC-two-layer. Red: Decentralized scheme. Dashed: Ethanol concentration set point at the top of the distillation column.

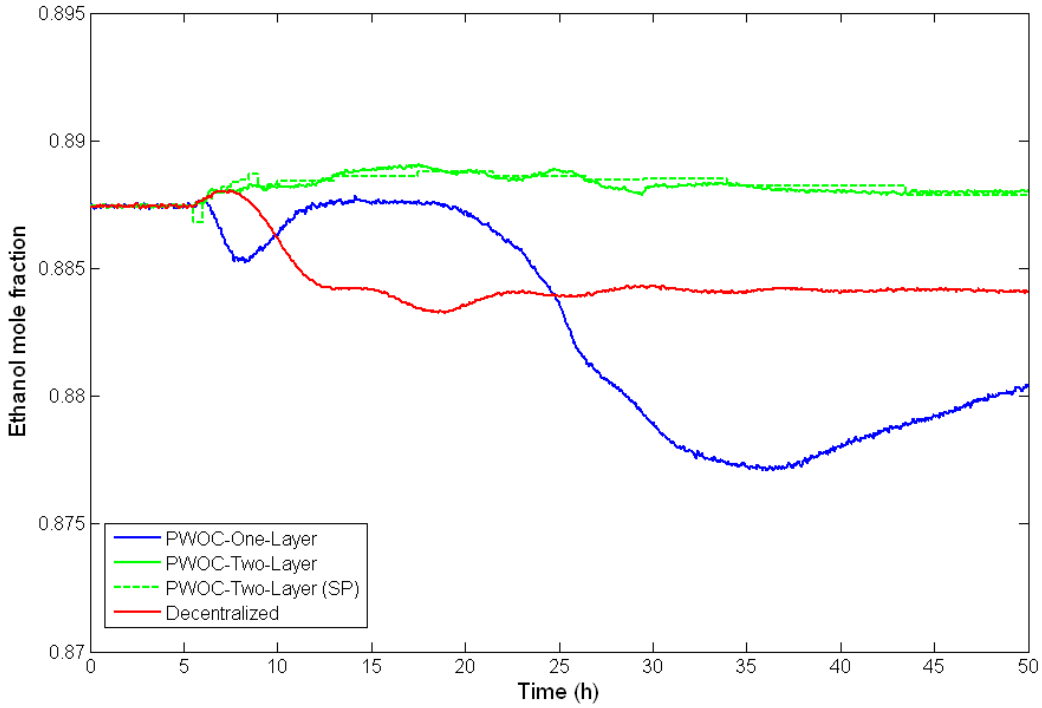

Figure 6.16 Ethanol mole fraction at the top of the rectification column for Scenario 1. Blue: PWOC-one-layer. Green: PWOC-two-layer. Red: Decentralized scheme. Dashed: Ethanol concentration set point at the top of the rectification column.

Following with the analysis of the purification section, it must be also noticed that the PWOC-two-layer does not allow large deviations in composition at the top of the distillation and rectification columns (as a result of the control performance objective), while at the same time reduces the operating costs in the purification section (economic objective). Unfortunately, the tight control in composition is accomplished by abrupt changes in the distillate flow rates (Figure 6.18) which ultimately affect the operation of the molecular sieves unit (Figure 6.20), increasing regeneration costs and reducing the plantwide profitability, and eventually compromising the quality of the final product by reaching values close to the specification limit from time to time (Figure 6.19).

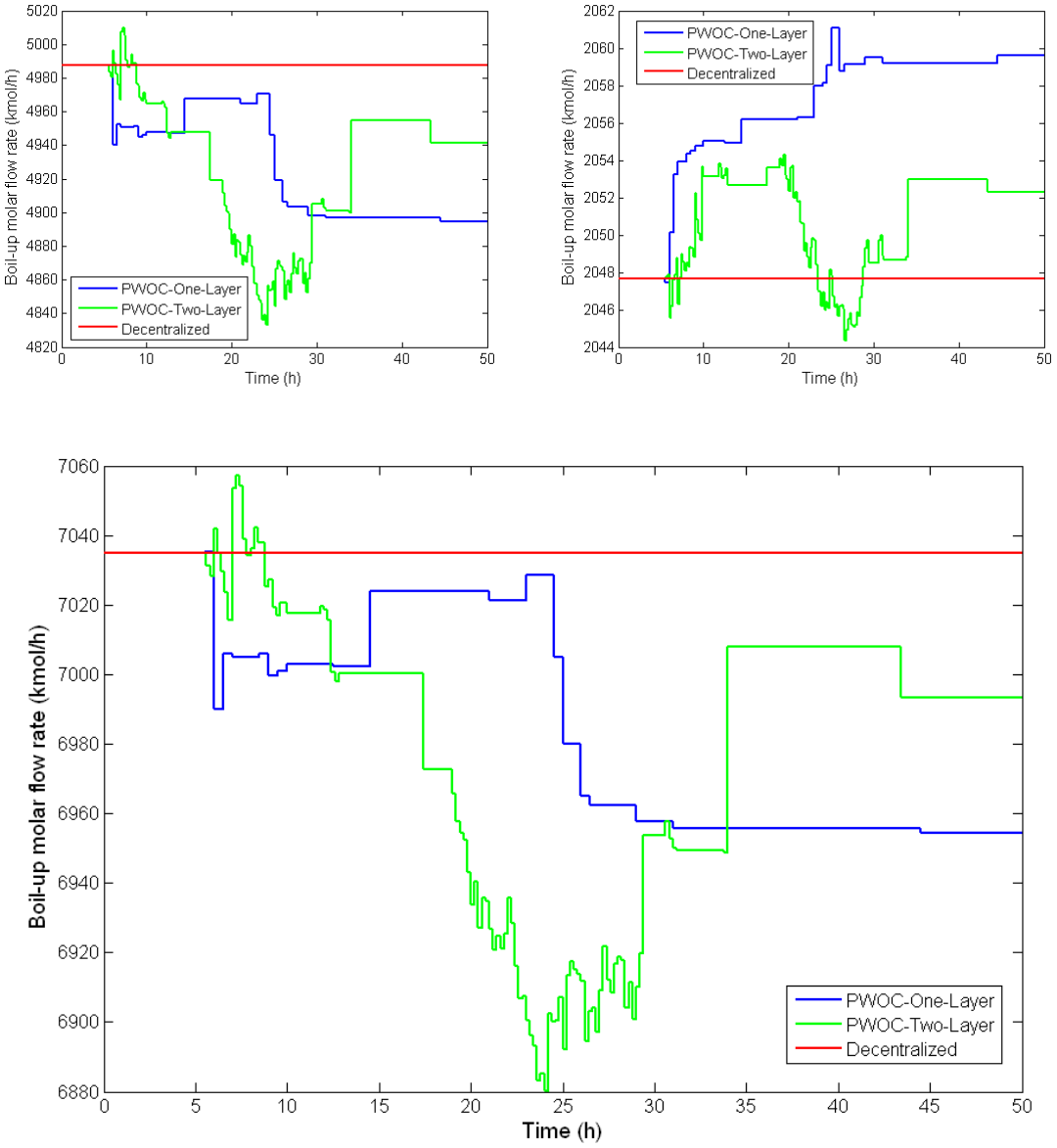

Figure 6.17 Boil-up molar flow rates in the purification section for Scenario 1. Distillation column (top-left), Rectification column (top-right), Sum of boil-up molar flow rates of the distillation and rectification columns as a measure of their energy consumption (bottom). Blue: PWOC-one-layer. Green: PWOC-two-layer. Red: Decentralized scheme.

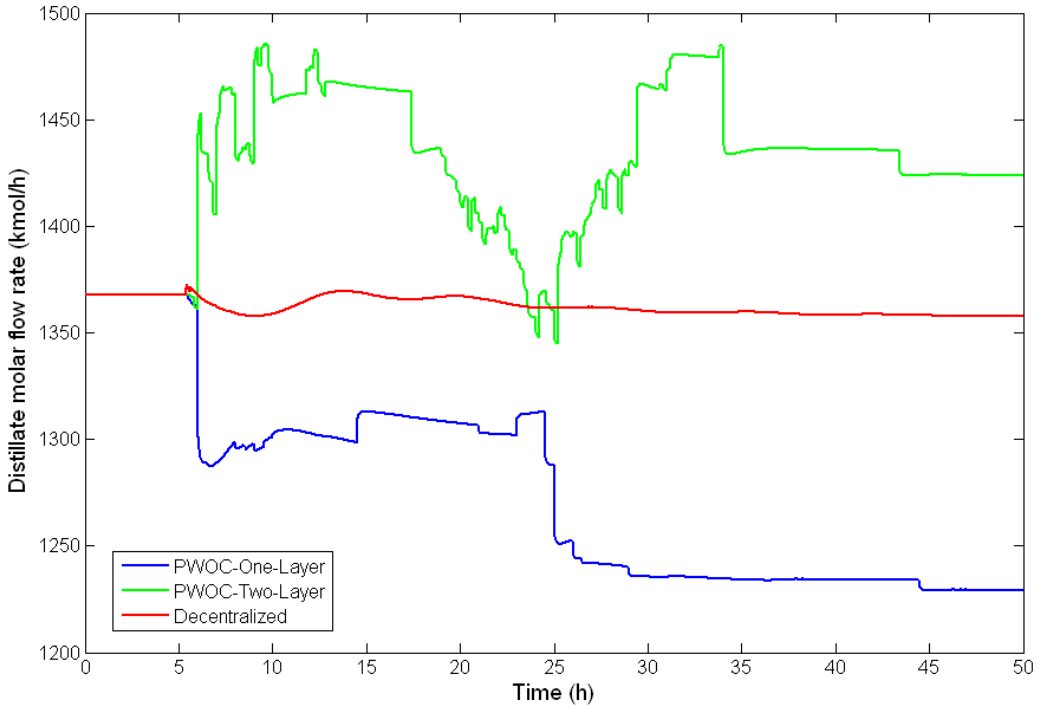

Figure 6.18 Distillate flow rates for Scenario 1. Blue: PWOC-one-layer. Green: PWOC-two-layer. Red: Decentralized scheme.

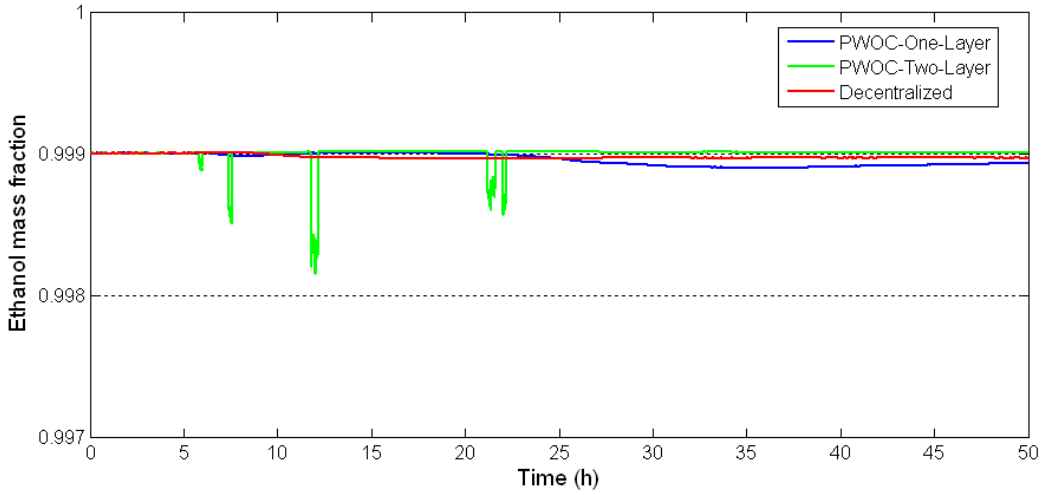

Figure 6.19 Ethanol mass fraction in the final product leaving the molecular sieves unit for Scenario 1. Blue: PWOC-one-layer. Green: PWOC-two-layer. Red: Decentralized scheme. Set point: 0.999; specification limit: 0.998.

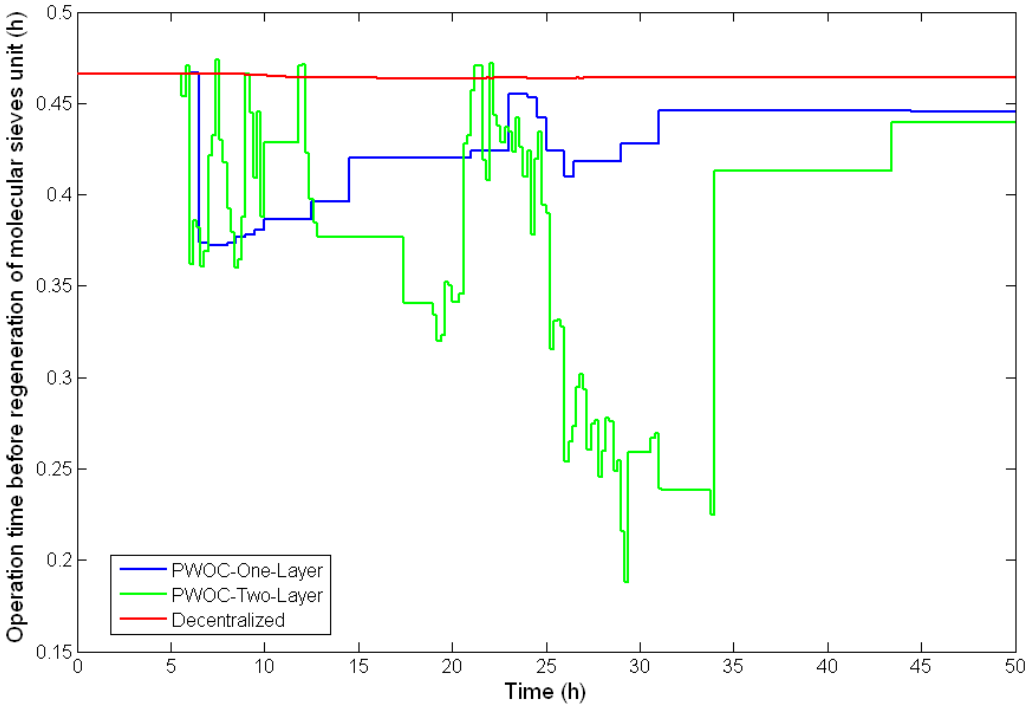

Figure 6.20 Operation time before regeneration of the molecular sieves units for Scenario 1. Blue: PWOC-one-layer. Green: PWOC-two-layer. Red: Decentralized scheme.

By far, the comparison of the different Plantwide Control schemes for dealing with the known disturbance in Scenario 1 has been presented. After analyzing the results taking into account not only the dynamic behavior of the main state variables in the process, but also the plantwide manipulated variables profiles applied by the PWOC-one-layer, the PWOC-two-layer and the decentralized scheme, it is possible to conclude that the three plantwide schemes applied resulted in different performance due to the fact that they pursue different objectives: a pure economical objective for the PWOC-one-layer, a pure control performance objective for the decentralized, and a good balance between the pure economical and the pure control performance for the PWOC-two-layer. As it was evidenced in this section, if the aim of a process production plant is to operate at maximal profitability, the PWOC-one-layer scheme is the best option. However, as stated by **Engell (2009)**, stability of the Direct Optimizing Control has not be proven yet, as it has been done for the integration between the RTO-MPC (i.e. two-layer architecture) and for the conventional decentralized schemes. Therefore, it is possible to think that still much work is needed for convincing the industrial sector about relying on the Plantwide Optimizing Control- One-Layer approach instead of using the second layer that introduces the MPC controller, or the pure decentralized architecture. Finally, it is important to mention that the intention of this work, as it will be shown also in Scenario 2 and Scenario 3 (sections 6.3.5 and 6.3.6 respectively), is to show

that besides of being successful in leading the process to maximal profitability where a known disturbance enters the process, the PWOC-one-layer is a very suitable and successful architecture capable to overcome even worst-case scenarios in which the pure decentralized scheme appears to be weak.

Before presenting the comparative results of the performance of the different Plantwide control schemes for facing the next disturbance scenario (in Section 6.3.5), denoted as Scenario 2 (i.e. unknown disturbance + model mismatch), additional results are presented in the following sections. First, in Section 6.3.2, representative results are shown, in order to demonstrate the advantages of using the Shrinking approach proposed in Section 5.2 as part of the strategy for solving the D-RTO problem that arises in the PWOC formulation. Then, in Section 6.3.3, three different replicas for solving the PWOC-one-layer using the MIPT algorithm are compared, in order to show the reproducibility capacity of the method despite the fact of being stochastic in nature. Finally, in Section 6.3.4, the performance of the MIPT and the Localized Random Search (LRS) algorithms in the PWOC-one layer and PWOC-two layer formulations is compared for dealing with the disturbance in Scenario 1.

6.3.2. PWOC-one-layer: Comparison of Shrinking vs. No Shrinking for Scenario 1

The Shrinking approach proposed in Section 5.2 has the purpose of reducing the search space of the D-RTO problem according to the capability of each plantwide manipulated variable for rejecting known and unknown disturbances that negatively impact the process profitability. The main advantage of using the shrinking approach is that the probability of change for each manipulated variable is a function of their capability for rejecting each disturbance; in other words, by implementing the shrinking approach, the optimization algorithm does not waste time testing large changes in the manipulated variables that just reject in a weak manner (or are not able to reject) the disturbances. In the case without shrinking, each manipulated variable is allowed to change from its lower to its upper bound, without any other restriction, whereas the shrinking approach bounds the search region according to the standard deviation calculated for each manipulated variable. Precisely, this standard deviation contains the information about the cause-effect relationship between each manipulated variable and each disturbance. In order to evaluate the performance of the shrinking approach, several simulation studies applying the PWOC with and without shrinking the search region of the optimization problem were carried out. Figures 6.21 – 6.23

show representative results obtained for the PWOC-one-layer using the shrinking approach (blue line), compared to the results obtained when the same problem was solved without implementing the shrinking (black line). In both cases the optimization algorithm used was the MIPT, using as stopping criteria the maximum number of function evaluations (Nf_{eval} =30) and/or a maximum time for running the optimization routine (t_{limopt}=0.4 h). For comparison purposes, in Figure 6.21, besides the profitability objective function, also the profiles for the main plantwide manipulated variables (F_0, R_1, V_{B1}, R_2 and V_{B2}) are presented in Figures 6.22 and 6.23

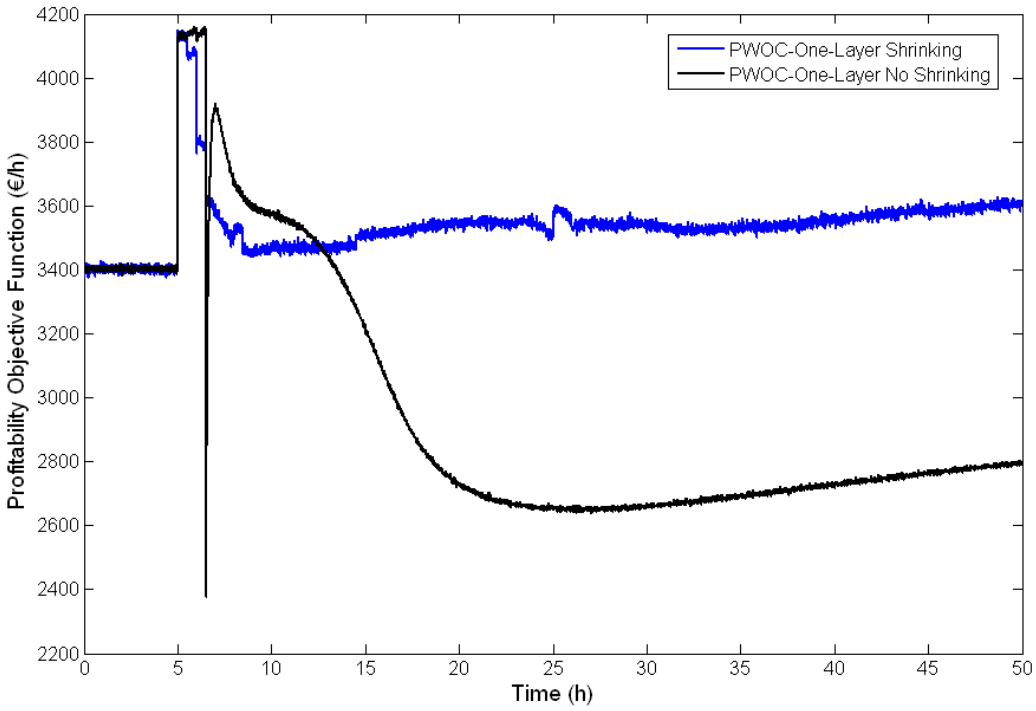

Figure 6.21 Profitability objective function PWOC-One-layer: Shrinking vs. No Shrinking for Scenario 1. Blue: PWOC-one-layer implementing search region shrinking. Black: PWOC-one-layer without shrinking.

As it can be seen in Figure 6.21, when the shrinking approach (blue line) is implemented in the solution strategy for solving the D-RTO problem, the process is led to a much higher profitability than when no shrinking is applied, being capable of successfully rejecting the disturbance that affected the process. In contrast, when no shrinking is used, the process profitability decreases considerably. This poor performance obtained when no shrinking is used can be understood analyzing the profiles of the main plantwide manipulated variables. It can be seen that when no shrinking is used (black line) each manipulated variable changes in a step-type policy with higher amplitude and longer period than when using shrinking

(blue line). Therefore, due to the wider search region where the algorithm must look for the optimal values of the decision variables, the optimization algorithm is not able of finding suitable movements of the plantwide manipulated variables, in a reasonable time, i.e. before meeting any stopping criterion, and it gets stuck in local minima that lead the process to lower profitability. In fact, in the ideal case where the shrinking and no shrinking approaches where run unlimitedly, both approaches would achieve the same performance.

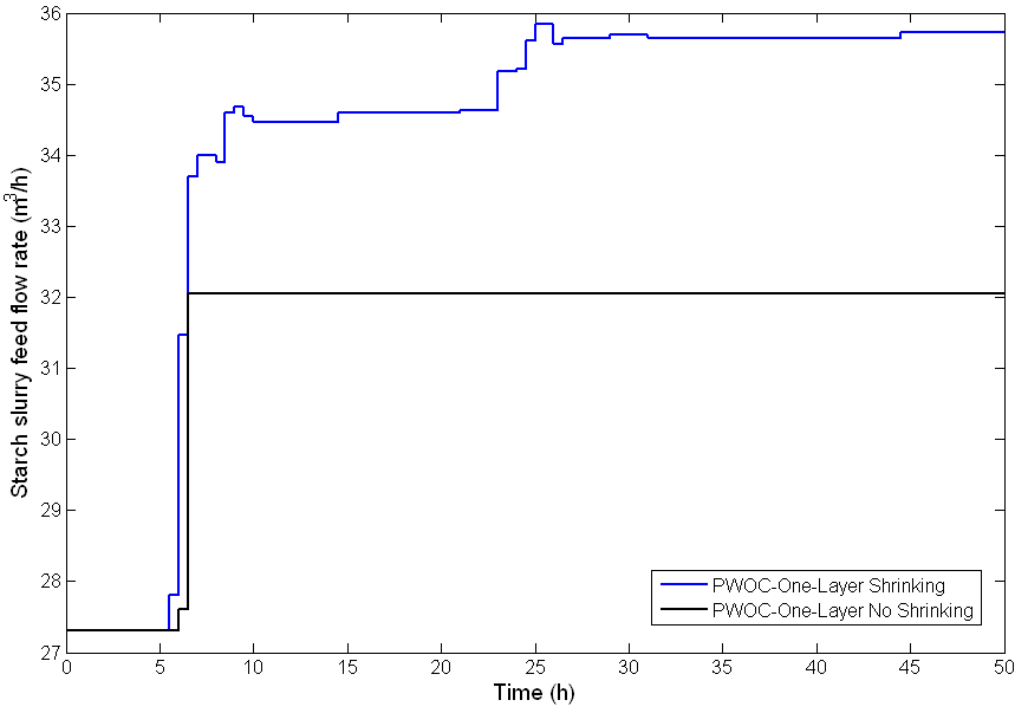

Figure 6.22 Starch slurry volumetric flow rate PWOC-One-layer: Shrinking vs. No Shrinking for Scenario 1. Blue: PWOC-one-layer implementing search region shrinking. Black: PWOC-one-layer without shrinking.

Finally, it is possible to conclude that when the shrinking approach is used as part of the solution strategy of the Plantwide Control problem for online applications (in which usually a stringent limit time exists for running the optimization), a very important improvement in the performance of the solution strategy is achieved. For the particular case analyzed, this improvement in optimization allowed the achievement of a much higher profitability. Furthermore, it has been also shown that when using the shrinking, smoother changes in the control actions are applied, which is also a very important issue regarding process stability and equipment protection.

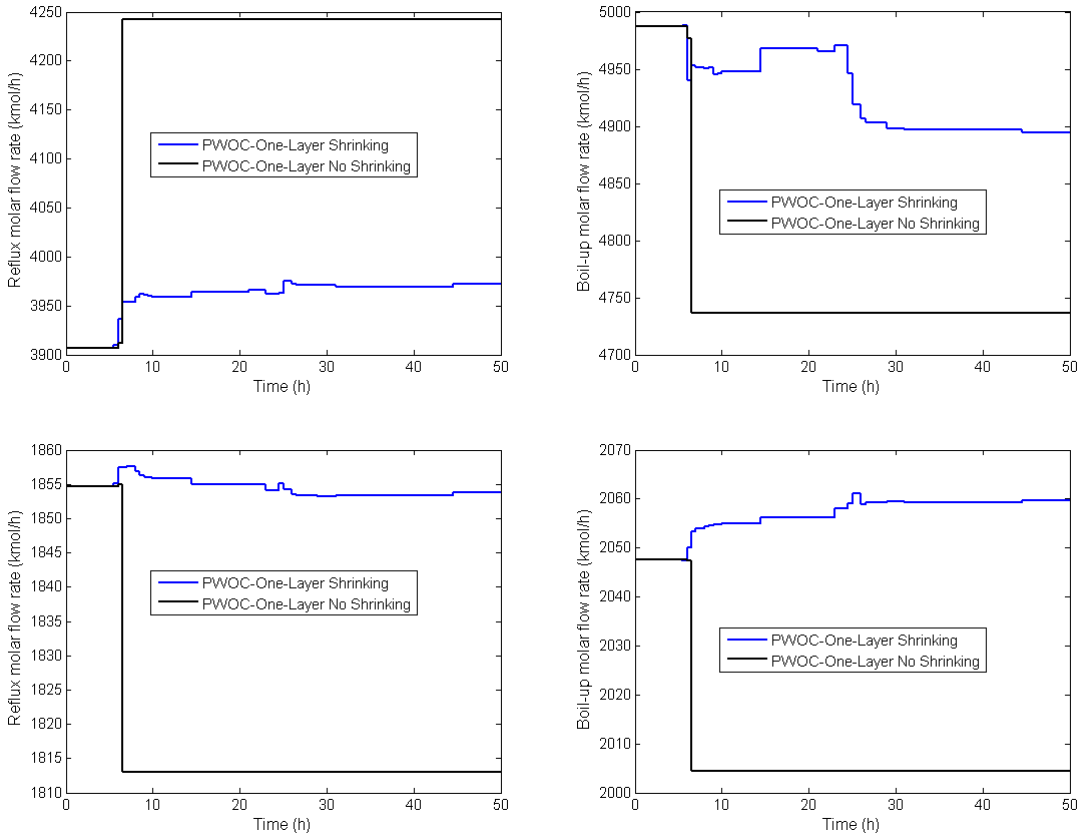

Figure 6.23 PWOC-One-layer: Shrinking vs. No Shrinking for Scenario 1. Reflux molar flow rate in the distillation column (top-left), Boil-up molar flow rate in the distillation column (top-right), Reflux molar flow rate in the rectification column (bottom-left), and Boil-up molar flow rate in the rectification column (bottom-right). Blue: PWOC-one-layer implementing search region shrinking. Black: PWOC-one-layer without shrinking.

6.3.3. PWOC-one-layer: Replicas Comparison of MIPT for Scenario 1

Given that the MIPT algorithm used for solving the D-RTO problem in the PWOC-one-layer is a stochastic method, the purpose of this section is to show that in spite of the random nature of the method, the results obtained by applying MIPT for solving the PWOC problem are reproducible following almost the same path and converging to almost the same optimal value at the end of the simulation period (i.e. 50 hours). The results presented in Figure 6.24 compare the profitability objective function for three different replicas in which the MIPT optimization algorithm was used in the application of the PWOC-one-layer scheme for facing a known disturbance (Scenario 1). Furthermore, Table 6.7 shows a comparison of the cumulative profitability value achieved in each case.

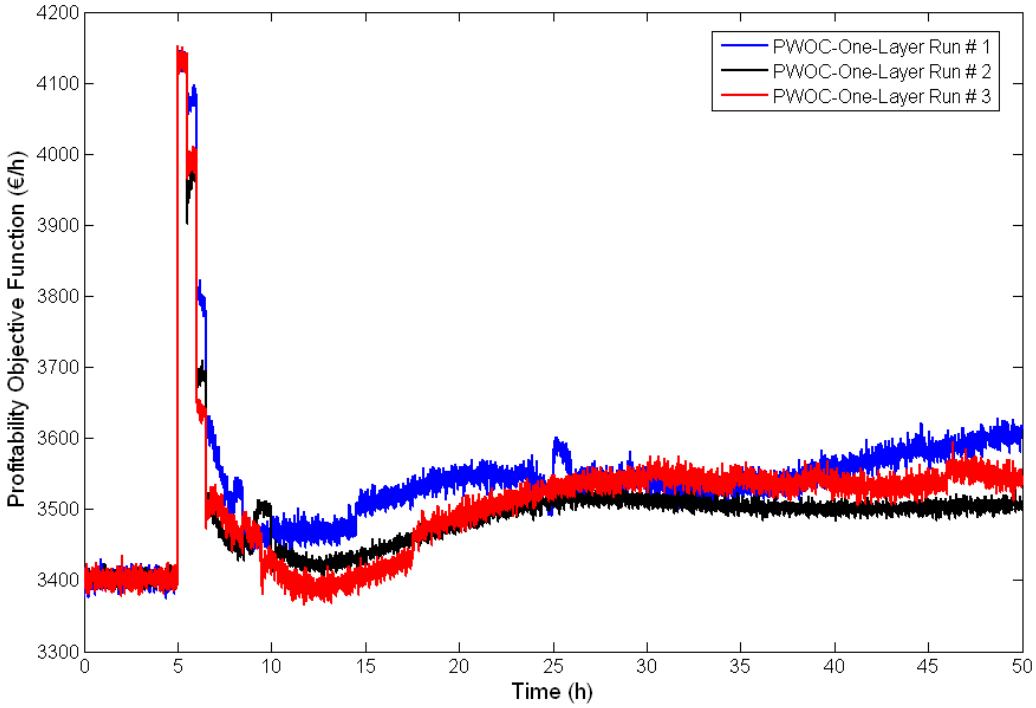

Figure 6.24 Profitability Objective function PWOC-one-layer: Comparison of different MIPT replicas.

Table 6.7 Cumulative Profitability Comparison in Scenario 1: Analysis of different Replicas

Plantwide Control Scheme	**Cumulative Profitability (€)**
PWOC-one-layer-Replica#1	1.769×10^5
PWOC-one-layer-Replica#2	1.746×10^5
PWOC-one-layer-Replica#3	1.753×10^5

As can be seen in Figure 6.24, the different replicas do not converge to exactly the same point due not only to the stochastic decisions made by the method, but also to the fact that the optimization problem solved is a multivariable problem (involving 8 decision variables) and may exhibit many local minima. However, it should be noticed that all replicas achieved almost the same cumulative profitability value (Table 6.7). Also, it is important to mention that the optimization stopped in most cases by the time criterion imposed. For this reason, the optimal value found may not be the global optimum but an operating point close to the optimum, obtained before the time limit was reached. From the comparison of the different replicas, it is possible to conclude that the results obtained by the MIPT algorithm are reproducible. This is an important fact that, together with the global character of the method, potentiates the use of MIPT for Plantwide Control applications.

All results shown until now for solving the problem stated in Scenario 1 were obtained using the MIPT algorithm described and evaluated in Chapter 5. In the following section, the MIPT is compared to the Localized Random Search (LRS) method, which is a stochastic local optimization algorithm, whose main advantage is the easiness of application, being very intuitive without requiring much programming effort, and therefore it might be of interest for industrial applications.

6.3.4. PWOC-one-layer: Comparison between MIPT and LRS for Scenario 1

In order to compare the performance of the MIPT and the Localized Random Search (LRS) algorithms, in this section the results obtained using both methods in terms of the profitability objective function are presented. Figure 6.25 shows the comparison between the profitability obtained with the PWOC-one-layer using the MIPT algorithm (blue line) and the PWOC-one-layer using the LRS algorithm (red line). Furthermore, the comparison of the two optimization algorithms is also made for the PWOC-two-layer case (Figure 6.26). In Figure 6.26, the differences obtained applying the PWOC-two-layer using the MIPT algorithm (blue line) and the PWOC-two-layer using the LRS algorithm (red line) can be clearly appreciated.

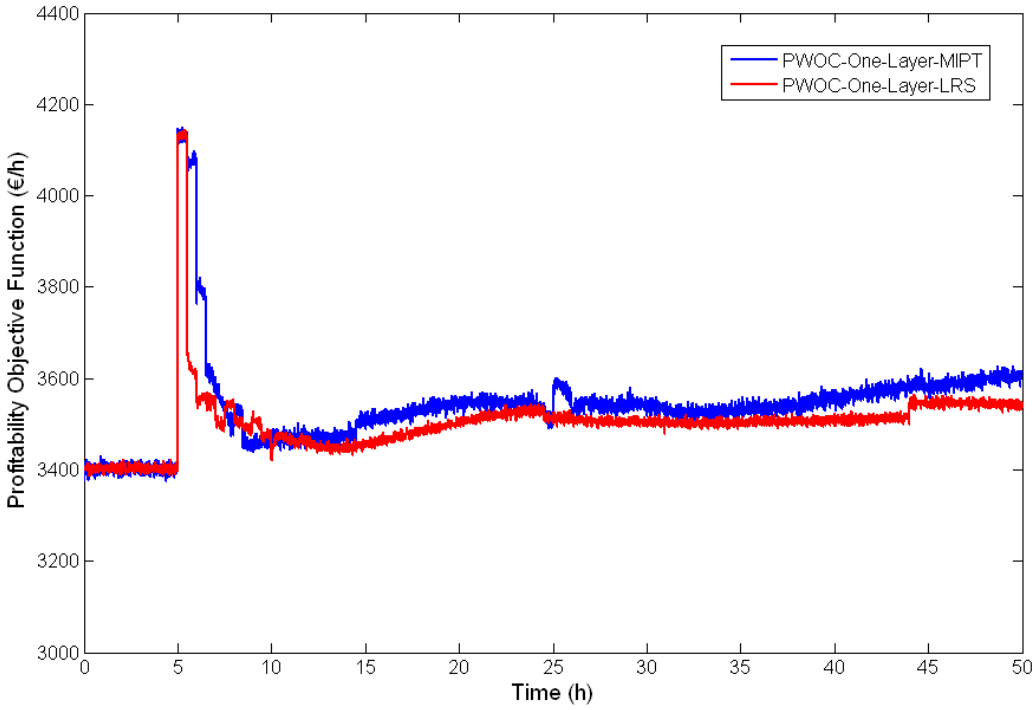

Figure 6.25 PWOC-one-layer: Comparison of the Molecular Inspired Parallel Tempering (MIPT) Algorithm (blue line) and the Localized Random Search (red line) for Scenario 1.

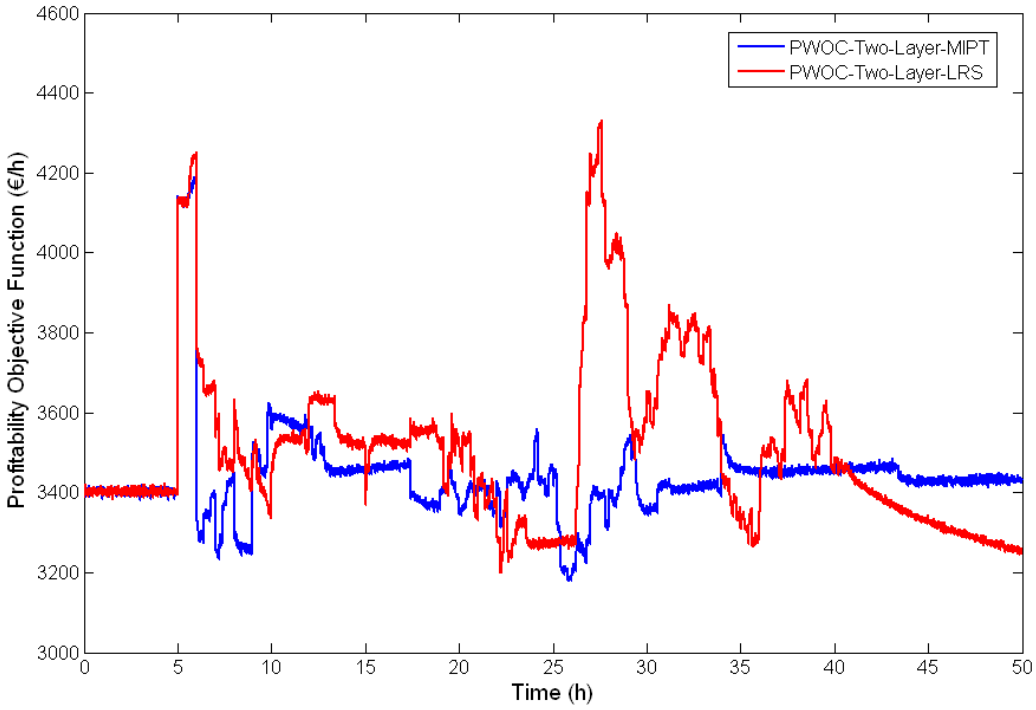

Figure 6.26 PWOC-two-layer: Comparison of the Molecular Inspired Parallel Tempering (MIPT) Algorithm (blue line) and the Localized Random Search (red line) for Scenario 1.

Analyzing the results presented in Figure 6.25 and Figure 6.26 it is possible to derive two main conclusions:

- Comparing the performance obtained for the PWOC-one-layer and PWOC-two-layer, it can be seen that the PWOC-two-layer scheme presents an unstable and aggressive behaviour (especially when the LRS algorithm is used), which is due to the conflict between the different objectives in the D-RTO and NMPC layers of the PWOC-two-layer approach. It is important to recall that for the D-RTO layer the main objective is to maximize the profitability in the process, but for the NMPC layer, the ultimate objective is to minimize a performance objective function which penalizes deviations of the state variables from their set points. So, although the profitability is also taken into account, the plantwide manipulated variables applied to the process are finally determined by the NMPC layer. It is also important to notice that both layers (the D-RTO and the NMPC) used the same process model, which discards any conflict as a result of model mismatch.
- Comparing the MIPT and LRS optimization algorithms in terms of the cumulative profitability achieved when facing the problem stated in Scenario 1 (Table 6.8), it can be seen that both methods have a very similar performance and that none of them

outperforms the other. According to the results presented in this section, it is possible to conclude that independently of the optimization algorithm used, the Plantwide Optimizing control methodology proposed in Chapter 4 is a very efficient and successful plantwide control architecture, capable of successfully rejecting known process disturbances.

Table 6.9 Cumulative Profitability Comparison in Scenario 1: MIPT vs. LRS

Plantwide Control Scheme	Cumulative Profitability (€)
PWOC-one-layer-MIPT	1.769×10^5
PWOC-one-layer-LRS	1.751×10^5
PWOC-two-layer-MIPT	1.719×10^5
PWOC-two-layer-LRS	1.753×10^5

Although the LRS optimization algorithm proved to be suitable for solving the problem stated in Scenario 1, in the following sections it is demonstrated that the main feature of the MIPT that outperforms LRS, namely its global character, is very useful for facing more challenging scenarios where the optimal operating point for the process moves further away from the nominal or previous optimal, as is the case addressed in Scenario 2 (Section 6.3.5) and Scenario 3 (Section 6.3.6).

6.3.5. PWOC Performance Evaluation: Scenario 2 - Unknown Disturbance with Model Mismatch

In this section, a comparison between the MIPT and LRS algorithms is presented when the PWOC-one-layer scheme (including shrinking of the search region) is used for counteracting the disturbance of Scenario 2, which is an unknown disturbance in the maximum biomass growth rate in the fermentation section that impact negatively the process profitability. The disturbance for this Scenario takes place at time t=5 hours, and the total time considered was 40 hours. As it can be observed in the process profitability of MIPT (green line) and LRS (magenta line) shown in Figure 6.27, the optimal operating point of the process moves further away from the profitability values reached in Scenario 1. The displacement of the system to a new global optimum due to the appearance of the disturbance can be better appreciated taking a look at the biomass control profiles shown in Figure 6.28 (optimal profile for Scenario 1 shown in blue). Comparing the optimal biomass behavior for Scenario 1 and Scenario 2 it is possible to observe a displacement of the optimal operating point of the system. For Scenario 1, the optimal operating point was displaced to a higher biomass

concentration than the nominal steady state. In contrast, due to the disturbance in the biomass growth rate, the optimal operating point in Scenario 2 is found at much lower biomass concentrations.

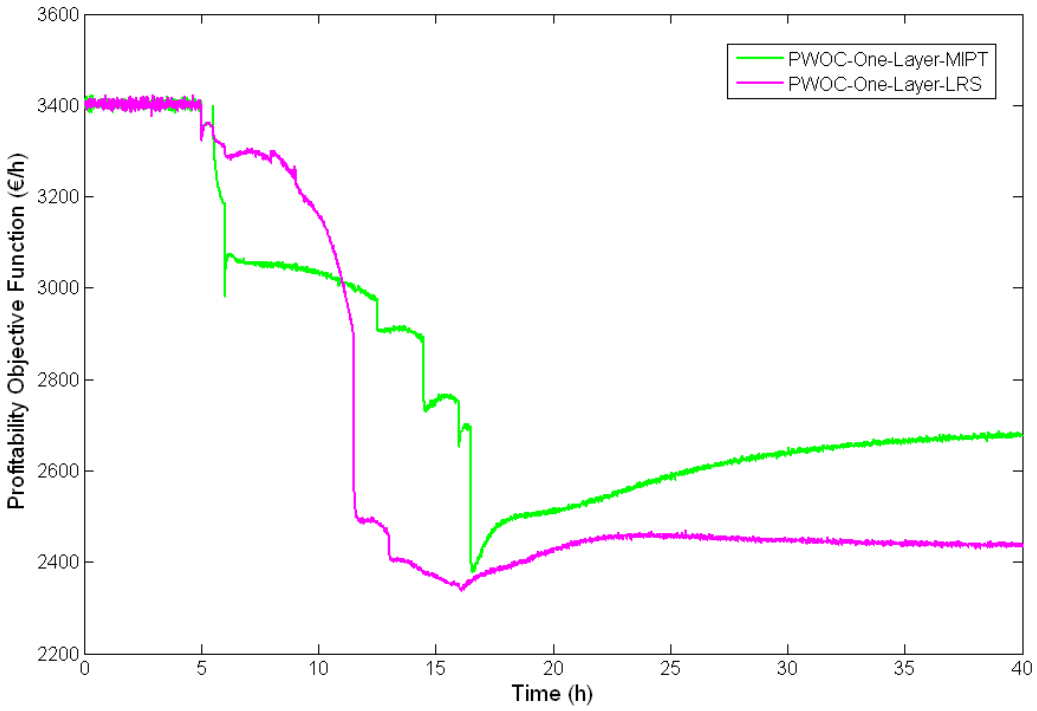

Figure 6.27 PWOC-One-Layer: Profitability Comparison of MIPT vs. LRS algorithms for Scenario 2. Green: MIPT. Magenta: LRS.

Figure 6.29 shows the behaviour of ethanol concentration in the fermentor using both algorithms. It is observed that the concentration of ethanol during fermentation was higher when the LRS algorithm was used compared with MIPT. However, a high concentration of ethanol in the fermentor does not necessarily leads to higher profitability values as it is seen in Figure 6.27, evidencing that the problem of maximizing the profitability in a chemical process not only requires to take into account the interactions between the different operating units, but also that the strategy for solving the corresponding optimization problem must consider an algorithm that assure an efficient exploration towards finding the global (or getting close to the global) optimum operating point.

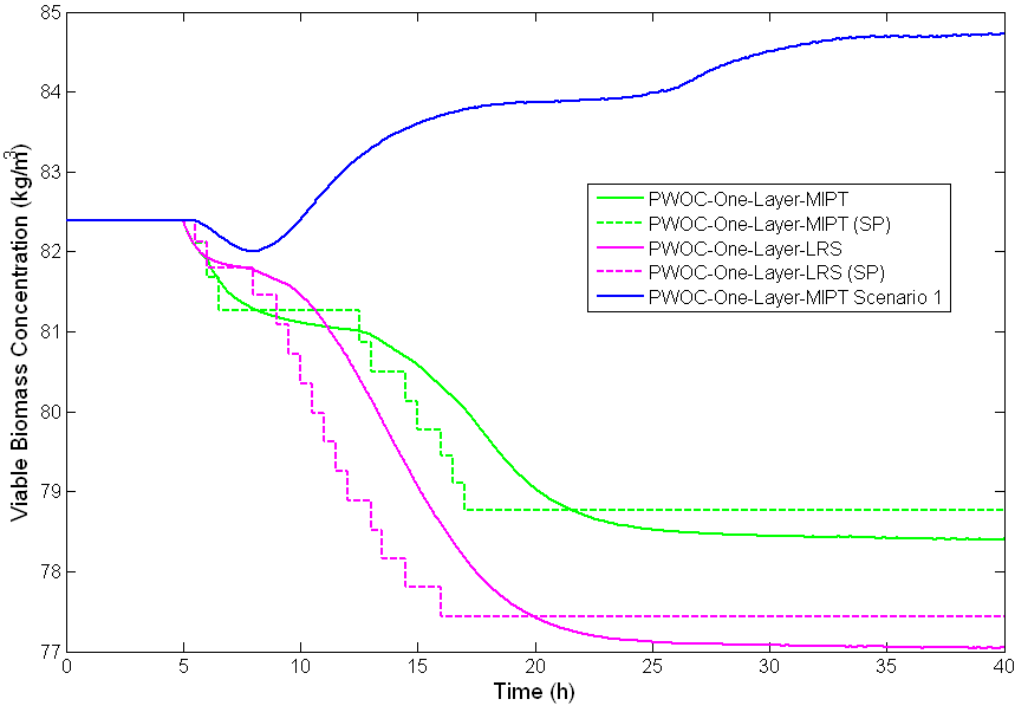

Figure 6.28 PWOC-One-Layer: Viable Biomass concentration in the fermentor. Comparison of MIPT vs. LRS for Scenario 2. Green: MIPT. Magenta: LRS. Blue: PWOC-one-layer MIPT for Scenario 1. Dashed: Biomass concentration set point.

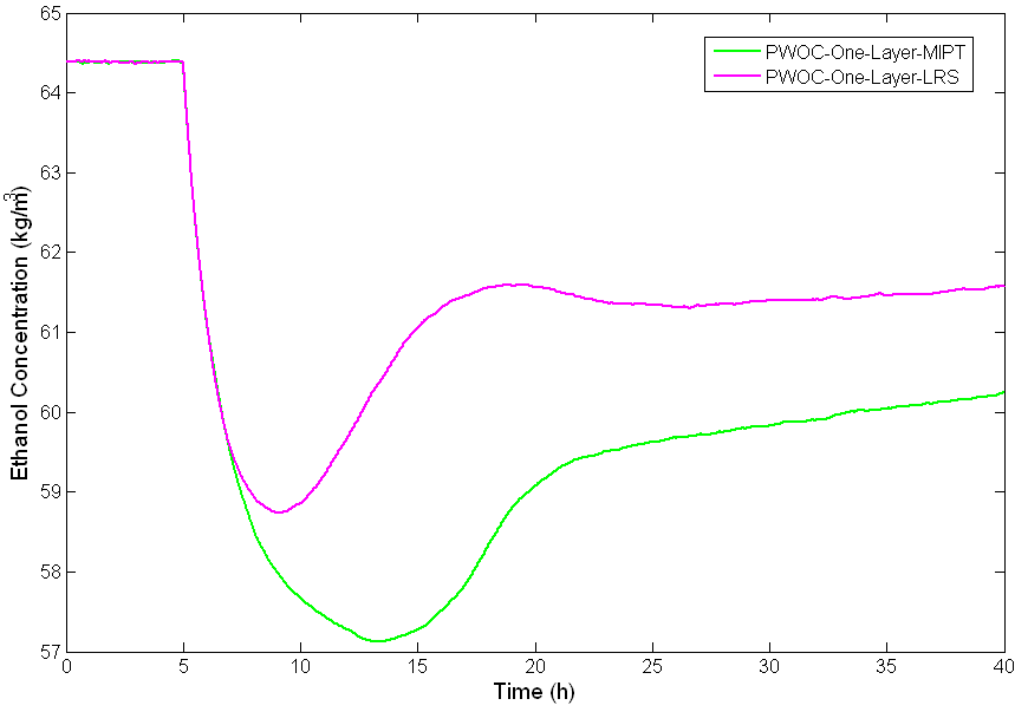

Figure 6.29 PWOC-One-Layer: Ethanol concentration in the fermentor. Comparison of MIPT vs. LRS algorithms for Scenario 2. Green: MIPT. Magenta: LRS.

A better understanding of the differences found in the profitability objective function when applying the MIPT and LRS algorithms for solving the PWOC problem can be obtained by analyzing the profiles of the main manipulated variables (Figure 6.30 and 6.31).

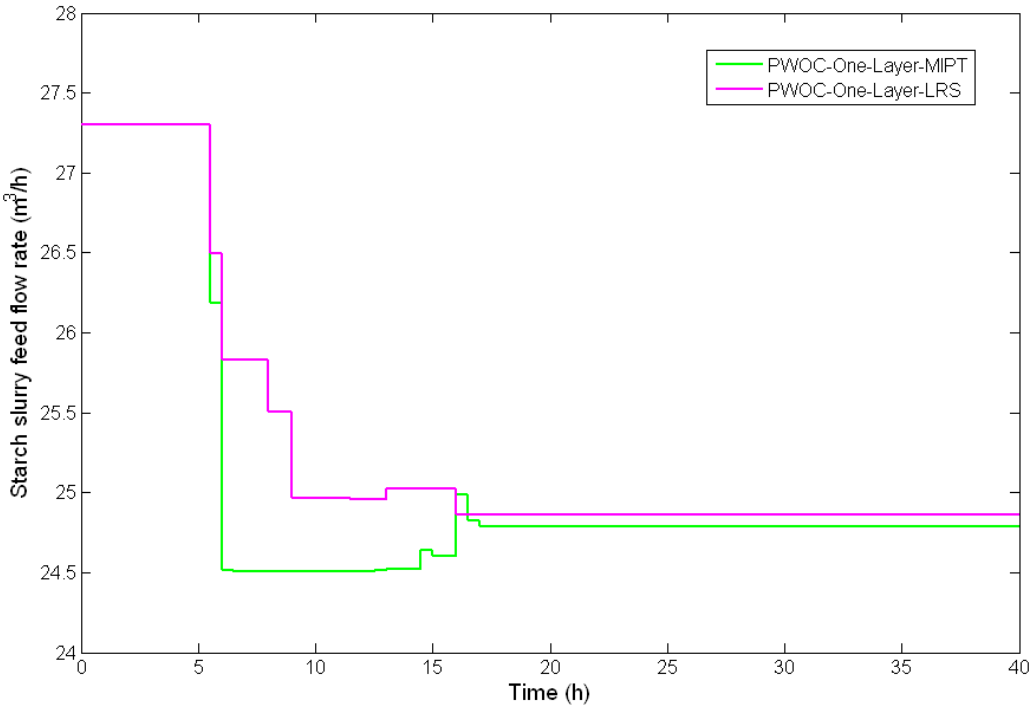

Figure 6.30 PWOC-One-Layer: Starch slurry feed flow rate. Comparison of MIPT vs. LRS algorithms for Scenario 2. Green: MIPT. Magenta: LRS.

It can be observed that even though the profile for F_0 shown in Figure 6.30 is very similar in both cases, the profiles for the other manipulated variables differ significantly. For example, analyzing in detail the profile for R_1 and VB_1 it is possible to see that both methods, MIPT (green line) and LRS (magenta line) found very different optimal values for those decision variables. Analyzing the profile for R_1 it is possible to appreciate the global character of the MIPT algorithm. In this case, both algorithms started increasing the R-value in order to reject the disturbance. However, whereas the MIPT (green line) was able to surpass a local optimum at around 3910 kmol/h, the LRS was unable to overcome the attraction exerted by that local minimum. A similar behavior is observed for the VB_2 profile, where once more the global feature of the MIPT is able to drive the system further away from the local optimum in which the LRS stays stalled (around 2030 kmol/h). Finally, it should be noticed that the problem is not the magnitude of the steps in the manipulated variables between different trials, because both methods are able to combine small and large step changes when

needed. This effect can be observed in the profile of VB_1 (Figure 6.31). As it can be seen for this manipulated variable, the LRS moves VB_1 beyond its nominal value, and also beyond the optimum operating point found by the MIPT algorithm, which on the contrary, and in spite of having explored also larger changes for VB_1, it was able to come back to the region where the global optimum is located.

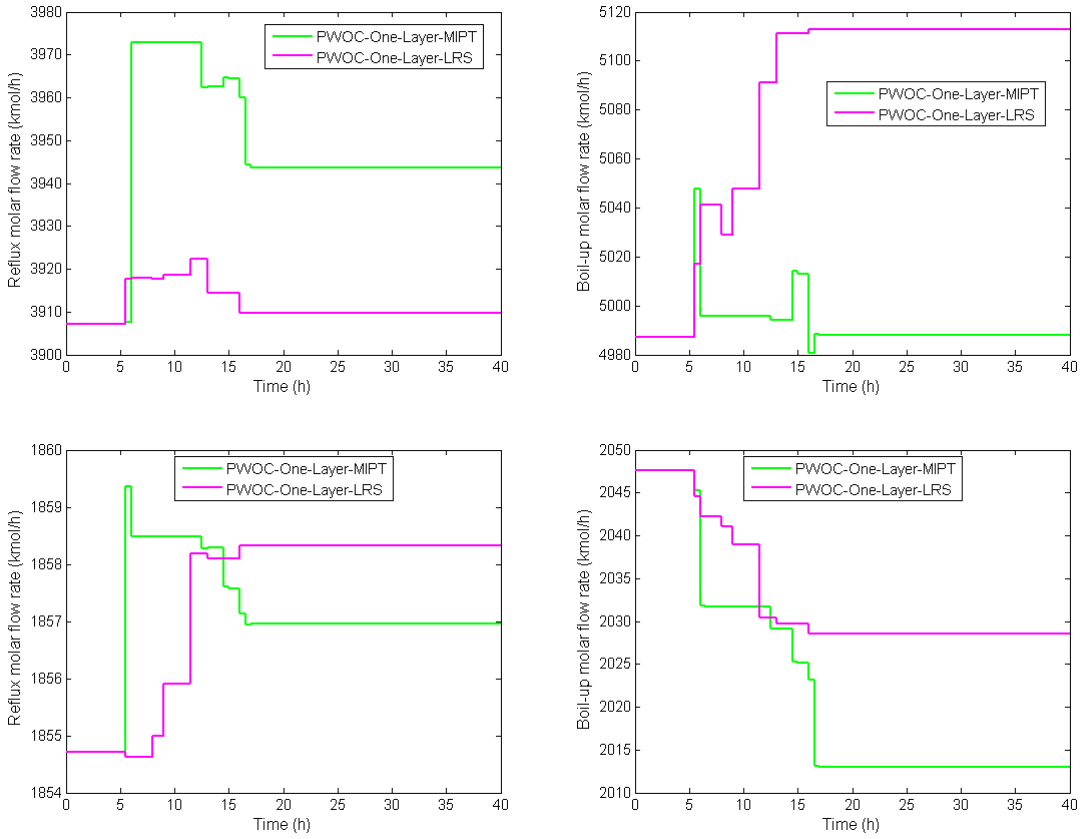

Figure 6.31 PWOC-One-Layer for facing Scenario 2: Plantwide manipulated variables in the separation section. Top-left: Reflux rate in distillation column. Top-right: Boil-up rate in distillation column. Bottom-left: Reflux rate in rectification column. Bottom-right: Boil-up rate in rectification column. Comparison of MIPT vs. LRS algorithms. Green: MIPT. Magenta: LRS.

For concluding this section, it is important to remark that although the LRS algorithm showed almost the same performance than the MIPT algorithm for facing Scenario 1, a very big different performance was obtained for both methods when they were used for implementing the PWOC-one-layer problem for facing the disturbance in Scenario 2. This is due to the fact that in the case of Scenario 2, a more challenging worst case disturbance was evaluated, which tested the global character of the algorithms.

Finally, in order also to show the advantages of the PWOC architecture over the Decentralized scheme, Figure 6.32 shows a comparison between the profitability objective

function when the PWOC-one-layer (green line) and the Decentralized 1 (black line) schemes are used for dealing with the disturbance Scenario 2. It can be seen that the PWOC-one-layer architecture (green line) is capable of leading the process to a high profitability value, even in the worst-case analyzed in this Section. In contrast, the Decentralized scheme (black line) leads the process to a very low cumulative and negative profitability value (see Table 6.9), and shows to be unable and unsuitable for dealing with the analyzed disturbance. Therefore, through this example, it has been demonstrated not only the global character and suitability of MIPT algorithm for dealing with such challenging disturbances, but also, it has been proved once more that the PWOC-one-layer architecture surpass the performance obtained by a typical decentralized scheme, demonstrating the advantages of the PWOC methodology proposed in this work.

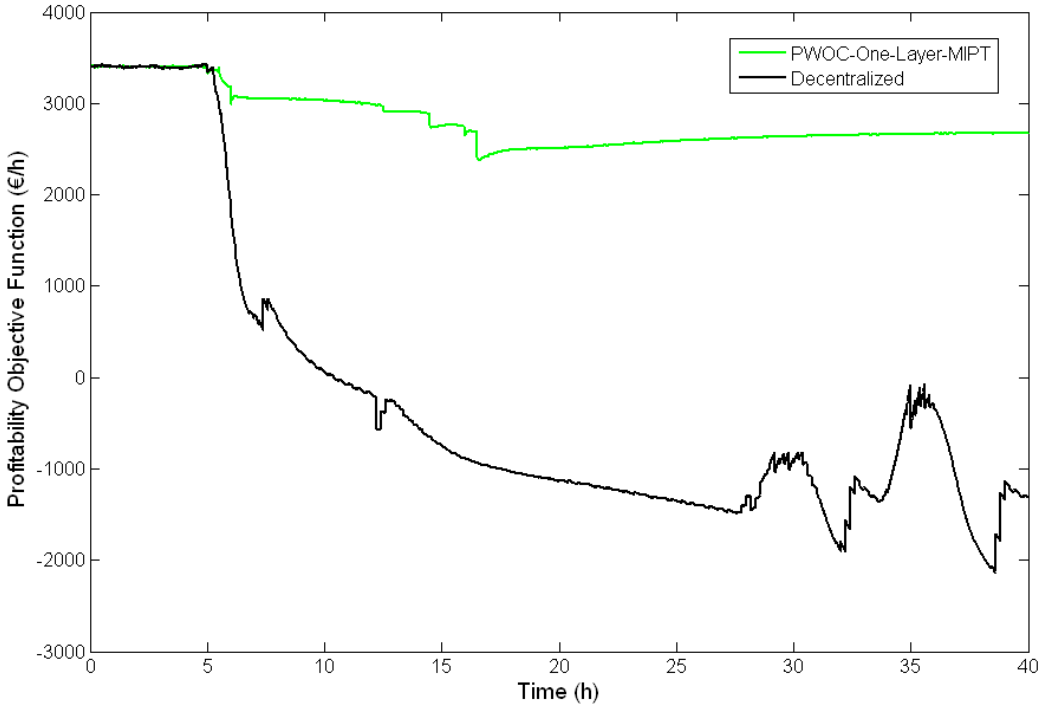

Figure 6.32 PWOC-One-Layer vs. Decentralized architecture: Profitability performance comparison for Scenario 2. Green: PWOC-one-layer-MIPT. Black: Decentralized.

Table 6.9 Cumulative Profitabilty Comparison in Scenario 2: PWOC vs. Decentralized

Plantwide Control Scheme	**Cumulative Profitability (€)**
PWOC-one-layer-MIPT	1.125×10^{5}
PWOC-one-layer-LRS	1.074×10^{5}
Decentralized	-8.464×10^{3}

6.3.6. PWOC Performance Evaluation: Scenario 3 - Increase in the Raw Material Price

Nowadays, the economical feasibility of the bio-ethanol industry strongly depends on the taxes exemption policy applied by the governments. In the particular case of Germany, a study by the Kiel Institute for World Economics (**Henke et al., 2003**) concludes that the industry of bio-ethanol in the country is not competitive at all without tax exemption. Such situation would get dramatically worst if the raw material prices increase as a result of the competition between food consumption and bio-fuels production. As such scenario will jeopardize even more the economical feasibility of the industry, the purpose of this Section is to show the potential use of the Plantwide optimizing control architecture for dealing with such worst-case scenario. The scenario analyzed here considers a very pessimistic situation, in which the starch raw material price increases in 100%, varying from 0.16 €/kg to 0.32 €/kg. This disturbance takes place at time t=5 hours, and the total time considered for the process was 40 hours. Results for this case study are shown in Figure 6.33 - 6.37, where the performance of the PWOC-one-layer (blue) using the Molecular Inspired Parallel Tempering (MIPT) algorithm is compared with the performance obtained when the Decentralized plantwide architecture (black) is used, and also using the PWOC-one-layer, but solving the D-RTO problem by the Localized Random Search optimization algorithm (red).

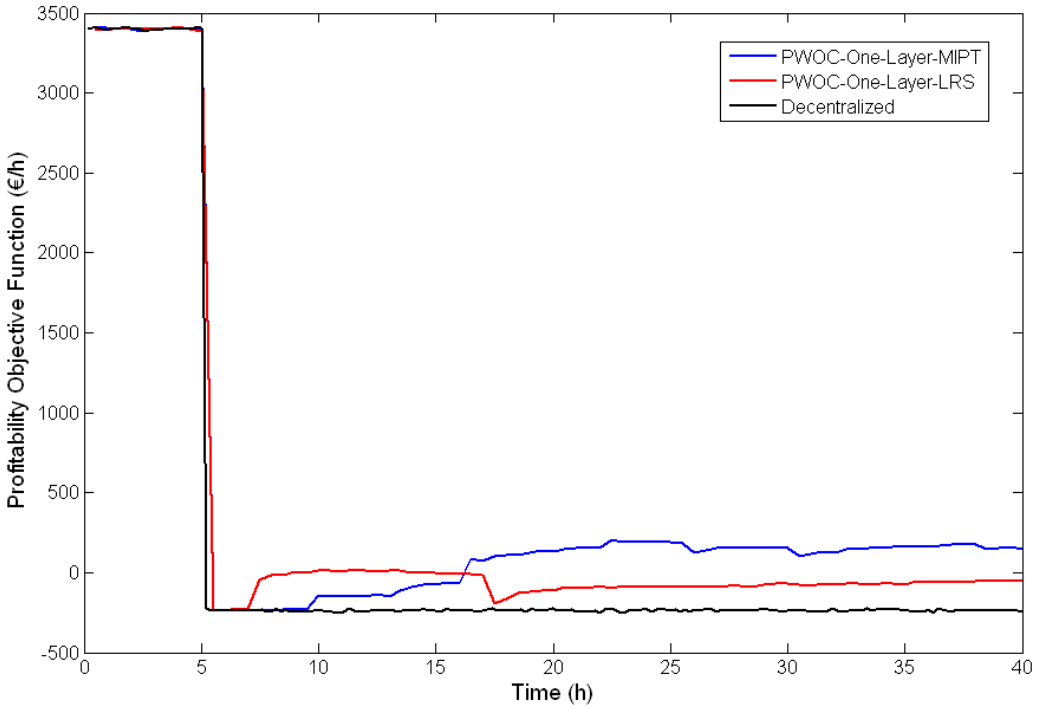

Figure 6.33 Comparison of profitability objective function values for Scenario 3: price change in the raw material. Blue: PWOC-one-layer-MIPT. Black: Decentralized approach. Red: PWOC-one-layer-LRS.

Table 6.10 Cumulative Profitabilty Comparison in Scenario 3: PWOC vs. Decentralized

Plantwide Control Scheme	Cumulative Profitability (€)
PWOC-one-layer-MIPT	626.32
PWOC-one-layer-LRS	-3.659×10^{3}
Decentralized	-9.479×10^{3}

Figure 6.33 shows the profitability objective function when a worst case in the price change impacts the process. In this very pessimistic scenario, the objective function for the different plantwide architectures analyzed decreases considerably, as expected, even leading the process to a non viable operation from an economical point of view, just after the change in the raw material price was introduced. As the Decentralized Plantwide Control architecture does not take explicitly into account the process profitability, and as in this scenario the analyzed "disturbance" does not affect the state variables in the process (i.e. the controlled variables stay at their nominal steady state values), the decentralized scheme is not "aware" of its effect on the plantwide performance of the process. Therefore, the decentralized scheme does not take any action on the manipulated variables in order to reject the disturbance, as it can be appreciated in Figure 6.34 for F_0, which is kept constant at its nominal steady state value (i.e. with a small oscillation around the nominal value due to the noise effect). Of course, it can be argued that the plant manager and/or plant operators are aware of such disturbance, and thus, they would have the chance to adapt the process conditions to this price fluctuation, for example, by changing the set points and re-tuning the PID parameters of the decentralized scheme. However, such adaption will depend on the operators own experience and will also require not only to set the product flow rate to a different value, but also to re-tune all other decentralized loops which is not an easy task in a highly interconnected process as the bio-ethanol case study. In contrast to the Decentralized scheme, the PWOC-one-layer architecture shows to be able of dealing with the challenging disturbance for this scenario. As it is shown in Table 6.10, the PWOC-one-layer that implemented the MIPT algorithm for solving the D-RTO problem presents the best performance, leading the process to a cumulative profitability of 626 €, meaning that for the analyzed operating period, the PWOC-one-layer architecture was able to avoid economical losses. The strategy followed by the PWOC-one-layer consisted in decreasing the raw material flow rate (Figure 6.34); however, this was not the only plantwide manipulated variable that changed. In fact, the other 7 plantwide manipulated variables also changed in order to synergistically reject the disturbance. Although the profiles for all other Plantwide manipulated variables is not shown, it is possible to observe in Figure 6.35, where the

efficiency of ethanol production in terms of kg ethanol produced/kg ungelatinized starch consumed is presented, that the optimal profile applied for the manipulated variables by the PWOC-one-layer leads the process to a much better use of the raw material in the process for accomplishing the main task, which is producing ethanol while maximizing profitability.

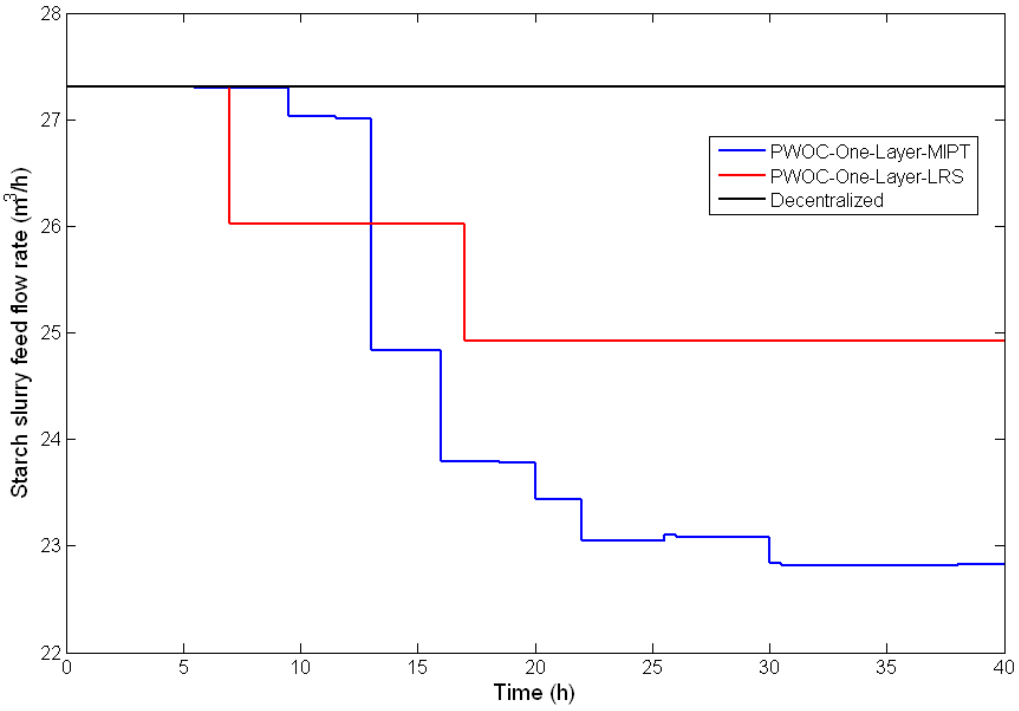

Figure 6.34 Comparison of starch slurry feed flow rates for Scenario 3: price change in the raw material. Blue: PWOC-one-layer-MIPT. Black: Decentralized approach. Red: PWOC-one-layer-LRS.

Finally it is also important to notice, that despite of the lower feed flow rate used to maximize the profitability, the PWOC-one-layer still satisfies the constraint imposed on the minimal flow rate of product of F_{20}>=80000 Ton/year (i.e F_{20} >=10.1 Ton ethanol/h), as it is shown in Figure 6.36. Furthermore, it is important to observe that even though the decentralized scheme (black line) in this Scenario maintained the maximum product flow rate (when compared to the PWOC schemes), which is an important term that contributes very positively in the calculation of the profitability objective function (Equation 6.1). This behavior does not assure good profitability, because as it is evidenced once more, the problem of leading the process to maximal profitability is a plantwide control problem that should not be addressed from a decentralized perspective in which the different operating units are considered as isolated entities.

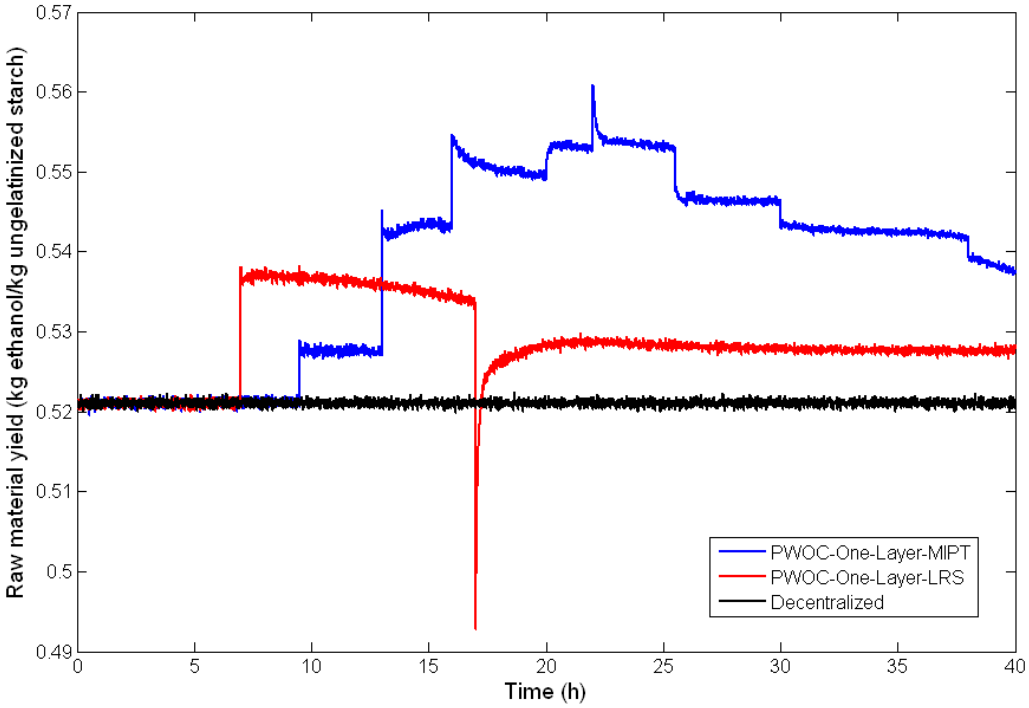

Figure 6.35 Comparison of raw material yield during ethanol production for Scenario 3: price change in the raw material. Blue: PWOC-one-layer-MIPT. Black: Decentralized approach. Red: PWOC-one-layer-LRS.

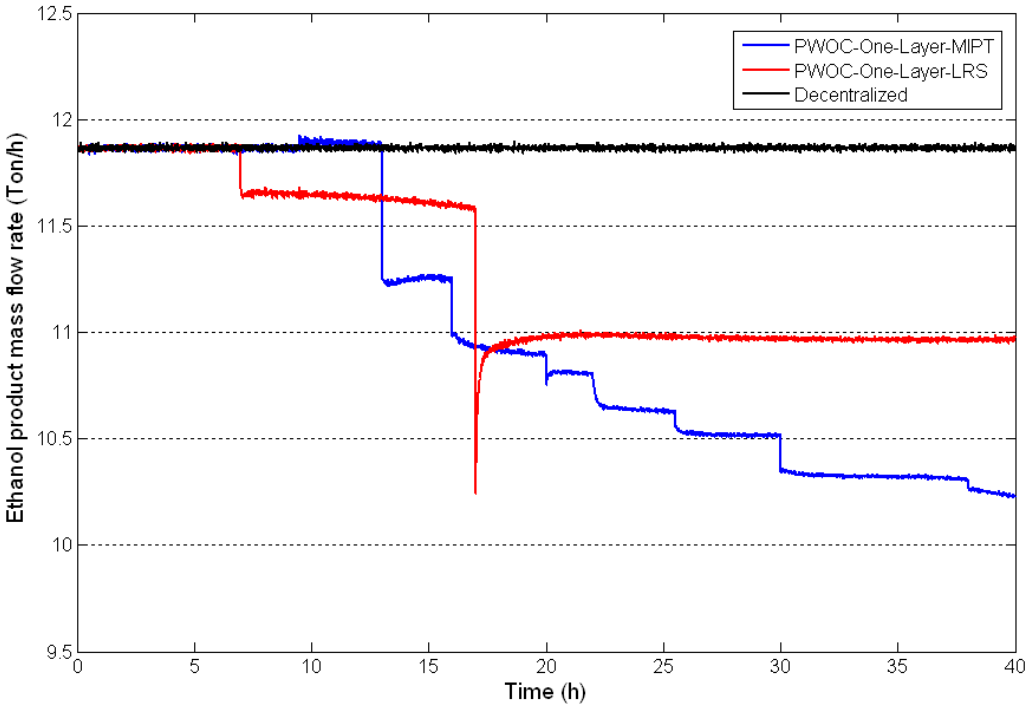

Figure 6.36 Comparison of ethanol product mass flow rates for Scenario 3: price change in the raw material. Blue: PWOC-one-layer-MIPT. Black: Decentralized approach. Red: PWOC-one-layer-LRS. Constraint: Flow rate≥10.1 Ton/h.

For closing this section, a brief mention about the comparison between the results obtained using the Molecular Inspired Parallel Tempering (MIPT) Algorithm and the Localized random Search (LRS) for solving the D-RTO problem in the PWOC-one-layer, should be done. As it can be seen in Figure 6.33, the LRS algorithm was the first to respond after the price change (at around 7 hours of operation, whereas the MIPT responded at around 9.5 hours). However, at time 17 h the profitability suddenly decreases and it cannot be restored for the rest of the period. Sudden drops in profitability are usually caused by relatively short-term improvements achieved during the optimization. In these cases, the profitability initially increases but after some hours (usually close to the optimization horizon) it starts to decrease again because the operating condition can not be sustained. Then, the optimizer must find new actions that drive the process again towards high profitability values. If the optimizer is able to reach the global optimum from the beginning, it will lead to a long-term sustainable increase in profitability.

6.4. Chapter conclusions

PWOC has been applied to the bio-ethanol process, showing much better results from an economical point of view than when the process is only controlled by a conventional decentralized control scheme. It has been demonstrated that PWOC is a very promising alternative for controlling a complete chemical or biochemical processes in which the economical feasibility is at risk when disturbances appear.

The novel shrinking approach was successfully tested resulting in an improvement of the solution of the D-RTO problem, which was evidenced by obtaining higher productivities (for the same number of function evaluations and/or limit time for the optimization routine) than when no shrinking was used.

Additionally, comparing the PWOC-one-layer and the PWOC-two-layer, it is possible to conclude that the former achieves higher profitability. However, its success strongly depends on the model accuracy, and its main drawback is that stability issues have not been proved yet. On the other hand, the PWOC-two–layer case, tracks very well the state variables in the process, but does not guarantee good profitability. However, its main advantage is that it is more robust due to the presence of the MPC-layer.

Finally, it was corroborated that the MIPT algorithm has an excellent performance, and that it is a suitable optimization algorithm for solving the optimization problem that arises in PWOC. MIPT showed to be capable of finding an optimal solution in the three different disturbance scenarios analyzed, even in the worst cases (unknown disturbance and price increase of the raw material), and in doing so, allowed the PWOC strategy to lead the process to the highest cumulative profitability values.

7. Final Conclusions and Outlook

The fuel Bio-ethanol industry is currently a very important part of the worldwide economy, which has experienced an accelerated growth in the last years, because bio-ethanol, as an environmentally friendly fuel, is considered an attractive alternative energy source with the potential of having a much lower contamination impact that the one caused by the use of oil-based fuels. However, despite the growing market and favorable predictions, ethanol industry is at risk because the process is claimed to be economically infeasible, non-sustainable without governmental subsidies, and non-competitive with today's fuel oil prices. In order to contribute for assuring the economical feasibility of the bio-ethanol industry from a process system engineering point of view, in this work, the plantwide control problem of the bio-ethanol process has been addressed as an optimizing control problem based on Dynamic Real-Time Optimization (D-RTO). The main reasons that motivated this are: the process is highly nonlinear and characterized by the coupling of slow and fast dynamics; there exist interactions between different operating units which cannot be neglected; the quality and availability of the raw material change often introducing disturbances into the process; and finally, the economical feasibility of the process can be effectively assured only if this is the main control objective of the plantwide strategy.

In spite of having been studied for more than 40 years, the plantwide control problem of chemical and biochemical processes is still a top problem for academics but also for the industry. Thanks to the advances and the emerging of very fast computers and communication tools during the last decades, a new spectrum of possibilities has been opened for improving the plantwide control strategies in the process industry. Some recent issues, namely, the integration of optimization and control layers in a multilayer architecture and the formulation of the plantwide problem as a single layer scheme, appear to be not only realizable for a whole process, but also have proved to be more suitable for addressing the plantwide control problem when the objective is not only to regulate the process at fixed predefined set points, but to drive the process to the fulfilment of an economical objective stated by the particular process. However, the decentralized architecture continues to be the most frequently used alternative for addressing the control problem of a complete process.

The main reason for this preference relies on the easiness of implementation and understanding of the operation of the PID controllers. However, it must be noticed that even if regulation of the controlled variables at fixed set points (as done by the typical decentralized architecture) results in a good performance in terms of error deviation, it might deteriorate the profitability of the process, because when a disturbance enters the process, the optimal operating point may also move. How much this point moves can not be generalized because it depends on the process and the nature of the disturbances. If well it is completely true that over the years the process industry has been operating under fixed set point policies relying on PID-SISO loops without reporting enormous economical losses, it is also true as stated by **Prett and García (1988)**, that the apparent savings in doing so (i.e. minimization of both design effort and maintenance) are in the majority of cases nonexistent and in the long run result in more costs than the use of multivariate techniques. Therefore, the main purpose of this work has been to solve the plantwide control problem for the bio-ethanol production process from an optimizing control perspective.

This work presents a novel contribution to the research in plantwide control, proposing a methodology for solving the problem of controlling a whole process, the continuous bio-ethanol process from starch, towards reaching maximal profitability. In summary, the main contributions of this thesis are the following:

- The proposal of a **novel methodology** for plantwide control, denoted as **Plantwide Optimizing Control** (PWOC): This methodology, based on the optimizing control concept, has as main objective to provide the steps required for designing the control system of a complete process, which leads the process to maximal profitability even in the presence of disturbances. The PWOC methodology is divided in two main tasks. First, a local control-oriented task should be carried out, whose aim is the design of the local control loops required for the fulfilment of the control objectives related to safe operation and environmental and equipment protection. The second is a plantwide-oriented task, in which the available degrees of freedom are used in order to drive the process towards maximal profitability. The novel plantwide optimizing control methodology was tested in three challenging scenarios in which disturbances of different nature, namely, the change in the raw material quality, change in the kinetics of the microorganism, and change in the raw material price, affected the process. In these three scenarios, PWOC was compared with a typical decentralized architecture and proved to be the best option in economic terms, that is, it led the process to the highest cumulative profitability.

- The proposal of a **novel algorithm for global optimization**, denoted as **Molecular Inspired Parallel tempering (MIPT)**: Since the core of the PWOC methodology proposed is the formulation and solution of a Dynamic Real Time Optimization problem, in this work, the new MIPT stochastic optimization method was developed. MIPT presented a very good performance (in terms of the number of function evaluations and success ratio for reaching the global optimum) in solving different types of global optimization problems. The MIPT algorithm was compared in several case studies to other well-established stochastic algorithms, and in all cases proved to be a very well suited method for global optimization. The strength of the MIPT algorithm is that, when searching for an optimum, it combines very well the global character with the local refinement. The global character is provided by the explorer-type molecules, which allow the efficient exploration of a wider region of the space of decision variables. Due to the presence of the refiner molecules, the algorithm is also able to keep exploring promising local regions (i.e. local refinement). The combination of these two effects enormously increases the capacity of the algorithm for finding the global optimum. MIPT was used inside the formulation of the PWOC for the three disturbance scenarios analyzed, demonstrating to be able of finding an optimal solution in all cases and resulting in a more profitable operation.

- The proposal of a **new stochastic-based approach for shrinking the search region of the optimization problem**: The purpose of the shrinking approach was to reduce the search space of the optimization problem, in order to have a higher success ratio in finding the global optima solution (or close to the optimal), when solving the D-RTO problem that arises in PWOC, in a short time. This is an important fact that needs to be taken into account in online applications, because in such applications, the time for reaching an optimal solution every time that the optimization routine is called is short because the decision variables of the optimization problem must be quickly applied to the process for ensuring maximal profitability. The shrinking approach was also applied inside the PWOC methodology for solving the control problem of the bio-ethanol process when facing three challenging disturbance scenarios. Comparing to the case in which the PWOC was implemented without shrinking the search region, it was concluded that the use of the shrinking approach allows the optimization algorithm to find a much higher value for the profitability objective function than when no shrinking is used. This result confirms the advantages of the stochastic-based shrinking approach and shows that

it is not a blind approach, but on the contrary, it is a guided approach that uses information of the causal relationship between the disturbances and manipulated variables (through the analysis of the effect that they exert on the state variables), for taking the decisions on how much to reduce the search region according to the capability of each manipulated variable for rejecting a particular disturbance or a decrease in the profitability objective function.

Finally, some ideas for future work towards complementing the contributions given in this thesis are the following:

- The incorporation of the very important topics of data reconciliation, soft-sensors development and on-line parameter identification into the PWOC methodology, in order to close the gap between the theory developed here (tested in simulation studies) and real applications.
- To formulate a parallelized version of the MIPT algorithm, in order to take advantage of its formulation (i.e. each molecule could be run in an independent processor) for speeding up the convergence to the Global Optimum, reducing CPU time.
- To extend the application of the shrinking approach for being used also in deterministic formulations.

References

Ahmetović, E., M. Martín, I.E. Grossmann (**2010**) *Optimization of Energy and Water Consumption in Corn-based Ethanol Plants*. Carnegie Mellon University (http://egon.cheme.cmu.edu/Papers/Water_consumption_CornethanolAhmetovicMartinGrossmann.pdf). Last access: 18.03.2010

Al-Asheh, S., F. Ganat, N. Al-Lagtah (**2004**) *Separation of ethanol-water mixtures using molecular sieves and biobased adsorbents*. Chem. Eng. Res. Des. 82, 855-864.

Alvarado-Morales, M., J. Terra, K.V. Gernaey, J.M. Woodley, R. Gani (**2009**) *Biorefining: Computer aided tools for sustainable design and analysis of bioethanol production*. Chem. Eng. Res. Des. 87, 1171-1183.

Andrade, G.V.N., E.L. **Lima** (**2009**) *Control structure design for an ethanol production plant.* In: R.M.B. Alves, C.A.O. do Nascimento, E.C. Biscaia Jr. (Eds.), 10th International Symposium on Process Systems Engineering - PSE2009, Salvador, 1551-1556.

Araujo, A.C.B. (**2007**) *Studies on Plantwide Control*. Ph.D. Dissertation. Norwegian University of Science & Technology, Trondheim.

Araujo, A.C.B., M. Govatsmark, S. Skogestad (**2007a**) *Application of plantwide control to the HDA process. I - Steady-state optimization and self-optimizing control.* Control Eng. Practice 15, 1222-1237.

Araujo, A.C.B., E.S. Hori, S. Skogestad (**2007b**) *Application of Plantwide Control to the HDA Process. II - Regulatory Control*. Ind. Eng. Chem. Res. 46, 5159-5174.

Araujo, A., S. **Skogestad** (**2008**) *Control structure design for the ammonia synthesis process*. Comp. Chem. Eng. 32, 2920-2932.

Arifeen, N., R. Wang, I.K. Kookos, C. Webb, A.A. Koutinas (**2007**) *Process Design and Optimization of Novel Wheat-Based Continuous Bioethanol Production System*. Biotechnol. Prog. 23, 1394-1403.

Baba, N., Y. Mogami, M. Kohzaki, Y. Shiraishi, Y. Yoshida (**1994**) *A hybrid algorithm for finding the global minimum of error function of neural networks and its applications*. *Neural Netw.* 7, 1253-1265.

Baldea, M., A. Araujo, S. Skogestad, P. Daoutidis (**2008**) *Dynamic Considerations in the Synthesis of Self-Optimizing Control Structures*. AIChE J. 54, 1830-1841.

Banga, J.R., A.A. Alonso, R.P. Singh (**1997**) *Stochastic dynamic optimization of batch and semicontinuous bioprocesses*. Biotechnol. Prog. 13, 326-335.

Bartee, J.F., M.A. Macharia, P.D. Noll, M.E. Tay (**2008**) *Integrated model predictive control of batch and continuous processes in a biofuel production process*. US Patent Appl. US2008/0109200 A1.

Bartusiak, R.D. (**2007**) *NLMPC: A platform for optimal control of feed- or product-flexible manufacturing*. In: R. Findeisen, , F. Allgöwer, L.T. Biegler (Eds.), Assessment and future directions of NMPC, Springer-Verlag, Berlin, 367-381.

Bequette, W. (**2006**) *Process Control - Modeling Design and Simulation*. Prentice Hall, Upper Saddle River NJ.

Beverley, K.J., J.H. Clint, P.D.I. Fletcher (**1999**) *Evaporation rates of pure liquids measured using a gravimetric technique*. Phys. Chem. Chem. Phys. 1, 149-153.

Biegler, L.T., V.M. Zavala (**2009**) *Large-scale nonlinear programming using IPOPT*. Comp. Chem. Eng. 33, 575-582.

Bittner, E., A. Nußbaumer, W. Janke (**2008**) *Make life simple: Unleash the full power of the parallel tempering algorithm*. Phys. Rev. Lett. 101, 130603.

Brandam, C., X.M. Meyer, J. Proth, P. Strehaiano, H. Pingaud (**2003**) *An original kinetic model for the enzymatic hydrolysis of starch during mashing*. Biochem. Eng. J. 13, 43-52.

Buckley, P.S. (**1964**) *Techniques of Process Control*. John Wiley & Sons Inc., New York.

Calvo, F. (**2009**) *Non-genetic global optimization methods in molecular science: An overview*. Comput. Mater. Sci., 45, 8-15.

Castro, J.J., F. J. **Doyle** III (**2004**) *A pulp mill benchmark problem for control: application of plantwide control design*. J. Proc. Control 14, 329-347.

Cheng, R., J.F. Forbes, W.S. Yip (**2007**) *Price-driven coordination method for solving plant-wide MPC problems*. J. Proc. Control 17, 429-438.

Clerc, M., J. **Kennedy** (**2002**) *The particle swarm - Explosion, stability, and convergence in a multidimensional complex space*. IEEE Trans. Evol. Comput. 6, 58-73.

Costa, A.C., D.I.P. Atala, R.M. Filho, F. Maugeri (**2001**) *Factorial design and simulation for optimization and determination of control structures for extractive alcoholic fermentation.* Proc. Biochem. 37, 125-137.

Costa, A.C., L.A.C. Meleiro, R.M. Filho (**2002**) *Non-linear predictive control of an extractive alcoholic fermentation process*. Process Biochem. 38, 743-750.

Csendes, T., L. Pál, J.O.H. Sendín, J.R. Banga (**2008**) *The GLOBAL optimization method revisited*. Optim. Lett. 2, 445-454.

da Silva, F.L., M.I. Rodrigues, F. Maugeri (**1999**) *Dynamic modelling, simulation and optimization of an extractive continuous alcoholic fermentation process*. J. Chem. Tech. Biotech. 74, 176-182.

Daubert, T.E., R.P. Danner, H.M. Sibul, C.C. Stebbins (**1989**) *Physical and Thermodynamic properties of pure chemicals - Data Compilation*. Taylor & Francis, Washington.

Dias, M.O.S., T.L. Junqueira, R.M. Filho, M.R.W. Maciel, C.E.V. Rossell, D.I.P. Atala (**2009a**) *Optimization of Bioethanol Distillation Process - Evaluation of Different Configurations of the Fermentation Process*. In: R.M.B. Alves, C.A.O. do Nascimento, E.C. Biscaia Jr. (Eds.), 10th International Symposium on Process Systems Engineering – PSE2009, Salvador, 1893-1898.

Dias, M.O.S., A.V. Ensinas, S.A. Nebra, R.M.l Filho, C.E.V. Rossell, M.R.W. Maciel (**2009b**) *Production of bioethanol and other bio-based materials from sugarcane bagasse: Integration to conventional bioethanol production process*. Chem. Eng. Res. Des. 87, 1206-1216.

Dixon, L.C.W., G.P. **Szegö** (**1978**) *Towards global optimization 2*. North-Holland Publishing Company, Amsterdam.

Dréo, J., A. Pétrowski, P. Siarry, E. Taillard (**2006**) *Metaheuristics for Hard Optimization*. Springer, Berlin.

Earl, D.J., M.W. **Deem** (**2005**) *Parallel tempering: Theory, applications and new perspectives*. Phys. Chem. Chem. Phys., 7, 3910-3916.

Earl, D.J., M.W. **Deem** (**2008**) *Monte Carlo simulations*. In: A. Kukol (Ed.), Molecular modeling of proteins (Methods in molecular biology 443), Humana Press, Totowa NJ, 25-36.

Eberhart, RC, Y. **Shi** (**2001**) *Particle swarm optimization: developments, applications and resources*. dProc. Congress on evolutionary computation, Seoul, 81–6.

Eberhart, R.C., J. Kennedy, Y. Shi (**2001**) *Swarm intelligence*. Morgan Kaufmann Publishers, San Francisco.

Egea, J.A., E. Balsa-Canto, M.-S.G. Garcia, J.R. Banga (**2009**) *Dynamic Optimization of Nonlinear Processes with an Enhanced Scatter Search Method*. Ind. Eng. Chem. Res. 48, 4388-4401.

Ehnström, L., J. Frisenfelt, M. Danielsson (**1991**) *The biostil process*. In: B. Mattiasson, O. Holst. (Eds.) Extractive Bioconversions. Marcel Dekker Inc., New York, 303-321.

Engell, S. (**2007**) *Feedback control for optimal process operation*. J. Proc. Control 17, 203-219.

Engell, S. (**2009**) *Online Optimizing Control: The Link between Plant Economics and Process Control*. In: R.M.B. Alves, C.A.O. do Nascimento, E.C. Biscaia Jr. (Eds.), 10th International Symposium on Process Systems Engineering – PSE2009, Salvador, 79-86.

Faber, R., T. Jockenhövel, G. Tsatsaronic (**2005**) *Dynamic optimization with simulated annealing*. Comp. Chem. Eng. 29, 273-290.

Favre-Nicolin, V., R. **Cerný** (**2002**) *FOX, 'free objects for crystallography': a modular approach to ab initio structure determination from powder diffraction*. J. Appl. Crystallogr. 35, 734-743.

Findeisen, W., F.N. Bailey, M. Brdys, K. Malinowski, P. Tatjewski, A. Wozniak (**1980**) *Control and coordination in hierarchical systems*. Wiley, New York.

Floudas, C.A., C.E. **Gounaris** (**2009**) *A review of recent advances in global optimization*. J. Global Optim. 45, 3-38.

Franceschin, G., A. Zamboni, F. Bezzo, A. Bertucco (**2008**) *Ethanol from corn: a technical and economical assessment based on different scenarios*. Chem. Eng. Res. Des. 86, 488-498.

Franke, R., J. **Doppelhamer** (**2007**) *Integration of advanced model based control with industrial IT*. In: R. Findeisen, , F. Allgöwer, L.T. Biegler (Eds.), Assessment and future directions of NMPC, Springer-Verlag, Berlin, 399-406.

Franke, R., L. **Vogelbacher** (**2006**) *Nonlinear model predictive control for cost optimal startup of steam power plants*. Automatisierungstechnik 54, 630-637.

Frenkel, D., B. **Smit** (**2002**) *Understanding molecular simulation: from algorithms to applications*. Academic Press, San Diego.

Garcia, C.E., M. **Morari** (**1984**) *Optimal operation of integrated processing systems. Part II: Closed-loop on-line optimizing control*. AIChE J. 30, 226-234.

Gardiner, C.W. (**1994**) *Handbook of stochastic methods*. 2nd edition, Springer-Verlag, Berlin.

Geyer, C.T. (**1992**) *Practical Markov chain Monte Carlo*. Stat. Sci., 7, 473-483.

Glazer, A.N., H. **Nikaido** (**1994**) *Microbial Biotechnology: Fundamentals of Applied Microbiology*, W.H. Freeman and Co., New York.

Glover, F., G.A. **Kochenberger** (**2003**) *Handbook of Metaheuristics*. Kluwer Academic Publishers, New York.

Gmehling, J., U. Onken, W. Arlt, P. Grenzheuser, U. Weidlich, B. Kolbe, J. Rarey (**1990**) *Vapor liquid equilibrium data collection. Alcohols and phenols*. Dechema, Frankfurt.

Gonçalves, L. R. B., G.S. Suzuki, R.C. Giordano, R.L.C. Giordano (**2001**) *Kinetic and mass transfer parameters of maltotriose hydrolysis catalyzed by glycoamylase immobilized on*

macroporous silica and wrapped in pectin gel. Appl. Biochem. Biotechnol. 91-93, 691-702.

Green, D.W., R.H. **Perry** (**2008**) Perry's chemical engineers' handbook. 8th edition. McGraw-Hill.

Grunert, M. (**2005**) *Bioethanol – Situation in Deutschland und Anbauverfahren*, Sächsische Landesanstalt für Landwirtschaft, Dresden.

Haelssig, J.B., A.Y. Tremblay, J. Thibault (**2008**) *Technical and Economic Considerations for Various Recovery Schemes in Ethanol Production by Fermentation*. Ind. Eng. Chem. Res. 47, 6185-6191.

Hansmann, U.H.E. (**1997**) *Parallel tempering algorithm for conformational studies of biological molecules*. Chem. Phys. Lett. 281, 140-150.

Hedar, A.-R., M. **Fukushima** (**2003**) *Minimizing multimodal functions by simplex coding genetic algorithm*. Optim. Methods Software, 18, 265-282.

Hedar, A.-R., M. **Fukushima** (**2006**) *Tabu search directed by direct search methods for nonlinear global optimization*. Eur. J. Oper. Res. 170, 329-349.

Henke, J.M., G. Klepper, N. Schmitz (**2003**) *Tax Exemption for Biofuels in Germany: Is Bio-Ethanol Really an Option for Climate Policy?*. 2003 International Energy Workshop, Laxenburg, Austria.

Henke, S., P. Kadlec, Z. Bubník (**2009**) Physico-chemical properties of ethanol - Compilation of existing data. J. Food Eng. (in press). doi:10.1016/j.foodeng.2009.06.050.

Hirsch, M.J., C.N. Meneses, P.M. Pardalos, M.G.C. Resende (**2007**) *Global optimization by continuous grasp*. Optim. Lett. 1, 201-212.

Hoch, P.M., J. **Espinosa** (**2008**) *Conceptual Design and Simulation Tools Applied to the Evolutionary Optimization of a Bioethanol Purification Plant*. Ind. Eng. Chem. Res. 47, 7381-7389.

Hong, J. (**1986**) *Optimal Substrate Feeding Policy for a Fed Batch Fermentation with Substrate and Product Inhibition Kinetics*. Biotech. Bioeng. 28, 1421-1431.

Huang, H.-J., S. Ramaswamy, U.W. Tschirner, B.V. Ramarao (**2008**) *A review of separation technologies in current and future biorefineries*. Sep. Purif. Technol. 62, 1-21.

Jacobi, A., F. **Hartmann** (**2005**) *Breeding of cereal crops for the production of bioethanol*. Zuckerindutrie 130, 694-696.

Jacques, K.A., T.P. Lyons, D. R. Kelsall (**2003**) *The alcohol textbook*. 4th edition. Nottingham University Press, Nottingham.

Jang, J., C.T. Sun, E. Mizutani (**1997**) *Neuro-fuzzy and soft computing*. Prentice Hall, Upper Saddle River NJ.

Jarzebski, A.B., J.J. Malinowski, G. Goma (**1989**) *Modeling of ethanol fermentation at high yeast concentrations*. Biotech. Bioeng. 34, 1225-1230.

Jezowski, J., R. Bochenek, G. Ziomek (**2005**) *Random search optimization approach for highly multi-modal nonlinear problems*. Adv. Eng. Software 36, 504-517.

Jockenhövel, T., L.T. Biegler, A. Wächter (**2003**) *Dynamic optimization of Tennessee Eastman process using OptControlCentre*. Comp. Chem. Eng. 27, 1513-1531.

Kadam, J.V., M. Schlegel, W. Marquardt, R.L. Tousain, D.H.v. Hessem, J.v.d. Berg, O.H. Bosgra (**2002**) *A two-level strategy of integrated dynamic optimization and control of industrial processes*. In: J. Grievink, J. van Schijndel (Eds.), 12th European Symposium on Computer Aided Process Engineering - ESCAPE 12, Amsterdam, 511-516.

Kadam, J.V., W. Marquardt, M. Schlegel, T. Backx, O.H. Bosgra, P.J. Brouwer, G. Dünnebier, D. van Hessem, A. Tiagounov, S. de Wolf (**2003**) *Towards integrated dynamic real-time optimization and control*. In: Foundations of Computer-Aided Process Operations - FOCAPO 2003 - Conference Proceedings, Coral Springs, 593-596.

Kadam, J.V., W. **Marquardt** (**2004**) *Sensitivity-based solution updates in closed-loop dynamic optimization*. In: 7th International Symposium on Dynamics and Control of Process Systems - DYCOPS 7, Cambridge.

Karuppiah, R., A. Peschel, I.E. Grossmann, M. Martin, W. Martinson, L. Zullo (**2008**) *Energy Optimization for the Design of Corn-Based Ethanol Plants*. AIChE J. 54, 1499-1525.

Kennedy, J., R.C. **Eberhart** (**1995**) *Particle swarm optimization*. In: Proc. IEEE Conf. on Neural Networks, Piscataway NJ, 1942-1948.

Kempe, F. (**2008**) *Optimierung einer Druckwechseladsorptionanlage zur Entwässerung von Bioethanol*. Diplomarbeit. Fachhochschule Lausitz, Seftenberg.

Kirkpatrick, S., C.D. Gelatt, M.P. Vecchi (**1983**) *Optimizing by simulated annealing*. Science 220, 671-680.

Konda, N.V.S.N.M., G.P. Rangaiah, P.R. Krishnaswamy (**2005**) *Plant- Wide Control of Industrial Processes: An Integrated Framework of Simulation and Heuristics.* Ind. Eng. Chem. Res. 44, 8300-8313.

Konda, N.V.S.N.M., G.P. Rangaiah, D.K.H. Lim (**2006**) *Optimal Process Design and Effective Plantwide Control of Industrial Processes by a Simulation-Based Heuristic Approach.* Ind. Eng. Chem. Res. 45, 5955-5970.

Küpper, A., S. **Engell** (**2008**) *Engineering of online optimizing control - A Case Study: Reactive SMB Chromatography*. In: 17th IFAC World Congress – Conference Proceedings, Seoul.

Kwiatkowski, J.R., A.J. McAloon, F. Taylor, D.B. Johnston (**2006**) *Modeling the process and costs of fuel ethanol production by the corn dry-grind process*. Ind. Crops Products 23, 288-296.

Lacks, D.J. (**2003**) *Real-Time Optimization in Nonlinear Chemical Processes: Need For Global Optimizer*. AIChE J. 49, 2980-2983.

Larsson, T., S. **Skogestad** (**2000**) *Plant-Wide Control - A Review and a New Design Procedure*. Model. Ident. Control 21, 209-240.

Larsson, T., M.S. Govatsmark, S. Skogestad, C.C. Yu (**2003**) *Control structure selection for reactor, separator, and recycle processes*. Ind. Eng. Chem. Res. 42, 1225-1234.

Lausch, H.R., G. Wozny, M. Wutkewicz, H. Wendeler (**1998**) *Plant-wide control of an industrial process*. Trans. IChemE Part A 76, 185-192.

Leibtag, E. (**2008**) *Corn prices near record high, but what about food costs?* Amber waves 6, 10-15.

Li, J., R.R. Rhinehart (**1998**) *Heuristic random optimization*. Comp. Chem. Eng. 22, 427-444.

Li, Y., V.A. Protopopescu, N. Arnold, X. Zhang, A. Gorin (**2009a**) *Hybrid parallel tempering and simulated annealing method*. Appl. Math. Comput. 212, 216-228.

Li, Y., M. Mascagni, A. Gorin (**2009b**) *A decentralized parallel implementation for parallel tempering algorithm*, Parallel Computing, 35, 269-283.

Licht, F.O. (**2006**) *World Ethanol and Biofuels Report*. F.O. Licht, Kent.

Lin, C.-Y., C.K. Hu, U.H.E. Hansmann (**2003**) *Parallel Tempering Simulations of HP-36*. Proteins: Struct. Funct. Genet. 52, 436-445.

Lu, J.Z. (**2003**) *Challenging control problems and emerging technologies in enterprise optimization*. Control Eng. Practice 11, 847-858.

Luyben, W.L. (**1990**) *Process Modelling, Simulation and Control for Chemical Engineers*. 2nd edition. McGraw Hill Higher Education, Singapore.

Luyben, W.L., B.D. Tyreus, M.L. Luyben (**1998**) *Plant-Wide Process Control*. McGraw-Hill, New York.

Luyben, W.L. (**2002**) *Plantwide Dynamic Simulators in Chemical Processing and Control*. Marcel Dekker Inc., New York.

Macedo, E.A., A.M. **Peres** (**2001**) *Thermodynamics of ternary mixtures containing sugars. SLE of D-fructose in pure and mixed solvents. Comparison between modified UNIQUAC and modified UNIFAC*. Ind. Eng. Chem. Res. 40, 4633-4640.

Maiorella, B.L., C.R. Wilke, H.W. Blanch (**1981**) *Alcohol production and recovery*. Adv. Biochem. Eng. 20, 43-49.

Maiorella, B.L., H.W. Blanch, C.R. Wilke (**1984**) *Biotechnology report-Economic evaluation of alternative ethanol fermentation processes*. Biotechnol. Bioeng. 26, 1003-1025.

Manenti, F., M. **Rovaglio** (**2007**) *Integrated multilevel optimization in large-scale poly(ethylene terephthalate) plants*. Ind. Eng. Chem. Res. 47, 92-104.

Marlin, T. (**2000**) *Process Control: Designing Processes and Control Systems for Dynamic Performance*. 2nd edition. McGraw-Hill Higher Education, Boston.

Maurya, M.R., R. Rengaswamy, V. Venkatasubramanian (**2003**) *A systematic framework for the development and analysis of signed digraphs for chemical processes*. Ind. Eng. Chem. Res. 42, 4811-4827.

McMillan, G.K. (**2005**) *Good Tuning: A Pocket Guide*. 2nd edition. ISA: The Instrumentation, Systems, and Automation Society, Durham NC.

McAvoy, T.J., N. **Ye** (**1993**) *Base control for the Tennessee Eastman process*. Comp. Chem. Eng. 18, 383-413.

Meleiro, L.A.C., F.J. Von Zuben, R.M. Filho (**2009**) *Constructive learning neural network applied to identification and control of a fuel-ethanol fermentation process*. Eng. Applic. Artificial Intelligence 22, 201-215.

Mercangöz, M., F.J. **Doyle** III (**2007**) *Distributed model predictive control of an experimental four-tank system*. J. Proc. Control 17, 297-308.

Metropolis, N.A., A.W. Rosenbluth, M.N. Rosenbluth, A.H. Teller, E. Teller (**1953**) *Equation of State Calculations by Fast Computing Machines*. J. Chem. Phys. 21, 1087-1092.

Michalik, C., R. Hannemann, W. Marquardt (**2009**) *Incremental single shooting - A robust method for the estimation of parameters in dynamical systems*. Comp. Chem. Eng. 33, 1298-1305.

Monbouquette, H.G. (**1987**) *Models for high cell density bioreactors must consider biomass volume fraction: cell recycle example*. Biotech. Bioeng. 29, 1075-1080.

NBPBCO – National Biobased Products and Bioenergy Coordination Office. *The U.S. dry-mill ethanol industry.* U.S. Department of Energy. (http://www.brdisolutions.com/pdfs/drymill_ethanol_industry.pdf) Last access: 19.03.2010.

Neumaier, A. (**2004**) *Complete search in continuous global optimization and constraint satisfaction*. Acta Numerica 13, 271-369.

Nishiwaki, A., I.J. **Dunn** (**1999**) *Analysis of the performance of a two-stage fermentor with cell recycle for continuous ethanol production using different kinetic models*. Biochem. Eng. J. 4, 37-44.

NPGA - National Propane Gas Association. *Energy costs*. U.S. Department of Energy. (http://www.npga.org/i4a/pages/index.cfm?pageid=914). Last access: 18.03.2010.

Ochoa, S., A. Yoo, J.-U. Repke, G. Wozny, D.R. Yang (**2007**) *Modeling and Parameter Identification of the Simultaneous Saccharification-Fermentation Process for Ethanol Production*. Biotechnol. Prog. 23, 1454-1462.

Ochoa, S., A. Yoo, J.-U. Repke, G. Wozny, D. R. Yang (**2008**) *Modeling and Identification of the Bio-ethanol Production Process from Starch: Cybernetic vs. Unstructured Modeling*. Comp. Aided Chem. Eng. 25, 707-712.

Ochoa, S., J.-U. Repke, G. Wozny (**2009a**) *Plantwide Optimizing Control for the Bio-ethanol Process*. In: Proceedings of International Symposium on Advanced Control of Chemical Processes - ADCHEM 2009, Istanbul.

Ochoa, S., J.-U. Repke, G. Wozny (**2009b**) *Integrating Real-Time Optimization and Control for Optimal Operation: Application to the Bioethanol Process*. Biochem. Eng. J. (in press). doi:10.1016/j.bej.2009.01.005.

Ochoa, S., J.-U. Repke, G. Wozny (**2009c**) *A New Parallel Tempering Algorithm for Global Optimization: Applications to Bioprocess Optimization*. Comp. Aided Chem. Eng. 26, 513-518.

Ochoa, S., J.-U. Repke, G. Wozny (**2009d**) *A New Algorithm for Global Optimization: Molecular-Inspired Parallel Tempering*. Comp. Aided Chem. Eng. 27, 279-284.

Ochoa, S., G. Wozny, J.-U. Repke, (**2010a**) *Plantwide Optimizing Control of a Continuous Bioethanol Production Process.* Submitted to J. Proc. Control.

Ochoa, S., G. Wozny, J.-U. Repke (**2010b**) *A New Algorithm for Global Optimization: Molecular-Inspired Parallel Tempering.* Submitted to Comp. Chem. Eng.

O'Dwyer, A. (**2009**) Handbook of PI and PID Controller Tuning Rules. 3rd edition. Imperial College Press, London.

Phisalaphong, M., N. Srirattana, W. Tanthapanichakoon (**2006**) *Mathematical modeling to investigate temperature effect on kinetic parameters of ethanol fermentation*. Biochem. Eng. J. 28, 36-43.

Prett, D.M., C.E. **Garcia** (**1988**) *Fundamental Process Control*. Butterworth, Stoneham.

Price, R.M., P.R. Lyman, C. Georgakis (**1994**) *Throughput manipulation in plantwide control structures*. Ind. Eng. Chem. Res. 33, 1197-1207.

Rawlings, J.R., B.T. **Stewart** (**2008**) C*oordinating multiple optimization-based controllers: New opportunities and challenges*. J. Proc. Control 18, 839-845.

Reimelt, S., F. Winkler, K. Mögel, M. Kirchhof (**2002**) *Bioethanol Technology of Lurgi Life Science*. Zuckerindustrie 127, 770-781.

Riva, M., D. Fessas, L. Franzetti, A. Schiraldi (**1998**) *Calorimetric characterization of different yeast strains in doughs*. J. Thermal Analysis 52, 753-764.

Roehr, M. (**2001**) *The biotechnology of ethanol: classical and future applications*. Wiley-VCH, Weinheim.

Roman, R., Z.K. Nagy, M.V. Cristea, S.P. Agachi (**2009**) *Dynamic modelling and nonlinear model predictive control of a fluid catalytic cracking unit*. Comp. Chem. Eng. 33, 605-617.

Scattolini, R. (**2009**) *Architectures for distributed and hierarchical model predictive control - A review*. J. Proc. Control 19, 723-731.

Schmitz, N. (**2003**) *Bioethanol in Deutschland*. Landwirtschaftverlag GmbH, Münster.

Schneider, J.J., S. **Kirkpatrick** (**2006**) *Stochastic optimization*. Springer-Verlag, Berlin.

Schug, A., W. Wenzel (**2004**) *Predictive in-silico all atom folding of a four helix protein with a free energy model*. J. Am. Chem. Soc. 126, 16737.

Seborg, D.E., T.F. Edgar, D.A. Mellichamp (**2004**) *Process Dynamics and Control*. 2nd edition. John Wiley & Sons, Hoboken NJ.

Sikorski, A. (**2002**) *Properties of star-branched polymer chains – Application of the replica exchange Monte Carlo method*. Macromolecules 35, 7132-7137.

Skogestad, S. (**2000**) *Plantwide control: The search for the self-optimizing control structure*. J. Proc. Control 10, 487-507.

Smith, J.M., H.C. Van Ness, M.M. Abbott (**2005**) Introduction to Chemical Engineering Thermodynamics. 7th edition. McGraw-Hill Higher Education, Boston.

Solis, F.J., R.J.-B. **Wets** (**1981**) *Minimization by random search techniques*. Math. Oper. Res. 6, 19-30.

Spall, J.C. (**2003**) *Introduction to Stochastic Search and Optimization*. John Wiley & Sons Inc., Hoboken, NJ.

Spall, J.C. (**2004**) *Stochastic optimization*. In: J.E. Gentle, W.K. Härdle, Y. Mori (Eds.) Handbook of Computational Statistics. Springer, Berlin.

Srinivasan, B., S. Palanki, D. Bonvin (**2003**) *Dynamic optimization of batch processes I. Characterization of the nominal solution*, Comp. Chem. Eng. 27, 1-26.

Stephanopulous, G., C. **Ng** (**2000**) *Perspectives on the synthesis of plant-wide control structures*. J. Proc. Control 10, 97-111.

Suman, B., P. **Kumar** (**2006**) *A survey of simulated annealing as a tool for single and multiobjective optimization*. J. Oper. Res. Soc. 57, 1143-1160.

Sun, Y., N.H. **El-Farra** (**2008**) *Quasi-decentralized model-based networked control of process systems*. Comp. Chem. Eng. 32, 2016-2029.

Swendsen, R.H., J.S. **Wang** (**1986**) *Replica Monte Carlo simulation of spin-glasses*. Phys. Rev. Lett. 57, 2607-2609.

Szitkai, Z., Z. Lelkes, E. Rev, Z. Fonyo (**2002**) *Optimization of hybrid ethanol dehydration systems*. Chem. Eng. Processing 41, 631-646.

Tan, C.M. (**2008**) *Simulated Annealing*. In-teh, Croatia.

Thomas, D.J., W.A. **Atwell** (**1999**) *Starches*. American Association of Cereal Chemists, St. Paul MN.

Toumi, A., S. **Engell** (**2004**) *Optimization-based control of a reactive simulated moving bed process for glucose isomerization*, Chem. Eng. Sci. 59, 3777-3792.

Tosukhowong, T., J.M. Lee, J.H. Lee, J. Lu (**2004**) *An introduction to dynamic plant-wide optimization strategy for an integrated plant*. Comp. Chem. Eng. 29, 199-208.

Trvzskâ de Gouvêa, M., D. **Odloak** (**1998**) *One layer real time optimization of LPG production in the FCC unit: Procedure, advantages and disadvantages*. Comp. Chem. Eng. 22, S191-S198.

Vane, L.M. (**2008**) *Separation technologies for the recovery and dehydration of alcohols from fermentation broths*. Biofuels, Bioprod. Bioref. 2, 553-588.

Vasudevan, S., G.P. Rangaiah, N.V.S.N.M. Konda, W.H. Tay (**2009**) *Application and Evaluation of Three Methodologies for Plantwide Control of the Styrene Monomer Plant*. Ind. Eng. Chem. Res. 48, 10941-10961.

Venkat, A.N. (**2006**) *Distributed model predictive control: Theory and applications*. Ph.D. Dissertation, University of Wisconsin-Madison, Madison.

Venkat, A.N., J.B. Rawlings, S.J. Wright (**2007**) *Distributed model predictive control of large-scale systems*. In: R. Findeisen, F. Allgöwer, L.T. Biegler (Eds.) Assessment and future directions of NMPC. Springer-Verlag, Berlin, 591-605.

Vora, N., P. **Daoutidis** (**2001**) *Dynamics and Control of an Ethyl Acetate Reactive Distillation Column*. Ind. Eng. Chem. Res. 40, 833-849.

Wang, J.-F., C.-X. Li, Z.-H. Wang, Z.-J. Li, Y.-B. Jiang (**2007**) *Vapor pressure measurement for water, methanol, ethanol, and their binary mixtures in the presence of an ionic liquid 1-ethyl-3-methylimidazolium dimethylphosphate*. Fluid Phase Equilibria 255, 186-192.

Walter, A., F. Rosillo-Calle, P. Dolzan, E. Piacente, K. Borges da Cunha (**2008**) *Perspectives on fuel ethanol consumption and trade*. Biomass and Bioenergy 32, 730-738.

Xu, G., C. Shao, Z. Xiu (**2008**) *A modified iterative IOM approach for optimization of biochemical systems*. Comp. Chem. Eng. 32, 1546-1568.

Ying, C.M., B. **Joseph** (**1999**) *Performance and stability analysis of LP-MPC and QP-MPC cascade control systems*. AIChE J. 45, 1521-1534.

Yiqing, L., Y. Xigang, L. Yongjian (**2007**) *An improved PSO algorithm for solving non-convex NLP/MINLP problems with equality constraints*. Comp. Chem. Eng. 31, 153-162.

Zabinsky, Z.B. (**1998**) *Stochastic Methods for Practical Global Optimization*. J. Global Optim. 13, 433-444.

Zabinsky, Z.B. (**2009**) *Random Search Algorithms.* University of Washington. (http://courses.washington.edu/inde510/516/RandomSearch4.05.2009.pdf) Last access: 18.03.2010.

Zanin, A.C., M. Trvzskâ de Gouvêa, D. Odloak (**2000**) *Industrial implementation of real-time optimization strategy for maximizing production of LPG in a FCC unit*. Comp. Chem. Eng. 24, 525-531.

Zanin, A.C., M. Trvzskâ de Gouvêa, D. Odloak (**2002**) *Integrating real-time optimization into the model predictive controller of the FCC system*, Control Eng. Practice 10, 819-831.

Zavala, V.M., C.D. Laird, L.T. Biegler (**2007**) *Fast implementations and rigorous models: Can both be accommodated in NMPC?* Int. J. Robust Nonlinear Control 18, 800-815.

Zavala, V.M. (**2008**) *Computational Strategies for the Optimal Operation of Large-Scale Chemical Processes*. Ph.D. Dissertation. Carnegie Mellon University, Pittsburgh PA.

List of own Publications

1. Lyubenova, V., S. **Ochoa**, J.-U. Repke, M. Ignatova, G. Wozny (**2007**) *Control of one Stage Bio Ethanol Production by Recombinant Strain*. Biotechnol. & Biotechnol. Equip. 21 (3), 372-376.

2. **Ochoa**, S., A. Yoo, J.-U. Repke, G. Wozny, D.R. Yang (**2007**) *Modeling and Parameter Identification of the Simultaneous Saccharification-Fermentation Process for Ethanol Production*. Biotechnol. Prog. 23, 1454-1462.
3. **Ochoa**, S., A. Yoo, J.-U. Repke, G. Wozny, D.R. Yang (**2007b**) *Cybernetic and Unstructured Modelling of the Simultaneous Saccharification – Fermentation Process for Bio-Ethanol Production*. In: Proceedings of the European BioPerspectives Conference, Cologne.
4. **Ochoa**, S., A. Yoo, J.-U. Repke, G. Wozny, D. R. Yang (**2008**) *Modeling and Identification of the Bio-ethanol Production Process from Starch: Cybernetic vs. Unstructured Modeling*. Comp. Aided Chem. Eng. 25, 707-712.
5. **Ochoa,** S., V. Lyubenova, J-U. Repke, M. Ignatova, G. Wozny (**2008b**) *Adaptive Control of the Simultaneous Saccharification - Fermentation Process from Starch to Ethanol*. Comp. Aided Chem. Eng. 25, 489-494.
6. **Ochoa**, S., J.-U. Repke, G. Wozny (**2009a**) *Plantwide Optimizing Control for the Bio-ethanol Process*. In: Proceedings of International Symposium on Advanced Control of Chemical Processes - ADCHEM 2009, Istanbul.

7. **Ochoa**, S., J.-U. Repke, G. Wozny (**2009b**) *Integrating Real-Time Optimization and Control for Optimal Operation: Application to the Bioethanol Process*. Biochem. Eng. J. (in press). doi:10.1016/j.bej.2009.01.005.
8. **Ochoa**, S., J.-U. Repke, G. Wozny (**2009c**) *A New Parallel Tempering Algorithm for Global Optimization: Applications to Bioprocess Optimization*. Comp. Aided Chem. Eng. 26, 513-518.
9. **Ochoa**, S., J.-U. Repke, G. Wozny (**2009d**) *A New Algorithm for Global Optimization: Molecular-Inspired Parallel Tempering*. Comp. Aided Chem. Eng. 27, 279-284.
10. **Ochoa**, S., G. Wozny, J.-U. Repke, (**2010a**) *Plantwide Optimizing Control of a Continuous Bioethanol Production Process.* Submitted to J. Proc. Control.
11. **Ochoa**, S., G. Wozny, J.-U. Repke (**2010b**) *A New Algorithm for Global Optimization: Molecular-Inspired Parallel Tempering.* Submitted to Comp. Chem. Eng.
12. Yoo, A., S. **Ochoa**, J.-U. Repke, G. Wozny, D.R. Yang (**2007**) *Cybernetic Modelling of Simultaneous Saccharification & Fermentation (SSF) Process for Bio-ethanol Production*. In: Proceedings of the KIChE Spring meeting, Korea.

List of Oral Presentations in International Conferences

1. **Keynote Lecture**: *Plantwide Optimizing Control for the Bio-ethanol Process*. International Symposium on Advanced Control of Chemical Processes **ADCHEM 2009.** Istanbul, Turkey. July 12-15.
2. *A New Algorithm for Global Optimization: Molecular-Inspired Parallel Tempering*. 10th International Symposium on Process Systems Engineering, **PSE'09.** Salvador-Bahia-Brazil, August 16–20, 2009.
3. *Plantwide Optimizing Control: Bio-Ethanol Process Case Study*. **AIChE 2008** Annual Meeting. Philadelphia, USA. November 16-21, 2008.
4. *Integrating Real-Time Optimization and Control for Optimal Operation: Application to the Bio-ethanol Process.* 10th International Chemical and Biological Engineering Conference **CHEMPOR 2008**, Braga, Portugal. September 4-6, 2008.

Appendix A. MIPT Toolbox Developed in MATLAB

A.1. MIPT Toolbox Instructions

1. Creating the objective function

The objective function must be created as a .m file in MATLAB using the following structure:

```
[Fobj,feasible]=myfunctionname(decisionvariables)
Fobj = …
feasible = …
```

Fobj is the value of the objective function to be ***minimized***. feasible is a binary variable. feasible should be set to 1 if the set of decision variables provides a feasible result (all constraints are satisfied, i.e. linear, non-linear, equality, inequality); otherwise, feasible should be set to 0.
The name of the .m file should correspond to the name provided to the function (i.e., myfunctionname.m)

2. Defining the optimization options

The following is a list of the most important options and their corresponding default values for the MIPT optimization procedure:

NumberOfMolecules: Number of molecules used in the optimization.
[positive integer | {'3*numberofvariables'}]
MaxIter: Maximum number of iterations allowed.
[positive scalar | {Inf}]
TolFun: Termination tolerance on function value evaluated during a certain number of stall iterations.
[positive scalar | {1e-6}]
RepulsionForceConst: Value of the repulsion force constant.
[positive scalar | {5}]
RandomForceConst: Value of the random force constant
[positive scalar | {5e-4}]

Metropolis: Type of Metropolis conditions used

['none' | {'explorers only'} | 'refiners only' | 'both']

MetropolisConstant: Value of the constant used for the Metropolis condition

[positive scalar | {1e3}]

MinFracExplorers: Minimum fraction of explorer molecules

[positive fraction | {0.5}]

InitNumberRefiners: Initial number of refiner molecules. It must be consistent with the minimum fraction of explorer molecules!

[positive integer | {1}]

MinFrictionCoeff: Minimum value of the friction coefficient

[positive scalar | {1e-9}]

MaxFrictionCoeff: Maximum value of the friction coefficient

[positive scalar | {1}]

CutoffDist: Interaction force cut-off distance

[positive scalar | {0.25*sqrt(numberofvariables)}]

StallIterLimit: Number of iterations over which average change in objective function value at current point is less than options.TolFun

[positive scalar | {500*numberOfVariables}]

MaxFunEvals: Maximum number of function (objective) evaluations allowed

[positive scalar | {3000*numberOfVariables}]

TimeLimit: Total time (in seconds) allowed for optimization

[positive scalar | {Inf}]

ObjectiveLimit: Minimum objective function value desired

[scalar | {-Inf}]

Display: Controls the level of display

['off' | 'iter' | 'diagnose' | {'final'}]

DisplayInterval: Interval for iterative display

[positive integer | {10}]

AutoSave: Automatically save the results in a .mat file

[{'off'} | 'on']

PlotType: Type of plot for final results.

numberfunceval plots the best value of the objective function vs. the number of function evaluations.

iterations plots the best value of the objective function versus the number of iterations of the algorithm.

[{'none'} | {'numberfunceval' | 'iterations'}]

You can create and save the optimization options using the following commands:

```
myoptions=miptoptimset('param1',value1,'param2',value2,…);
save myoptionsfile myoptions
```

Any unspecified parameters are set to the default value for that parameter. It is sufficient to type only the leading characters that uniquely identify the parameter. Case is ignored for parameter names. NOTE: For values that are strings, correct case and the complete string are required. Additional information can be found typing **help miptoptimset** or **help miptoptimget** in the command window of MATLAB.

3. Defining the optimization problem

The most important parameters of the optimization problem include:

```
Objective: Function handle of the objective function for minimization.
x0: Starting point
lb: Lower bounds of decision variables
ub: Upper bounds of decision variables
options: Options structure
```

The optimization problem can be created and saved using the following commands:

```
myproblem = miptproblem(@myfunctionname,x0,lb,ub,myoptions);
save myproblemfile myproblem
```

x0, lb and ub can be saved as variables before the definition of the problem, or they can be typed as vectors during the definition of the problem. Type **help miptproblem** in the command window of MATLAB for additional information.

4. Executing the optimization

You can execute the optimization using the following command:

```
mipt(myproblem)
```

Depending on the selected display option, you will see the results of the optimization on the command window of MATLAB, and depending on the plot option, you will also get a graphical summary of the performance at the end of the optimization.

The results will be saved automatically after finishing the optimization in the current work folder. The name of the file will contain the date and time at which optimization is finished. Type **help mipt** in the command window of MATLAB for more information.

A.2. MIPT Algorithm Pseudo-Code

```
MIPT Algorithm
1   Call Initialization
2   while stop_flag = FALSE
3       iter = iter + 1          Update iteration number
4       gamma = exp(log(gmin)+(log(gmax)-log(gmin))*(nm-molrank)/(nm-1))
                Update friction coefficients of molecules
5       frep = 0            Variable initialization for summation
6       for i = 1 to nm
7           for j = 1 to nm
8               d(i,j) = norm(x(i)-x(j))     Intermolecular distance
9               if 0 < d(i,j) < dcutoff and molclass(i) = 1 then
10                  frep(i) = frep(i) - (x(j)-x(i))/(d(i,j)^3)
                            Intermolecular repulsion force
11              end
12          end
13          fbm(i) = normal_random(ndv)  Random force vector
14          dx(i) = (K1*frep(i) + K2*fbm(i))/gamma(i)    Molecular displacement
15          xnew(i) = x(i) + dx(i)           New molecular position
16          Fobjnew(i) = objfunct(xnew(i))   New objective function evaluation
17          nFeval = nFeval + 1       Update number of function evaluations
18          dG(i) = (Fobjnew(i) – Fobj(i))/(max(Fobj)-min(Fobj))
                                  Calculation of normalized free energy change
19          P(i) = exp(-K3*gamma(i)*dG(i)) Acceptance criterion
20      end
21      Call Molecules_update_subroutine
22      mopt = index of feasible molecule with best objective function value
23      if objfunct(x(mopt)) < Fopt then
24          Fopt = objfunct(x(mopt)) Optimal value of the objective function
25          xopt = mopt                  Position of the optimal molecule
26      end
27      evaluate stop_conditions
28      if any(stop_conditions) = TRUE then
29          stop_flag = FALSE
30      end
31  end
32  print Fopt, xopt, iter, nFeval
```

***Initialization* procedure**
Input Data:
1 *ndv* = Number of decision variables
2 *nm* = Number of molecules
3 *niter* = Number of maximum iterations
4 *tol* = Tolerance in the objective function
5 *objfunct(x)* = Objective function evaluated at position *x*
Load Parameters:
6 *gmin* = Lowest friction coefficient
7 *gmax* = Largest friction coefficient
8 *K*1 = Repulsion force constant
9 *K*2 = Stochastic force constant
10 *K3* = Constant used in the Metropolis criterion
11 *minfexp* = Minimum fraction of explorers during optimization
12 *dcutoff* = Cut-off distance for intermolecular forces
Initialization of variables:
13 *iter* = 0 Number of iterations
14 *nFeval* = 0 Number of function evaluations
15 *stop_flag* = FALSE Status of stopping conditions
Initialization of molecules:
16 **for** *i* = 1 **to** *nm*
17 *molclass(i)* = 1
Classification of molecules (0 = Refiner, 1 = Explorer)
18 *x*(*i*) = **uniform_random**(*ndv*)
Setting initial position vector of molecules
19 *Fobj*(*i*) = *objfunct*(*x*(*i*)) Initial objective function evaluation
20 *nFeval* = *nFeval* + 1 Update number of function evaluations
21 **end**
22 *R* = set of indices of refiner molecules
23 *molrank* = sort index of molecules according to feasibility (descending) and objective function (ascending)
24 *mopt* = index of feasible molecule with best objective function value

***Molecules_update_subroutine* procedure**
1 **for** *i* = 1 **to** *nm*
2 **if** *molclass*(*i*) = 1 **and** *P*(*i*) > **uniform_random then**
3 *x*(*i*) = *xnew*(*i*) Update molecular position
4 *Fobj*(*i*) = *Fobjnew*(*i*) Update objective function value
5 **if** *feasible* **and** *Fobj*(*i*) < **max**(*Fobj*(*r*)) **then**
6 *molclass*(*i*) = 0 Molecule set as refiner
7 **if sum**(*molclass*) < *nm***minfexp*
8 *r* = index of refiner molecule with highest Fobj
9 *molclass*(*r*) = 1 Set molecule as explorer
10 **end**
11 **end**
12 **elseif** *feasible* **and** *dG*(*i*) < 0 **then**
13 *x*(*i*) = *xnew*(*i*) Update molecular position
14 *Fobj*(*i*) = *Fobjnew*(*i*) Update objective function value
15 **end**
16 **end**
17 *molrank* = sort index of molecules according to feasibility (descending) and objective function (ascending)
18 **for** *i* = 1 **to** *nm*
19 **if** *molrank*(*i*) < *nm*-**sum**(*molclass*) **then**
20 *molclass*(*i*) = 0 Update refiners
21 **else**
22 *molclass*(*i*) = 1 Update explorers
23 **end**
24 **end**

Appendix B. Global Optimization Problems

B.1. Dixon-Szegö Test Functions

Dixon and Szegö (1978) proposed a set of challenging set functions for testing global optimization algorithms. Some of these functions (all of them showing multiple local minima) were selected for testing the performance of MIPT vs. other well-established optimization methods. The details of the selected functions are presented here.

Easom function

- Number of variables: 2
- Search region: $-10 < x_j < 10$, j = 1, 2.
- Definition:

$$f_{obj}(x_1, x_2) = -\cos(x_1)\cos(x_2)\exp\left(-(x_1-\pi)^2 - (x_2-\pi)^2\right) \quad \text{(B.1)}$$

- Global minimum: $x_1^* = \pi$, $x_2^* = \pi$, $f_{obj}^* = -1$

Goldstein and Price function

- Number of variables: 2
- Search region: $-2 < x_j < 2$, j = 1, 2.
- Definition:

$$\begin{aligned} f_{obj}(x_1, x_2) &= a(x_1, x_2) \cdot b(x_1, x_2) \\ a(x_1, x_2) &= 1 + (x_1 + x_2 + 1)^2 \cdot (19 - 14x_1 + 3{x_1}^2 - 14x_2 + 6x_1x_2 + 3{x_2}^2) \\ b(x_1, x_2) &= 30 + (2x_1 - 3x_2)^2 * (18 - 32x_1 + 12{x_1}^2 + 48x_2 - 36x_1x_2 + 27{x_2}^2) \end{aligned} \quad \text{(B.2)}$$

- Global minimum: $x_1^* = 0$, $x_2^* = -1$, $f_{obj}^* = 3$

Shubert function

- Number of variables: 2
- Search region: $-10 < x_j < 10$, j = 1, 2.
- Definition:

$$f_{obj}(x_1, x_2) = \left(\sum_{i=1}^{5} i\cos((i+1)x_1 + i)\right)\left(\sum_{j=1}^{5} j\cos((j+1)x_2 + j)\right) \quad \text{(B.3)}$$

- Multiple global minima: $f_{obj}^* = -186.7309$

Hartmann-3 function

- Number of variables: 3
- Search region: $0 < x_j < 1$, j = 1, 2, 3.
- Definition:

$$f_{obj}(\mathbf{x}) = -\sum_{i=1}^{4} c_i \exp\left(-\sum_{j=1}^{3} a_{ij} \left(x_i - p_{ij} \right)^2 \right) \qquad \text{(B.4)}$$

- Global minimum: $x_1^* = 0.114614$, $x_2^* = 0.555649$, $x_3^* = 0.852547$, $f_{obj}^* = -3.862782$

Table B.1. Parameters of Hartmann-3 function

i	a_{ij}			c_i	p_{ij}		
	$j=1$	$j=2$	$j=3$		$j=1$	$j=2$	$j=3$
1	3.0	10	30	1.0	0.6890	0.1170	0.2673
2	0.1	10	35	1.2	0.4699	0.4387	0.7470
3	3.0	10	30	3.0	0.1091	0.8732	0.5547
4	0.1	10	35	3.2	0.0381	0.5743	0.8828

Hartmann-6 function

- Number of variables: 6
- Search region: $0 < x_j < 1$, j = 1, ..., 6.
- Definition:

$$f_{obj}(\mathbf{x}) = -\sum_{i=1}^{4} c_i \exp\left(-\sum_{j=1}^{6} a_{ij} \left(x_i - p_{ij} \right)^2 \right) \qquad \text{(B.5)}$$

- Global minimum: $x_1^* = 0.201690$, $x_2^* = 0.150011$, $x_3^* = 0.476874$, $x_4^* = 0.275332$, $x_5^* = 0.311652$, $x_6^* = 0.657300$, $f_{obj}^* = -3.32237$

Table B.2. Parameters of Hartmann-6 function

i	a_{ij}						c_i	p_{ij}					
	$j=1$	$j=2$	$j=3$	$j=4$	$j=5$	$j=6$		$j=1$	$j=2$	$j=3$	$j=4$	$j=5$	$j=6$
1	10	3	17	3.5	10	30	1.0	0.1312	0.1696	0.5596	0.0124	0.8283	0.5886
2	0.05	10	17	0.1	10	35	1.2	0.2329	0.4135	0.8307	0.3736	0.1004	0.9991
3	3	3.5	1.7	10	10	30	3.0	0.2348	0.1451	0.3522	0.2883	0.3047	0.6650
4	17	8	0.05	10	10	35	3.2	0.4047	0.8828	0.8732	0.5743	0.1091	0.0381

Shekel functions

- Number of variables: 4
- Search region: $0 < x_j < 10$, j = 1, …, 4.
- Definition:

$$f_{obj,m}(\mathbf{x}) = -\sum_{i=1}^{m} \frac{1}{c_i + \sum_{j=1}^{4} (x_i - a_{ij})^2} \tag{B.6}$$

- Global minimum: $x_1^* = 4$, $x_2^* = 4$, $x_3^* = 4$, $x_4^* = 4$,

$$f_{obj,m}^* = \begin{cases} -10.1532, & m = 5 \\ -10.4029, & m = 7 \\ -10.5364, & m = 10 \end{cases}$$

Table B.3. Parameters of Shekel functions

i	a_{ij}				c_i
	$j=1$	$j=2$	$j=3$	$j=4$	
1	4	4	4	4	0.1
2	1	1	1	1	0.2
3	8	8	8	8	0.2
4	6	6	6	6	0.4
5	3	7	3	7	0.4
6	2	9	2	9	0.6
7	5	5	3	3	0.3
8	8	1	8	1	0.7
9	6	2	6	2	0.5
10	7	3.6	7	3.6	0.5

B.2. Nonlinear Steady-State Model of a Biochemical Reaction Network

The complete model for the pathway of ethanol production by *Saccharomyces cerevisiae*, and the corresponding optimization problem are presented by **Xu et al. (2008)**. The optimization problem used as for testing the MIPT algorithm is the following:

$$\max_{X_1,X_2,X_3,X_4,X_5,Y_1} V_{PK}$$

subject to:

$$\begin{aligned}
&V_{in} - V_{HK} = 0\\
&V_{HK} - V_{PFK} - V_{Pol} = 0\\
&V_{PFK} - V_{GAPD} - 0.5V_{Gol} = 0\\
&2V_{GAPD} - V_{PK} = 0\\
&2V_{GAPD} + V_{PK} - V_{HK} - V_{Pol} - V_{PFK} - V_{ATPase} = 0\\
&V_{in} - Y_1 + 3.7X_2 = 0\\
&V_{Pol}\left(1+\left(\frac{2}{X_2}\right)^{8.25}\right)\left(\frac{1.1}{0.7X_2}+2.43\right) - 1.1Y_6 = 0\\
&1.0832V_{Gol}\left(R_2^2 + 164.084L_2^2T_2^2\right) - Y_7X_4ADP\left(2.519R_2 + 0.656T_2L_2^2\right) = 0\\
&X_1X_5Y_2 - V_{HK}\left(6.2\times10^{-4} + 0.11X_5 + 0.1X_1 + X_1X_5\right) = 0\\
&50X_2X_5R_1Y_3 - V_{PFK}\left(R_1^2 + 3342L_1^2T_1^2\right) = 0\\
&V_{GAPD}\left(1+\frac{0.25}{X_3}+\frac{0.18}{NAD}\left(1+\frac{AMP}{1.11}+\frac{ADP}{1.5}+\frac{X_2}{2.5}\right)\left(1+\frac{0.25}{X_3}\right)\left(1+\frac{NADH}{0.00029433}\right)\right) - Y_4 = 0\\
&Y_5V_{Gol} - Y_7V_{PK} = 0\\
&Y_8X_5 - V_{ATPase} = 0\\
&V_{PK} \le 2V_{in}\\
&Y_{k0} \le Y_k \le 50Y_{k0},\quad k = 1,2,3,4,5,8
\end{aligned} \tag{B.7}$$

with

$$\begin{aligned}
&Y_6 = 14.31;\ Y_7 = 203;\ Y_9 = 0.042\\
&NAD^+ = \frac{2}{Y_9+1}\\
&NADH = \frac{2Y_9}{Y_9+1}\\
&ADP = \frac{1}{2}\left(\sqrt{12X_5 - 3X_5^2} - X_5\right)\\
&AMP = 3 - X_5 - ADP\\
&L_1 = \frac{1+0.76AMP}{1+40AMP}\\
&R_1 = 1 + 0.3X_2 + 16.67X_5 + 50X_2X_5\\
&T_1 = 1 + 1.5\times10^{-4}X_2 + 16.67X_5 + 0.0025X_2X_5\\
&R_2 = 1 + 125.94X_4 + 0.2ADP + 2.519X_4ADP\\
&T_2 = 1 + 0.02X_4 + 0.2ADP + 0.004X_4ADP\\
&L_2 = \frac{1+0.05X_3}{1+5X_3}
\end{aligned} \tag{B.8}$$

B.3. Unstructured model of Ethanol Production

The system considered by the unstructured model is composed of three main state variables: Glucose (G), Cells (X) and Ethanol (E) concentrations. The cells concentration in the batch depends on the cell's growth and cell's death rates as follows:

$$\frac{dX}{dt} = \mu X - K_d X \tag{B.9}$$

$$\mu = \mu_m \left(\frac{G}{k_s + G + \frac{G^2}{K_{ss}}} \right) \left(1 - \frac{E}{E_m} \right) \tag{B.10}$$

μ is the specific growth rate in h^{-1}, K_d is the cell's death rate in h^{-1}, k_s is the saturation growth constant in g/L, K_{ss} is the substrate growth inhibition constant in g/L, and E_m is the ethanol inhibition constant for growth in g/L. Besides substrate limitation, the cell's growth expression shown in Equation (B.10) includes inhibition caused by both substrate (glucose) and product (ethanol).

Glucose produced during the saccharification is given by the first term on Equation (B.11). The second and third term represent the fraction of glucose that is used for cell growth (including maintenance) and ethanol production respectively.

$$\frac{dG}{dt} = -\left(\frac{\mu X - K_d X}{Y_{X/G}} \right) - \left(\frac{qX}{Y_{E/G}} \right) - K_{cm} X \tag{B.11}$$

q is the ethanol specific production rate in h^{-1}, $Y_{X/G}$ is the yield coefficient of cell growth in g/g, $Y_{E/G}$ is the yield coefficient of product in g/g and K_{cm} is the rate of glucose consumption for cell maintenance in h^{-1}.

Finally, the ethanol is produced only by cells at the rate:

$$\frac{dE}{dt} = qX \tag{B.12}$$

$$q = q_m \left(\frac{G}{k_{sp} + G + \frac{G^2}{K_{ssp}}} \right) \left(1 - \frac{E}{E_{mp}} \right) \tag{B.13}$$

q_m is the maximum specific production rate in h^{-1}, k_{sp} is the saturation production constant in g/L, K_{ssp} is the substrate production inhibition term in g/L, and E_{mp} is the ethanol inhibition constant for production in g/L.

The objective function for this problem was defined taking into account the normalized mean of the squared error (*MSE*) for the *X*, *S*, *G* and *E,* as:

$$\min_{pk}\left(F_{obj}\right) = \min\left(MSE_X + MSE_S + MSE_G + MSE_E\right) \tag{B.14}$$

where p_k represent the 12 parameters of the model to be identified: μ_m, k_s, K_{ss}, E_m, K_d, q, k_{sp}, K_{ssp}, E_{mp}, K_{cm}, Y_{XG} and Y_{EG}.

The normalized MSE for each variable is described as:

$$MSE_y = \frac{1}{n} * \sum_{i=1}^{n} \left(\frac{y_{\exp,i} - \hat{y}_i}{\max(y_{\exp,i})} \right)^2 \tag{B.15}$$

where $y_{\exp,i}$ and $\hat{y}_i$ (for *i=1,2..,n*) are respectively the experimental data reported and the value predicted by the model for the variable *y*; and *n* is the number of available experimental data used for identification.

The initial conditions of the fermentation are: 220 g/L of glucose and 0.2 g/L of biomass. The simulation time is 72 hours. The model is solved using Euler's method with a step of 0.1 hours.

B.4. Ethanol fed-batch fermentation

The dynamic model for fed-batch production of ethanol by means of *Saccharomyces cerevisiae*, using glucose as raw material is given by:

$$\frac{dV}{dt} = F \tag{B.16}$$

$$\frac{dX}{dt} = \mu X - \frac{FX}{V} \tag{B.17}$$

$$\frac{dS}{dt} = \frac{-\mu X}{Y} + \frac{F(S_{in} - S)}{V} \tag{B.18}$$

$$\frac{dP}{dt} = qX - \frac{FP}{V} \tag{B.19}$$

Where V, X, S and P are the state variables Volume, Biomass, Substrate (glucose) and Product (ethanol) concentration respectively. F is the substrate flow rate and S_{in} is the concentration of substrate in the feed. The kinetic expressions for cells' growth and ethanol production are given by:

$$\mu = \left(\frac{\mu_0}{1 + \frac{P}{K_p}} \right) \left(\frac{S}{K_S + S} \right) \tag{B.20}$$

$$q = \left(\frac{q_0}{1 + \frac{P}{K_p'}} \right) \left(\frac{S}{K_s' + S} \right) \tag{B.21}$$

The parameters of the model are given in Table B.4. The initial conditions for the state variables and the constraints for the states (in this case only for the volume) and for the control variables are given in Table B.5.

The substrate flow feed rate profile is described by a cosine parameterization:

$$F(t) = a_0 + a_1 \cos\left(w_1 \left(\frac{t - t_0}{t_f - t_0} \right) + \phi_1 \right) + a_2 \cos\left(w_2 \left(\frac{t - t_0}{t_f - t_0} \right) + \phi_2 \right) \quad \text{(B.22)}$$

The objective function to be maximized is the productivity of the process defined as:

$$\max_{F(t)} \left[Productivity \right] = \min_{a_0, a_1, a_2, w_1, w_2, \phi_1, \phi_2} \left[-P(t_f) V(t_f) \right] \quad \text{(B.23)}$$

The total fermentation time considered was 54 hours.

Table B.4 Model parameters for the ethanol fermentation process taken from **Hong (1986)**

Parameter	**Description**	**Value**
μ_0 (1/h)	Maximum Biomass growth rate	0.408
q_0 (1/h)	Maximum Ethanol production rate	1
K_s (g/l)	Monod Constant	0.22
K_s' (g/l)	Monod Constant	0.44
K_p (g/l)	Substrate Inhibition Constant	16
K_p' (g/l)	Product Inhibition Constant	71.5
Y (gX/gS)	Yield Factor	0.1
S_{in} (g/l)	Substrate Input Concentration	150

Table B.5 Initial conditions for the ethanol fermentation process taken from **Hong (1986)**

Variable	**Bounds**		**Initial**
	Lower	**Upper**	**Condition**
V (l)	0	200	10
X (g/l)	0	-	1
S (g/l)	0	-	150
P (g/l)	0	-	0
F (l/h)	0	12	-

Appendix C. Additional information of the bio-ethanol production process model

C.1. Model parameters and operating conditions

The model parameters, including the kinetics and the operating conditions used in the model of the hydrolysis stage are shown in Table C.1.

Table C.1 Model parameters and operating conditions for the starch hydrolysis stage

Parameter/ Operating condition	Description	Value	Units
k_g	Kinetic factor for gelatinization	1.116×10^{18}	h^{-1}
E_{ag}	Activation Energy for gelatinization	1.083×10^{8}	J/kmol
k_{mlt}	Kinetic constant for dextrins production	421.2	kg/Uh
K_{de}	Kinetic factor for alpha-amylase deactivation	2.484×10^{34}	h^{-1}
E_{ade}	Activation Energy for denaturation	2.242×10^{8}	J/kmol
a_{act}[1]	Specific Alpha-amylase Activity	5×10^{7}	U/kg
T_L	Liquefaction temperature	365	K
ρ_L	Density	1037	kg/m^3
$A_{T,L}$	Cross section of the liquefaction tank	12.5	m^2
K_3	Kinetic constant	7.56×10^{-5}	kg/Uh
k_m	Michaelis-Menten constant	0.45	kg/m^3
k_i	Product inhibition constant	0.52	kg/m^3
g_{act}[2]	Specific Gluco-amylase Activity	7×10^{7}	U/kg
$A_{T,S}$	Cross section of the saccharification tank	45.45	m^2
T_S	Saccharification temperature	333	K
P_L	Liquefaction pressure	1.2	atm
P_S	Saccharification pressure	1.2	atm

[1,2] Specific activity of alpha-amylase and gluco-amylase from *Bacillus subtillis* and *Aspergillius niger*, respectively.

Table C.2 shows the kinetics parameters and operating conditions considered for the fermentation stage.

Table C.2 Model parameters and operating conditions for the fermentation stage

Parameter/ Operating condition	**Description**	**Value**	**Units**
μ_{max}	Maximum specific growth rate	0.4233	1/h
E_m	Inhibition constant by product	80	kg/m^3
X_m	Biomass concentration when cell grows ceases	330	kg/m^3
A_1	Constant in equation 4.37	1	
A_2	Constant in equation 4.37	1	
K_s	Monod constant	4.074	kg/m^3
K_i	Inhibition constant by substrate	4.218×10^{-3}	m^3/kg
Y_{XS}	Limit cellular yield	0.1204	kg/kg
M_x	Maintenance coefficient	0.2548	h^{-1}
Y_{PX}	Yield of product	4.7135	kg/kg
M_p	Ethanol production associated to growth	0.1	h^{-1}
k_{dT}	Coefficient of death by temperature	2.48×10^{-14}	h^{-1}
k_{dP}	Coefficient of death by ethanol	0.3928	m^3/kg
γ_x	Ratio of concentration of intracellular to extracellular ethanol	390	kg/m^3
$A_{T,F}$	Cross section of the Fermentor tank	75	m^2
T_F	Fermentor temperature	305	K
P_F	Fermentor pressure	1.2	Atm

The operating conditions and design parameters of the distillation and rectification columns are summarized in Table C.3. In addition, each adsorption unit (T-303/304) consists of a bed of 1000 kg of molecular sieves with a pore size of 3 Å.

In Table C.4, the level-, pressure- and composition-control loops implemented in the plant as local control strategy (Section 6.1.1) are presented including their corresponding set point values and tuning parameters.

Table C.3 Operating conditions and design parameters for the purification section

Parameter	**Distillation**	**Rectification**
Feed trays	30	20, 42
Feed temperature (K)	368	368, 358
Top pressure (atm)	0.3	1
Number of trays	37	43
Tray diameter (m)	3	2
Weir height (cm)	0.03	0.02
Tray pressure drop (mm Hg)	5	5

Table C.4 Local control strategy: Set points and tuning parameters

Controller ID	**Set point**	**Tuning parameters[§§]**
LC-1	H_{Lsp}=6 m	F_{2ss}=90.16 m^3/h K=50 m^2/h
LC-2	H_{Ssp}=11 m	F_{4ss}=90.2 m^3/h K=100 m^2/h
LC-3	H_{Fsp}=12 m	F_{6ss}=222.52 m^3/h K=200 m^2/h
LC-4	H_{B1sp}=5 m	B_{1ss}=7762 kmol/h K=-5000 kmol/m h
LC-5	H_{D1sp}=3 m	D_{1ss}=1347.2 kmol/h K=-5000 kmol/m h
LC-6	H_{B2sp}=3 m	B_{2ss}=1089.8 kmol/h K=-5000 kmol/m h
LC-7	H_{D2sp}=2 m	Q_{c2ss}=7.2×10^{10} J/h K=5×10^9 J/m h
PC-1	P_{t1sp}=225 mmHg	Q_{c1ss}=2.2×10^{11} J/h K=2.5×10^8 J/m h
PC-2	P_{t2sp}=760 mmHg	D_{2ss}=290.37 kmol/h K=2 kmol/ mmHg h
AC-1	$X_{v,F\text{-}sp}$= $X_{v,F\text{-}opt}$, is a variable SP (given by the D-RTO layer).	F_{5ss}=0 m^3/h K_{F5}=-0.001 m^6/ kg h F_{8ss}=0.576 m^3/h K_{F8}=0.5 m^6/ kg h

[§§] The tuning parameters were determined as follows: First, an initial set of parameters was found according to Shinskey's correlations given in **O'Dwyer (2009)**. Then, each parameter was sequentially fine-tuned by using dynamic simulations of the plant and guidelines given by **McMillan (2005)**.

C.2. Parameter identification and structural validation of the fermentation model

The model of the fermentation stage was introduced and described in Equations (4.32) – (4.58). The fermentation kinetics was modeled as reported by **Costa et al. (2002)**. In this section, the fermentation model is used to describe two different sets of fermentation experimental data in order to i) identify the best set of parameters for describing the kinetics of the process considered, which is a continuous fermentation with high biomass concentration and cells recycle; and ii) to assess the adequacy of the model structure (Equations 4.32 – 4.43), by using the model structure for describing a completely different set of data. The model structure validation is carried out using experimental data of batch fermentation with low biomass concentration and no cells recycle.

Parameter identification

The parameter identification was carried out using experimental data reported by **Jarzebski et al. (1989)**. The objective function minimized for parameter identification was the Mean Square Relative Error (MSRE) for the state variables in the fermentor, namely: Viable yeast (X_v), total biomass (X_t), glucose (G) and ethanol concentrations (E), as shown in Equation (C.1). The optimization method used was the Molecular-Inspired Parallel Tempering (MIPT) algorithm presented in Chapter 3.

$$MSRE = \sum_{i=1}^{N_D}\left[\frac{(X_{V,i} - X_{V,model}(t_i))}{max(X_V)}\right]^2 + \sum_{i=1}^{N_D}\left[\frac{(X_{t,i} - X_{t,model}(t_i))}{max(X_t)}\right]^2 + \sum_{i=1}^{N_D}\left[\frac{(G_i - G_{model}(t_i))}{max(G)}\right]^2 + \sum_{i=1}^{N_D}\left[\frac{(E_i - E_{model}(t_i))}{max(E)}\right]^2 \quad \text{(C.1)}$$

where N_D is the number of experimental data and t_i is the time at which each experimental data was taken.

Results of parameter identification are presented in Figure C.1, showing the comparison between the model used in this work (red line) and the experimental data reported by **Jarzebsky et al. (1989)**, for the total biomass, viable biomass, glucose and ethanol concentrations. The objective function value in the parameter identification for the model used in this work was *MSRE*=0.0193, indicating a very good fit between the experimental

data and the model, which is confirmed by an analysis of Figure C.1. Predictions for Biomass (total and viable) and glucose presented the best fit to experimental data, whereas ethanol predicted by the model presents a higher deviation from the data, which can be caused by the high dispersion of the experimental data after 50 hours. The best set of parameters identified has been already presented in Table C.2.

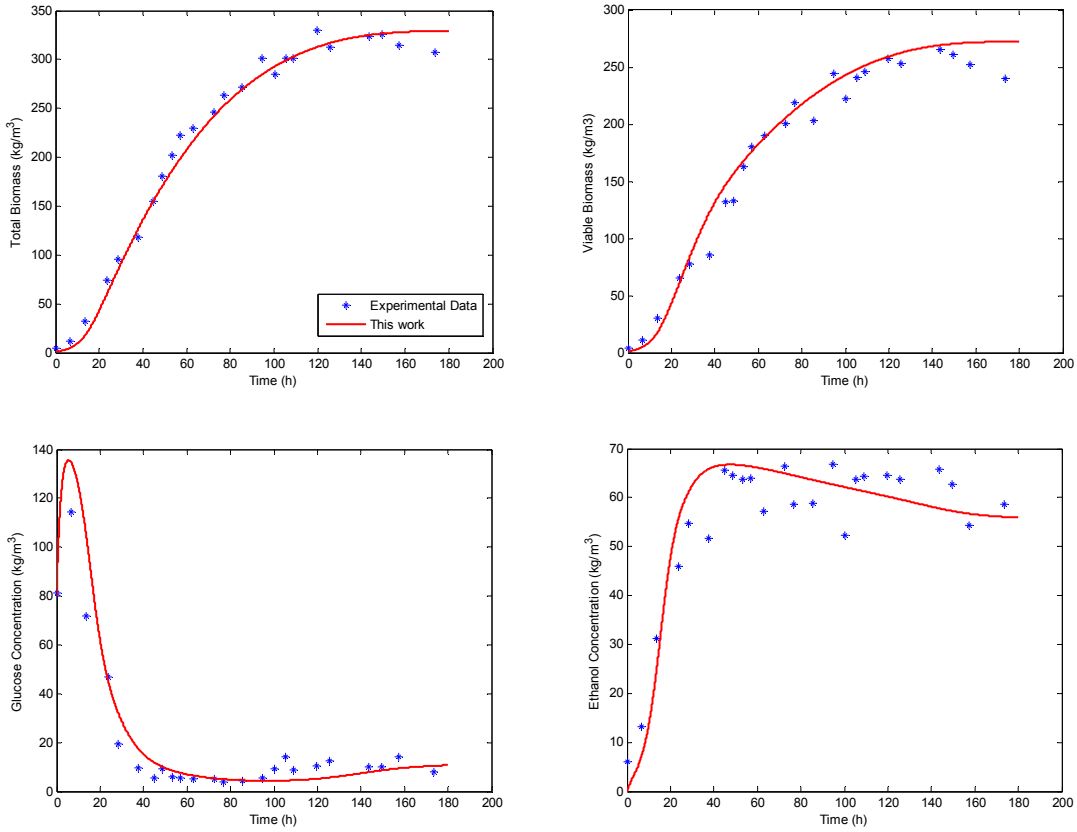

Figure C.1 Comparison of experimental data and the model used in this work after parameter identification for continuous ethanol fermentation with cells recycle and high biomass. Top left: Total biomass; Top right: Viable biomass; Bottom left: Glucose concentration; Bottom right: Ethanol concentration. The data points are the Experimental data from **Jarzebsky et al (1989)** and the red line describes the model predictions.

Model Structure Validation

In order to validate the model structure, experimental data from a batch fermentation process were used. For that purpose, batch fermentation experiments were performed using the yeast *Saccharomyces cerevisiae* 46 EDV and a culture medium with the following composition: 118.4 g/l glucose, 2 g/l $(NH_4)_2SO_4$, 2.72 g/l KH_2PO_4, 0.5 g/l $MgSO_4$·7H2O and 1 g/l yeast extract. Temperature and pH were controlled at 28 °C and 4.5 respectively. The bioreactor used was a 2-Liter glass cylinder (1.7 liters working volume) equipped with a six-

blade turbine stirrer and an Applikon control system. Yeast inoculum concentrations of 2% (w/v) were used corresponding to an initial population of living cells of approximately 10^7 CFU/mL. Ethanol and glucose concentrations were determined from density measurements using an Anton Paar DMA 4500, whereas the biomass was measured spectrophotometrically at 620 nm wavelength using a Spekol 11. It is important to notice that these experimental data were taken in a batch lab-scale bioreactor without cells recycle, and with a low biomass concentration, in contrast to the experimental data by **Jarzebky et al. (1989)** that were used for parameter identification, where a continuous fermentation with cell recycle at high biomass concentration was evaluated. Therefore, the purpose of using the new set of batch experimental data is to validate only the model structure (Equations 4.32 – 4.43), for which new parameters should be identified.[***]

The error function to be minimized in this case is the same than that described by Equation (C.1), but without the viable yeasts term, because the set of experimental data only include data for total biomass, glucose and ethanol. Figure C.2 shows the comparison between the model and the new set of experimental data, for the total biomass, glucose and ethanol concentrations. As it can be observed, the model is in good agreement with the experimental behavior (MSRE = 0.00435), especially for the glucose and ethanol predictions. The highest deviation is observed in the biomass concentration, which can be explained by the accuracy of biomass determination.

It is observed that the model structure used in this work for the fermentation model, which was taken from **Costa et al. (2002)**, is a reliable structure for representing the ethanol fermentation from glucose for a wide range of operating conditions: either batch or continuous mode, with or without cells recycle, and high or low biomass concentration.

[***] The parameters of the model change as a result of the different operating conditions (biomass concentration, substrate concentration, etc.), different microorganism strain and also different substrate quality.

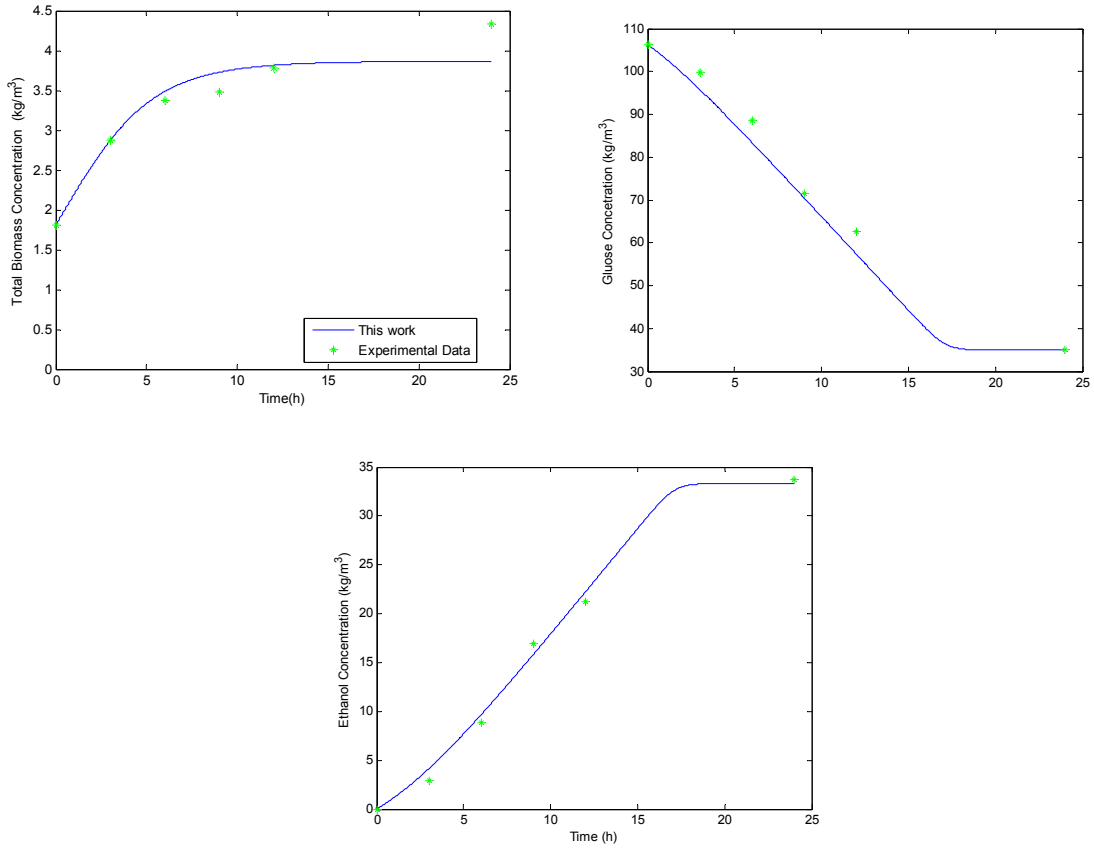

Figure C.2 Comparison of experimental data and simulation models after parameter identification for batch ethanol fermentation without cells recycle and low biomass concentration. Top: Total biomass; Top right: Glucose concentration; Bottom Ethanol concentration. Data points: Experimental data; Blue Red line: Model used in this work.

C.3. Phase equilibrium calculation and additional constants and model parameters

The Vapour-Liquid equilibrium in the trays of the distillation and rectification columns is described by Equation (4.65), rewritten in Equation (C.2).

$$y_{j,i} = x_{j,i} \cdot \left(\frac{\gamma_j P_{v,j}}{\sum_{k=1}^{Nc} x_k \gamma_k P_{v,k}} \right)_i \qquad \text{(C.2)}$$

where γ_j and $P_{v,j}$ are the activity coefficient and the vapor pressure, respectively. The activity coefficients are calculated using the UNIQUAC model as given by Equation (C.3)

$$\gamma_i = \exp\left(\ln\gamma_{i,c} + \ln\gamma_{i,r}\right) \tag{C.3}$$

where $\gamma_{I,c}$ and $\gamma_{I,r}$ are the combinatorial and residual activity contributions, which are given by Equation (C.4) and (C.5), respectively.

$$\ln\gamma_{i,c} = \ln\left(\frac{\phi_i}{x_i}\right) + 1 - \left(\frac{\phi_i}{x_i}\right) \tag{C.4}$$

$$\ln\gamma_{i,r} = Q_i\left(1 - \ln\left(\sum_j \theta_j\tau_{ji}\right) - \sum_j \frac{\theta_j\tau_{ij}}{\sum_j \theta_j\tau_{ji}}\right) \tag{C.5}$$

where Q_i is a molecular area parameter for component *i*, whereas ϕ_i, θ_i, and τ_{ij} are the molecular volume fraction and molecular area fraction of component i and temperature-dependent interaction parameters, given by Equations (C.6) – (C.8).

$$\phi_i = \frac{R_i^{2/3}x_i}{\sum_j R_i^{2/3}x_j} \tag{C.6}$$

$$\theta_i = \frac{Q_i x_i}{\sum_j Q_j x_j} \tag{C.7}$$

$$\tau_{ij} = \exp\left(-\frac{a_{ij} + b_{ij}(T - T_0)}{T}\right) \tag{C.8}$$

where R_i, a_{ij} and b_{ij} are the molecular volume parameter and the UNIQUAC interaction constants for component i, and T and T_0 are the system temperature and the reference temperature.

The vapor pressure in Equation (C.2) is calculated according to Antoine's equation:

$$\ln P_{s,i} = A_i - \frac{B_i}{T + C_i} \qquad \text{(C.9)}$$

Table C.5 and C.6 show the parameters used for the phase equilibrium calculations for the three-component system: Ethanol-water-glucose. The parameters for the calculation of the activity coeffcients were taken from **Macedo and Peres (2001)**, whereas the Antoine parameters are those reported by **Gmehling et al. (1990)**. The vapour pressure of the heavy components (i.e. glucose, starch, non-fermentable) was assumed to be zero for the whole range of temperatures considered.

Table C.5 UNIQUAC interaction parameters for the system ethanol-water-glucose taken from **Macedo and Peres (2001)**

Parameter	Value	Units
R_1	2.5755	
R_2	0.92	
R_3	8.1528	
Q_1	2.588	
Q_2	1.4	
Q_3	7.92	
a_{11}	0	K
a_{22}	0	K
a_{33}	0	K
a_{12}	249.06	K
a_{21}	-132.51	K
a_{13}	178.83	K
a_{31}	9.1123	K
a_{23}	96.5267	K
a_{32}	-68.6157	K
b_{11}	0	
b_{22}	0	
b_{33}	0	
b_{12}	0	
b_{21}	0	
b_{13}	0	
b_{31}	0	
b_{23}	0.277	
b_{32}	-0.069	
T_0	298.15	K

Table C.6 Antoine Parameters (Temperature in K, Pressure in mm Hg) taken from **Gmehling et al. (1990)**

Parameter	Value
A_E	8.1122
B_E	1592.864
C_E	-46.966
A_w	8.07131
B_w	1730.63
C_w	-39.574

On the other hand, the expressions used for calculating thermodynamic variables of mixtures are the following:

$$h_{l,i} = \sum_j x_j C_{pl,j,i} T_{t,i} \tag{C.10}$$

$$h_{v,i} = \sum_j y_j C_{pl,j,i} T_{t,i} + \lambda_i \tag{C.11}$$

$$\lambda_i = \sum_j y_j \lambda_{j,i} \tag{C.12}$$

where

$$C_{pl,w,i} = a_{cp,w} + b_{cp,w} T_{t,i} + c_{cp,w} T_{t,i}^2 \tag{C.13}$$

$$C_{pl,E,i} = a_{cp,E} \ln\left(1 - \frac{T_{t,i}}{T_{c,E}}\right) + b_{cp,E}\left(1 - \frac{T_{t,i}}{T_{c,E}}\right) + c_{cp,E} + d_{cp,E}\left(\frac{T_{t,i}}{T_{c,E}}\right) + e_{cp,E}\left(\frac{T_{t,i}}{T_{c,E}}\right)^2 + f_{cp,E}\left(\frac{T_{t,i}}{T_{c,E}}\right)^3 \tag{C.14}$$

$$\lambda_{w,i} = a_{\lambda,w} + b_{\lambda,w} T_{t,i} \tag{C.15}$$

$$\lambda_{E,i} = a_{\lambda,E}\left(1 - \frac{T_{t,i}}{T_{c,E}}\right)^{b_{\lambda,E}} \exp\left(\frac{c_{\lambda,w} T_{t,i}}{T_{c,E}}\right) \tag{C.16}$$

The parameters for the calculation of specific heat and vaporization enthalpy of water were taken from **Smith et al. (2005)**. The corresponding parameters for ethanol were taken from **Henke et al. (2009)**. These are presented in Table C.7. Additional physicochemical properties are included in Table C.8.

Table C.7 Additional thermodynamic parameters taken from **Smith et al. (2005)** and **Henke et al. (2009)**

Parameter	Value	units
$a_{cp,w}$	7.243×10^{4}	J/kmol K
$b_{cp,w}$	10.3925	J/kmol K^2
$c_{cp,w}$	-1.4965×10^{-3}	J/kmol K^3
$a_{\lambda.,w}$	5.5968×10^{7}	J/kmol
$b_{\lambda.,w}$	-4.0387×10^{4}	J/kmol K
$a_{cp,E}$	1.28×10^{5}	J/kmol K
$b_{cp,E}$	2.986×10^{3}	J/kmol K
$c_{cp,E}$	7.779×10^{4}	J/kmol K
$d_{cp,E}$	2.1405×10^{5}	J/kmol K
$e_{cp,E}$	-3.4487×10^{5}	J/kmol K
$f_{cp,E}$	6.6786×10^{5}	J/kmol K
$a_{\lambda.,E}$	5.043×10^{7}	J/kmol
$b_{\lambda.,E}$	0.4989	
$c_{\lambda.,E}$	0.4475	
$T_{c,E}$	513.92	K

Table C.8 Physicochemical properties of components

Parameter	Value	units
w_{co2}	44	kg/kmol
w_E	46	kg/kmol
w_w	18	kg/kmol
w_G	180	kg/kmol
w_S	342	kg/kmol
ρ_E	790	kg/m^3
ρ_w	1000	kg/m^3

C.4. Distillation Model Validation

Before validating the model for the distillation columns, it is necessary first to verify that the vapor-liquid equilibrium (VLE) model adequately describes the system. Figure C.3 shows a comparison of the UNIQUAC model used to describe the VLE (Appendix C.3) versus reported experimental data (**Green and Perry, 2008**). As it can be seen, there is a good agreement between the experimental data and the UNIQUAC, with an average absolute error of 2.1% in

ethanol composition and a maximum absolute error of 3.5%. It can be noticed that the largest deviations are observed in the range of 30-70% ethanol (molar basis), and that the UNIQUAC model satisfactorily predicts the azeotrope at around 89%mol of ethanol. Therefore, it is concluded that the UNIQUAC model and its corresponding parameters can be used to predict equilibrium data in the ethanol-water system.

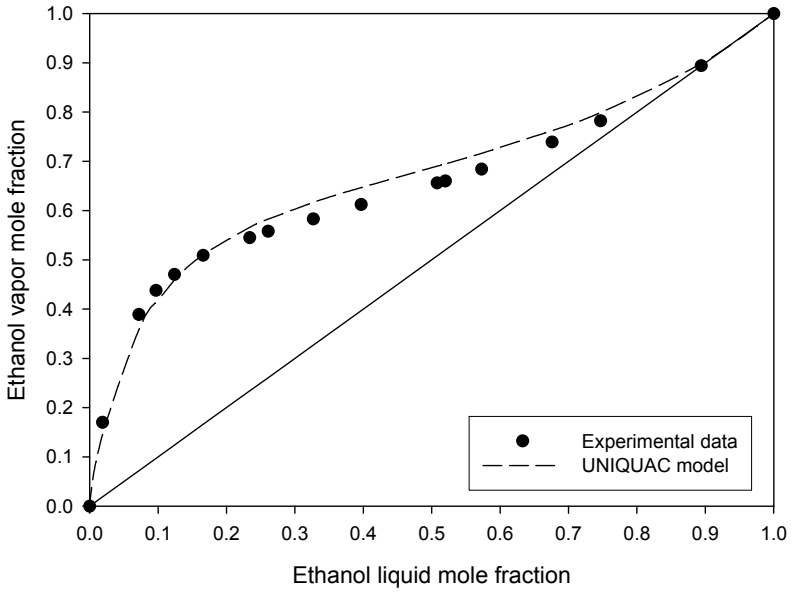

Figure C.3 Ethanol-water Vapor-Liquid Equilibrium. Experimental data (**Green and Perry, 2008**) vs. UNIQUAC model (**Gmehling et al., 1990**).

The distillation and rectification models were validated using simulated data obtained from Aspen Plus. The validation procedure was the following. Both columns were separately simulated in:

- Aspen Plus using *Radfrac* columns under the conditions identified as optimal (See Table C.3)
- Simulink using the dynamic model of the columns presented in Section 4.1.4.2, until it reached a steady state, for the same optimal design parameters (Table C.3) and input values (Table 4.3.).

The comparison between the validation data (e.g. Aspen simulated data) and the Simulink model for the temperature profiles across the column, and the profiles for the ethanol concentration in the liquid phase, for the Distillation and rectification columns is shown in Figures C.4 and C.5, respectively. Table C.9 shows the average and maximum deviation of these variables between the Aspen model and the model presented in Chapter 4. The

deviation in composition is the absolute value expressed as %mol. The deviation in temperature is presented relative to the temperature obtained in Aspen Plus.

Table C.9 Comparison of distillation and rectification models presented in 4.1.4.2 versus Aspen Plus

		Average deviation	**Maximum deviation**
Distillation column	**Composition**	0.05% mol	0.58% mol
	Temperature	0.16%	3.89%
Rectification column	**Composition**	0.44% mol	4.93% mol
	Temperature	0.16%	1.57%

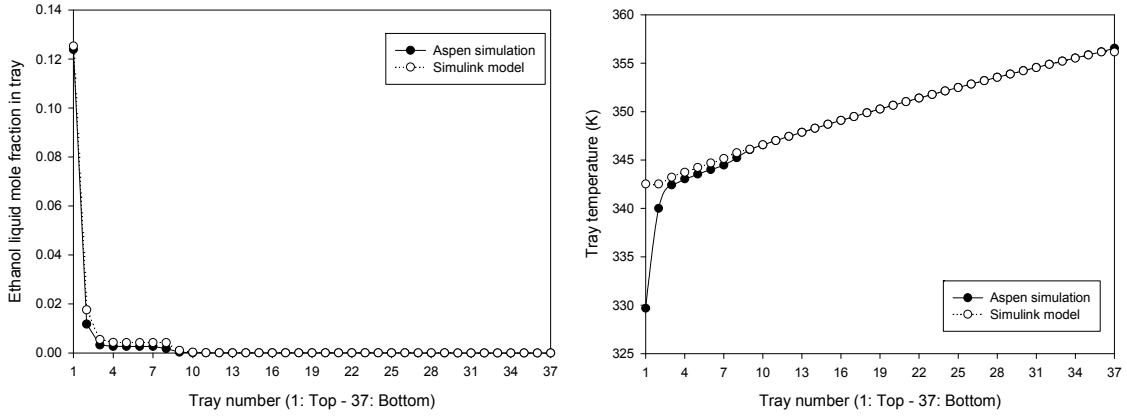

Figure C.4 Comparison between the distillation column model presented in Chapter 4 and results obtained using Aspen Plus. Left: Ethanol molar fraction; Right: Tray temperature.

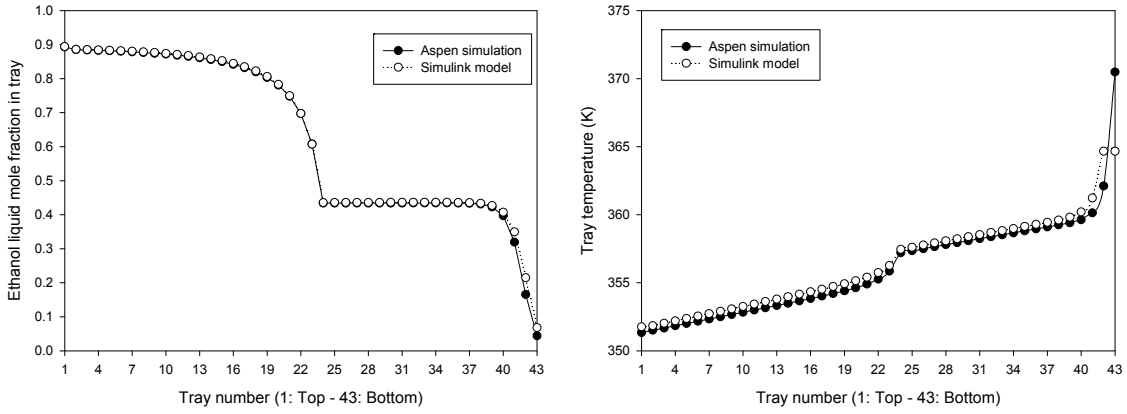

Figure C.5 Comparison between the rectification column model presented in Chapter 4 and results obtained using Aspen Plus. Left: Ethanol molar fraction; Right: Tray temperature.

As can be seen in Table C.8 and Figure C.4, for the distillation case, the model developed in this work and implemented in in Simulink is in excellent agreement with the Aspen Plus results for most of the trays in the column. The main deviation between the model and the Aspen data lies on the temperature of the condenser stage, basically because of the assumption of no sub-cooling in the total condenser for the Simulink model. On the other hand, for the rectification case, analyzing results shown in Table C.8 and in Figure C.5 it is possible to conclude that the Simulink model used in this work is in very good agreement with the Aspen plus model, and that the maximum deviation between the model predictions and the Aspen simulated data is observed for the concentration profile at the bottoms of the column (trays 40-43).

After comparing the simulink model for the distillation and rectification columns with total and partial condenser respectively, it is possible to conclude that the model described in Chapter 4 for the Distillation and Rectification is a suitable model for being used in the simulation studies.

C.5. Initial conditions of the process

A summary of the initial (optimal steady-state) conditions of the process are summarized in Tables C.10 and C.11.

Table C.10 Initial values of state variables in reactors

Variable \ Equipment	Liquefaction tank (R-101)	Saccharification tank (R-102)	Fermentor (R-201)
Level (m)	6.00	11.00	12.00
Ungelatinized starch concentration (kg/m^3)	0.86	0.85	0.83
Gelatinized starch concentration (kg/m^3)	0.19	0.19	0.08
Maltotriose concentration (kg/m^3)	260.57	6.20	2.51
Alpha-amylase concentration (kg/m^3)	0.00	0.00	0.00
Non-fermentables concentration (kg/m^3)	109.38	109.34	44.32
Glucose concentration (kg/m^3)	0.00	272.32	0.83
Glucoamylase concentration (kg/m^3)	0.00	0.34	0.14
Ethanol concentration (kg/m^3)	0.00	0.00	64.39
Viable biomass concentration (kg/m^3)	0.00	0.00	82.39
Total biomass concentration (kg/m^3)	0.00	0.00	119.23
CO_2 concentration (kg/m^3)	0.00	0.00	1.22

Table C.11 Initial values of state variables in columns

Tray	Distillation				Rectification		
	%mol Ethanol	%mol Water	Holdup (kmol)	Temp (K)	%mol Ethanol	Holdup (kmol)	Temp (K)
1 (Bottom)	0	0.99638	278.4	356.15	7.26E-15	166.7	379.94
2	0	0.99771	36.8	356.15	3.65E-14	13.2	379.94
3	7.51E-16	0.99770	36.8	355.83	1.74E-13	13.2	379.79
4	3.23E-15	0.99770	36.8	355.52	8.18E-13	13.2	379.64
5	1.04E-14	0.99770	36.7	355.19	3.84E-12	13.2	379.49
6	3.14E-14	0.99770	36.7	354.87	1.80E-11	13.2	379.34
7	9.33E-14	0.99770	36.7	354.54	8.47E-11	13.2	379.18
8	2.76E-13	0.99770	36.7	354.20	3.98E-10	13.2	379.03
9	8.14E-13	0.99770	36.7	353.87	1.87E-09	13.2	378.87
10	2.41E-12	0.99770	36.7	353.52	8.82E-09	13.2	378.72
11	7.11E-12	0.99769	36.7	353.18	4.15E-08	13.2	378.56
12	2.10E-11	0.99769	36.7	352.83	1.96E-07	13.2	378.41
13	6.23E-11	0.99769	36.7	352.48	9.22E-07	13.2	378.25
14	1.84E-10	0.99769	36.7	352.12	4.35E-06	13.2	378.09
15	5.47E-10	0.99769	36.7	351.76	2.05E-05	13.2	377.93
16	1.62E-09	0.99769	36.6	351.39	9.69E-05	13.2	377.74
17	4.81E-09	0.99769	36.6	351.02	0.00046	13.2	377.48
18	1.43E-08	0.99769	36.6	350.64	0.00215	13.1	376.83
19	4.25E-08	0.99768	36.6	350.26	0.00998	13.0	374.68
20	1.26E-07	0.99768	36.6	349.87	0.04318	12.5	368.91
21	3.76E-07	0.99768	36.6	349.48	0.11270	8.9	363.23
22	1.12E-06	0.99768	36.6	349.08	0.31731	7.6	357.93
23	3.34E-06	0.99768	36.6	348.68	0.53574	6.8	356.01
24	9.98E-06	0.99767	36.6	348.27	0.65428	6.4	355.33
25	2.98E-05	0.99765	36.5	347.85	0.71927	6.3	354.96
26	8.90E-05	0.99758	36.5	347.41	0.75925	6.2	354.68
27	0.00027	0.99741	36.5	346.93	0.78608	6.1	354.46
28	0.00079	0.99688	36.5	346.36	0.80524	6.1	354.25
29	0.00236	0.99531	36.4	345.52	0.81955	6.1	354.06
30	0.00688	0.99078	36.2	344.29	0.83061	6.0	353.88
31	0.00688	0.99312	22.7	343.59	0.83938	6.0	353.70
32	0.00687	0.99313	22.7	343.13	0.84649	6.0	353.53
33	0.00687	0.99313	22.7	342.66	0.85234	6.0	353.36
34	0.00706	0.99294	22.7	342.14	0.85723	6.0	353.19
35	0.00906	0.99094	22.6	341.22	0.86136	6.0	353.02
36	0.02870	0.97130	22.0	337.48	0.86488	6.0	352.85
37	0.18854	0.81146	129.0	337.48	0.86791	6.0	352.69
38					0.87053	6.0	352.52
39					0.87281	6.0	352.35
40					0.87480	5.9	352.18
41					0.87654	5.9	352.01
42					0.87808	5.9	351.85
43					0.88743	46.1	351.75

Appendix D. Process Design

In order to test the plantwide control methodology from an optimization perspective, the first step was the development of an optimal process design. For this purpose, the model developed in Section 4.1 was used. The process was designed to achieve a nominal production of 100.000 Ton ethanol/year (12.63 Ton/h for 330 days of operation during 24h/day) using a mash of starchy material as feed. The following aspects were considered during the process design stage:

1. For the conversion of starch to ethanol, a yield of only 90% was considered. Thus, the theoretical mass flow of ungelatinized starch required is 24.7 Ton/h. The raw material is considered to consist of: nonfermentable matter (25%), ungelatinized starch (60%) and water (15%).
2. According to **Karuppiah (2008)**, the amount of alpha-amylase and glucoamylase needed in the liquefaction and saccharification steps is 0.05% and 0.12% the weight of starch slurry, respectively. That is, flow rates of 20.6 kg/h alpha-amylase and 49.5 kg/h glucoamylase are required.

The main design parameters were obtained using sensitivity analysis, minimizing a pure economic objective function related to the capital and operating costs in the process. The economic objective function used for the sensitivity analysis is given in Equation (D.1):

$$C_{Total} = \sum_{year=0}^{10} C_{Liq} + C_{Sac} + C_{Fer} + C_{Distil} + C_{Recti} + C_{RawMaterial} - Profit \quad \text{(D.1)}$$

where the total cost in Euros (C_{Total}) was evaluated for a period of 10 years of operation. C_{Liq}, C_{sac}, C_{Fer}, C_{Distil} and C_{Recti} are the costs in the liquefaction, saccharification, fermentation, distillation and rectification sections, respectively. $C_{RawMaterial}$ and *Profit* is the difference between the costs related to raw material consumption and the incomes generated from the commercialization of the product. The costs for the liquefaction, saccharification and fermentation tanks consider only the capital costs related to the size of each tank (assuming L/D =1.5, and vertical cylindrical vessels), as shown in Equations (D.2) – (D.4) (**Hoch and Espinosa, 2008**).

$$C_{Liq} = 17330\left(\frac{4V_L}{1.5\pi}\right)^{0.7} a \quad \text{(D.2)}$$

$$C_{Sac} = 17330\left(\frac{4V_S}{1.5\pi}\right)^{0.7} a \quad \text{(D.3)}$$

$$C_{fer} = 17330\left(\frac{4V_F}{1.5\pi}\right)^{0.7} a \quad \text{(D.4)}$$

where *a* is the annualized cost of the equipment, calculated as:

$$a = \frac{i(1+i)^y}{(1+i)^y - 1} \quad \text{(D.5)}$$

y represents the years of operation considered (10 years), and *i* is the annual interest rate. For this process, the annual interest rate used was 42% (**Franceschin et al., 2008**).

The capital costs for the distillation and rectification columns were calculated using the expressions reported by **Hoch and Espinosa (2008)** (D.6 – D.7), which take into account the cost for the shell (C_{shell}) and the cost of the trays (C_{trays}) in the columns. The operating costs for each column consider the energy consumption of the reboiler (Q_{Reb}) and the condenser (Q_{cond}).

$$C_{Column} = C_{Shell} + C_{Trays} + C_{Reb} + C_{Cond} \quad \text{(D.6)}$$

$$C_{Column} = 1190\, F_{BM} f_q\, L^{0.87} D^{1.23} + 1044\, F_{BM,trays} f_q f_{NT} N_T\, D^{2.2146} + C_{steam} Q_{reb} + C_{Cool} Q_{cond} \quad \text{(D.7)}$$

where *L* is the height of the column, *D* is the column diameter and N_T is the total number of stages. The parameters F_{BM}, $F_{BM,trays}$, f_q, and f_{NT} are the bare module and the contingency for the shell and the stages, respectively. Considering steel as construction material and assuming a height equal to $L=N_T*D/2$, the following expressions for the total cost in the columns are obtained:

$$C_{Distil} = 12190\left(\frac{Nt_D}{2}\right)^{0.87} {D_D}^{2.1} + 1044\, Nt_D\, {D_D}^{2.2146} + C_{steam} Q_{reb} + C_{Cool} Q_{cond} \quad \text{(D.8)}$$

$$C_{\mathrm{Rec}ti} = 12190\left(\frac{Nt_R}{2}\right)^{0.87} D_R{}^{2.1} + 1044\, Nt_R\, D_R{}^{2.2146} + C_{steam}Q_{reb} + C_{Cool}Q_{cond} \quad \text{(D.9)}$$

Steam (C_{steam}) and cooling costs (C_{cool}), taken from **Hoch and Espinosa (2008)**, are C_{steam}=22.62 €/MW and C_{Cool}=3.82 €/MW.

In total, seven design parameters were selected for sensitivity analysis, namely the liquid volume of the liquefaction, saccharification and fermentation tanks, and the number of trays and feed tray location for the distillation and rectifications columns. The sensitivity analysis for process design was carried out as follows. Each parameter was changed between the lower and upper bounds shown in Table D.1, while keeping all other parameters at their nominal values (initial estimates) if they have not been analyzed yet, or at their optimal values if they have already been analyzed. The procedure was sequentially solved in the order presented in Table D.1. The results of the sensitivity analysis that led to the optimal design of the process are shown in Figure D.1.

Table D.1 Design parameters and their values considered for sensitivity analysis

Design Parameter	**Variation Interval**	**Nominal value (initial estimate)**	**Optimal Value**
Liquefaction Tank Volume V_L (m^3)	40 – 100	50	90
Saccharification Tank Volume V_s (m^3)	40 – 1000	70	600
Fermentation Tank Volume V_F (m^3)	400 – 1500	700	1080
Number of trays in Distillation column	30 – 38	36	37
Feed Tray in Distillation column	5 – 35	20	30
Number of trays in Rectification column	4 – 47	39	43
Feed Tray in Rectification column	2 – 40	4	20

Table D.1 shows the range of values considered for each design parameter and the optimal value obtained after analyzing the sensitivity of the economic objective function with respect to these parameters.

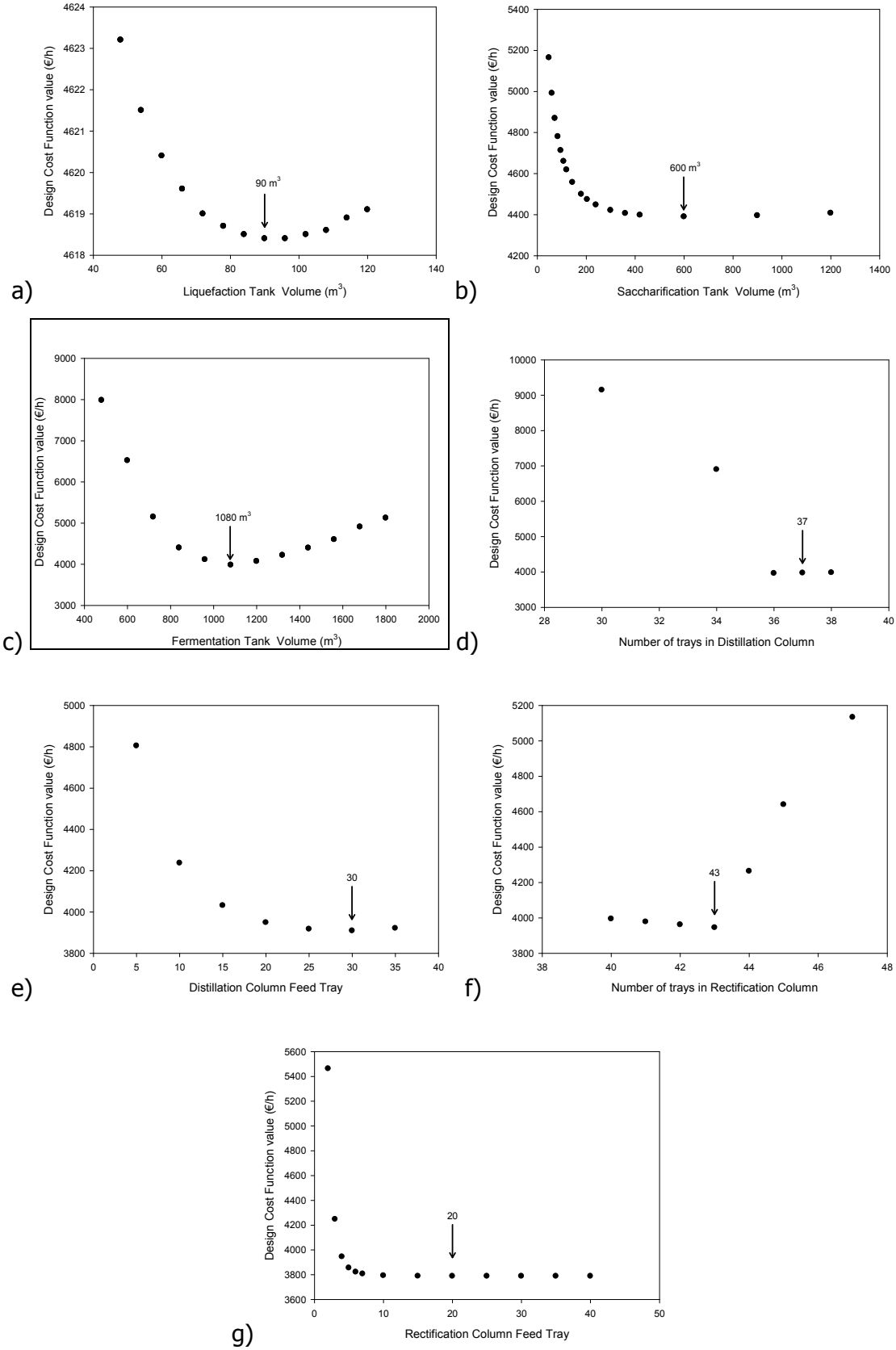

Figure D.1 Sensitivity analysis of the main process design parameters. a) Liquifier volume, b) Saccharificator volume, c) Fermentor volume, d) Number of trays in distillation column, e) Distillation column feed tray, f) Number of trays in rectification column, g) Rectification column feed tray